Investigations into the Simulation of Free-Radical Polymerization

by

Mark Thomas Langdon Rees

A thesis submitted in partial
fulfillment of the requirements
for the degree of Doctor of Philosophy in Chemistry.

Department of Chemistry,
The University of Canterbury.

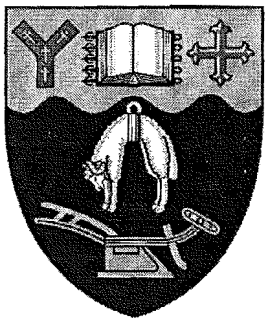

February 1999

'Out of the crooked timber of mankind no straight thing was ever made'

Emmanuel Kant

Abstract

A suite of simulation strategies has been developed that is well suited to the simulation of free-radical polymerization in general and pulse initiated polymerization (PIP) in particular. It has been shown that the appropriate use of these techniques can accurately yield the solution of the population-balance differential equations that characterize PIP, and can do so in a short period of time. During this study it became clear that many of truths elucidated about the solution of the differential equations for PIP, also hold true for the solution of the differential equations for free-radical polymerization in general. Although this study focussed entirely on PIP systems, this assertion is based on the many similarities in the mathematics of these two systems of differential equations.

A detailed analysis of the error incurred by these solution methods has been performed. Using this analysis as a basis several recommendations have been made concerning steps that can be taken to reduce the effect of this error upon the final molecular weight distribution. Two case studies have been undertaken where this suite of techniques has been used to test kinetic models and to extract rate parameters from experimental data.

In the presented study, both analytic and numerical strategies have been used to solve the population-balance differential equations that give a microscopic description of PIP. Analytic solution strategies proved to be too computationally expensive to implement, as well as too difficult to change to reflect changes to the kinetic model being used. In contrast to this, finite-difference based numerical methods produced solutions rapidly, ones that contained minimal error. Moreover, it has been shown that these methods can be used to model a wide range of PIP systems.

This investigation confirmed that the population-balance differential equations for dead chains and living radicals have different mathematical characteristics. Of particular relevance to this study was the fact that population-balance differential equations for the living radicals are more complicated and more prone to error, when solved numerically, than the differential equations for dead chain species. This means that a simpler, less computationally expensive method can be used to solve the differential equations for dead chain species than that which is used to solve the differential equations for living radical species.

The first of the two modeling studies performed in this thesis probed the mechanism of

termination in the free-radical polymerization of methyl methacrylate. A method for extracting this information from a molecular weight distribution measured by Matrix-Assisted-Laser-Desorption-Ionization Mass Spectrometry was developed. This analysis provided strong evidence that the termination mechanism of methyl methacrylate is dominated by the disproportionation mechanism at 0°C.

The second modeling study explored the kinetics of a PIP where radicals are created by an initiator which is bifunctional and which is sensitive to light in the visible region of the spectrum. This series of simulations confirmed that this initiator can be used to carry out meaningful PIPs.

Acknowledgments

There are a few people that I would like to thank for their contributions to my thesis:

Foremost amongst these is my supervisor, Greg Russell. It is a tribute to Greg's thoughtful approach to supervising my Ph.D. that I have found the time spent studying for my thesis enjoyable and stimulating. In particular, I have valued Greg's enthusiasm for my work, sense of humor, accessibility, and essays on a broad range of topics and respected, among other things, his erudition.

Dr. Hans Heuts for a wealth of good ideas and for supervising some of my work.

Professor Bob Gilbert for his support of my thesis and for an inflatable sheep to which I have formed a close personal bond.

Dr. Tom Davis and a number of the members of his research group for their ideas and collaboration. In particular, to Dr. Mike Zammit and Dr. Dax Kukulj for letting me sleep on their couch.

Greg Smith for the proof reading of this thesis and for constantly impressing me with his unsurpassable ability to turn weet-bixs into graphs and Chris Ferguson for his friendship.

And finally Sarah for Lake Hawea and other epiphanies.

Contents

List of Figures

List of Tables

Chapter 1

Introduction

1.1 Preamble

Free-radical polymerization is a process of undeniable commercial relevance, as well as a subject of academic interest. As such it provides an interesting case study of the interaction of industry and the academy, an example of the limitations and advantages of both forms of enquiry. Industry brings impetus, resources, and focus to the study of this procedure, while the academy brings rigor, divorced criticism, and excellence. Separated each produces a body of knowledge that is either outcome focussed or esoteric. Together they can bring an in-depth relevant understanding.

Commercially an understanding of free-radical polymerization is imperative. Industry seeks the ability to tailor polymerization to the requirements of the final product. As an academic subject free-radical polymerization provides an environment where a range of chemical theories can be tested and developed. An important example of this is that of radical reactivity, where semi-empirical models fail to explain the rate and specificity of simple radical reactions.

Although the enquiry that forms this thesis is unashamedly academic, much of its motivation comes from the questions that industry might ask. In this work, methods are developed that extend the applicability of techniques that can be used to extract information about the microscopic chemical processes that lie at the heart of polymerization, information that can be used to tailor polymerization and extend chemical understanding.

1.2 Free-Radical Polymerization

1.2.1 Basic Reaction Scheme

Free-radical polymerization is a chain mechanism that has at its heart four types of chemical process. These are: (1) radical formation; (2) propagation; (3) chain transfer and (4) bimolecular termination, by disproportionation and combination. The standard kinetic scheme for free-radical polymerization, a scheme that includes all of these processes, is as follows

$$\text{Initiator} \xrightarrow{k_d f} 2\text{R}_1 \tag{1.1}$$

$$\text{R}_i + \text{M} \xrightarrow{k_p^i} \text{R}_{i+1} \tag{1.2}$$

$$\text{R}_i + \text{X} \xrightarrow{k_{tr,X}^i} \text{R}_1 + \text{D}_i \tag{1.3}$$

$$\text{R}_i + \text{R}_j \xrightarrow{k_{td}^{i,j}} \text{D}_i + \text{D}_j \tag{1.4}$$

$$\text{R}_i + \text{R}_j \xrightarrow{k_{tc}^{i,j}} \text{D}_{i+j} \tag{1.5}$$

In this reaction scheme, R_i and D_i are defined as living radical species and dead polymer chains that contain i units of monomer (M) respectively, 'Initiator' denotes a molecule of initiator and X is defined as a species to which a growing radical chain can transfer its activity, for example solvent (S). Here, k denotes a rate coefficient, where this rate coefficient is subscripted to indicate to which reaction it pertains, and superscripted according to its chain-length dependence. For example, $k_{td}^{i,j}$ is the rate coefficient for termination by disproportionation, where this rate coefficient depends upon i and j, the chain lengths of both terminating radicals. Note that $k_t^{i,j} = k_{tc}^{i,j} + k_{td}^{i,j}$ in all circumstances and that the 'American' convention for termination rates has been employed, i.e., $R_{term} = 2<k_t>\text{R}^2$; here $<k_t>$ is the chain-length average value of k_t (see equation 1.17) and R the total concentration of living radicals.

Although each of these processes can be represented as a simple equation, each reaction is more complicated that it at first may seem. As these reactions play a important role in all that follows, a detailed description will be given of each of these processes.

Chain Initiation

Chain initiation (equation 1.1) begins by the activation of the initiator species via thermal or photochemical means. This activation causes the homolytic cleavage of a molecule of initiator, producing two primary radical species (R_0). A rate constant, k_d, is defined for this process. Once the primary radicals have been formed, a number of fates can befall them: they can recombine with each other, annihilating the radical activity; they can react with another species; or they can add to monomer, initiating free-radical polymerization. The propensity of a freshly created primary radical to add monomer and begin free-radical polymerization is quantified via the symbol f, the initiator efficiency. The initiator efficiency is defined as the fraction of primary radical fates that lead to free-radical polymerization. The initiator efficiency is closely linked to how fast a primary radical diffuses out of its solvent cage; hence, it is highly dependent on the initiator–solvent system. Note that at low polymer concentrations f is approximately equal to 0.5.

Hence, chain initiation really consists of two processes: (1) initiator decomposition (equation 1.6) and (2) the addition of primary radicals to monomer (equation 1.7).

$$\text{Initiator} \xrightarrow{k_d} 2R_0 \tag{1.6}$$

$$R_0 + M \xrightarrow{k_{p,I}} R_1 \tag{1.7}$$

In equation 1.7, $k_{p,I}$ is the rate constant for propagation for primary radicals. Rather than explicitly dealing with all reactions of primary radicals it is customary to take a simpler approach: the rate of production of R_1 via initiation is written as

$$\left[\frac{dR_1}{dt}\right]_{\text{init}} = 2fk_d[\text{Initiator}] \tag{1.8}$$

If polymerization is initiated by a short laser pulse, i.e., pulsed-laser polymerization, then equation 1.6 is written as

$$\text{Initiator} \xrightarrow{\phi} 2R_0 \tag{1.9}$$

If it is assumed that the length of time necessary for the initiation of a polymer chain is negligible, then the radical concentration, expressed as ρ, produced when a laser pulse causes

initiator to dissociate into two radicals can be calculated according to:

$$\rho = \frac{2\Phi n_{ph}}{V} \tag{1.10}$$

Here Φ is the quantum yield, n_{ph} is the number of absorbed photons in moles and V is the irradiated volume. The overall quantum yield Φ is equal to the number of radicals that actually start polymerization divided by the product of the number of absorbed photons and the number of radicals produced when the initiator dissociates. This overall quantum yield is the product of the primary quantum yield (or laser efficiency) ϕ and the initiator efficiency f. The laser efficiency indicates the fraction of absorbed photon which results in the generation of primary radicals. The number of absorbed photons can be calculated via Beer's law[2]

$$n_{ph} = \frac{E_p}{E_\lambda}(1 - 10^{-\varepsilon.c.l}) \tag{1.11}$$

In this expression, E_p is the pulse energy, E_λ is the energy of a mole of photons of wavelength λ, ε is the molar absorptivity, c is the concentration of absorbing species and l is the path length of the irradiated sample. The product of $\epsilon.c.l$ is known as the absorbance, A.

Chain Propagation

The process of chain propagation (equation 1.2) is at the core of free-radical polymerization. It is through this process that the living radical chains grow to such extraordinary lengths. A propagation reaction occurs when the radical center of a living chain attacks a monomer species. Typically, this attack occurs at the least substituted end of a substituted asymmetrical olefin, i.e. tail attack.[34] As the propagation reaction involves the conversion of monomer into polymer, it not only produces long polymer species, but consumes monomer. This means that if the so called 'long chain' approximation is made that the rate of propagation, R_{prop}, is equal to the rate of monomer consumption, i.e.,

$$R_{prop} = -\frac{d\mathrm{M}}{dt} = \mathrm{M}\sum_{i=0}^{\infty} k_{\mathrm{p}}^{i}\mathrm{R}_i \tag{1.12}$$

Recently, experimental studies have suggested that the rate coefficient for propagation de-

pends upon the chain length of the attacking radical species for the first five or so propagation steps, i.e., $k_p^i > k_p^\infty$ for $i \leq 5$, where k_p^∞ is the long-chain propagation rate coefficient.[34] Theoretical studies on the propagation of ethylene by Heuts et al.[24] have borne out this suggestion. In this work, *ab initio* quantum mechanical techniques were applied to calculate the geometry, energy and vibrational modes of the attacking radical, monomer and appropriate transition state 'species'. The results of these calculations were then used with the transition state theory formalism to predict the preexponential and activation energies for the Arrenhius rate expression. This theory suggested that the rate coefficient for the propagation for small radical species should be greater than that for large radical species, in particular, that $k_p^1 \approx 10 k_p^\infty$.[23]

Frequently, the rate coefficients of chemical reactions can depend on features of the chemical system, such as viscosity. Although k_p is independent of viscosity up to very high conversion, there are some suggestions of solvent effects. For example, some experimental evidence has been found of such effects during the polymerization of styrene and methyl methacrylate in benzyl alcohol.[35] Nonetheless, it is normally assumed that k_p is independent of solvent identity.

Chain Transfer

Chain transfer is the first process considered here that produces dead polymer chains. The transfer reaction involves the transferal of the radical activity from a radical species to some other chemical species, denoted above as X, converting the growing radical into a dead polymer chain. This X may be a molecule of solvent, transfer agent or monomer. The transfer reaction involves two steps if X is not a molecule of monomer. The first involves the transferral of the radical activity to X, i.e.,

$$R_i + X \xrightarrow{k_{tr,X}^i} D_i + X^\bullet \tag{1.13}$$

and the next step typically involves a propagation (equation 1.14) reaction between $X^\bullet$ and monomer.

$$X^\bullet + M \longrightarrow R_1 \tag{1.14}$$

This scheme assumes that the rate of reaction 1.14 does not occur slowly. If this process were slow then X would be more correctly termed an inhibitor or retarder. The propensity of a system to undergo chain transfer is normally quantified by the chain transfer constant, $C_{tr,X}$.

$$C_{\mathrm{tr,X}} = \frac{k_{\mathrm{tr,X}}}{k_{\mathrm{p}}} \tag{1.15}$$

Two mechanisms have been proposed for the first step in the chain transfer process. These are the transfer of an atom or group to or from the growing radical to X via a homolytic substitution mechanism.[34] For transfer to monomer in ethylene, a recent theoretical study has suggested that the favored mechanism involves abstraction from, rather than transfer to, the monomer species.[25]

It is clear from equation 1.3 that the transfer reaction has no effect upon the total concentration of radicals, and thus no effect upon the polymerization kinetics. However, this is only true if the rate constants (in particular that for termination) are assumed to be chain-length independent. As $k_{\mathrm{t}}^{i,j}$ does decrease as the chain length of the radicals increases, an increase in the number of small radicals by transfer will normally increase $<k_{\mathrm{t}}>$, the average value of the termination rate coefficient. The effect of transfer upon the dead polymer chain molecular weight distribution (MWD) is more direct. Transfer increases the number of small dead polymer species in the MWD.

Chain Termination

Bimolecular termination has a strong effect upon the kinetics and MWDs of free-radical polymerization. Chain termination affects the kinetics by decreasing the concentrations of radical species and the MWDs by producing dead polymer chains. It is well known that bimolecular termination can occur via two mechanisms: termination by the combination mechanism (equation 1.5) and by the disproportionation mechanism (equation 1.4). Although both mechanisms have the same effect upon polymerization kinetics, they produce dead polymer species of different chain lengths. The disproportionation termination mechanism yields two dead polymer chains of chain length equal to the reacting radicals. The mechanism of disproportionation involves the abstraction of a hydrogen from one radical species by the other, producing two dead polymer chains, one with a saturated, the other with an unsaturated endgroup. In contrast to this, the combination termination mechanism gives one dead polymer chain that has a chain length equal to the sum of the chain lengths of the two reacting species.

The rate of the termination reaction is very fast, e.g. of the order of $10^8 - 10^{10}$ L.mol.s^{-1} for

small radicals.[19] So rapid, in fact, that the reaction rate is diffusion limited.[3] The diffusion coefficients of the radicals are dependent on the mass of the diffusing species, leading to a chain-length dependent rate coefficient for the termination reaction between a radical of chain length i and j.

There are three types of diffusion normally associated with radical-radical termination, these being: (1) translational diffusion; (2) segmental diffusion; and (3) reaction diffusion. The first stage of termination involves the centers of mass of both radicals species diffusing together. The next stage, segmental diffusion, has the chain ends diffusing together. Once the chain ends are close, the chemical process of termination takes place very quickly. To describe the diffusion involved in the termination process at high monomer conversion a third type of diffusion is also included: reaction diffusion. This is the diffusion of the radical center as a result of the addition of monomer.

It is believed that at low conversion segmental diffusion is the rate controlling step and that at higher conversions translational diffusion takes over. However, recent modelling studies have indicated that centre of mass diffusion could be rate controlling at low conversion as well.[45]

It should be noted that the rate coefficient for termination is the rate of this diffusion process; the actual chemical termination of the two radical species is effectively instantaneous. Moreover, it is important to point out that the rate at which the radical species diffuse together is independent of termination mechanism. That is, the net rate of diffusion for two radicals that will terminate by the disproportionation mechanism is the same as the rate of diffusion for two radicals that terminate by the combination mechanism. Thus the rate of termination by the combination mechanism is the same as that for the disproportionation mechanism. The difference between the two, which is normally thought of as a difference in rate, merely reflects the fact that the chance of a radical-radical encounter pair disproportionating is normally different from the likelihood of it combining. This means that one should talk about the proportion of radical-radical encounter pairs that disproportionate, f_{td}, and those that combine, f_{tc}, rather than the rate coefficients of termination by disproportionation and by combination.

The rate of termination is defined as:

$$-\frac{d\mathrm{R}}{dt} = 2\sum_{i=0}^{\infty}\sum_{j=0}^{\infty} k_{\mathrm{t}}^{i,j}\mathrm{R}_i\mathrm{R}_j \qquad \text{where } \mathrm{R} = \sum_{i=0}^{\infty}\mathrm{R}_i \tag{1.16}$$

and the average rate of termination is defined as:

$$<k_t> = \frac{\sum_{i=0}^{\infty}\sum_{j=0}^{\infty} k_t^{i,j} R_i R_j}{\sum_{i=0}^{\infty} R_i \sum_{i=0}^{\infty} R_i} \tag{1.17}$$

1.2.2 Population-Balance Differential Equations

The reaction scheme presented above is useful in that it lays out in a logical manner all of the processes believed to be important. From this reaction scheme it is possible to infer a modest amount of information about how each chemical process affects the kinetics and MWDs of these systems. However, what is of more use is to write down a system of population-balance differential equations (equations 1.18 – 1.25), i.e., equations that model the rate of change in the concentration of all species with time. These differential equations are obtained from the reaction scheme by considering how each type of reaction affects the concentration of a particular species. For example, it is clear that chain propagation has two effects. It decreases the concentration of radicals of chain length $i-1$ and increases the concentration of radicals of chain-length i.

This means that the differential equations for each species contain a number terms originating from the different reactions. For example, consider equation 1.20. This is the general differential equation for a radical of chain-length i. The first two terms come from chain propagation. The next term is a result of chain transfer. This involves the removal of radicals as they transfer their activity to another species. The final term describes the decrease in radical concentration caused by bimolecular termination. However, not all reactions directly affect the concentrations of all species. For example, the differential equation 1.20 contains no term directly related to chain initiation.

In general, differential equation 1.20 describes the rate of change in the concentration of radicals containing i monomer units as a function a time. If the value of this differential equation is positive, then the concentration of R_i is increasing, while if $\frac{dR_i}{dt}$ is negative, then the concentration of R_i is decreasing. These differential equations include two types of term: loss and gain terms. The loss terms describe the effects of reactions that reduce the concentration R_i, e.g., bimolecular termination, while the gain terms describe the effects of reactions that

increase the concentration of R_i, e.g., propagation 'in' from R_{i-1}.

The population-balance differential equations that describe the rate of change of the concentration of dead polymer species contain only gain terms. This is because this reaction scheme only contains reactions that produce dead polymer, none that consume it. Most of the differential equations for dead polymer species contain three terms: for termination by combination; termination by disproportionation; and transfer.

In theory, it is possible for a radical species to grow to any chain length, i.e., there is no theoretical limit on the maximum possible chain length. However, it is not possible to model an infinite number of differential equations. To avoid this problem an arbitrary maximum chain length is chosen and a single differential equation included for longer species (equation 1.21 for growing radicals and equation 1.25 for dead polymer chains). The maximum, or truncation, chain length (L) is chosen to minimize the impact of treating all chains of a greater chain length as if they were the same chain length. A reasonable criterion for deciding upon a value of L is to choose it so that R_L makes up no more that 0.5% of the total concentration of radicals. The value of L for dead polymer chains is normally set equal to L for living radicals. The value of L used throughout this thesis is 5000. It should be noted though, that a sensible value of L is system dependent.

Living Radicals:

$$\frac{dR_0}{dt} = R_{init} - k_p^0 M R_0 - 2R_0 \sum_{j=0}^{L} k_t^{0,j} R_j \tag{1.18}$$

$$\frac{dR_1}{dt} = k_p^0 M R_0 - k_p^1 M R_1 + X\left(\sum_{i=1}^{L} k_{tr,X}^i R_i - k_{tr,X}^1 R_1\right) - 2R_1 \sum_{j=0}^{L} k_t^{j,1} R_j \tag{1.19}$$

$$\frac{dR_i}{dt} = k_p^{i-1} M R_{i-1} - k_p^i M R_i - k_{tr,X}^i X R_i - 2R_i \sum_{j=0}^{L} k_t^{i,j} R_j \qquad 2 \le i < L \tag{1.20}$$

$$\frac{dR_L}{dt} = k_p^{L-1} M R_{L-1} - k_{tr,X}^L X R_L - 2R_L \sum_{j=0}^{L} k_t^{j,L} R_j \tag{1.21}$$

Dead Chains:

$$\frac{dD_0}{dt} = 2R_0 \sum_{j=0}^{L} k_{td}^{0,j} R_j + k_{tc}^{0,0} R_0 R_0 \tag{1.22}$$

$$\frac{d\mathrm{D}_1}{dt} = 2\mathrm{R}_1 \sum_{j=0}^{L} k_{\mathrm{td}}^{1,j}\mathrm{R}_j + k_{\mathrm{tr,X}}^{1}\mathrm{XR}_1 + \sum_{j=0}^{1} k_{\mathrm{tc}}^{j,1-j}\mathrm{R}_j\mathrm{R}_{1-j} \tag{1.23}$$

$$\frac{d\mathrm{D}_i}{dt} = 2\mathrm{R}_i \sum_{j=0}^{L} k_{\mathrm{td}}^{i,j}\mathrm{R}_j + k_{\mathrm{tr,X}}^{i}\mathrm{XR}_i + \sum_{j=0}^{i} k_{\mathrm{tc}}^{j,i-j}\mathrm{R}_j\mathrm{R}_{i-j} \qquad 2 \leq i < L \tag{1.24}$$

$$\frac{d\mathrm{D}_L}{dt} = 2\mathrm{R}_L \sum_{j=0}^{L} k_{\mathrm{td}}^{L,j}\mathrm{R}_j + k_{\mathrm{tr,X}}^{L}\mathrm{XR}_L + \sum_{i=0}^{L}\sum_{j=0}^{L} k_{\mathrm{tc}}^{i,j}\mathrm{R}_i\mathrm{R}_j - \sum_{i=0}^{L-1}\sum_{j=0}^{i} k_{\mathrm{tc}}^{j,i-j}\mathrm{R}_j\mathrm{R}_{i-j} \tag{1.25}$$

The only part of these differential equations that requires additional explanation is the combination term in differential equation 1.25. To calculate the contribution of combination to the long chain differential equation we sum all the possible ways that a radical may combine, i.e., $\sum_{i=0}^{L}\sum_{j=0}^{L} k_{\mathrm{tc}}^{i,j}\mathrm{R}_i\mathrm{R}_j$ and take away all of the ways a radical can combine to form a dead polymer chain of chain length less than L. Also note that it is assumed that primary radicals do not undergo chain transfer reactions.

The differential equations presented here are at the heart of this thesis. A considerable amount of time will be spent developing methods for solving these differential equations. Following on from this, these solution techniques will be used to perform novel simulation studies of polymerization systems. Because of their prominence in what follows, some time will be spent delving into their mathematical characteristics.

Put briefly, differential equations 1.18 - 1.21 are numerous, non-linear, stiff and coupled.

Stiffness

Stiffness is a fundamental characteristic of some differential equations that results in them being difficult to solve numerically. Before explaining stiffness one distinct point is required to be noted that will not be introduced in detail until later in this chapter. This is that a numerical solution produces a solution that contains error while an analytic solution produces a solution that is error free. To explain what stiffness is, and to illustrate the effects that it can have on the solution of differential equations, we will consider the paradigm example of a stiff differential equation, which is

$$y'' = f(x)y \tag{1.26}$$

Equation 1.26 is a second-order differential equation. For positive values of $f(x)$, y (the solution to equation 1.26) is the sum of two exponentials. For example, suppose $f = 100$, then

$$y = Ae^{-10x} + Be^{10x} \qquad A, B = \text{constant} \tag{1.27}$$

Often the desired solution to such an equation is the decaying exponential. Thus if we integrated equation 1.26 with the initial conditions:

$$y(0) = 1 \qquad y'(0) = -10 \tag{1.28}$$

the true solution is $y = e^{-10x}$. However, when solving equation 1.26 numerical integration methods will produce an answer that starts off decaying as $y = e^{-10x}$, but then 'explodes' as e^{10x} when x becomes large. The reason for this clear: any error in the numerical integration, no matter how small, is equivalent to a small admixture at the origin of the unwanted solution e^{10x}. Thus

$$y_{numerical} \approx e^{-10x} + \varepsilon\, e^{10x} \tag{1.29}$$

No matter how small ϵ is, sooner or later the second term will dominate.

In general, stiff differential equations are difficult to solve because their solution contains two parts, each changing on a very different scale. This means that the numerical solution of a stiff differential equation is limited by the part of the solution that is changing on a scale that one is often not interested in. Frequently, the part of the solution of interest is the large time-scale solution. However, in trying to obtain this large time-scale solution we are limited by the small time-scale, or transient part, of the solution. This is because far smaller integration steps must be used to model the transient part of the solution than would be necessary to describe the long time-scale part of the solution. Thus even though a large step size could be used to describe the large time-scale solution accurately, using such an integration step will incur a lot of error in the transient part, causing the solution to diverge overall.

This is the case for the solution of differential equations 1.18 – 1.21; their solution has two parts that change on different scales. To illustrate this we will jump ahead of ourselves for a moment and consider pulsed initiation polymerization (PIP), rather than continuously-

initiated polymerization, because the cause of stiffness is clearer when the initiation profile is not constant. The transients in the solution of the differential equations for PIP originate from the wave-like nature of the radical chain-length distribution. These transients cause the solution of these differential equations to change rapidly as a radical waves passes by. The long time-scale part of the solution is derived from bimolecular termination. Termination decreases the concentration of radical species as time passes. Propagation affects the concentrations of the radical species on a smaller time scale than termination; these differential equations are stiff.

This means that when solving these differential equations we are limited by the effort we must expend on accurately modeling the transient part of the solution. If the solution did not contain these propagation-derived transients then the solution of these differential equations would require significantly less effort.

Having said this, the situation with the system of differential equations for PIP is a little different from typical stiff systems, for the transient part of the solution, the radical waves, is not irrelevant. In modelling this type of polymerization we are not only interested in the total radical concentration, but also the wave-like nature of the radical chain-length distribution. For it is this wave-like radical chain-length distribution that eventually leads to the peaks in the dead polymer MWD which are characteristic of PIP. Thus the extra effort spent describing the solution transients does have benefits, in that it means that the important fine structure of the radical chain-length distribution is well described; this is an important aspect of a PIP simulation.

Many techniques have been developed for dealing with stiff differential equations; a number of these will be used in this thesis.[6][13][20]

Coupling

When more than one differential equation is used to describe the properties of a physical or chemical system it is very likely that those differential equations will be coupled. Consider differential equations 1.30 and 1.31. These differential equations are coupled to one another because the value of one depends upon the solution of the other. For example, the value of the differential equation 1.30 depends upon the value of the solution to differential equation 1.31,

y_2.

$$y_1' = a_1 y_1 - a_2 y_2 \tag{1.30}$$

$$y_2' = a_3 y_2 - a_4 y_1 \qquad a_i = \text{constant} \tag{1.31}$$

The population-balance differential equations for free-radical polymerization are coupled in four ways.

Coupling Due to the Propagation Reaction For all but the first differential equation, $\frac{dR_0}{dt}$, the differential equations for radicals of chain-length i are coupled to those for chain-length $i-1$. This coupling comes from the propagation term $k_p^{i-1} M R_{i-1}$.

Coupling Due to the Transfer Reaction In contrast to propagation, transfer couples only the differential equation for R_1. This differential equation is coupled via the term $X \sum_{i=1}^{L} k_{tr,X}^{i} R_i$. This terms means that the differential equations for R_1 is coupled to the differential equations for all other growing radicals.

Coupling Due to the Termination Reaction - Living Radical Differential Equations The termination reaction couples each differential equation to all others, and affects all of the differential equations for living radicals. The term that introduces the coupling is $2R_i \sum_{j=0}^{L} k_t^{i,j} R_j$.

Coupling Due to the Termination Reaction - Dead Polymer Chain Differential Equations The last form of coupling is between the living and dead polymer chain differential equations. The differential equations for dead polymer species depend upon the concentrations of living radical species. Hence the differential equations for dead polymer species are coupled to those for the growing radical species.

The coupled nature of these differential equations has a number of effects. Primarily, it means that all of the coupled differential equations, hence, all the differential equations for this system, must be solved at the same time. For example, again consider differential equation 1.20. The value of this differential equation depends on the values of the solutions to all the other radical differential equations. Thus to be able to solve differential equation 1.20 we must

know the solution to all other differential equations. This means that this system of differential equations must be solved in concert, i.e., each differential equation solved simultaneously.

In chapter three, we will see that the numerical solution of differential equations introduces error. Another effect of the coupling of differential equations is that an error in the solution of one differential equation affects all of the differential equations that are coupled to it. For example, suppose that when solving differential equation 1.20 for radicals of chain-length 10, i.e., $i = 10$, that positive 10% error was incurred, i.e., the value of R_{10} increased as a result of error by 10%. Because these differential equations are highly coupled, this error would affect all of the living radical differential equations and a large proportion of dead polymer differential equations. In chapter three it will become clear that the coupled nature of these differential equations has significant effects upon the temporal dependence of the numerical error (see for example section 3.10.3)

Non-linearity

A differential equation is defined as being linear if the function F (equation 1.32) is linear in terms of the variables $t, y.y', y''..., y^{(n)}$, i.e., it does not contain terms such as, i.e., yy', y^2, or $\cos(y)$

$$F(t, y.y', y''..., y^{(n)}) = 0 \tag{1.32}$$

Thus a differential equation is said to be non-linear if it does contain cross terms such as yy'. In addition to this, a system of differential equations is said to be non-linear if it contains terms that are the product of the solutions to other differential equations in that system. For example, equation 1.34 is a non-linear differential equation, as it contains a term that is the product of the solution to equation 1.33 and 1.34, $a_3 y_2 y_1$.

$$y_1' = a_1 y_1 + a_2 y_2 \tag{1.33}$$

$$y_2' = a_3 y_2 y_1 \qquad a_i = \text{constant} \tag{1.34}$$

The non-linearity is introduced into differential equations 1.18 to 1.25 via the termination reaction. All of the differential equations for the living radical species include a term similar to

$2R_i \sum_{0=1}^{L} k_t^{i,j} R_j$. Expanding this term we have that

$$2R_i k_t^{i,0} R_0 + 2R_i k_t^{i,1} R_1 + 2R_i k_t^{i,2} R_2 + 2R_i k_t^{i,3} R_3 + 2R_i k_t^{i,4} R_4 ... \tag{1.35}$$

This is a series of non-linear terms, as it contains terms that are the product of the solution of two different equations. This means that the differential equations for living radical species are non-linear in the same sense that equation 1.34 is non-linear. The dead polymer differential equations are also non-linear as they contain a series of terms analogous to equation 1.35.

Non-linear differential equations are normally more difficult to solve numerically than linear ones, as they are frequently sensitive to numerical error.[13] However, they are often impossible to solve analytically.

1.2.3 Intermittently-Initiated Polymerization

The initiation process for most free-radical polymerizations involves the addition of a constant, or slowly changing, concentration of radicals. These radicals are created continuously, as was described in section 1.2.1, by thermal or photochemical means. Hence, this type of polymerization can be called continuously-initiated polymerization. As the rate of initiation is effectively constant, at least until initiator consumption becomes important, the kinetics of these systems quickly reach a 'steady state'. A steady state involves the balance between the concentration of radicals added and those taken away, i.e., a balance between the rates of initiation and termination. At the steady state the total concentration of radicals becomes constant. This steady-state radical concentration can be calculated by applying the steady-state approximation to the differential equation for the total radical concentration (equation 1.36).

$$\frac{dR}{dt} = R_{init} - 2<k_t>R^2 = 0 \qquad R = \sum_{i=0}^{\infty} R_i \tag{1.36}$$

This expression can be solved for the steady-state total radical concentration, i.e.,

$$R_{ss} = \sqrt{\frac{R_{init}}{2<k_t>}} \tag{1.37}$$

However, what is of greater interest is the rate of monomer consumption, for this can be easily measured experimentally. Making the long chain assumption, the rate of polymerization, or monomer consumption, is equal to:

$$-\frac{d\mathrm{M}}{dt} = k_\mathrm{p}\mathrm{MR} \tag{1.38}$$

If we replace the total radical concentration in equation 1.38 with the steady-state radical concentration we obtain

$$-\frac{d\mathrm{M}}{dt} = k_\mathrm{p}\mathrm{M}\sqrt{\frac{R_{init}}{2<k_\mathrm{t}>}} \tag{1.39}$$

Assuming a steady state, this expression can then be solved to yield

$$\ln(\frac{\mathrm{M}_0}{\mathrm{M}_t}) = \sqrt{\frac{k_\mathrm{p}^2 R_{init}}{2<k_\mathrm{t}>}}\ t \tag{1.40}$$

In this expression, M_0 is the initial monomer concentration and M_t is the monomer concentration at time t. All other symbols have their normal definitions. This means one can extract the ratio of $\frac{k_\mathrm{p}^2}{<k_\mathrm{t}>}$ by plotting experimental data for monomer consumption as $\ln(\frac{\mathrm{M}_0}{\mathrm{M}_t})$ against time and evaluating the slope of this plot. It is clear from equation 1.40 that this analysis yields only the ratio of rate coefficients $\frac{k_\mathrm{p}^2}{<k_\mathrm{t}>}$. While this does provide some kinetic information, what is more useful is the individual rate coefficients. Hence, what is required is some procedure from separating the values of k_p and $<k_\mathrm{t}>$. Some options are now discussed.

The Rotating Sector Method

To overcome the limitations of the steady state one is forced to work under non-steady-state conditions. The easiest means of stopping a polymerizing system from obtaining a steady state is to use a time-dependent initiation profile, i.e., to intermittently initiate the polymerization. Whereas, in a continuously-initiated system, such as that described above, a steady stream of radicals is added, in an intermittently-initiated polymerization the rate of initiation varies with time in a periodic manner. Although there are many ways of varying the rate of initiation with time, by far the most widely used involves a light source and a photosensitive initiator.

For a long time the most prominent way of creating an initiation profile that changed with time was the rotating-sector technique. This technique has the polymer vessel contained within

a rotating annulus that has a sector removed. A light source is placed outside the annulus such that the annulus precludes light reaching the polymerization vessel unless the open sector is next to the light source. This means that as the annulus rotates there are times where light impinges on the system (when the removed sector is adjacent to the light source) and times when it does not. Hence, there are periods of high and zero (or at least low) rates of initiation. From this experiment a combination of rate constants ($k_p/<k_t>$) different from that obtained from steady-state experiments ($k_p^2/<k_t>$) can be extracted. By combining these two pieces of information it is possible to extract the individual values of the rate constant for propagation and that for termination. Although combining these two pieces of information did yield the required kinetic information, little could be concluded from the results. The values of k_p and $<k_t>$ varied by orders of magnitude between groups and experimental setups. One of the reasons for this large variation was that different conditions were established in the each of the two experiments used in this method, i.e., steady and non-steady state polymerization. Given chain-length dependent termination, this means that $<k_t>$ is different for each experiment, contrary to assumption. Thus the method breaks down. This all meant that a better method needed to be found for measuring these rate coefficients.

Olaj's Method Using Laser Based Initiation

In an important paper in 1987, Olaj et. al.[37] proposed a new method that overcame the limitations of previous attempts to extract the rate coefficient for propagation. This method, which is now recommended by IUPAC [5], produces a value of k_p independently of all other rate constants. Moreover, it has been shown that this method for determining k_p is not affected by other polymerization reactions or by the mechanism of termination.[37][40]

The Pulse Initiated Polymerization (PIP) Method

In a nutshell, the PIP method involves initiating a polymerization with periodic bursts of initiation, i.e., laser pulse mediated cleavage of initiator that is instantaneous relative to all other processes. Next it involves measuring the MWD of resulting dead polymer chains by gel permeation chromatography (GPC) and locating the low molecular weight side inflection point of the first peak in this distribution. Finally it involves using the chain length of this point to

calculate the value of k_p. The key relationship of this method is that the position of the low molecular weight inflection point is equal to

$$i_{poi} = k_p M t_0 \tag{1.41}$$

In this expression, i_{poi} is the chain length of the point of inflection, M the monomer concentration and t_0 is the time between laser pulses. Several insights are required to understand how this method works. Firstly, that there is a critical chain length that most radicals will grow to in the time between bursts of initiation and that this chain length is equal to $k_p M t_0$. Next that this critical chain length can be extracted from the dead chain MWD. And finally that the inflection point is positioned reasonably close to this critical chain length.

Initiation Profile - the Periodic Creation of Radical Species

The initiation profile for a PIP, by definition, must consist of a series of bursts of initiation similar to that shown in figure 1-1. In this figure the concentration of radicals added by a burst of initiation, frequently created by a laser, is ρ and the period between laser pulses is t_0. In figure 1-1 t_0 is equal to 0.1 s. Thus the frequency of the laser is $1/t_0$ (as distinct from the frequency of the laser light). Note that although the most common means of creating this type of profile involves a pulsed laser-photosensitive initiator system, other methods have been used. For example, van Herk et.al.[54] have performed pulsed electron beam polymerization of styrene in latex particles. Pulsed electron beams were used in this study rather than a pulsed laser as an electron beam can penetrate further into this heterogeneous medium.

The Total Radical Concentration as a Function of Time The total radical concentration profile that is created by this initiation profile is shown in figure 1-2. The rate parameters of this data are: $k_t = 1 \times 10^8$ L.mol^{-1}.s^{-1}, $\rho = 1 \times 10^{-6}$ mol.L^{-1}, and $t_0 = 0.1$ s. This figure contains several noteworthy features. Firstly, the total radical concentration has the same periodicity as the initiation profile. The total radical concentration increases by ρ every t_0 seconds; next the total radical concentration declines due to bimolecular termination throughout an dark period (that is the time between two bursts of initiation). Note that bimolecular termination occurs throughout the whole initiation period, it is not only confined to the moments straight

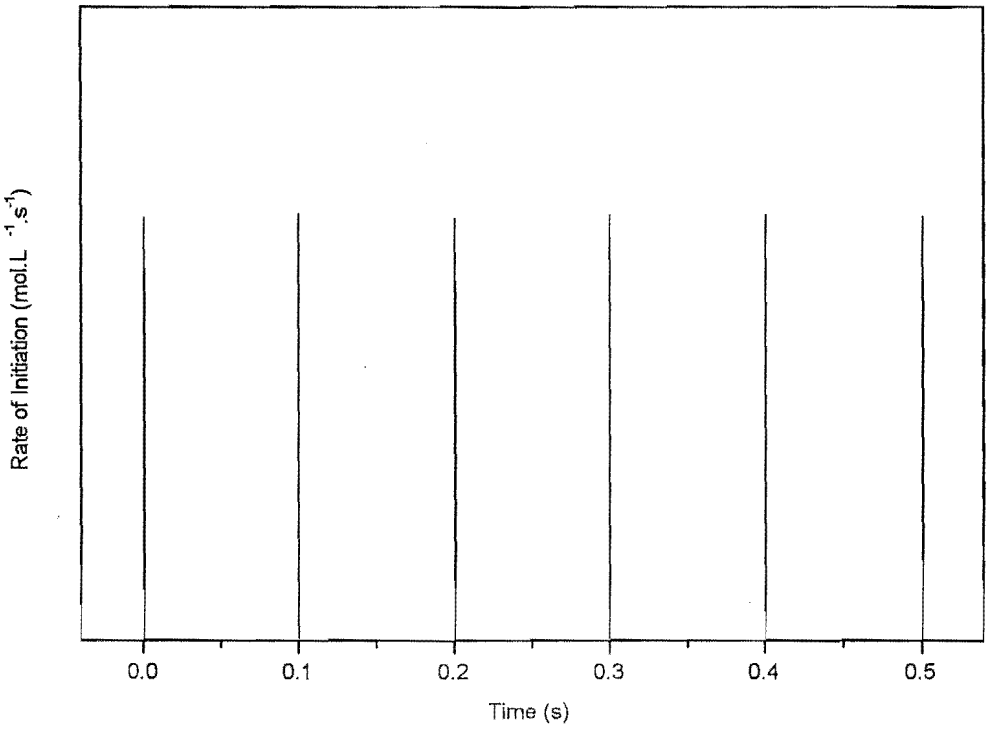

Figure 1-1: The initiation profile for a pulse initiated polymerization. Note that $t_0 = 0.1$ s.

after the arrival of a laser pulse. Nonetheless the rate of termination decreases as the time since the laser pulse increases (see figure 1-2). The time dependence of the total radical concentration during the period between two laser pulses is described by a simple expression (see chapter two for the derivation of this expression). This expression is:

$$R_t = \frac{R_{max}}{1 + 2k_t R_{max} t} \tag{1.42}$$

In this expression, R_t is the total radical concentration at time t, R_{max} is the maximum radical concentration (the concentration of radicals straight after the arrival of a laser pulse).

The final feature of these plots that will be discussed is the pseudo-steady state in the total radical concentration. This is a repeating pattern in the total radical concentration that has the

same periodicity as the initiation profile. Instead of a constant radical concentration (steady state) there exists a radical concentration profile that is repeated every initiation period (pseudo-steady state). Once this pseudo-steady state has been established the total radical concentration repeats the same pattern every initiation period. The pseudo-steady state normally takes three to eight initiation periods to establish. By definition, the radicals added during the pseudo-steady-state period (ρ) must be equal to those that are lost by termination, i.e.,

$$\rho = 2 \int_{t=0}^{t=t_0} k_t \mathrm{R}^2 \tag{1.43}$$

This expression can be used in conjunction with equation 1.42 to derive an expression for the maximum radical concentration, R_{max}. This expression is:

$$R_{max} = \frac{\rho}{2} + \sqrt{\frac{\rho^2}{4} + \frac{\rho}{2k_t t_0}} \tag{1.44}$$

Radical Chain-Length Profile It is well known that the radical chain-length distribution in an intermittently-initiated free-radical polymerization consists of a series of evenly spaced Poisson distributions, where the spacing between these distributions is $k_p M t_0$, the mean chain length a living chain grows in t_0 seconds. A Poisson distribution is a probabilistic distribution that is found in a wide range of real-world problems. This distribution describes the occurrence of a random events, ones as diverse as: the times when a piece of radioactive material emits particles; the times when customers arrive at a service station; the times when accidents occur at a particular intersection; and the time it takes for a growing radical chain to add one monomer unit. The Poisson distribution describes the distribution of living chains because propagation is a Poissonian, or stochastic, process. It depends upon the random encounter between of appropriately activated monomer and growing chain. Because of this, not all growing chains add the same number of monomer units in the same period of time. This means that even radical species that are created at the same time, i.e., by pulsed initiation, are not necessarily the same chain length at some later time. Figure 1-3 contains an example of a radical chain-length distribution for a PIP, the rate parameters used in this calculation are: $k_p = 100$

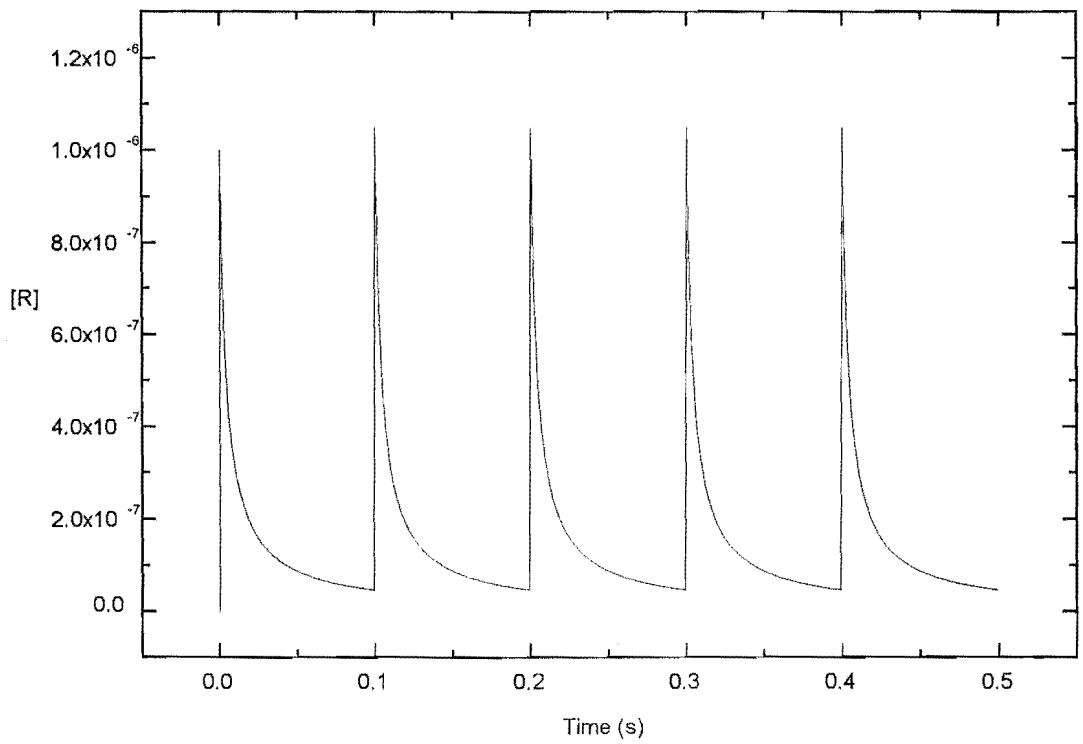

Figure 1-2: The temporal dependence of the total radical concentration in a PIP.

$\text{L.mol}^{-1}\text{.s}^{-1}$; $\text{M} = 10.0\ \text{mol.L}^{-1}$; $k_\text{t} = 1 \times 10^7 \text{L.mol}^{-1}\text{.s}^{-1}$; $\rho = 1 \times 10^{-6} \text{mol.L}^{-1}$; $t_0 = 0.1$ s; and this simulation was run for one second. This distribution is shown at $t = 0.09$ seconds after a burst of initiation. It is clear from figure 1-3 that the chain lengths of the radical species are distributed about the most probable chain length ($k_\text{p}\text{M}t$) with appreciable width. It is also clear from this figure that the width of these chain-length distributions increases as time passes. This is a result of the accumulation of random events.

Molecular Weight Distribution of Dead Polymer Chains A dead polymer chain-length distribution for an intermittently-initiated free-radical polymerization is shown in figure 1-4 and that same distribution transformed to $w(\log_{10} M)$ against $\log_{10} M$ is displayed in figure 1-5. These plots contain a number of features that are symptomatic of intermittently-initiated

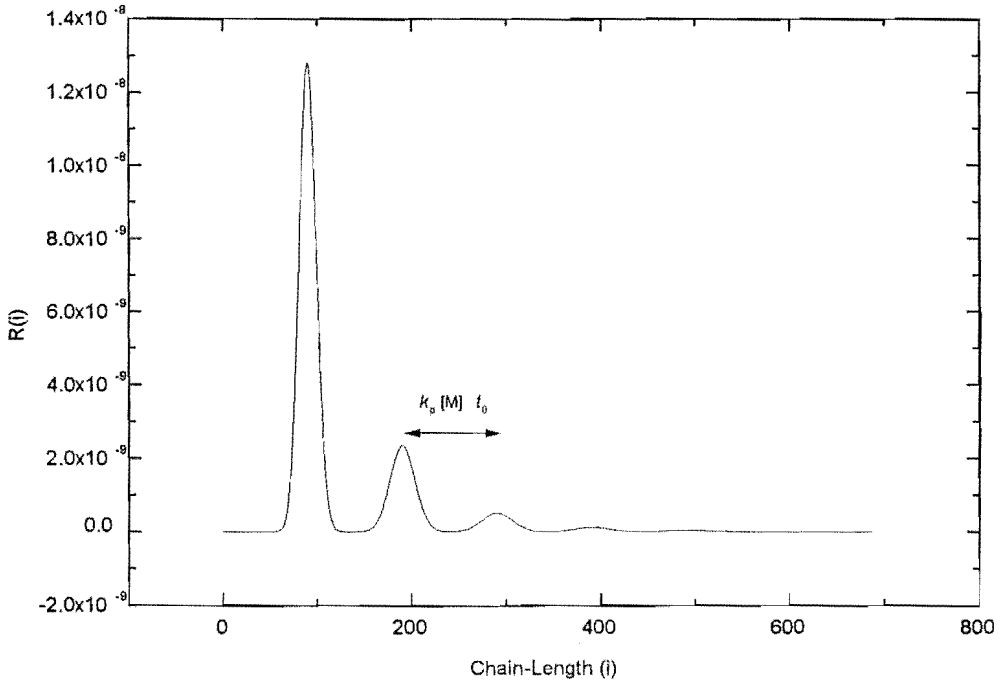

Figure 1-3: The radical chain-length distribution in an intermittently-initiated polymerization.

free-radical polymerization. For example, the dead polymer chain-length distribution contains several peaks, and these peaks are positioned at chain lengths that are approximately equal to jk_pMt_0 (j is a counting number). Moreover, these peaks extend further to high molecular weight than they do to low molecular weight. To understand the position and shape of these peaks, an explanation has to be given of the process of converting living radicals into dead polymer chains.

Two pieces of information are needed to explain these features. The first concerns the rate of polymer production. The total radical concentration and therefore the rate of termination decreases with time after a burst of initiation. As the rate of termination is equal to the rate of dead polymer production (neglecting chain transfer), more dead polymer is produced early in the time period than is produced at the end. This means that the dead polymer MWD is

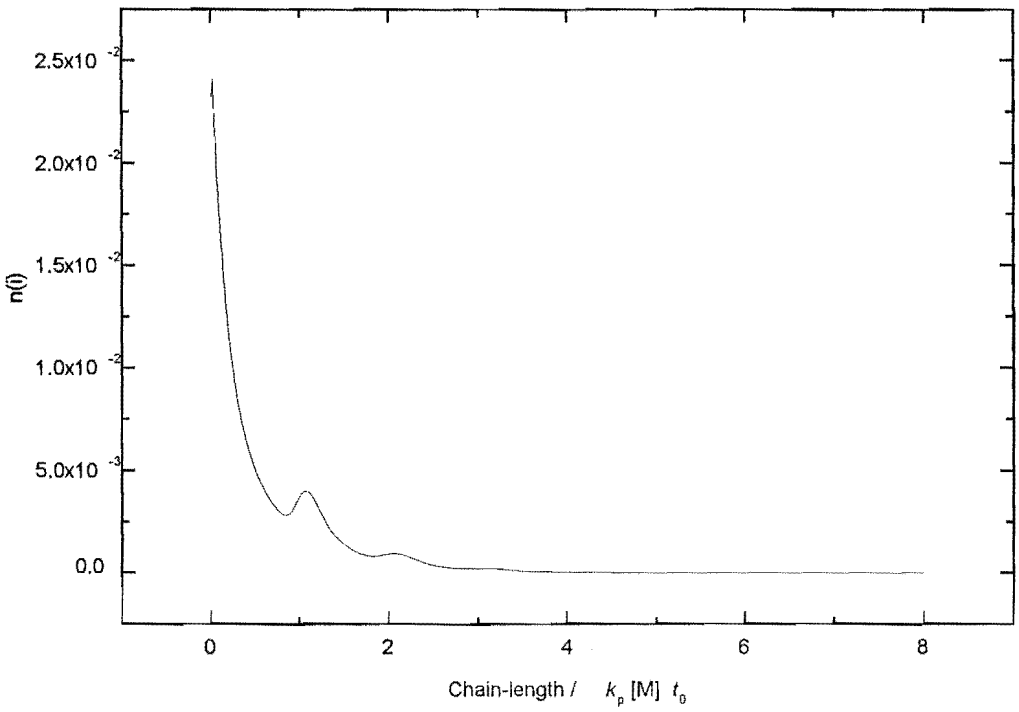

Figure 1-4: Number distribution of dead polymer chains formed in a intermittently-initated free radical polymerization. Rate parameters: all rate parameters as per figure 1-3 and termination via the disproportionation mechanism only.

biased towards chain lengths that correspond to dead polymer produced at the start of the time period. Secondly, the radical chain-length distribution also changes as the time since a burst of initiation increases. The concentrations of all species decrease due to termination and move to higher chain length because of propagation. These two changes are illustrated in figure 1-6. In this discussion it is assumed that termination occurs only by the disproportionation termination mechanism.

Combining the change in the rate of dead polymer production and the changes in the radical chain-length distribution allows us to explain the shape of the dead polymer chain-length distribution. The dead polymer chain-length distribution can be thought of as being the weighted sum of copies of the radical chain-length distribution throughout an initiation period.

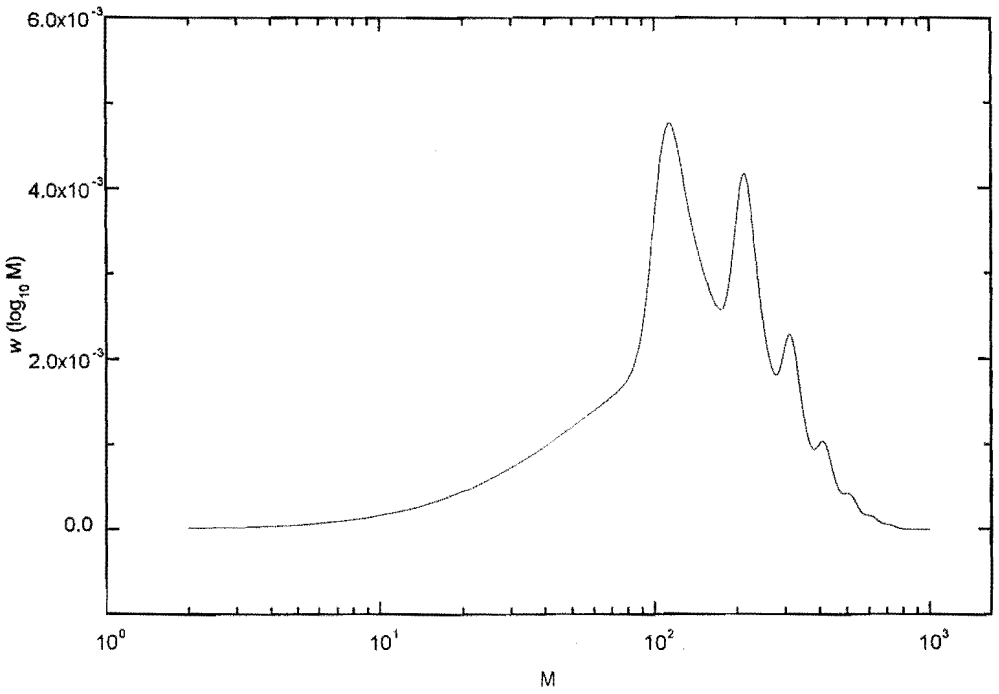

Figure 1-5: GPC type distribution of dead polymer chains formed in a intermittently-initated free radical polymerization. Rate parameters: all rate parameters as per figure 1-3 and termination via the disproportionation mechanism only.

The weighting originates from the fact that the amount of polymer produced declines with time so that the dead polymer MWD is dominated by the shape of the radical distribution early in an initiation period.

To consider the way this works we will divide time into intervals of $(k_{\mathrm{p}}\mathrm{M})^{-1}$ seconds. It should be noted that this discretization of time is no more than a useful simplification, because termination and propagation processes can occur at all times.

Straight after the arrival of a laser pulse the rate of termination is high and because of this a lot of dead polymer is produced. At this stage a copy of the current living radical chain-length distribution is added to the dead polymer chain-length distribution. Hence, at this stage the dead polymer chain-length distribution consists of a series of peaks centered around $jk_{\mathrm{p}}\mathrm{M}t_0$.

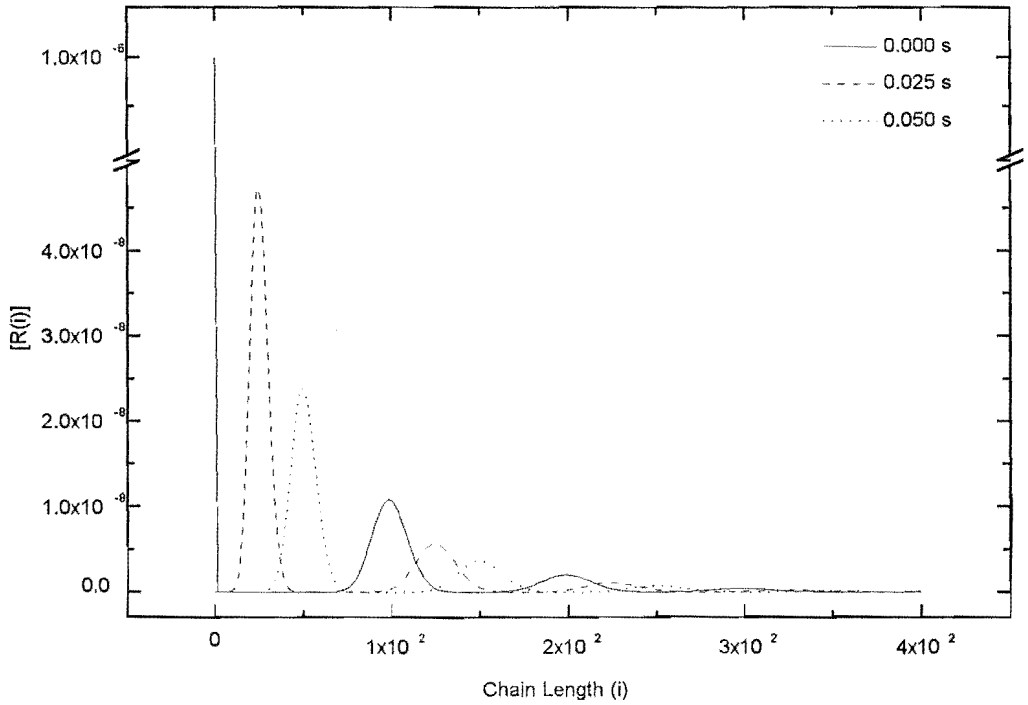

Figure 1-6: The living radical chain-length distribution at several times after the arrival of a burst of intiation. All rate parameters are the same as for figure 1.3.

At $(k_p M)^{-1}$ seconds after the arrival of an initiation burst, the positions of the peaks in the living radical chain-length distribution have increased by one. Moreover, the concentration of radicals has decreased due to termination. At this point another copy of the living radical chain-length distribution is added to the dead polymer chain-length distribution. This means that our model of the dead polymer chain-length distribution is the sum of two copies of the living radical distribution with peaks slightly offset and the second distribution containing less polymer.

These changes to the living radical chain-length distribution continue: the peaks move to high chain length and radicals are removed by bimolecular termination. As time passes more copies of the radical distribution are added to the dead polymer distribution.

Thus the reason why the peaks are positioned at higher chain length is that each peak in the dead polymer MWD is the sum of a series of peaks of diminishing height that extend to higher chain length. Moreover, the reason that these peaks are unsymmetrical is that the heights of the peaks in this sum diminishes as time passes.

It is important to note that the actual position of the peak maximum is controlled by the relative rates of propagation and termination. For example, if termination occurs much faster than propagation then lots of dead polymer will be added while the peaks in the radical distribution are still positioned at $jk_{\mathrm{p}}\mathrm{M}t_0$, i.e., before the radicals have a chance to grow. In contrast to this, if the rate of propagation is very much greater than the rate of termination then radicals will grow well past $jk_{\mathrm{p}}\mathrm{M}t_0$ before lots of dead polymer is formed. Thus the peak maximum will move to higher chain length, i.e., the position of the peak maximum is greater than $jk_{\mathrm{p}}\mathrm{M}t_0$.

Extracting the Value of the Rate Constant for Propagation One of the important insights of Olaj and coworkers[37] was that there exists a critical chain length that a radical species is most likely to grow to between burst of initiations. Assuming that propagation is chain-length independent this critical chain length, i_{crit}, is described by equation 1.45

$$i_{crit} = k_{\mathrm{p}}\mathrm{M}t_0 \tag{1.45}$$

Although this was an important realization, what was more significant was the fact that the value of this critical chain length could be extracted from the dead polymer MWD. For if one is able to extract the value of i_{crit}, then using independently known values of the monomer concentration and the time between laser pulses one can calculate the rate coefficient for propagation. The crucial step in this process is, therefore, locating a feature in the dead chain MWD that corresponds to the critical chain length.

The Location of the Critical Chain Length: the Low Molecular Weight Side Inflection Point vs the Peak Maximum In their original paper Olaj et. al.[37] suggested, and showed empirically, that the low molecular weight point of inflection of the primary peak of the dead chain MWD could be used as a measure of the critical chain length. Although there is

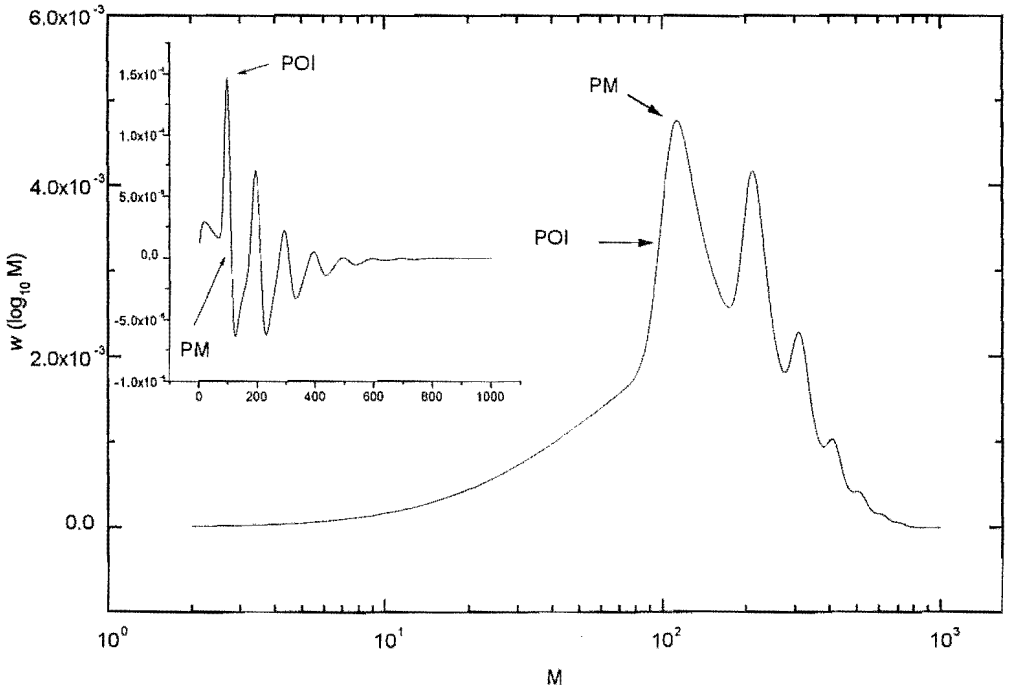

Figure 1-7: A MWD for a PIP with the position of the peak maximum (PM) and point of inflection (POI) indicated. The inlay contains the dervative of this distribution with respect to chain-length.

no theoretical reason for using this point, it is typically within 5% of the critical chain length and is easily extracted from experimental data, as an inflection point is a maximum or minium in the first derivative of the MWD (see the inlay of figure 1-7). For example, the position of the critical chain length in the MWD shown in figure 1-7 is 100, while the point of inflection is at chain-length 97. Therefore, in this case, using the inflection point as an estimate of the critical chain length introduces 3% error. Disagreeing with the idea that the inflection point is always the best feature of the MWD to extract the value of i_{crit} from, Schweer and Sarnecki[47] argued that sometimes the peak maximum of the first peak is closer to i_{crit}. They went on to classify PIPs as being in the high or low termination limit, where the product of the rate coefficient for termination, the concentration of radicals added by a laser pulse, and t_0 define

whether a polymerization is in the high or low termination limit. If a polymerization is in the high termination limit then the chain length of the peak maximum provides the best estimate of the critical chain length, while in the low termination limit the point of inflection is closest to i_{crit}.

However, the rate coefficient for propagation also affects which feature provides the best estimate of i_{crit}. If the rate of termination is high, relative to the rate of propagation, then the peak maximum is closest to the critical chain length (the high termination limit). In contrast to this, if the rate of termination is small relative to the rate of propagation, then the peak maximum is at a chain length higher than the critical chain length and the point of inflection provides a better estimate of the critical chain length (the low termination limit). Thus it is important to note that it is not only the rate of termination, but also the rate of propagation that decides which feature of the MWD provides the best estimate of i_{crit}.

The polymerization modeled above (figure 1-7) is in the low termination limit, and hence the inflection point should be closer to i_{crit} than the peak maximum. This is in fact the case. The peak maximum occurs at a chain length of 117, thus it overestimates the critical chain length by 17%. This means that the point of inflection (3% error) is closer to i_{crit} than the peak maximum.

The Criteria for Reliability The PIP method is a robust method for extracting the rate coefficient for propagation. Not only is it insensitive to a wide range of side reactions, e.g., transfer, and to effects such as chain-length dependent termination (see below), but it also has an in-built 'consistency check'. It was clear from figure 1-5 that the dead polymer chain-length distribution contains more than one peak. These additional peaks appear at chain lengths that are multiples of $k_p M t_0$. These peaks can be used for two purposes. Firstly, the appearance of an additional peak in the dead polymer MWD confirms that PIP conditions have been established.[8] Secondly, these peaks can be used to check the value of k_p extracted from the first peak, i.e., the critical chain length that corresponds to $2k_p M t_0$ can be extracted from the low molecular weight point of inflection of the second peak, and this chain length also used to calculate k_p.

In addition to the check built into a single experiment, multiple experiments can be per-

formed where one or several experimental parameters are changed. For example, frequently a series of experiments are performed where the concentration of radicals added by an initiation burst is varied. This can be done by changing the initiator concentration or laser intensity. This change should not affect the position of the inflection point[1], but it should alter the relative peak intensity. Thus if one performs these experiments and the value of k_p changes significantly then little confidence should be placed in the value of k_p obtained.

This having been said, one of the best ways to establish the reliability of any rate constant is by computer-based simulation. By comparing simulated and experimental data, frequently MWDs, conclusions can be drawn about the rate coefficient that has been extracted and the kinetic model used (see below).

Other data that can be extracted from the Pulse Initiated Method Although the strength of the PIP method is its ability to provide accurate values of the rate coefficient for propagation, techniques have been developed to extract other kinetic information from pulse initiated polymerization.

Rate Coefficient for Termination The rate coefficient for termination affects both the kinetics and MWD of a free-radical polymerization. Many workers in this field have realized this and attempted to extend understanding of termination as well as measure values of $<k_t>$. However, methods designed to measure this parameter have encountered many difficulties. Foremost amongst these is the fact that k_t is not really a constant at all, but varies with the chain length of the two radicals involved in the termination process. An indication of the difficulties in accurately measuring $<k_t>$ can be found in the *Polymer Handbook*.[4] Here the values of $<k_t>$ for methyl methacrylate and styrene at 25°C are spread over one and a half orders of magnitude.

To rectify this, several authors have developed methods for extracting the rate coefficient from laser polymerized material. The first two methods were developed by Olaj et. al.[38][39] These methods use the number and weight average molecular weights respectively, in combination with several other rate parameters to evaluate $<k_t>$. However, it is well known that the

[1] A small effect may be seen as a result of the peak maximum becoming a more appropriate measure of the critical chain-length.

values of these molecular weight averages are susceptible to effects such as the occurrence of transfer and the failure of SEC to pick up the large numbers of low molecular weight chains. Thus the value of $<k_t>$ extracted by these methods is also sensitive to these effects. Another method for extracting $<k_t>$ has been developed by Buback and Lämmel.[11] This is based upon a comparison of the area under the dead polymer MWD between the first and second, and the second and third points of inflection. Taking the ratio of these areas allows the value of $<k_t>$ to be extracted. One of the advantages of this method is that it ignores the regions of the MWD where the signal to noise ratio is high, i.e., the low and high molecular weight regions. Another method also used by Buback et. al.[9] involves a single pulse experiment. In these experiments a polymerization is initiated by a single laser pulse and the decay in the total radical concentration is measured indirectly by time-resolved vibrational spectroscopy.

Computer based simulation of PIP MWDs can be used extract a value of $<k_t>$. The shape of a PIP MWD is influenced by the dimensionless constant $<k_t>\rho t_0$ (see [37] and chapter 6). Thus the value of this constant can be obtained by fitting theory to experiment. If the values of t_0 and ρ can be obtained independently, then $<k_t>$ can be evaluated. Of course obtaining the value of t_0 is trivial; the difficult part of this procedure is obtaining an accurate value of ρ. However, several methods can be used to do this including a method developed by Moad et. al.[32]

Rate Constant for Transfer Several research groups have used the PIP method to determine transfer rate coefficients. Hutchinson and co-workers[26] determined the transfer coefficients for transfer to n–dodecyl mercaptan in methyl methacrylate, styrene, and ethyl methacrylate at a temperature range of $20 - 80°C$. By adding sufficient transfer agent, they were able to produce transfer-dominated conditions. Buback and co-workers[10] designed a method to determine the value of k_p and C_M ($k_{tr,M}/k_p$) from one PIP experiment. Buback et. al. noted that application of packages of high frequency pulses that were separated by long dark time intervals should give rise to distinct regions in the dead polymer MWD. The packages of high frequency laser pulses should create typical PIP conditions which allow the determination of k_p, while the long interval should produce transfer-dominated conditions from which C_M can be extracted. In this study, the PREDICI simulation package was used to model results.

1.3 Computer-Based Simulation

1.3.1 Introduction

Numerical simulation has always had an important role to play in the development of an understanding of free-radical polymerization. Although the simulation methods used have changed as the power and availability of computing resources have increased, many of the underlying principles remain the same. The concept of using a mathematical model to describe the processes that take place during a polymerization and of manipulating that model to make predictions, and extract kinetic information are as relevant today as they were fifty years ago. This being said, the computer based modelling that can now be routinely performed on a desktop computer is many orders of magnitude more sophisticated than that which was possible half a century ago. The days when a dead polymer MWD could only be described in terms of a handful of moments have passed. It is now possible to solve the differential equations that describe simple polymerization systems in a modest length of time. Moreover, it is no longer necessary to linearize data before extracting kinetic information. The advent of computer based non-linear least squares analysis has meant that complex kinetic relationships can now be fitted to experimental data, for example consider the analysis of copolymerization kinetics.

1.3.2 The Benefits of Computer-Based Simulation

The benefits that computer based modelling have brought to the understanding of free-radical polymerization are many. Firstly, it is only through modeling, in the broadest sense of the word, that we are able to deconvolute the various rate parameters that affect experimental observables. For example, a common measurement performed on polymerization systems is the rate of monomer consumption. However, the rate of monomer consumption alone provides little information. This value is system dependent and influenced by a number of reactions, i.e., the macroscopic observable of rate of monomer consumption of itself provides little direct information about the microscopic rates of the system. Nonetheless, in section 1.2.3 we saw that by developing a model of the kinetics of these systems it is possible to extract the ratio $k_p^2/<k_t>$. Thus the modeling of kinetic systems suggests ways of analyzing experimental data so that kinetic parameters can extracted.

Moreover, there are many situations where the kinetics are so complicated that the only way that rate parameters can be extracted is by directly simulating experimental data. For example, by fitting a simulation to an entire experimental MWD.

Secondly, the simulation of free-radical polymerization allows kinetic models, i.e., combinations of reaction mechanisms and rate coefficients, to be tested. For example, suppose we extracted the rate coefficients for propagation and termination from a continuously-initiated polymerization. One of the ways that we can test these values is to run a computer based simulation and attempt to reproduce the experimental data. From this comparison, conclusions could be drawn about the quality of these rate parameters. In addition to this, a comparison of simulated and experimental results allows decisions to be made about which reactions are important in a particular system. For example, suppose we wish to test whether chain transfer is important during the polymerization of a certain monomer. By proposing two models, one with and one without the chain transfer reaction and comparing the predictions of those models with experiment, we might be able to decide if chain transfer is important. This procedure can also be used to examine the impact of kinetic or experimental effects, such as chain-length dependence or chromatographic broadening.

Lastly, numerical simulation means that the sensitivity of experimental data to a method of analysis can be explored. It is all too easy to analyze experimental data for a rate parameter without knowing how sensitive the data and/or method of analysis are to the value of that parameter. Performing simulations with a wide range of parameter values allows conclusions to be made about the error in the parameter. For example, the analysis of two sets of experimental data may yield rate parameters that appear to be significantly different in value. However, little can be said about the chemical meaning of such a difference until information about the sensitivity of the data to the method of analysis has been obtained.

1.3.3 What is Required of a Good Simulation Strategy?

Having established that simulations help us to develop an understanding of free-radical polymerization, how should we decide what properties a good simulation strategy should have? In what follows a number of criteria will be established. A good simulation strategy should fulfill them all.

Ease of use

A simulation strategy is of little use if it can not be easily used. Ideally a simulation strategy should be able to be used by those not versed in high-level mathematics. It should be part of the suite of software routinely used by a polymer chemist, alongside, for example, software used for GPC analysis.

Consistency

A simulation strategy should work for a range of different conditions. To be of any use, such a strategy must work under all of the normal polymerization conditions. Moreover, it should not be significantly more prone to error under certain conditions than others. For example, suppose a study was performed where the rate coefficient for transfer was systematically varied in order to explore the effects of chain transfer upon the dead chain MWD. If the solution strategy used incurred a lot more error when the rate of transfer was high, then this could cause the wrong conclusions to be drawn about the effects of chain transfer. Hence, a good solution strategy should work consistently for a wide range of polymerization conditions.

Applicability to Novel Situations

A good modelling strategy should be able to be applied to a new variant of free-radical polymerization without having to be reanalyzed. For example, suppose, as we will in chapter six, that we want to separate dead polymer chains based on the number of initiator-derived end-groups they contain. Furthermore, suppose that the simulation strategy to be used had never been used to solve differential equations of this type before. Ideally a good simulation strategy should be able to be used to model this system without the need for reanalysis, that is, without a study having to be performed where the numerical error incurred in solving those differential equations is measured.

Transparency

A simulation strategy should be easily understood. Its workings should be easy to understand and inspect. Using a transparent solution strategy makes it is less likely that mistakes will be made as a result of that method being used inappropriately. For example, if a simulation

strategy is poorly understood and its inner workings are not easily probed, then it is more likely that it will be used in an inappropriate situation or manner. Thus it is more likely that it will produce nonsensical results.

Efficiency

The last criteria is the most important. The efficiency of a solution strategy is defined as the amount of computational effort that must be spent to produce a solution of a certain accuracy (see chapter three for an elaboration of this definition). If little computational effort must be spent to produce a solution of high accuracy then a solution strategy is said to be efficient. Efficient solution strategies give the best possible results in the shortest time.

1.3.4 The Simulation of Pulse Initiated Polymerization

To date we have talked in general terms about the simulation of free-radical polymerization. However, the main concern of this work is the simulation of intermittently-initiated free-radical polymerization. This simulation involves obtaining the solution of differential equations 1.18 – 1.25 for the initiation profile shown in figure 1-1.

The simulation of this type of polymerization is significantly more difficult than that of continuously-initiated polymerization. The main reason for this is that an intermittently-initiated polymerization does not reach a steady state, hence the steady-state assumption can not be made. Moreover, the periodic initiation that is central to PIP changes the structure of the solution to differential equations 1.18 – 1.25, making it more difficult to acquire a numeric solution. In section 1.2.2, we saw that transients in the solution to a system of differential equations makes them more difficult to solve, i.e., this is the problem of stiffness. The solution to the differential equations for PIP contains more transients than a continuously-initiated free radical polymerization. The waves in the radical chain-length distribution (see figure 1-3) are transients in the total radical concentration (see figure 1-2). Thus intermittently initiating a free-radical polymerization stiffens the differential equations that model it. Furthermore, the structure of these differential equations is such that even differential equation solvers that are normally suited to stiff systems perform poorly (see chapter four for a detailed explanation of this). For these reasons this thesis concentrates on PIP simulations. Because they provide a

stringent test of simulation methods, there is every reason to believe that the conclusions are general, and hold for simulation of all free-radical polymerizations.

In this thesis a wide range of different numerical and analytic techniques will be used to model PIP. These techniques will be used to model differential equations 1.18 – 1.25 with a periodic initiation profile. By analyzing the error in the solution and the time taken to obtain it, conclusions will be drawn about that solution strategy as a method for simulating PIP. Furthermore, several novel simulation strategies will be developed that are especially suited to modelling PIP.

PIP Simulation Strategies in the Literature

Many different methods have been used to model PIP. These include a wide range of different approaches to this problem. However, to date there has not been a systematic evaluation of these methods; here such an analysis will be performed. Several of these methods will be examined in this thesis.

The first type of approach solves the differential equations numerically via solution methods suited to stiff systems. Unfortunately such studies were forced either to use unphysically small values of the truncation chain length, L or perform calculations that took large amounts of CPU time on very fast computers. Moad et. al.[16] used a NAG library routine (utilizing an implicit method) to solve a system of 160 differential equations. Even this very limited system took 16 minutes on a Cray YMP-2 computer. A conservative estimate of the CPU time needed to extend this calculation is the number of additional species to the power of three, so the time required to model a modest system of differential equations is huge. In a more recent study[30], the Gear Algorithm was used to solve a system 2000 differential equations for a period of twenty laser pulses (2.0 seconds). This calculation took 26 hours on a Silicon Graphics Challenge XL supercomputer. Finally, Hutchinson et. al.[26] have used the implicit Runge-Kutta method (the DASSL package) to explore the effects of chain transfer upon PIP MWDs. Several numerical methods of this type have been applied in this thesis.

A number of authors have used the Monte Carlo Algorithm to model PIP. One approach[29][22] is based on the Master equation[21] and includes explicitly all possible chemical reactions. Another approach[36] uses a hybrid approximating variant of the Monte Carlo algorithm. Both of

these methods required many hours of computer time. The Monte Carlo algorithm has been applied and extended in this thesis.

Another method that has been used to simulate PIP is known as the discrete Galerkin h-p-method.[55] This method has been used in the form of the software package PREDICI to study PIP (for example [7][12]). The discrete Galerkin h-p- method has not been studied in this thesis. However, while this method has been successfully used by several groups of workers it does not excel in all of the criteria outlined above: for example, this method is not easily understood by non-mathematicians. This means that the person running the calculation will normally have very little idea of the way the solution is being obtained. Hence, this person will normally have very little idea of when and when not to place confidence in the output of the program. However, this is not to suggest that a far less successful, but more easily understood method should always be used in place of such a method, just that methods that are treated as 'black boxes' by those that operate them should be treated with care. It was hoped that a computer program could be written that implemented the discrete h-p- Galerkin method, so that this method could be compared with those described this thesis. Unfortunately, time constraints meant that this could not be completed. There exists the possibility for this work to be undertaken in the future.

Analytic solution strategies have also been used to simulated PIP. In their original paper Olaj et. al.[37] developed an analytic treatment of PIP that they have extended in a large number of publications, for example[57][58]. This has lead to the development of an iterative treatment for simulation of PIP[40][41], as well as extending their original method to include chain transfer.[57][58] The formalism of Aleksandrov et. al.[1] has also been used to simulate PIP.[47] Another analytic method involves the use of generating functions to integrate differential equations 1.18 – 1.25. The first publication using this method dealt with only a single pulse[31], but different workers have extended this to multiple pulses.[17] The analytic solution strategy developed by Olaj et. al., Aleksandrov et. al. and a novel analytic solution have been used in this thesis.

1.3.5 Thesis Outline

This thesis is divided into seven chapters. In **chapter two**, three analytic solutions to the differential equations for PIP will be implemented and assessed, these being a novel solution obtained by the author of this thesis; Olaj et. al.'s solution[37]; and the solution obtained by Aleksandrov et. al.[1] The next three chapters focus on numerical solution techniques, and in particular on finite-difference based solution strategies. In chapter three the methodology for assessing these strategies is developed and tested on the Euler method (the simplest finite-difference based solution method). In **chapter four**, a suite of different numerical techniques are applied and assessed using the methodology of the previous chapter. In **chapter five**, an understanding of the numerical solution of the differential equations for dead polymer chains is developed. The next chapter, **chapter six**, contains two case studies, where the methods developed in the previous chapters are used to simulate real-world polymerization. Finally, the last chapter, **chapter seven**, contains a set of conclusions and recommendations.

Chapter 2

Analytic Solution Techniques

2.1 Introduction

In this chapter, three methods of simulating pulse-initiated polymerization (PIP) will be described. Each method is based upon an analytic solution of the population-balance differential equations that characterize this type of polymerization. Two of these analytic solutions have been taken from the literature[1][37], while the third (see section 1.2) has been developed by the author of this thesis. Here a study is performed of how well these solutions are suited to the task of simulating PIP. That is, we will try to answer the following questions: Are these solutions computationally efficient?; How much error, if any, do these solutions introduce into the kinetics and/or final MWD?; Are these solutions flexible to changes, or additions, to the reaction scheme for free-radical polymerization?; And can these solutions be used as the heart of a method for routinely simulating PIP? To answer these questions, each solution will be used to model a simple PIP system (see below). The times taken to perform these calculations, as well as the MWDs produced, will then be compared and the applicability of these solutions discussed.

Analytic solutions to differential equations are symbolic mathematical solutions. They are solutions obtained through the direct mathematical manipulation of those equations. Although many methods have been developed to analytically solve differential equations, the solutions presented in this chapter have been obtained using only two. The first is direct integration, for an example see section 1.2. The second approach involves the judicious use of dimensionless

constants as the basis for building up a solution. The formalism developed in section 2.3 illustrates this type of approach.

Analytic solutions are exact solutions to differential equations for a particular kinetic system (this is in contrast to numerical solutions which are inexact). Although these solutions do not contain numerical error, frequently error-introducing assumptions are made to reduce the complexity of both their derivation and final form. The steady-state approximation is an example of this type of assumption. All of the expressions outlined in this chapter involve the use such an assumption: the pseudo-steady-state assumption. This means that they are exact solutions for a PIP in a pseudo-steady-state.

A PIP is said to have reached a pseudo-steady-state if the total radical concentration repeats the same time profile every t_0 seconds (for an example of this repeating pattern see figure 1-2). Thus, by making the pseudo-steady-state assumption we assume that a polymerization has a total radical concentration that is changing in this way. This assumption ignores both the period of time before this profile is established, as well as effects that alter the total radical concentration profile to remove it from the pseudo-steady-state. As the length of the pre-pseudo-steady-state is normally far shorter than the length of the pseudo-steady-state (approximately 5 as compared with 100s of initiation periods), ignoring this phase of the polymerization will normally incur little error. Moreover, ignoring effects such as initiator consumption that could remove a system from the pseudo-steady-state are justified on the basis of experimental evidence.[12]

To illustrate the simplifying effects of this type of assumption, a simple differential equation has been solved with and without it. Although this differential equation, and the simplifying assumption used, are not identical to those involved in the modelling of PIP, they do illustrate the effects that well chosen assumptions can have on the analytic derivation of the solution of differential equations. The model differential equation examined, equation 2.1, is a simple first-order differential equation.

$$\frac{dy}{dt} = 1 - 2y \tag{2.1}$$

In this expression, $\frac{dy}{dt}$ is the rate of change in y with time t. To solve this equation without a simplifying assumption, one uses mathematical manipulations to transform it into what is

known as its characteristic form, i.e.,

$$\frac{dy}{dt} + 2y - 1 = 0 \tag{2.2}$$

This expression can then be integrated to yield

$$y(t) = \frac{1}{2} + ae^{-2t} \tag{2.3}$$

Equation 2.3 is the solution to equation 2.1, as such it describes the value of y at time t. In this expression a is a constant of integration. To use equation 2.3 to predict the value of y at a certain t, the value of a must be calculated; this is done using an initial condition. An initial condition is the value of the solution at $t = 0$. For example, suppose that we know that $y = 1$ when $t = 0$. This means that

$$a = \frac{1}{2} \tag{2.4}$$

and thus,

$$y(t) = \frac{1}{2}(1 + e^{-2t}) \tag{2.5}$$

Equation 2.5 is the exact solution to equation 2.1, i.e., a solution such that $y = 1$ when $t = 0$.

Now equation 2.1 will be solved making use of a simplifying assumption. Suppose that we are only interested in the time invariant solution to equation 2.1, i.e., the value of y that does not depend on time. To obtain this solution we can either use equation 2.5 or we can make the steady-state assumption, i.e., assume that

$$\frac{dy}{dt} = 0 \tag{2.6}$$

Hence, from equation 2.1,

$$1 - 2y = 0 \tag{2.7}$$

or

$$y = \frac{1}{2} \tag{2.8}$$

It is clear that the complexity of this solution and its derivation are reduced by making assump-

tion 2.6. Figure 2-1 contains a plot of equations 2.3 and 2.8 as a function of time. It follows from this figure that the two solutions are in close agreement for all but the first 3 seconds, the non-steady-state period. Nonetheless, as we are only interested in the steady-state solution this is of little concern. This analysis has shown that the use of an appropriate assumption, such as

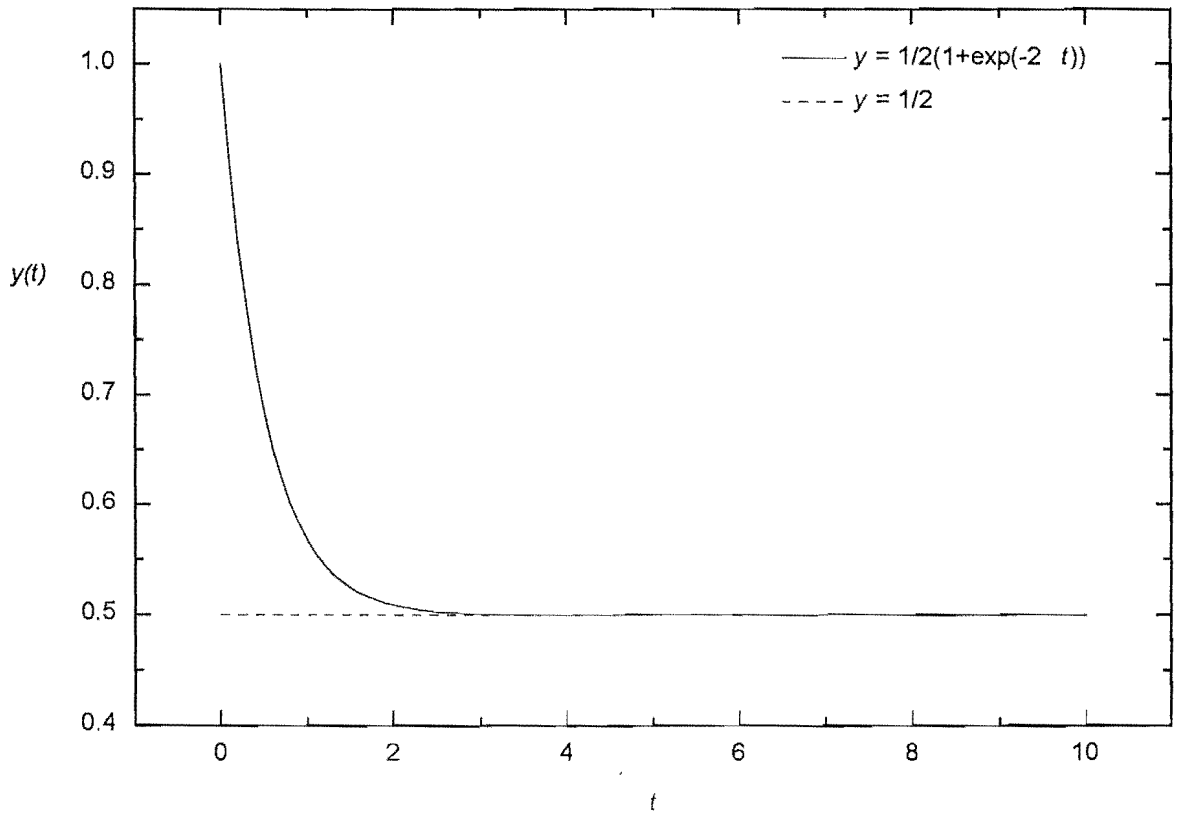

Figure 2-1: A comparison of the analytic solution to equation 2.1 obtained with, and without the steady-state assumption.

the steady state, or pseudo-steady state assumption, can make differential equations easier to solve. In fact, there are many cases when an analytic solution can only be obtained when this type of assumption is made. The pseudo-steady state has been made during the development of all of the methods studied in this chapter. Each solution is the analytic solution to the

Rate Parameter	Value	Units
k_p	100	L.mol.s^{-1}
M	10	mol.L^{-1}
k_t	1×10^{7}	L.mol.s^{-1}
ρ	1×10^{-6}	mol.L^{-1}
Freq. of Initiation	10	Hz
t_{sim}	2	s
λ	1	–

Table 2.1: Default rate parameters used in all calculations in chapter two.

population-balance differential equation for a PIP in the pseudo-steady state where different additional assumption have been made in the derivation of each solution.

2.1.1 Model System

To test the analytic solutions presented in this chapter, each solution was used to model the kinetics and MWD for a simple PIP system. This model system is a simplified version of the reaction scheme, and therefore the differential equations, outlined in chapter one – it does not include chain transfer or allow any of the rate coefficients to be chain-length dependent. Also no closure, or truncation, assumption has been made to obviate the difficulty of dealing with an infinite number of differential equations. This is because it is possible to generate the analytic solution to an infinite number of differential equations.

In addition to using the same set of differential equations throughout this chapter, the same set of rate parameters will also be used. These are shown in table 2.1. In this table, all symbols have their normal definitions and $\lambda = k_{td} \,/\, (k_{td} + k_{tc})$, t_{sim} is the length of the simulation and 'Freq of Initiation' is, as its name suggests, the frequency of periodic initiation.

This chapter is divided into four further sections. In the following three sections, the three analytic solutions are derived and preliminary results are presented. In the final section the computer time required, and solution results are compared.

2.2 The Method of Integrating Factors

The first analytic solution makes use of the method integrating factors (MOIF) (see below) and has been derived by the author of this thesis.

The derivation of an expression for the chain-length distribution for dead polymer chains begins with the population-balance differential equations for living radical species. Each of these differential equations (except for $\frac{dR_0}{dt}$) is transformed into its characteristic form, i.e., $\frac{dy}{dt} + ay + b = 0$, where a and b are constants, by the method of integrating factors. These differential equations are then integrated in the same manner as equation 2.2 was integrated. The solution that is obtained contains a constant of integration that must be evaluated before the expression can be used. To evaluate the constant of integration we use the initial conditions (see below). This yields an expression for the concentration of living radicals of chain length i at time t. This process is repeated for several values of i until a general solution becomes obvious. This general solution is then substituted into the differential equations for the dead polymer chains (equations 1.22 to 1.25) and attempts are made to solve this expression.

An inspection of the differential equations for the living radical species (equations 1.18 to 1.21) shows that rate of change in the concentration of a radical of chain length i depends upon the concentration of radicals of chain length $i-1$ for all radical chain lengths except primary radicals. This means that an expression for the concentration of radicals of chain length $i-1$ must be found before the differential equation for radicals of chain length i can be solved. To overcome this problem we begin by solving the differential equation for primary radicals. The solution of this differential equation is then used to solve the differential equation for radicals containing one monomer unit. Hence, we move up the radical chain-length distribution solving the differential equations in numerical order.

Expressions for the concentration of two further species must be known before beginning this derivation. These are the concentration of monomer and the total concentration of radical species, R, where R is defined as

$$\mathrm{R} = \sum_{i=0}^{\infty} \mathrm{R}_i \tag{2.9}$$

The concentration of monomer is assumed to be equal to its initial concentration. This is a reasonable assumption as PIPs are normally only performed to low conversion ($\approx 1\%$). On the other hand, an expression has to be derived for the total concentration of radicals. The derivation of this expression is given in section 2.2.1 below.

One final comment must be made on this derivation. It concerns the initial conditions. In

the solution of equation 2.1 we saw that it is necessary to solve for the constant of integration using the initial conditions. The initial conditions used in the solution to equations 1.18 to 1.21 are the concentrations of radicals of chain length i just after the arrival of a burst of initiation, i.e., at the start of an initiation period. For example, the initial conditions used to evaluate the constant of integration for primary radicals, R_0^{last}, is equal to

$$R_0^{last} = (R_0)_{t=t_0} + \rho \tag{2.10}$$

In this expression, $(R_0)_{t=t_0}$ is the concentration of primary radicals just before the arrival of the periodic initiation and ρ is the concentration of radicals added by a burst of initiation. However, one does not know the value of $(R_0)_{t=t_0}$ until one has solved for the constant of integration. To avoid this problem the values of R_i^{last}, i.e., the initial conditions, are, as yet, not given explicit values in this derivation.

2.2.1 An Analytic Expression for the Total Radical Population

There exists an analytic expression that describes the way that the total radical concentration of living radicals changes with the time between successive bursts of initiation in the pseudo-steady state. Although the derivation of this expression is well known, it is given here as it serves as an introduction to the general approach used in the following novel derivation.

The derivation of an expression for the total radical concentration begins with the differential equation that describes the rate of change in total radical concentration (equation 2.11). In the absence of a continuous initiation process, such as thermal initiation, this differential equation contains a single term, that for the removal of radicals by bimolecular termination. To solve this equation, we use a standard integration technique.

$$\frac{d\,R}{dt} = -2k_t R^2 \tag{2.11}$$

$$\int_{t=0}^{t=t_0} \frac{d\,R}{R^2} = -\int_{t=0}^{t=t_0} 2k_t\, dt \tag{2.12}$$

Integrating, where a is the constant of integration.

$$\frac{1}{\mathrm{R}} + a = 2k_t t \tag{2.13}$$

Here $\mathrm{R} = \mathrm{R}_{max}$ when $t = 0$, therefore

$$a = \frac{-1}{\mathrm{R}_{max}} \tag{2.14}$$

so that,

$$\mathrm{R}_t = \frac{\mathrm{R}_{max}}{2k_t t\mathrm{R}_{max} + 1} \tag{2.15}$$

The symbols in equation 2.15 are defined as:

- R_t is the total radical concentration at time t (mol.L^{-1});
- R_{max} is the maximum radical concentration, i.e., the radical concentration at $t = 0$ (mol.L^{-1});
- k_t is the rate constant for termination (L.mol^{-1}.s^{-1});
- t is the time since the last laser pulse (s).

The maximum total concentration of radicals, $\mathrm{R}_{\mathrm{max}}$, is dependent on the concentration of radicals added by a burst of initiation, the rate coefficient for termination and the time between bursts of initiation (see equation 1.44).

2.2.2 An Analytic Expression for the Living Radical Chain-Length Distribution

Now that we have an expression for the total concentration of radicals, we can begin solving the differential equations for R_i. For the reasons mentioned above this has to begin with the differential equation for primary radicals.

The Solution of The Differential Equation for Primary Radicals

To solve $\frac{d\mathrm{R}_0}{dt}$ the technique that was used to solve the differential equation for the total radical concentration is used. The differential equation for primary radicals is rearranged and equation

2.15 is substituted into it.

$$\int \frac{d\,\mathrm{R_0}}{\mathrm{R_0}} = -\int (k_\mathrm{p}\mathrm{M} + 2k_\mathrm{t}(\frac{\mathrm{R}_{max}}{2k_\mathrm{t}t\mathrm{R}_{max}+1})dt \tag{2.16}$$

Integrating, where a is the constant of integration,

$$\ln \mathrm{R_0} = -k_\mathrm{p}\mathrm{M}t - \ln(2k_\mathrm{t}t\mathrm{R}_{max}+1) + a \tag{2.17}$$

To obtain a value of a we use the initial conditions. These say that the concentration of $\mathrm{R_0}$ just after the arrival of the last burst of initiation must be equal to R_0^{last}. Hence,

$$a = \ln \mathrm{R}_0^{last} \tag{2.18}$$

Thus, the expression for the concentration of primary radicals in an intermittently initiated free-radical polymerization is

$$\mathrm{R_0} = \frac{\mathrm{R}_0^{last}}{(2k_\mathrm{t}t\mathrm{R}_{max}+1)} \exp(-k_\mathrm{p}\mathrm{M}t) \tag{2.19}$$

Equation 2.19 predicts all of the features of the time dependence of the concentration of primary radicals in a PIP. These are:

- A decrease in radical concentration due to propagation;
- The loss of radicals because of bimolecular termination;
- The dependence of the radical concentration on the initial concentration of radicals;
- The periodicity in the concentration of the same frequency as the periodicity of the initiation profile. Although this is not clear from the form of equation 2.19, it appears because of the periodicity of the initial conditions.

2.2.3 The Solution of the Differential Equation for Radicals Containing One Monomer Unit

The next differential equation that will be solved is that for radicals containing one monomer unit. This equation can be solved because an expression has been derived for the temporal dependence of the concentration of primary radicals. This is done by substituting both equations 2.15 and 2.19 into the differential equation for radicals of chain length one.

$$\frac{d\,\mathrm{R_1}}{dt} = k_\mathrm{p}\mathrm{M}\left(\frac{\mathrm{R}_0^{last}}{(2k_\mathrm{t}t\mathrm{R}_{max}+1)}\exp(-k_\mathrm{p}\mathrm{M}t)\right) - k_\mathrm{p}\mathrm{M}\mathrm{R_1} + \frac{2k_\mathrm{t}\mathrm{R_1}\mathrm{R}_{max}}{2k_\mathrm{t}t\mathrm{R}_{max}+1} \tag{2.20}$$

This expression is then rearranged to give equation 2.21.

$$\frac{d\,\mathrm{R_1}}{dt} + \left(k_\mathrm{p}\mathrm{M} + 2k_\mathrm{t}\left(\frac{\mathrm{R}_{max}}{2k_\mathrm{t}t\mathrm{R}_{max}+1}\right)\right)\mathrm{R_1} = \frac{k_\mathrm{p}\mathrm{M}\mathrm{R}_0^{last}}{(2k_\mathrm{t}t\mathrm{R}_{max}+1)}\exp(-k_\mathrm{p}\mathrm{M}t) \tag{2.21}$$

To transform equation 2.21 into its characteristic form we use the method of integrating factors. The method of integrating factors transforms a differential equation to its characteristic form by multiplying it by an integrating factor. For example, a differential equation of the form of equation 2.22

$$\frac{dy}{dt} + A(t)y = B(t) \tag{2.22}$$

is transformed into 2.24 by multiplying it by a factor η. Here η is defined as

$$\eta = \exp\left(\int A(t)dt\right) \tag{2.23}$$

The resulting differential equation is

$$\frac{d\,(\eta y)}{dt} = \eta B(t) \tag{2.24}$$

Equation 2.24 can be solved in the same way that equations 2.1 and 2.11 were solved. So that the final solution to equation 2.22 is

$$y = \frac{1}{\eta}\left[\int \eta B(t)dt + a\right] \tag{2.25}$$

Applying this method to equation 2.21, we use an integrating factor

$$\eta = \exp\left(\int\left(k_{\mathrm{p}}\mathrm{M} + \frac{2k_{\mathrm{t}}\mathrm{R}_{max}}{2k_{\mathrm{t}}t\mathrm{R}_{max}+1}\right)dt\right) \tag{2.26}$$

$$= \exp\left(k_{\mathrm{p}}\mathrm{M}t + \ln(2k_{\mathrm{t}}t\mathrm{R}_{max}+1)\right) \tag{2.27}$$

This integrating factor can then be used to transform equation 2.21 to equation 2.28.

$$\frac{d\left(\eta\mathrm{R}_1\right)}{dt} = k_{\mathrm{p}}\mathrm{M}\mathrm{R}_0^{last} \tag{2.28}$$

Equation 2.28 is then integrated, producing equation 2.29.

$$\eta\mathrm{R}_1 = k_{\mathrm{p}}\mathrm{M}\mathrm{R}_0^{last}t + a \tag{2.29}$$

Therefore,

$$\mathrm{R}_1 = \frac{k_{\mathrm{p}}\mathrm{M}\mathrm{R}_0^{last}t + a}{2k_{\mathrm{t}}t\mathrm{R}_{max}+1}\exp(-k_{\mathrm{p}}\mathrm{M}t) \tag{2.30}$$

This expression contains a constant of integration a that has to be evaluated. This is done by solving it using the initial conditions (equation 2.31)

$$\mathrm{R}_1 = \mathrm{R}_1^{last} \qquad \text{when } t = 0 \tag{2.31}$$

Thus,

$$a = \mathrm{R}_1^{last} \tag{2.32}$$

Therefore the final solution is

$$\mathrm{R}_1 = \frac{k_{\mathrm{p}}\mathrm{M}\mathrm{R}_0^{last}t + \mathrm{R}_1^{last}}{2k_t t\mathrm{R}_{max}+1}\exp(-k_{\mathrm{p}}\mathrm{M}t) \tag{2.33}$$

Now that a solution has been obtained for radicals of chain length one, the same procedure is used to generate the solution to the differential equation for radicals of chain length two. This in turn allows us to solve the differential equation for radicals of chain length three. Hence, we can continue to generate the solutions to differential equations for radicals of greater and greater chain length. Fortunately this must only be done for radicals up to chain length four,

because the form of the general solution becomes clear at this stage. The general solution to the differential equations for radicals of chain length i is

$$\mathrm{R}_i = \frac{\exp(-k_\mathrm{p}\mathrm{M}t)}{2k_\mathrm{t}t\mathrm{R}_{max}+1}\sum_{j=0}^{i}\mathrm{R}_j^{last}\frac{(k_\mathrm{p}\mathrm{M}t)^{i-j}}{(i-j)!} \tag{2.34}$$

It should be noted that equation 2.34 is general and assumption free solution to the radical chain-length distribution (it is the implementation, not the derivation of this expression that involves the pseudo-steady-state assumption). It will become clear when we address the two other analytic solutions that this is the only analytic solution about which this can be said. The other analytic solutions are not general or assumption free.

An appraisal of the single pulse limit of this expression, i.e., $\mathrm{R}_j^{last} = 0$ for $j \geq 1$, reveals that this expression is intuitively correct. In the limit when only a single laser pulse is applied to the polymerization system equation 2.34 reduces to equation 2.35, the correct expression for the radical chain-length distribution in the single pulse limit is:

$$\mathrm{R}_i = \frac{\exp(-k_\mathrm{p}\mathrm{M}t)}{2k_\mathrm{t}t\mathrm{R}_{max}+1}\mathrm{R}_{\mathrm{max}}\frac{(k_\mathrm{p}\mathrm{M}t)^{i}}{i!} \tag{2.35}$$

Equation 2.35 is "intuitively" correct because it takes the form of an a Poisson distribution attenuated by termination. i.e., a Poisson distribution multiplied by equation 2.15. Note that again $\mathrm{R}_{\mathrm{max}}$ is defined by equation 1.42.

Again, this expression predicts all of the features that are expected of the living radical chain-length distribution. It predicts that the radical chain-length distribution should be

- A Poisson distribution with a most probable chain length of $k_\mathrm{p}\mathrm{M}t$;
- That the concentration of all radicals should decrease because of bimolecular termination (the denominator of the pre-summation term);
- That the most probable chain length (MPCL) increases as time passes (because $k_\mathrm{p}\mathrm{M}t$ increases as time passes).

The only feature of the radical chain-length distribution predicted by equation 2.34 that can not be inferred from its general form is the periodicity of the solution. A PIP radical

chain-length distribution contains a series of equally spaced Poisson distributions, however, equation 2.34 appears to predict just a single Poisson distribution. Nonetheless, this equation does predict a periodic radical chain-length distribution if the right initial conditions are used, i.e., the right set of R_j^{last} values.

It was noted above that the initial conditions can not be defined explicitly. This is because a expression for R_i is required before the initial value of R_i can be calculated.

To calculate the initial conditions for equation 2.34, we begin with radicals that have survived one initiation period. Using equation 2.34 we predict the radical chain-length distribution for radicals that have survived one initiation period. This calculation is possible because the initial conditions for this calculation are known. These are: $R_0^{last} = \rho$ and $R_i^{last} = 0$ for $i \geq 1$.

The results of this calculation are then used as the initial conditions for a calculation to predict the chain-length distribution for radicals that have lived two initiation periods. Equation 2.34 and these initial conditions are then used to predict the radical chain-length distribution for radicals that have lived three initiation periods. Hence this means that the radical chain-length distribution for species that have survived four initiation periods can be predicted. This calculation is carried out for enough initiation periods to well and truly cover the whole radical chain-length distribution, typically seven initiation periods. Each of the seven radical chain-length distributions are then summed (including that for radicals initiated by the last laser pulse, which contributes $R_0^{last} = \rho$ and $R_i^{last} = 0$ for $i \geq 1$) to give the required initial conditions.

This calculation is based on the idea that it is possible to treat a single radical wave separately from the rest of the chain-length distribution. That is, a single radical wave can be modeled, if the total radical concentration is treated correctly (equation 2.15), without having to worry about the other radical waves. Note that this assumption will only be true when the rate coefficient for termination is chain-length independent and subsequent radical waves are well separated (see chapter six for an example of when this is not the case).

Note that the initial conditions must be generated in this manner, rather than just using equation 2.34 and the initial conditions $R_0^{last} = \rho$ and $R_i^{last} = 0$ for $i \geq 1$ to generate the radical chain-length distribution after periodic time intervals. This calculation would not give the correct initial conditions because it implies that the rate of termination decreases continuously with time, rather than increasing every t_0 seconds. However, this calculation would give the

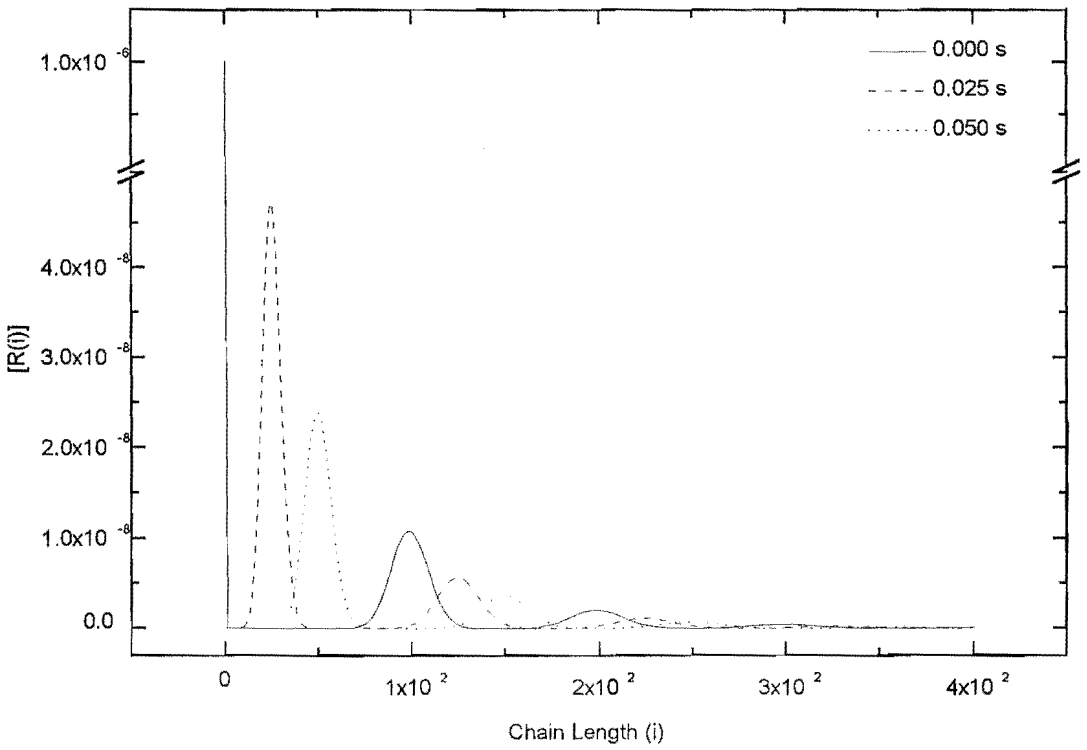

Figure 2-2: The time evolution of the living radical chain-length distribution. The times shown in this figure correspond to the length of time since the last burst of initiation.

correct result for a single pulse experiment.

Having calculated the initial conditions, equation 2.34 can be used to predict the living radical chain-length distribution at any time between two bursts of initiation. Figure 2-2 contains three sample calculations where equation 2.34 has been used to predict the living radical chain-length distribution at 0.000, 0.025, and 0.050 seconds after a burst of initiation.

2.2.4 An Analytic Expression for the Dead Polymer Chain-length Distribution

Although this expression for the living radical chain length is useful (extensive use is made of it in chapters three and four), an expression for the dead polymer chain-length distribution would be more useful as it can be used to make predictions that can easily be compared with experiment. To calculate the dead polymer chain length distribution the expressions for the living radical chain-length distribution are substituted into the differential equations for dead polymer chains (equation 1.24). The total radical concentration is then replaced by the analytic expression for the total radical concentration (equation 2.15). This yields equation 2.36.

$$(\mathrm{D}_i)_t = \int_0^t \left(2k_{\mathrm{td}}\mathrm{R}_i\left(\frac{\mathrm{R}_{max}}{2k_{\mathrm{t}}t\mathrm{R}_{max}+1}\right) + k_{\mathrm{tc}}\sum_{j=0}^{i}\mathrm{R}_{i-j}\mathrm{R}_j \right) dt \qquad i \geq 0 \qquad (2.36)$$

$$\text{where } \mathrm{R}_i = \frac{\exp(-k_{\mathrm{p}}\mathrm{M}t)}{2k_{\mathrm{t}}t\mathrm{R}_{max}+1}\sum_{j=1}^{i}\mathrm{R}_j^{last}\frac{(k_{\mathrm{p}}\mathrm{M}t)^{i-j}}{(i-j)!} \qquad (2.37)$$

In this expression $(\mathrm{D}_i)_t$ is the concentration of dead polymer chains of chain length i produced between 0 and t seconds. Although numerous attempts were made to solve these equations analytically, no solution could be found. Note that software package MATLAB has been used in an attempt to solved these equations and this also meet with no success. Thus, equation 2.36 was solved numerically. A computer program has been written to perform this numerical integration. This program uses an adaptive Simpson's integration algorithm.[13] Note that more sophiscated integration techniques, such as the Gauss-Hermitte or Gauss-Laguerre methods, have not be used to perform this numerical integration; these methods could meet with some success. In each case this integration is performed for one complete initiation period, i.e., $0 \leq t \leq t_0$. It was assumed that radicals lived for a maximum of seven initiation periods and a truncation chain length of 2000 was used. Figure 2-3 contains an MWD that has been calculated using equation 2.36. This plot illustrates how the MWD is affected by changes to the integration step size. This figure makes it clear that the integration step size has little effect the MWD. A detailed discussion of the results of the method will be given at the end of this chapter. These calculations typically took two hours of CPU time on a VAX mainframe.

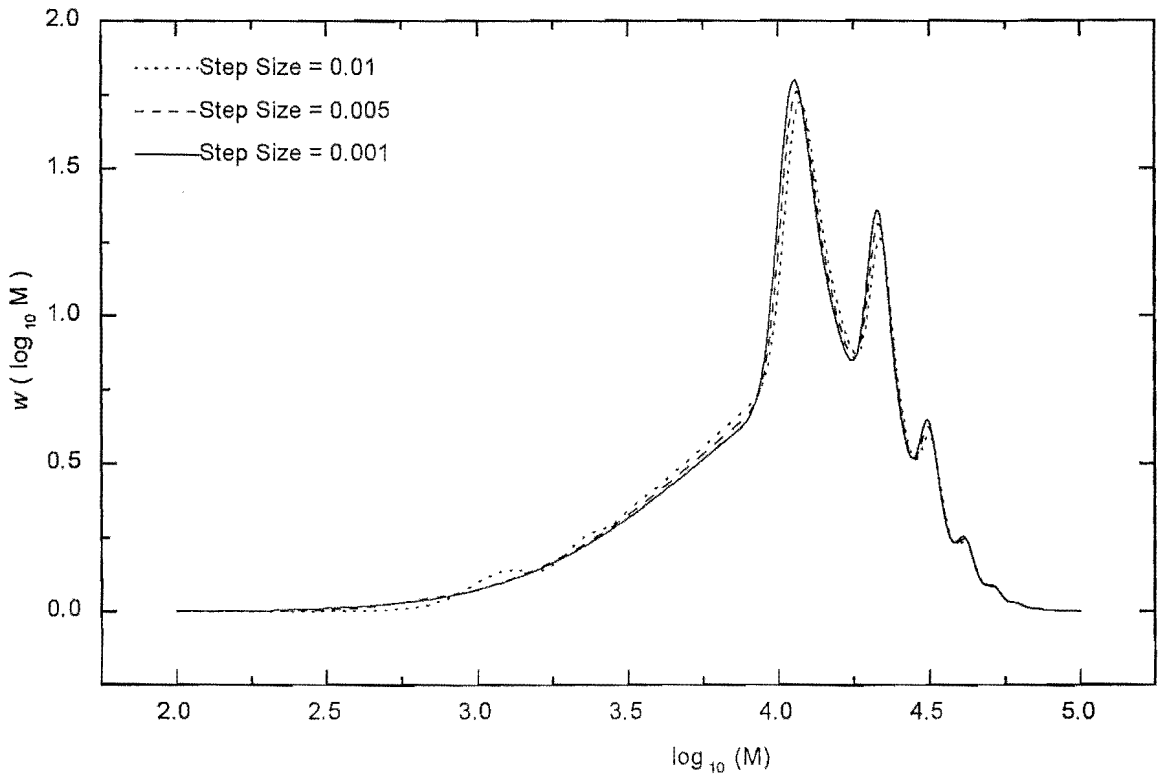

Figure 2-3: The effect of numerical integration step-size upon the MWD for the analytic solution based upon the method of integrating factors. The default rate parameters have been used in this simulation.

2.3 The Analytic Formalism Developed by Olaj Et. Al.

The next analytic solution studied here is the solution developed by Olaj et. al.[37] This analytic solution is derived in a completely different manner to the solution described above. Instead of solving the differential equations directly, Olaj et. al. derive expressions for the chain-length distribution of dead polymer in terms of several dimensionless constants. This derivation starts with an expression for the rate of termination for a radical of chain length i. This equation is then used as the basis for deriving two expressions for the dead polymer chain-length distribution, one for dead polymer formed by the disproportionation termination

mechanism and another for polymer formed by the combination termination mechanism. Both of these expressions assume that all radicals grow at the same rate, i.e., they ignore the stochastic nature of propagation. However, once expressions have been obtained for the dead polymer chain-length distribution, Poisson broadening is added.

2.3.1 The Rate of Termination as a Function of Chain length

Note that the rate of termination as a function of chain length is in no way related to normal chain-length dependencies. This expression is derived assuming that all rate coefficients are independent of the chain length of the reacting species. This expression merely describes the rate of termination for a radical of chain length i. As was stated above this derivation is based on the assumption that the PIP system has already reached a pseudo-steady state. A pseudo-steady state where the total radical concentration begins at R_{max}, the radical concentration just after the arrival of a laser pulse, and decays to a final radical concentration that is equal to R_{max} - ρ, where ρ is the concentration of radicals added by the laser pulse.

Here a dimensionless constant β is defined as the proportion of the total concentration of radicals that were generated by the last laser pulse, i.e.,

$$\beta = \frac{R_{I=0}}{\sum_{I \geq 0} R_I} \tag{2.38}$$

In this expression, I indicates which burst of initiation a radical was created in. For example, $R_{I=0}$ is the concentration of radicals added by the last laser pulse, i.e., here $R_{I=0}$ does not stand for the concentration of primary radicals. Using this nomenclature, the rate of termination, $(\nu_I)_t$, of radical species generated in pulse I at time t is equal to

$$(\nu_I)_t = -\frac{dR_I}{dt} = 2k_t R_I \sum_{I \geq 0} R_I \tag{2.39}$$

It is clear from this expression that the relative rate of consumption of radicals R_I, $\frac{(\nu_I)_t}{R_I}$ is independent of the concentration of R_I radicals specifically, and dependent only upon the total concentration of radicals.

$$\frac{(\nu_I)_t}{R_I} = 2k_t \sum_{I \geq 0} R_I \tag{2.40}$$

This means that the proportion of the total radical concentration made up of radicals created by laser pulse I stays the same throughout an initiation period. This is simply a consequence of termination being chain-length dependent in rate and also means that the concentration of R_I relative to the total radical concentration is governed by the same second-order rate law as the total radical concentration. Hence,

$$\frac{(R_I)_t}{(R_I)_{t=0}} = \frac{(\sum_{I \geq 0} R_I)_t}{(\sum_{I \geq 0} R_I)_{t=0}} = \frac{1}{1 + 2k_t R_{max} t} = f(t) \tag{2.41}$$

Thus $f(t_0)$ is equal to the proportion of radicals created by the last burst of initiation that are alive when the next burst of initiation arrives, i.e., $f(t_0) = (1 - \beta)$. This means that β can be redefined as

$$\beta = 1 - f(t_0) = \frac{2k_t R_{max}}{1 + 2k_t R_{max} t_0} \tag{2.42}$$

Moreover, by definition one notes that

$$\beta = \frac{\rho}{R_{max}} \tag{2.43}$$

This means that one can define

$$(\sum_{I \geq 0} R_I)_t = R_{max} f(t) \tag{2.44}$$

$$(R_I)_t = (R_I)_{t=0} f(t) \tag{2.45}$$

Substituting these expressions into equation 2.39 one has that the rate of termination at time t is equal to

$$(\nu_I)_t = 2k_t (R_I)_{t=0} R_{max} f^2(t) \tag{2.46}$$

In addition to this, one can define the concentration of radicals created by laser pulse I in terms of the concentration of radicals added by a burst of initiation, ρ, and the probability of surviving an initiation period,$1 - \beta$, i.e.,

$$(R_I)_{t=0} = (R_0)_{t=0}(1 - \beta)^I = \rho(1 - \beta)^I \tag{2.47}$$

Substituting equation 2.47 into equation 2.45 one gets

$$(\nu_I)_t = 2k_t\rho(1-\beta)^I \mathrm{R}_{\max} f^2(t) \tag{2.48}$$

This gives the rate of termination of radicals at time t. However, what is of greater interest is that equation 2.48 can be transformed to give the rate of termination as a function of chain length, L (note that in contrast to chapter one L is the chain length not the truncation chain length). To transform between chain length and t we assume that all radicals grow at the same rate, so that

$$L = k_p \mathrm{M} t \tag{2.49}$$

Thus, from equation 2.40 $f(L)$ is defined as

$$f(L) = \left(1 + \frac{2k_t \mathrm{R}_{\max}}{k_p \mathrm{M}}.L\right)^{-1} \tag{2.50}$$

This means that we can define the rate of termination in terms of given simulation parameters. Again $\mathrm{R}_{\max}$ is defined by equation 1.44.

$$\begin{aligned}
0 < L \leq L_0 \qquad & (\nu_0)_L = 2k_t \mathrm{R}_{\max}\rho f^2(L) \\
L_0 < L \leq 2L_0 \qquad & (\nu_1)_L = 2k_t \mathrm{R}_{\max}\rho(1-\beta) f^2(L-L_0) \\
2L_0 < L \leq 3L_0 \qquad & (\nu_2)_L = 2k_t \mathrm{R}_{\max}\rho(1-\beta)^2 f^2(L-2L_0) \ \ldots
\end{aligned} \tag{2.51}$$

In these expressions, $L_0 = k_p \mathrm{M} t_0$ and $1-\beta = f(L_0)$. Figure 2-4 shows the dependence of the rate of termination on the chain length of the growing radicals. This figure indicates that the rate of termination is strongly dependent on the chain length of the radical species. This plot displays two trends. Firstly, the rate of termination decreases as the chain length of the terminating radical increases. This trend is a result of the decrease in the concentration of radicals as chain length increases. Hence as the rate of termination depends on the concentration of radicals of chain length i, it also decreases with chain length. The second trend is the periodic increase in the rate of termination at chain lengths that are multiplies of $k_p \mathrm{M} t_0$. This is due to the increase in the rate of termination that occurs when a burst of initiation arrives. Thus, the rate

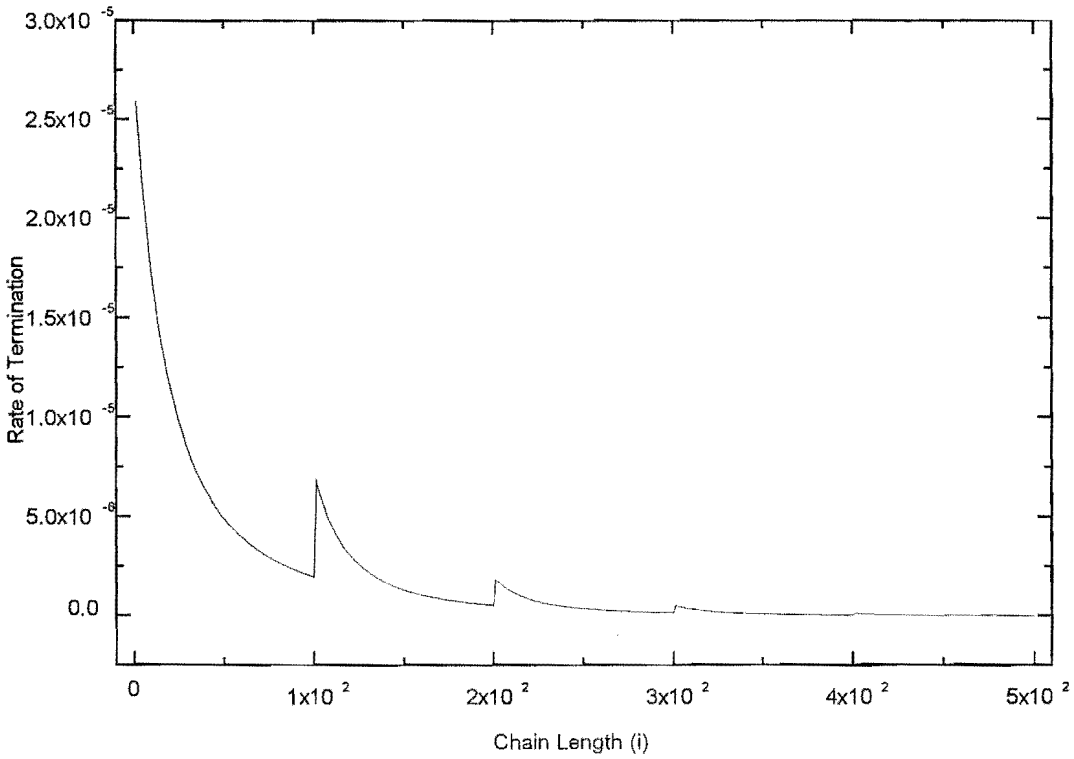

Figure 2-4: The rate of termination as a function of chain-length modelled by equation 2.51. Standard rate parameters were used in this calculation and the rate of termination has units of mol/L/s.

of termination is higher for chain lengths that are common at, or soon after a burst of initiation. This figure also indicates that the concentration of radicals is effectively zero after six initiation periods. It should be remembered in appraising figure 2-4 that Poisson broadening is ignored at this stage.

The next step in defining an expression for the dead chain-length distribution, depends upon the mode of termination. The two cases, termination by disproportionation and termination by combination are treated separately.

2.3.2 The Derivation of an Expression for the Dead Polymer Chain-length Distribution Produced When Termination Occurs Only Via the Disproportionation Termination Mechanism

The chain-length distribution for dead polymer chains formed by disproportionation follows simply from the expressions for the rate of termination as a function of chain length (equations 2.51), as the chain length of the dead polymer chains produced is equal to the length of the growing radicals at the moment when they terminate. This means that the concentration of radicals of chain length L, $x_D(L)$, is equal to

$$\begin{aligned} 0 < L \leq L_0 \qquad & x_D(L) = K\lambda(1 + KL)^2 \\ L_0 < L \leq 2L_0 \qquad & x_D(L) = K\lambda[1 + K(L - L_0)]^{-2}(1 - \beta) \\ 2L_0 < L \leq 3L_0 \qquad & x_D(L) = K\lambda[1 + K(L - 2L_0)]^{-2}(1 - \beta)^2 ... \end{aligned} \tag{2.52}$$

Here K is defined as

$$K = \frac{2k_t \mathrm{R}_{max}}{k_p \mathrm{M}} \tag{2.53}$$

and as usual

$$\lambda = \frac{k_{td}}{k_{td} + k_{tc}} \tag{2.54}$$

The prefactor K appears at the front of these expressions to ensure normalization. Figure 2-5 contains a plot of the dead polymer chain-length distribution for chains formed by the disproportionation mechanism described by equation 2.52. This dead polymer chain-length distribution is plotted as $i^2.\mathrm{D}_i$ against the log of the chain length ($\log_{10} i$), i.e., as the MWD that would be obtained from GPC. This distribution shows many of the typical PIP features. Notably, there are peaks at chain lengths equal to $jk_p \mathrm{M}t_0$, where j is a counting number.

Now that we have an expression for the distribution for dead polymer chains, the assumption that all radicals from a particular pulse must be of the same chain length can be removed. This involves transforming a radical wave from a delta spike to a Poisson distribution. The Poisson distribution of chains with a most probable chain length L_{mp} is equal to

$$x_L = e^{-L_{mp}} \frac{(L_{mp})^L}{L!} \tag{2.55}$$

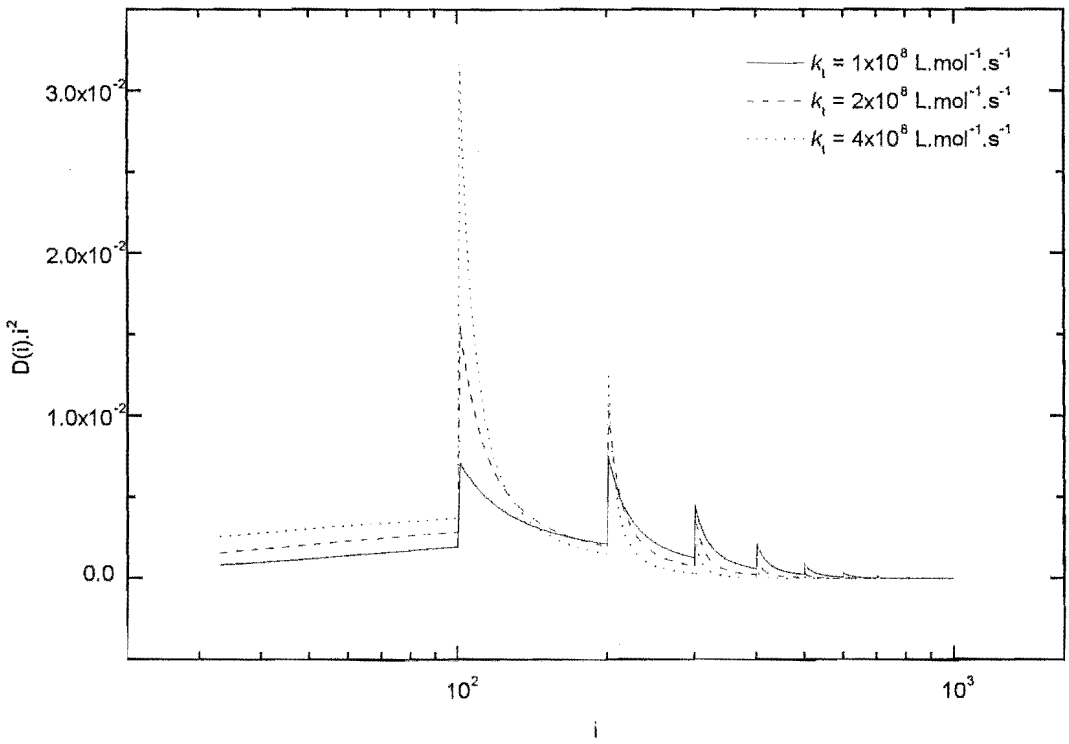

Figure 2-5: The dead polymer chain-length distribution predicted by equation 2.52 for three values of the rate coefficient for termination, with other rate parameters as standard.

Here x_L is the probability of that a radical of chain length L is a part of the radical wave with most probable chain length L_{mp}. This expression can be substituted into equation 2.52 to give the exact chain-length distribution of dead chains formed by termination by the disproportionation mechanism, $x_D(L)$,

$$x_D(L) = \frac{\lambda K}{L!} \int_{L=0}^{L_0} f^2(L_{mp}) \left(\begin{array}{c} e^{-L_{mp}}.(L)^{L_{mp}} + (1-\beta)e^{-(L_{mp}+L_0)}(L_{mp}+L_0)^L \\ +(1-\beta)^2 e^{-(L_{mp}+2L_0)}(L_{mp}+2L_0)^L \ldots \end{array} \right) dL \quad (2.56)$$

Note that this is the integral over a time period $t = 0$ to $t = t_0$ which has been transformed into the equivalent integral over $L = 0$ to $L = L_0$.

This expression can be used to predict the dead polymer chain-length distribution from parameters inputted into a standard PIP simulation. It is important to point out that this expression must be evaluated numerically. To calculate the dead chain MWD equation 2.56 has to be integrated over chain lengths $L = 0$ to $L = L_0$. Thus, this treatment not does give an analytic expression for the exact dead chain distribution, rather it yields an analytic expression for dead chain MWD based on the assumption that radicals created by the same burst of initiation are always the same length, but not an analytic expression for the exact dead polymer chain-length distribution (including Poisson Broadening). In this regard, this treatment gives a result analogous to the method of integrating factors: an analytic expression for some facet of the living radical chain-length distribution, but an expression for the exact dead chain-length distribution that has to be solved numerically. Figure 2-6 contains plots of three dead polymer chain-length distributions predicted by equation 2.56. The numerical integration of equation 2.56 was performed using the adaptive Simpson's algorithm. The sum of exponential terms that make up the integrand was truncated after seven terms, i.e., seven initiation periods. This calculation includes chains up to and including dead chains of chain length 2000. The dead polymer chain-length distribution has been plotted once again in its GPC form. The results are similar to those predicted by the analytic solution derived using the MOIFs. The implementation of this solution took one and a half hours of CPU time on a VAX mainframe.

2.3.3 The Derivation of an Expression for the Dead Polymer Chain-length Distribution Produced When Termination Occurs Only Via the Combination Termination Mechanism

The development of an expression of the dead polymer chain-length distribution formed when termination occurs via the combination mechanism is very similar to that for the disproportionation termination mechanism. For this reason the final expression will simply be stated.

$$X_R(L) = \frac{(1-\lambda)C}{L!}\int_{L=0}^{L_0} f^2(L_{mp}) \left(\begin{array}{c} e^{-2L_{mp}}(2L_{mp})^L + 2e^{-(2L_{mp}+L_0)}(2L_{mp}+L_0)^L(1-\beta) \\ +3e^{-(2L_{mp}+2L_0)}(2L_{mp}+2L_0)^L(1-\beta)^2 ... \end{array} \right) dL \tag{2.57}$$

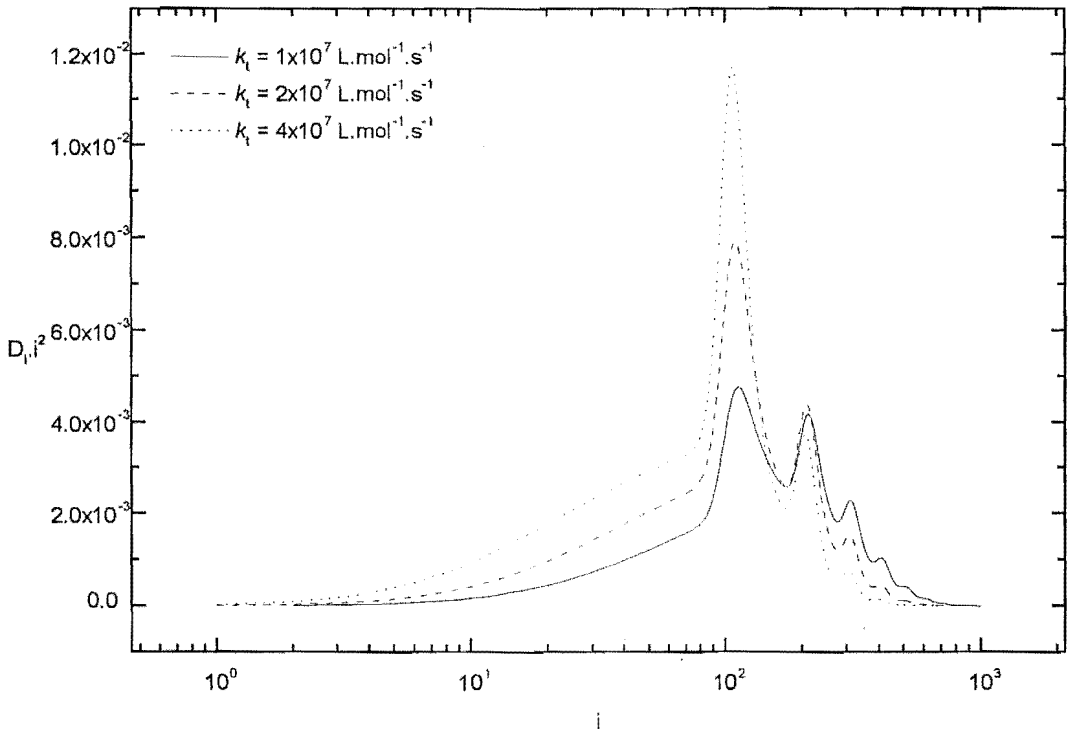

Figure 2-6: The dead polymer chain length distrbution for dead chains formed by the disproportionation mechanism described by the expression developed by Olaj et. al.

In equation 2.57 C stands for $\frac{K\beta}{2}$ and note that all of the significant changes between equations 2.57 and 2.56 are a result of the fact that disproportionation produces two chains of the same length as the terminating radical species while combination produces one dead polymer chain equal to the combined length of the two terminating radicals. Figure 2-7 contains a plot of the dead polymer chain-length distribution predicted by equation 2.57. A low value of $k_p = 5 \times 10^1 \text{L.mol}^{-1}.s^{-1}$ is used here. The reason for using a low value of k_p is to avoid having to deal with a large L for which it is difficult to evaluate the $L!$ and $(jL_{mp})^L$ terms. The distribution shown in figure 2-7 differs from figure 2-6 in all expected ways, for example dead polymer chains of higher chain length are formed and the distribution is broader. Again it is clear that this treatment does not give an analytic expression for the dead chain MWD, but

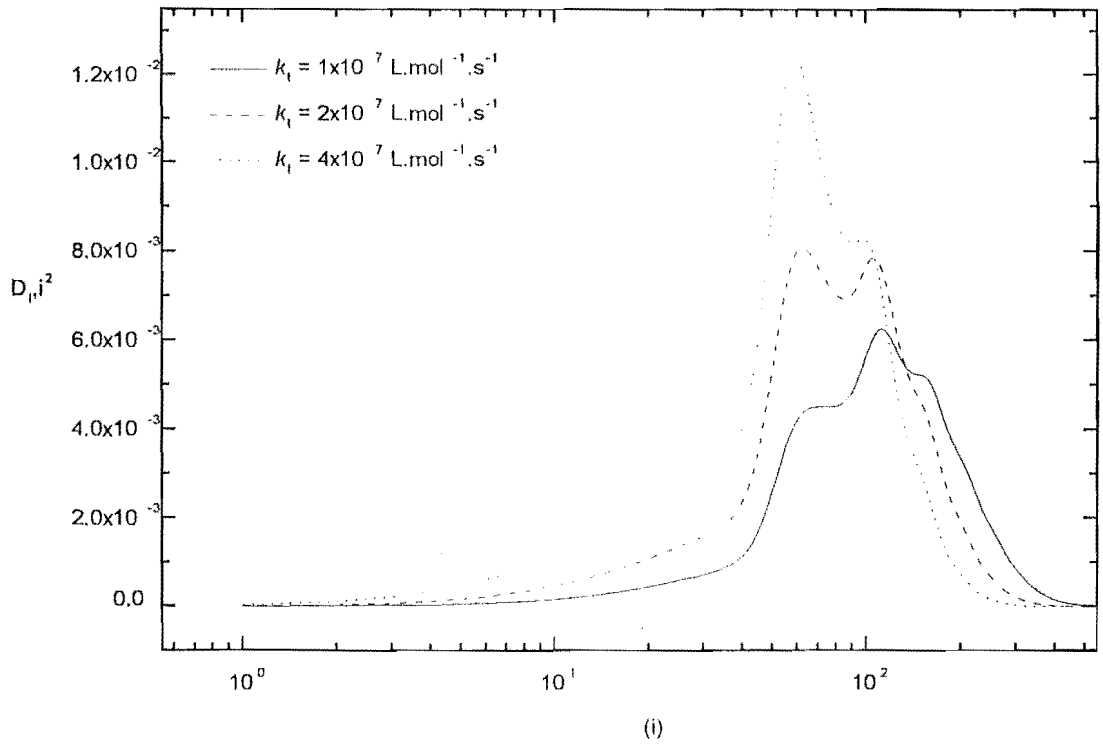

Figure 2-7: The dead polymer chain-length distribution for dead polymer chains formed exclusively via the combination termination mechanism modelled by the expression developed by Olaj et. al. (see text).

instead gives an expression that must be solved numerically.

2.4 The Analytic Expression Developed by Aleksandrov et. al., and other analytic methods

The last analytic expression to be described and tested here is the expression developed by Aleksandrov et. al.[1], an expression which has been used by Sarnecki et. al.[47] to explore the kinetics of PIP. The nomenclature and the form of this expression have been changed slightly for the sake of clarity. Aleksandrov et. al. used equation 2.58 to describe the dead polymer

chain-length distribution. Note that the expression used by Aleksandrov et. al. and Sarnecki et. al. describes the weight rather than the number molecular weight distribution. The number molecular weight distribution version of the expression is given here.

$$n(i) = \sum_{N=n^*}^{int(t/t_0)} \rho \int_{t=0}^{\tau} \sum_{j=0}^{2n^*} \frac{p_c + p_d}{t_T^n \, t_{\tau'}^2} d\tau' \tag{2.58}$$

In this expression,

- $t_{\tau'}$ is defined as $1 + 2k_t R_{max}\tau'$;
- t_T is defined as $1 + 2k_t R_{max}T$;
- t is the polymerization time (s);
- T is the time between laser pulses (s);
- τ and τ' are continuous time variables ranging from 0 to t_0;
- i is the chain length of the dead polymer species (s);
- n, N are the number of laser pulses
- ρ is the concentration of radicals added by a burst of initiation $(mol.L^{-1})$;
- R_{max} is the maximum radical concentration (the concentration straight after a burst of initiation) $(mol.L^{-1})$;
- n^* is the number of initiation periods the system requires to reach a pseudo-steady state;
- M is the monomer concentration $(mol.L^{-1})$;
- k_p is the rate coefficient for propagation $(L.mol.s^{-1})$;
- k_{tc} is the rate coefficient for termination by the combination mechanism $(L.mol.s^{-1})$;
- k_{td} is the rate coefficient for termination by the disproportionation mechanism $(L.mol.s^{-1})$;
- $\varkappa(n) = \frac{n}{2} + 1$ for even n; $\varkappa(n) = \frac{n+1}{2}$ for odd n; [1]

[1] Note this term was omitted by Sarnecki and Schweer [47] from their term for termination by combination.

- $k_t = k_{td} + k_{tc}$ (L.mol.s^{-1}).

and where

$$p_d = k_{td}\rho \frac{\exp(\frac{-k_p M(nt_0+\tau')}{1-\frac{k_p}{k_t}})((\frac{-k_p M(nt_0+\tau')}{1-\frac{k_p}{k_t}})^i}{i!} \tag{2.59}$$

$$p_c = k_{tc}\rho \frac{\exp(\frac{-k_p M(nt_0+2\tau')}{1-\frac{k_p}{k_t}})((\frac{-k_p M(nt_0+2\tau')}{1-\frac{k_p}{k_t}})^i \varkappa(n)}{i!} \tag{2.60}$$

Although equation 2.58 is more complicated than the two solutions given above, it contains the same features. It says that the dead polymer chain-length distribution can be represented as the sum of dead polymer chains formed over a small number of initiation periods once the polymerization has reached the pseudo-steady state ($int(t/t_0)$ initiation periods). It includes radicals that have been alive for a small number of initiation periods and allows termination to occur via either mechanism. This expressions accounts for the Poisson character of the living radical chain-length distribution through the terms p_c and p_d.

As the focus of this chapter is on the implementation rather than the derivation of analytic solutions, a detailed description of the derivation of this expression will not be given here. Nonetheless, one point about the derivation of this expression will be emphasized. Aleksandrov et. al. do not give an analytic solution to the integral that calculates the dead polymer chains produced during an initiation period. Therefore, their expression must be evaluated numerically in the same manner as the formulas developed in this thesis and those developed by Olaj et. al.

The dead polymer chain-length distribution modeled by equation 2.58 is shown in figure 2-8. Note that in this figure termination was allowed to occur only by the disproportionation mechanism. This figure and those for the two previous methods will be discussed in the following section. However it is worthwhile discussing the differences between the analytic solutions obtained using the MOIFs and by Aleksandrov et. al. at this time. It is clear from the form these solutions that there are many similarities, for example both analytic solutions are complex forms of the Poisson distributions, what is not as clear is the major differences. The analytic solution derived via the MOIFs is the completely general solution to the living radical differential equations for PIP. It can be used to describe the radical chain-length distribution in the pre-pseudo-steady state and pseudo-steady state stages of the polymerization. In contrast

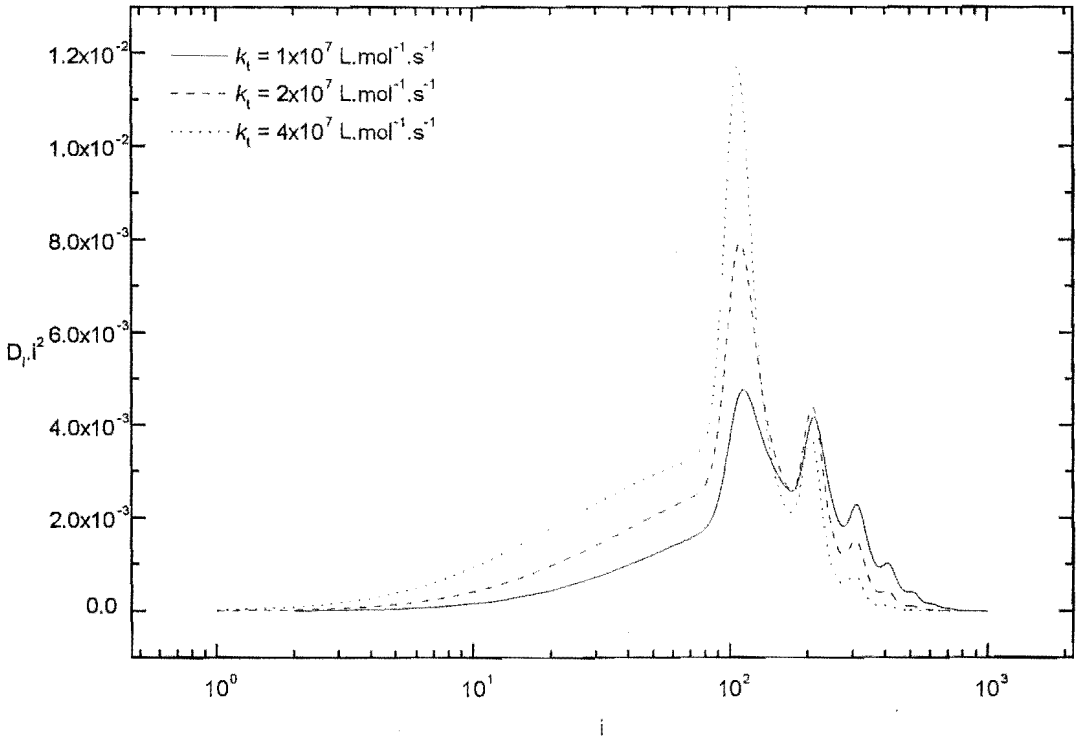

Figure 2-8: The dead polymer chain-length distribution predicted by the analytic expression developed by Aleksandrov et. al.

to this, the expression derived by Aleksandrov only holds for the pseudo-steady state stage of the polymerization and is therefore not a completely general solution. This difference is illustrated by the fact that one can simply alter the initial conditions used in equation 2.34 to obtained the single pulse limit, while the same limit cannot be found for equation 2.58. For these reasons equation 2.34 provides greater insight into the nature of the radical chain-length distribution than equation 2.58 and is therefore superior.

Several other analytic solutions have been derived for PIP. These include expressions obtained using generating functions[31][17] and those ignoring Poissionian broadening[18]. The expression obtained using the method of generating functions only holds for the pseudo-steady state phase of the polymerization and are therefore not as general as the analytic solution ob-

tained via the MOIFs. Meanwhile, although the analytic solution derived by Nikitin et. al.[18] holds for all stages of the polymerization, the exclusion of Poissionian broadening limits its usefulness.

2.5 Discussion

In the introduction to this chapter it was stated that the aim of this work was to explore how well analytic solutions are suited to routinely modeling PIP. To do this, computer programs have been written that implement three such solutions and these programs have been run extensively. To be able to decide whether these solutions, and indeed analytic solutions in general, have potential as effective solution strategies, we must consider several factors relating to their implementation, for example the computer time required to run these programs. Moreover, we will consider how easy it is to extend these solutions so that they can be used to model PIPs that include polymerization processes other than those included in this model system. To do this we will focus on the four questions mentioned in the introduction to this chapter.

2.5.1 Are These Solutions Computationally Efficient?

Analytic expressions can normally be evaluated efficiently on a computer. Typically this is because they are simple mathematical expressions that have to be evaluated only once. For example, the evaluation of the analytic solution to equation 2.1 (the simple differential equation studied at the start of this chapter) was effectively instantaneous. However, a significant amount of CPU time is required to evaluate any of the three analytic solutions studied in this chapter (see table 2.2). In each case, four factors contribute to this high computational cost: (1) they all contain an integrand that consists of a series of terms; (2) this integrand contains a large number of terms, one for each chain length (3) each case a factorial term must be calculated (this difficult and time consuming for larger numbers); and (4) in each case an integral must be evaluated numerically. Although each of these factors influence the computational cost, the numerical solution of the integral has the greatest effect. To solve an integral numerically, one divides the region of the integral into a series of small intervals (quadrature). The value of the integral can be then estimated by calculating the area in each of these small sections

Analytic Solution	CPU Time (hr)
MOIF	2.5
Olaj et. al.	2
Aleksandrov et. al.	1.5

Table 2.2: The amount of time required to evaluate the three analytic expressions studied in this chapter. See text for rate parameters.

and summing over all of these sections. Thus at the core of any numerical integration is the repeated evaluation of the integrand. For example, the numerical integration performed here required the integrand to be evaluated one thousand times per initiation period. Thus, if the evaluation of the integrand requires even a modest amount of computational effort, the numerical solution of that integral can incur significant computational cost. This is the case here: the integrands that must be evaluated are computationally expensive to evaluate. Note that frequently truncation chain lengths much larger than those used here will have to be used to model 'real-world' polymerizations. Increasing the truncation chain-length will drastically increase the computational cost.

Table 2.2 contains a summary of the CPU time required to evaluate each of the analytic solutions discussed here. In each case, the model parameter set was used. Each simulation allowed for living radical and dead polymer species up to and including a chain-length of 2000. The results shown in this table indicate that all of the analytic solutions take approximately the same time to implement, i.e., approximately 2 hours of CPU time. This is not surprising as the three analytic solutions presented are very similar – essentially the same steps need to be taken implementing all of these solutions.

Although in this chapter only three analytic solution strategies have been studied, the similarity of the essential features of these solutions suggests that any analytic solution of this type of polymerization (based on this kinetic model) will have the same form. Significantly, in each case only a semi-analytic solution could be found for the dead polymer chain-length distribution. This is likely to be a general feature of all analytic solutions for PIP. Hence, the performance of these three solutions can be used as the basis for drawing conclusions about analytic solutions to PIP in general. Hence it is concluded that analytic expressions for PIP are computationally expensive to evaluate. In subsequent chapters we will see that numerical methods can generate solutions with close to the same accuracy in significantly less time. This

means that analytic solutions to PIP do not have the advantages that typical analytic solutions have over typical numerical solutions, i.e., analytic solutions are not faster to use.

2.5.2 How Much Error, If Any, Do These Solutions Introduce into the Kinetics and/or Final MWD?

To assess the error incurred by these methods, MWDs predicted by each analytic solution are compared. Note that this comparison only provides indirect information about how well these solutions model the kinetics of these systems. Three MWDs, one for each solution, are presented in figure 2-9. This plot shows that there is extremely little difference between MWDs predicted by each of these expressions. In fact the difference that is present can be attributed to the adaptive quadrature used by the numerical integration technique. In effect the three methods are just three methods of arriving at the same result - similar although not exactly the same approximations are made in each case.

As this analysis compares three distributions that have been calculated by similar, although not identical, methods, it is possible that there is error present in all of these MWDs that this comparison would not illuminate. If each of these solutions incurred error in the same way then this comparison would tell us little. However, these solutions are different enough that it seems unlikely that each of these solutions will contain the same systematic error. Finally, these MWDs have also been compared with numerical solutions (see chapter three). This comparison between numerical and analytic solution indicated that these analytic solutions contain little error. A series of numerical calculations were performed where the step size and therefore the accuracy of the calculation was changed. The best agreement between the analytic and numerical solutions came when small step sizes were used in the numerical calculation, i.e., there is optimum agreement between the high accuracy numerical solution and the analytic solution. This suggests that these analytic solutions contain little error.

2.5.3 Are These Solutions Flexible to Changes, or Additions to, the Reaction Scheme for Free-radical Polymerization?

One of the obvious disadvantages of analytic solutions is their inflexibility to changes in the systems on which they are based. Commonly violated limitations of the reaction scheme used

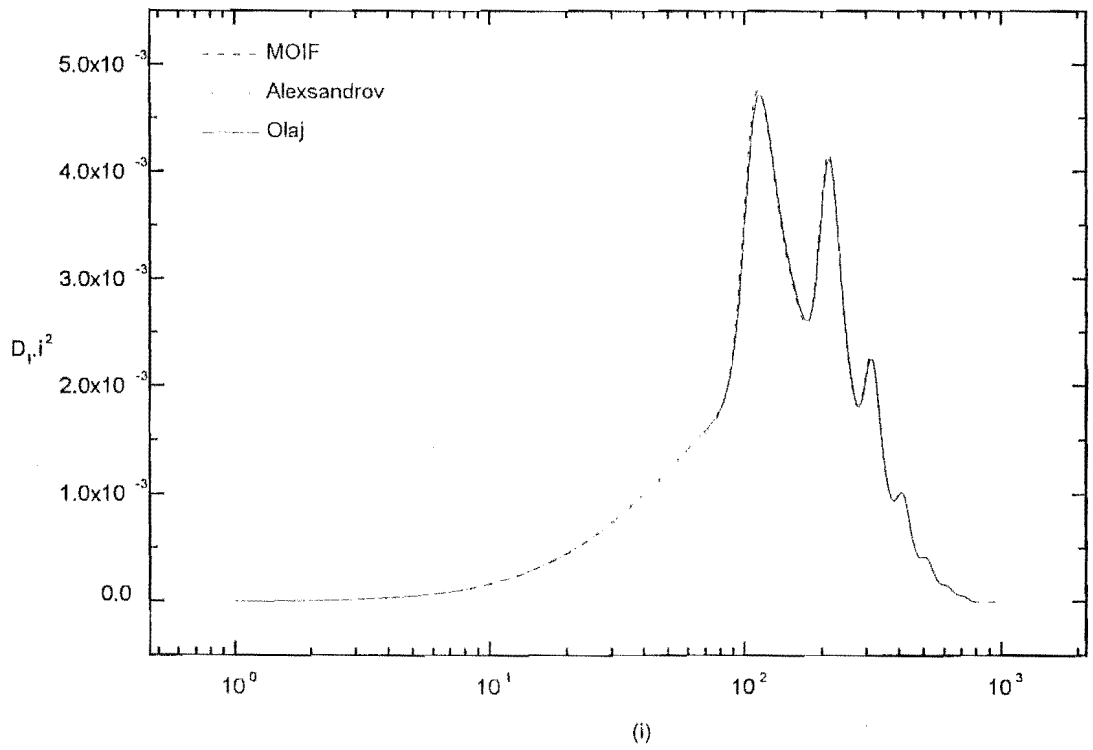

Figure 2-9: A comparison of MWDs calculated by the three analytic solution techniques outlined in this chapter. For rate parameters see text.

here include: occurrence of chain transfer; chain-length dependent termination; occurrence of "background" initiation; and non-pseudo-steady state conditions, e.g., initiator or monomer consumption, or pre- or post- effect experiments. For example, suppose it was concluded that chain transfer to monomer had a significant affect upon the MWD obtained from the PIP of a particular monomer. To explore this it might prove necessary model an experimental MWD with a simulated MWD based on a model to that includes chain transfer. To perform this modelling using an analytic expression one would need to completely re-derive the analytic expressions, a time consuming and difficult process as Olaj et. al. have illustrated in adding various perturbations to their basic PIP scheme.[57][58][42] On the other hand, if a numerical solution strategy is used (for example those outlined in chapters 3-5) all that needs to be done

is to simply add further terms to the differential equations to be solved – the method of solution need not be changed.

2.5.4 Concluding Remarks: Can These Solutions be Used as the Heart of a Method for the Routine Simulation PIP?

All of the methods described in this chapter can be used to simulate PIP. Each method accurately models the MWD for this type of polymerization and the required length of CPU time is not prohibitive. Moreover, it is possible to extend these formalisms to include many of the refinements frequently included in PIP simulation studies, e.g. transfer to monomer, chain-length dependent rate coefficients and initiator consumption.[57][58] However, in almost every regard these methods are surpassed by the numerical methods that follow. Numerical solution strategies obtain solutions in a shorter period of time and with greater flexibility. The only way that analytic solutions out-perform numerical solutions is in the accuracy of the solutions they obtain. Analytic solutions almost always incur less error than numerical solutions. However, with the right choice of numerical simulation parameters, in particular the integration step size (see chapter three), this error can be reduced to the point that it becomes insignificant. In short, by using analytic solutions one doesn't gain greater accuracy, and one sacrifices flexibility and computing time. Another potential disadvantage of analytic solutions over numerical solutions is that analytic solutions usually provide greater insight. While some insight - for example the Possionian form of solutions - is evident from the analytic solutions of this chapter, it is clear that the expressions are so complicated that they provide no great insight. So in this respect also the analytic solutions offer no significant advantage.

Finally, it is worthwhile pointing out the Schweer and Sarnecki [47] are the only workers to have used anyone else's analytic solutions. Otherwise, every method of analytic solution has only been used by those who developed it. On the other hand, many groups [7][26][16][44] have carried out PIP simulations using numerical methods. So in a sense workers have voted with their feet: numerical solutions are easier to implement, easier to understand, and easier to tailor the specific needs at hand. At the same time, they do not suffer from any significant disadvantages compared to analytic solutions.

Chapter 3

Numerical Solution Techniques: First Approaches

3.1 Introduction

The aim of the work described in the thesis is the development of solution methods that can be used to model pulsed initiation polymerization (PIP). To model this type of polymerization, such a method must be able to solve the differential equations that characterize it, and do so in a short period of time, without incurring too much error.

In the previous chapter, a series of analytic solutions that had the potential to achieve this aim were outlined and implemented. Unfortunately, these solutions failed as practical solution strategies, as they proved to be computationally expensive to implement, and very difficult to alter, if one wished to change the fundamental kinetic scheme. Because of the way that these methods failed, it was concluded that it is unlikely that any solution of this type could be used to simulate PIP routinely.

In this chapter, another type of solution method is introduced, implemented and refined. This type of method is known as a finite-difference based (FDB) numerical solution strategy. Finite-difference based methods attempt to solve differential equations via series of numerical approximations. A FDB method works by dividing the time between when the solution is known, the initial conditions, and the time when the solution is required into a series of small intervals. They then use simple approximations to generate the solution to a differential equa-

tion at the end of these intervals. As these methods use approximations, the final solutions that they produce contain error.

In this chapter, a significant amount of time will be spent measuring and understanding this error. This is important, as the presence of uncontrolled error in the final solution can lead to false conclusions being drawn about these polymerizing systems. To aid us in developing an understanding of the error incurred by all FDB methods, a detailed study is performed of the error incurred by the simplest of these methods, the Euler method.

Finally, in the last part of this chapter, a refinement of all FDB methods is developed that significantly improves their efficiency. This refinement customizes these methods so that they are particularly suited to solving the differential equations that characterize PIP.

To introduce FDB numerical methods they will be contrasted with the analytic solution strategies studied in the previous chapter.

3.2 Numerical Versus Analytic Solution Strategies

Numerical solution techniques approach the problem of solving differential equations in a different manner to analytic approaches. One of the major differences between these two approaches is in the type of solution they attempt to obtain. Whereas an analytic approach generates solutions that are mathematical expressions, numerical approaches produce the numerical value of the solution at a particular point in time. This difference, as well as several others, can be highlighted by using both methods to solve a simple differential equation (equation 3.1) subject to initial conditions (equation 3.2)

$$y'(t, y(t)) = 1 - t + 4y(t) \tag{3.1}$$

$$y(0) = 1 \tag{3.2}$$

In equation 3.1, $y'(t, y(t))$ is the rate of change in $y(t)$, where this rate of change depends on both t and $y(t)$. Equation 3.2 constrains the solutions of equation 3.1 to those that give a value of $y(0) = 1$, i.e., this is the value of y when $t = 0$.

The analytic, or exact, solution to equation 3.1 can be obtained by the use of one of a number of mathematical techniques, such as integration via the method of integrating factors.

The exact, or analytic solution, $\Phi(t)$, to equation 3.1, subject to the initial conditions of equation 3.2) is

$$y(t) = \Phi(t) = \frac{1}{4}t - \frac{3}{16} + \frac{19}{16}\exp(4t) \tag{3.3}$$

This is a typical analytic solution in that it describes the value required, $y(t)$, in terms of several variables and mathematical functions. One of the advantages of such an analytic solution is that it can be used to quickly generate the value of the solution at any point in time. For example, if the solution of equation 3.1 is needed at $t = 1$, then all one needs to do is substitute the time into equation 3.3 and evaluate that expression. In this case, the answer is $y(1) = 64.898$. It should be noted though that this is not always the case. There are many analytic solutions that are either too difficult, or too computationally expensive, to evaluate, for example those of the previous chapter. However, analytic solutions do have other advantages: for example, they can be used to infer information about the general nature of the solution. Take equation 3.3 for example. From the form of this expression and a knowledge of mathematical functions we can infer that when t is very low, the $\frac{1}{4}t$ term will dominate the behavior and the solution will change linearly with time. However, as t increases, the exponential term will quickly dominate and at moderately high values of t the solution will be a simple exponential growth expression, i.e., $y(t) \approx \exp(4t)$.

In contrast to this, finite-difference methods do not try to generate general mathematical expressions. Instead, they aim to generate the numerical value of the solution at a particular time. That is, a numerical solution is never a mathematical expression of the form of equation 3.3; instead, it is a trail of the values of the solution leading from the initial conditions to the time where the final solution is required. As a mathematical expression is not produced, it is not possible to simply plug in a set of numbers and generate the final solution. Instead, one must run an often-lengthy computer calculation to generate the value(s) required. Furthermore, unlike an analytic solution, it is difficult to infer information about the nature of the solution simply by inspecting its form. Nevertheless, FDB techniques do have several advantages over analytic approaches. The most significant of these is that they are able to solve a far wider range of differential equations. In fact, of all the real world problems thay are described by differential equations, only a vanishingly few can be solved by analytic approaches, while the majority can be solved accurately numerically.

A finite-difference method, as its name suggests, works by replacing a differential equation by a finite equation. By doing this, these methods approximate a complex expression (the differential equation) by a simple expression (the finite equation). The simplest FDB method, the Euler method, does this by approximating the differential equation during a time interval by its value at the start of the time interval. This means that the integral of the differential equation during a time interval can be approximated by the size of that time interval multiplied by the value of the differential equation at the start of that interval, i.e.,

$$\int_{t_n}^{t_{n+1}} y'(t) \approx (t_{n+1} - t_n) y'(t_n) \tag{3.4}$$

$$= h y'(t_n) \tag{3.5}$$

In these expressions, $y'(t)$ is defined as the value of the differential equation at time t and h is the size of the time interval or the step size.

Equation 3.4 is an approximate expression for the amount that the solution changes during an interval of size h. Thus, if the value of the solution at the start of interval, $y(t_n)$, is known, equation 3.4 can be used to generate the value of the solution at the end of the time step, $y(t_{n+1})$. Expressed mathematically, this is the expression for the Euler method (equation 3.7), a method that will be used to solve differential equations in this work.

$$y(t_{n+1}) = y(t_n) + \int_{t_n}^{t_{n+1}} y'(t) \tag{3.6}$$

$$= y(t_n) + h y'(t_n) \tag{3.7}$$

The way that the Euler method finds the numeric value of a solution of differential equations is shown in figure 3-1. In this figure the 'Euler approximation' of the integral of the differential equation during a time step is shown as a black box, where the actual value of the differential equation during the interval is shown as a line. It is clear from this figure the Euler method's approximation of this integral is not always equal to the actual integral, i.e., $\int_{t_n}^{t_{n+1}} y'(t) \neq h y'(t_n)$. In fact, if it any stage during the time interval the differential equation is other than its initial value, then the Euler approximation introduces error (unless there is a fortuitous cancellation).

To illustrate the way that equation 3.7 can be used to solve a differential equation, it has

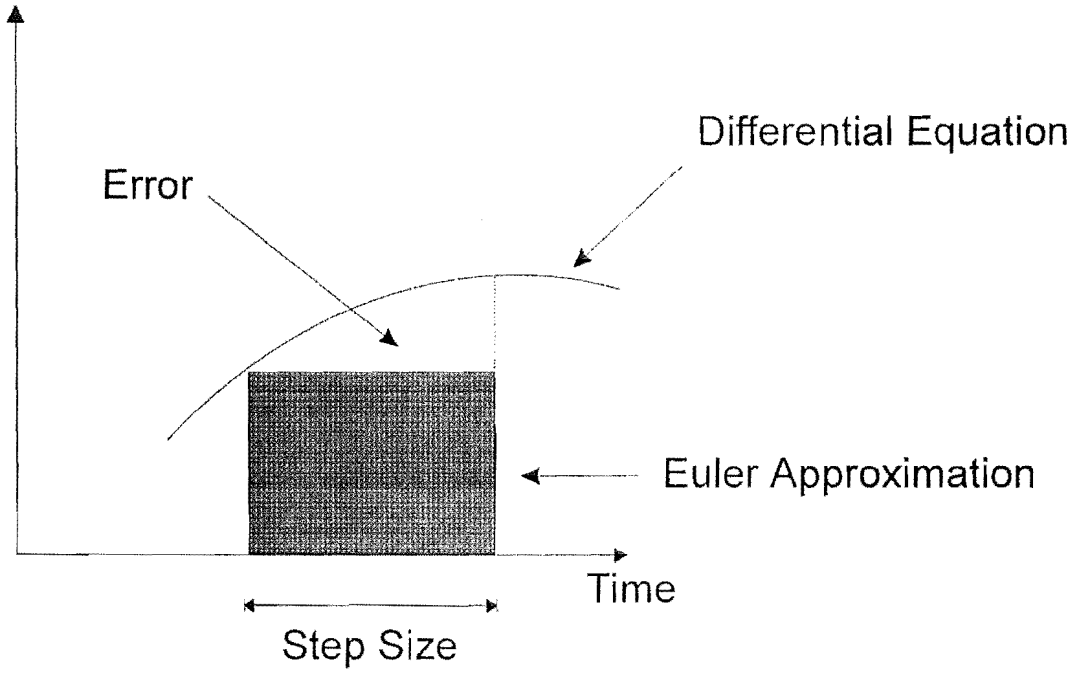

Figure 3-1: A schematic representation of the Euler method and the key features of the FDB numerical solution approach.

been used to solve equation 3.1. The Euler method begins with the initial conditions, i.e., $y(0) = 1$, and calculates the solution at $y(h)$. It then uses the solution $y(h)$ as the initial condition for the next step and calculates the solution $y(2h)$. The Euler method can be used over and over again until the solution at the final time has been calculated, i.e., $y(t_{final})$.

To solve equation 3.1 an integration step size of $h = 5.0 \times 10^{-3}$ s, i.e., 200 steps are taken to calculate the final solution at $t = 1$. Table 3.1 contains some of the values of the solution that are generated in the course of calculating the value of the solution at $t = 1$. This table illustrates how a numerical method moves forward in time generating new values of the solution as it goes.

A quick comparison of the final value of the solution shown in table 3.1 and that produced by the analytic formula (see above) reveals that these values are not identical; in fact, there is a 4% difference between them. This difference, known as solution error, is caused by the approximation of the differential equation (equation 3.1) during the time step, as explained above.

t	y′(t)	y(t)
0.00	5.00	1.00
0.10	7.31	1.60
0.20	10.74	2.48
0.30	15.83	3.78
0.40	23.41	5.70
0.50	34.66	8.54
0.60	51.38	12.75
0.70	76.23	18.98
0.80	113.16	28.24
0.90	168.02	41.98
1.00	249.55	62.39

Table 3.1: The solution of equation 3.1 by the Euler method.

h	y(1)	Φ(1) − y(1)
0.1	34.41	−30.49
0.05	45.59	−19.31
0.01	60.04	−4.86
0.005	62.39	−2.51
0.001	64.38	−0.52
0.0005	64.55	−0.35
0.0001	64.85	−0.05

Table 3.2: The error in the solution of equation 3.1 by the Euler method.

There are two major ways of reducing this error: 1) use a better approximation of the differential equations, i.e., a different expression to equation 3.4; 2) take smaller time steps. The effect that reducing the time step has on the error is shown in table 3.2. This table contains the solution of equation 3.1 by the Euler method for several values of the step size. As the step size decreases (more steps are taken) the difference between the exact and numerical solutions decreases (column three). Taking smaller steps decreases the error because it reduces the difference between the Euler approximation and the real value of the integral. This is because the Euler method is able to approximate the differential equations over a small interval more accurately than over a large time interval as the differential equations will normally change less in a small period of time than in a large period of time. Table 3.2 bears this out by showing that the numerical solution converges on the exact solution as the step size is decreased. Of course, this increase in accuracy comes at a cost. As the step size decreases and along with it the error incurred, the cost of obtaining the solution increases (with more steps, more computation is required to generate the solution).

In this discussion, we have seen that there are a number of major differences between analytic and numerical solution strategies. In summary, these are:

- The manner that they approach the solution of differential equations: analytic solution strategies employ a large array of standard mathematical strategies to solve differential equations, whilst numerical techniques involve the repeated use of simple approximations.

- The nature of the solution obtained: analytic solutions yield general mathematical expressions for the solution at any point in time; numerical solutions are the numerical values of the solution to one differential equation system from the initial conditions to some later time. This means that analytic solutions contain far more information about the general nature of the solution.

- The accuracy of the solution obtained: an analytic solution is an exact solution to the system from which it obtained. A number of error-introducing assumptions may be made to simplify the system being solved (see chapter two), but the solution obtained will be exact for that simplified system. A numerical solution on the other hand is not exact, and typically the amount of error in it can be reduced by decreasing the size of the integration

step.

- The systems to which they are applicable: of the differential equation systems that can be written down, vanishingly few have analytic solutions. In contrast to this, the majority of differential equations system can be solved accurately by a numerical solution algorithm.

3.3 Finite-Difference Methods

Central to any finite-difference method is the idea of dividing the period over which the differential equation has to be solved into many much smaller intervals. The strength of this technique is that it means that the a simple function can be used to describe the value of the differential equations as the function must only approximate the differential equations over a very short interval. Hence, the central assumption is that such a function can be used to approximate the differential equations during a time interval without introducing significant amounts of error. Once an appropriate approximate value for the differential equations during the time step has been found, then the amount that the solution to the differential equations changes during a time step can be estimated. This is done by multiplying the size of the interval by the rate of change during that interval (the value of the differential equations). From these two pieces of information – the solution at the start of the time step and the amount of change during the time step – it is possible to predict the value of the solution at the end of the time step. This is the essence of all finite-difference methods.

The two most important parts of calculating a solution via a finite-difference method are the choice of an appropriate step size and of an appropriate approximation function, e.g. $\int_{t_n}^{t_{n+1}} y'(t) \approx hy'(t_n)$ for the Euler method. If inappropriate choices are made for either of these components then a significant amount of error will be incurred. In the work that follows, we will see reappearing repeatedly the ideas of step size, of solution error, of the approximations that incur that error and of the concept of reducing that error by a number means. Because of their importance in what follows, these concepts are restated here.

- step size: the difference in time between the values of the solution that a finite-difference. method generates (h).

- Solution error: the difference between the exact and numerically generated solutions of a differential equation.
- Numerical approximation: the approximation of the differential equations during an integration step by a simple function.
- Ways of reducing solution error: solution error can be reduced by increasing the accuracy of the approximation of the differential equations, be it by decreasing the step size or using a more appropriate approximation function.

3.4 The Algorithm for Finite-Difference Based Numerical Solution Strategies

A series of computer programs have been written to implement the finite-difference based solution strategy explained above. All of these programs have at their core the same algorithm. The key steps in this algorithm are described below.

Initialization of Variables

The task that this algorithm performs first is the initialization of all the variables used in the calculation. When simulating intermittently initiated free-radical polymerization this involves setting the concentration of all species equal to zero apart from the initial concentration of primary radicals which is set equal to the concentration of radicals added by a burst of initiation. Also the monomer concentration is set equal to its initial concentration, i.e.,

$$R_0(0) = \rho \tag{3.8}$$

$$R_i(0) = 0 \qquad i \geq 1 \tag{3.9}$$

$$D_i(0) = 0 \qquad i \geq 0 \tag{3.10}$$

$$M(0) = M_0 \tag{3.11}$$

Evaluation of the Differential Equations

The next task is the evaluation of the differential equations. The values of all of the variables, for example the radical concentrations, are substituted into the differential equations, and these equations are evaluated. This yields the value of the differential equations at a particular time. Normally, this step is the most computationally expensive task in the prediction of the new value of the solution. This is because these equations are numerous and frequently involve the evaluation of large sums (see chapter one)

Calculation of the Next Value of the Solution

This step is at the core of all finite-difference based methods. The last values of the solution and the approximate values of the differential equations are combined to generate the new solution values, i.e.,

$$y(t_{n+1}) = y(t_n) + h\ A(t_n \text{ to } t_{n+1}) \tag{3.12}$$

Here $A(t_n \text{ to } t_{n+1})$ is the approximate value of the differential equations during the interval t_n to t_{n+1}.

Increment Time

The value of the simulation time is then increment by the size of the integration step.

$$t_{n+1} = t_n + h \tag{3.13}$$

Periodic Initiation

The current value of time is checked to ascertain whether it is equal to a multiple of the dark time, i.e., jt_0. If this is the case then the concentration of primary radicals (R_0) is increased by ρ.

Time Test

The solution of the differential equations continues until the simulation time is greater than the required time. If this is the case then the algorithm ends, otherwise the entire procedure

repeats.

3.5 Error in the Numerical Solution of Differential Equations

Previously it has be noted that numerical methods do not produce exact, error-free, solutions to differential equations. Rather, they produce solutions that contain error, where the amount of error in that solution depends on the solution strategy and differential equations involved. Here the different types of error incurred when using a numerical solution strategy will be discussed and methods of assessing and measuring that error developed. Having established these methods, we will begin to use this methodology to assess a simple numerical technique – the Euler method.

The error incurred by numerical solution strategies is a result of three types of approximation. Each approximation leads to a different type of error, these being round-off error, local truncation error, and global truncation error respectively. It should be noted that, although it is possible to describe each error type as if it were a separate effect, in any real calculation it is impossible for all but the most trivial cases to deconvolute each type of error.

3.5.1 Round-Off Error

Error is described as being 'round-off'error if it is a result of the way that a computer represents a number internally. For example, as a part of a calculation it might be necessary to divide 1 by 3. As the resulting number consists of an infinite series of threes, the computer must truncate it, as say 0.3333, and by doing so introduce error, in this case 0.01%. Typically, the magnitude of this type of error is so small that it may be ignored. It should be remembered though that this sort of error provides a lower bound on the error for any numerical calculation. That is, it is never possible to completely remove it when performing a numerical calculation. It should also be noted that as error is cumulative, the more times a function is evaluated the greater the amount of round-off error added to the solution. This means that it is not possible to achieve a desired level of accuracy simply by reducing the size of the time step, as a reduction in the time step increases the number of times the differential equations must be evaluated and subsequently the amount of round-off error that is added.

3.5.2 Local and Global Truncation Error

In contrast to round-off error, truncation error is not related to way in which the computer represents numbers internally, but to the way that the exact solution is approximated by the numerical method. For example, above we saw that the Euler method approximates the integral of a differential equation over a time interval by a simple box. Because of this approximation, there will normally be a difference between the exact and approximate solutions and this is known as the truncation error. Truncation error is the error that caused the majority of the difference between the analytic and numerical solutions to equation 3.1 (section 3.2).

Two types of truncation error are defined: these are called local (e_n) and global (E_n) truncation error respectively. Global truncation error is the difference between the final exact solution $\Phi(t_{final})$ and the final approximate solution $y(t_{final})$ and it is given by

$$E_n = \Phi(t_{final}) - y(t_{final}) \tag{3.14}$$

This error arises from two causes: (1) using an approximate formula to determine $y(t_{n+1})$ at each step; (2) the fact that the input data for each step is inexact, since in general $\Phi(t_n)$ is not equal to $y(t_n)$. If we assume that the input data is correct, then the only error in moving forward one step is due to the use of an approximate formula. This error is known as local truncation error.

The error of a particular numerical method is normally discussed in terms of the way that it depends on the step size. For example, the local truncation error of the Euler method is said to be of the order h^2. This means that the error added in one time step, assuming exact initial conditions, is proportional to the square of the step size. As h is typically far less that one, the greater the value of exponent to which h is raised the smaller the amount of error added by a time step, and subsequently the better the numerical method. Unfortunately, for all but the first time step it is impossible to deconvolute the two types of truncation error. So when talking of truncation error reference is normally made to the global truncation error. It is possible to derive the relationship between local and global truncation error, but this is beyond the scope of this thesis. A rule of thumb will be given that describes this relationship. For the complete derivation of this, refer to numerical mathematics textbooks, such as Burden and Faires.[13]

This rule of thumb says that the global truncation error should be proportional to h raised to an integer one less than that for the local truncation error. For example, the global truncation error for the Euler method is h^1. In this thesis, the scaling law for the local truncation error will be described when the numerical solution technique in question is introduced and then the rule of thumb invoked to predict the global truncation error. Note that it is important to have an expression for the global rather than the local truncation error, as only this error is relevant to analysis. As an example, the local truncation error in the Euler method is now derived.

3.5.3 Truncation Error in the Euler Method

The order of local truncation error generated by this method can be derived as follows. The solution predicted by the Euler method is subtracted from the Taylor series expansion of the exact solution, $\Phi(t)$ (equation 3.15). This difference is shown as equation 3.16.

$$\Phi(t+h) = \Phi(t) + h\Phi'(t) + \frac{h^2\Phi''(t)}{2!} + ... \tag{3.15}$$

The exact solution at $t+h$ is given by equation 3.15. Note that $\Phi'(t)$ denotes the first derivative with respect to time and that the n^{th} derivative is denoted by n accents.

$$\Phi(t_{n+1}) - y_{n+1} = \{\Phi(t_n) - y_n\} + h\{\Phi'(t_n) - y'_n\} + \frac{1}{2}\Phi''(t_n)h^2 + ... \tag{3.16}$$

Note that as h is less than one the higher order terms can be ignored. As local truncation error excludes error derived from inexact initial conditions, it can be assumed that $y(t_n) = \Phi(t_n)$ and $y'_n = \Phi'(t_n)$. Therefore, equation 3.16 reduces to

$$e_{n+1} = \Phi(t_{n+1}) - y_{n+1} = \frac{1}{2}\Phi''(t_n)h^2 \tag{3.17}$$

This suggests that the local truncation error in the Euler method is proportional to the step size squared, i.e., h^2. Therefore, as was stated above, the global truncation error is proportional to h.

3.6 The Assessment of the Truncation Error

Scaling laws of the above type are useful, in that they give an estimate of the accuracy of a numerical technique. However, they suffer from one fundamental limitation - they are system independent. They provide minimal information about the magnitude of truncation error that will be produced when a numerical technique is applied to a particular system of differential equations. For example, whereas one system of differential equations can be solved almost error free with a low-level technique, another may yield solutions high in error when solved with the same method. In other words, the order of the truncation error merely indicates how the error scales with step size, not the magnitude of the absolute error.

Considering the importance of differential equations in the modeling of a wide range of processes and interactions it is not surprising that there are mathematical techniques that provide a more comprehensive assessment of solution error. However, these techniques have limited applicability. Normally, they can be used only on simple systems that contain a small number of differential equations and provide limited information. As this criteria is not met by the system studied in this thesis, yet another strategy of error assessment must be employed. This strategy, which is the technique used extensively in this thesis, uses computer experiments to assess the magnitude of truncation error. To use this method one runs a series of computer experiments where the system of differential equations in question is solved with a wide range of solution strategies and for a large range of variables, e.g., step size. The error in the solution produced by the computer experiment is then measured (see later for error measurement techniques) and conclusions are drawn about the nature of the truncation error.

3.7 The Measurement of Truncation Error

The crucial step in any study of truncation error is the measurement of that error. There are two ways of estimating this error. The first group of methods are known as internal comparisons. These involve comparing a solution obtained at a moderate step size, i.e., low level of accuracy, with a solution obtained with a small step size, i.e., a high level of accuracy. For example, the error in the solution of a system of differential equations could be calculated with a step size of $h = 1 \times 10^{-8}$ s and this solution used as a standard for all subsequent calculations.

This method has an important limitation, which is that several types of error are not removed by decreasing the step size. For example, in a system where round-off error is important, simply decreasing the step size will not remove this error. Therefore, if the set of solution values obtained at a small step size is used as a reference for calculating the error, the truncation error estimated will be incorrect. This is because there is general error that is not removed by using a small step size. For instance, a numerical method may introduce a large amount of error, of which only a small amount is removed by decreasing the step size. If we were to measure the error introduced by this method relative to the solution obtained by the same method with a small step size, the resulting estimate of the error would grossly underestimate the error in the solution. There are ways of circumventing this problem, for example by comparing the solution obtained by one solution method with those obtained by another solution method. However, comparison of this type still yield values of the error that are relative to error in the solution obtained with a small step size..

The second type of error measurement strategy, called here external comparison, avoids this problem. With this method, error is measured by comparing simulated values with an exact analytic solution. For example, there exists an exact analytic expression that describes the way that the total concentration of radicals in an intermittently initiated free-radical polymerization changes with time (see chapter one). To assess the error using this analytic function, one uses this expression to predict the total radical concentration. Next one extracts the same parameter from the simulation data, and calculates the difference between the two. Although this method gives a value for the error that is not relative to another error containing solution (as the analytic solution is exact), it is also subject to a number of limitations. Primarily, these are a result of the paucity of analytic expressions for intermittently initiated polymerization. As this method relies on analytic expressions that describes some facet of this type of polymerization, we are constrained to measuring the error in values only where there exists an analytic expression. For example, we saw in chapter two that there exists no analytic expression for the dead polymer chain-length distribution in an intermittently initiated free-radical polymerization. Because of this, it is not possible to use a completely external comparison to estimate the error in this distribution, and we must resort to internal comparisons. In this study, error is mainly measured by external comparisons. In cases where there are no analytic expressions, internal

comparisons are used.

3.8 Error Standards

To implement the ideas outlined above, four error standards have been established. Each error standard uses one analytic expression, or external comparison, to probe the error introduced in the solution of the differential equations that model PIP. Although each error standard only investigates one facet of the solution error, collectively they can be used to develop a detailed understanding of the way that error is introduced.

3.8.1 Error Standard One

The first error standard uses the well known analytic expression for the total radical concentration in intermittently initiated polymerization. This expression (equation 3.18) describes the way that total radical concentration depends on the time since the last initiation. This equation was introduced in chapter one and only holds between bursts of initiation.

$$\mathrm{R}_t = \frac{\mathrm{R}_{max}}{2k_\mathrm{t}\mathrm{R}_{max}t + 1} \tag{3.18}$$

Here the symbols are defined as:

- R_{max} the maximum radical concentration, which is the radical concentration at time zero, just after the arrival of a laser pulse (mol.L^{-1});
- t time, the time in seconds since the arrival of the last laser pulse
- k_t the rate constant for termination (L.mol^{-1}.s^{-1});
- R_t the radical concentration at time t (mol.L^{-1}).

To employ this error standard the total radical concentration is calculated by taking the sum of the concentration of radicals of each chain length predicted by the numerical solution of the differential equation. The total radical concentration predicted by equation 3.18 is also

evaluated. These two values are then substituted into equation 3.19.

$$E_t = \left| \frac{(\mathrm{R}_t)_{analy} - (\mathrm{R}_t)_{sim}}{(\mathrm{R}_t)_{analy}} \right| \tag{3.19}$$

Here E_t is the error in the total radical concentration, $(\mathrm{R}_t)_{analy}$ is the total radical concentration from the equation 3.18 and $(\mathrm{R}_t)_{sim}$ is the total radical concentration from a simulation. The values of E_t are calculated after every integration step are summed to give the average error per initiation period (note the arithmetic mean has been used). Normally, this calculation is only performed after the system has reached pseudo-steady state (after five laser pulses), although calculations have been performed that monitor the error during the pre-pseudo-steady state of the polymerization (see below). This error standard returns a value that is an all-purpose estimate of the error added to this system. Note that it provides no information about how the error per integration step changes during the time between laser pulses. Moreover, it also does not provide detailed information concerning the error in the individual radical concentrations. However, as by definition the total radical concentration is the sum of the individual radical concentrations, it does provide some information about the error in the individual radical concentrations. Nonetheless, a method is developed that allows an in-depth analysis of the error in the individual radical concentrations (see below).

3.8.2 Error Standard Two

The second error standard makes use of the same analytic expression as error standard one. However, instead of calculating the average error over each initiation period, this error standard records the solution error for each integration step. This allows a graphical representation of the dependence of the solution error upon time to be made. This error standard provides information about how the error per integration step varies with the time since the laser pulse.

3.8.3 Error Standard Three

This error standard is based on a different analytic expression to the one used above. The analytic expression used in this standard describes the radical chain-length distribution as a function of time and has been developed as a part of this work (see chapter two). Recall that

this solution is exact.

$$R_i = \frac{\exp(-k_p M t)}{2k_t t R_{max} + 1} \sum_{j=0}^{i} R_j^{last} \frac{(k_p M t)^{i-j}}{(i-j)!} \tag{3.20}$$

Here the symbols are defined as above, and in addition:

- M is the monomer concentration (mol.L^{-1});
- k_p the rate constant for propagation (L.mol^{-1}.s^{-1});
- R_j^{last} is the concentration of radicals of chain length j at the arrival of the last laser pulse (mol.L^{-1}). In contrast to the earlier "analytic" use of equation 3.20, the values of $R_j^{last}$and R_{max} used now calculated naturally as a part of a numerical simulation: they are just the R_j^{last} and R_{max}values immediately after the arrival of a laser pulse. In this way equation 3.20 is relatively easy to use.

By using this expression, one can gain information about the chain-length dependence of error. That is, whereas error standard one analyses the error in the total radical concentration, this error standard focuses on the error in the concentrations of individual radical species. Evaluating this expression is computationally expensive so it must be used sparingly. This has been done by only calculating the error in a small number of radical species at select times. This error is then plotted against time and chain length. Usually five initiation periods are allowed to pass before the error is calculated.

3.8.4 Error Standard Four

The final error standard is the only one of the four used in this study that uses an internal, rather than external, comparison. To interrogate the error added by the various numerical solution strategies, this error standard records the rate of change in the concentrations of radicals of several chain lengths, for example $\frac{dR_0}{dt}$, $\frac{dR_1}{dt}$,and $\frac{dR_{10}}{dt}$. This is an important error standard as it provides information about the shape of, and the error incurred in, the actual equations that are being solved: the differential equations.

It should be noted that all of the error standards outlined above focus on the error incurred in the solution of the differential equations that model the concentrations of the radical species. A thorough investigation of both the effect of this error upon the dead polymer chain-length

distribution and the error incurred in the solution of the differential equations for these species will be performed in chapter five.

3.9 Solution Strategy Efficiency

In this chapter, I have gone in to considerable detail in describing the error incurred by finite-difference based solution techniques and developing methods for of measuring that error. However, another factor must be taken in to account when assessing solution strategies. This is the computational effort required to obtain the solution. For even if a solution strategy is able to produce a solution that is effectively error free, that solution strategy is of little use if the time taken to obtain that solution strategy is inordinately long. In this section, a method for assessing solution strategies that includes not only the error incurred but also the computational cost of obtaining that solution is developed. Central to this method is a parameter, ξ – the efficiency value. This parameter is defined as the product of the error incurred per initiation period, as measured by error standard one, the number of integration steps per pulse and the number of evaluations of the differential equations per integration step, i.e.,

$$\xi = E_{pulse} \cdot n_{steps} \cdot \sigma_{des} \tag{3.21}$$

In equation 3.21, E_{pulse} is the error added per pulse (assessed via error standard one), n_{steps} is the number of integration steps taken per pulse and σ_{des} is the number of evaluations of the differential equations per integration step. Note that this definition of the efficiency value has an empirical rather than a theoretical basis.

By defining the efficiency of the numerical solution in this manner we are assuming that most computationally expensive task in solving these equations is the evaluation of the differential equations. To test this assumption, simulation studies were performed that profiled the time taken for each part of the numerical solution. These simulations indicated that when bimolecular termination is allowed to occur only via the disproportionation mechanism, that the evaluation of the differential equations took 90% of the computer time needed to solve these differential equations. In contrast to this, when termination was allowed to also occur by the combination termination mechanism that this percentage increased to 98%. The results of

these simulations provide strong evidence in favor of defining the efficiency value in the above manner. It should also be noted that proportion of the computational effort spent on differential equation evaluation would increase as the number of differential equations to be solved increases.

Although the efficiency value is pivotal to the assessment of numerical solution strategies that follows, it must be treated with some care. In general, a low value of ξ indicates an efficient solution algorithm. Although this is generally true, this value must be coupled with the absolute values of the error and the computer time. For instance, there are trivial cases where the blind use of the efficiency value can lead to erroneous conclusions. Take the case, for example, where a numerical solution algorithm gives a solution that is high in error with almost no computational expense. Such a numerical method could give a low value of the efficiency value and yet still be a poor solution strategy. In light of this the efficiency value and the error per initiation period will be presented side by side throughout this thesis

The difference between the efficiency of a solution strategy and its efficiency value should be stressed. There is an important difference between the efficiency of the solution strategy (which we wish to increase) and the efficiency value (that we wish to decreases) and these may be easily confused.

3.10 The Development of the Euler Method: A Case Study

For the rest of the chapter, the methodology outlined above will be used to assess the simplest of the finite-difference based methods: the Euler method. This assessment will not only allow us to appraise the error incurred by the Euler method, but also to develop an understanding of the nature of error incurred. A significant amount of time will be spent explaining the origin of the solution error in these systems. This is important for two reasons. Firstly, knowledge of the error incurred by the Euler method can be used as a basis for understanding the error incurred by the more elaborate methods implemented in chapter four. Secondly, from this understanding several ideas for refinements to these methods, which increase the efficiency of these numeric solution techniques, are developed.

3.10.1 Differential Equations

In this study the Euler method will be used to solve the population-balance differential equations that characterize intermittently initiated free-radical polymerization. These equations are:

$$\frac{d\mathrm{R_0}}{dt} = R_{init} - k_p \mathrm{MR_0} - 2\mathrm{R_0} k_\mathrm{t} \sum_{j=0}^{L} \mathrm{R}_j \tag{3.22}$$

$$\frac{d\mathrm{R}_i}{dt} = k_p \mathrm{MR}_{i-1} - k_p \mathrm{MR}_i - 2\mathrm{R}_i k_\mathrm{t} \sum_{j=0}^{L} \mathrm{R}_j \qquad 1 \leq i < L \tag{3.23}$$

$$\frac{d\mathrm{R}_L}{dt} = k_\mathrm{p} \mathrm{MR}_L - 2\mathrm{R}_L k_\mathrm{t} \sum_{j=0}^{L} \mathrm{R}_j \tag{3.24}$$

Equation 3.22 is the population-balance differential equation for primary radicals, equation 3.23 is the differential equation for radicals species of chain lengths 1 to $L-1$ and equation 3.24 is the differential equations for radicals of length greater than or equal to L. In equations 3.22 - 3.24, R_i stands for the concentration of radicals of chain length i, k_p and k_t denote the rate coefficients for propagation and termination respectively, and M is the monomer concentration. The rate of initiation, R_{init}, is zero apart from at times jt_0, where j is a counting number, and t_0 the length of time (s) between bursts of initiation. At these times $\mathrm{R_0}$ is increased by ρ, the concentration of radicals added by a burst of initiation. All simulations include radical species up to, and including, a chain length of 5000 ($L = 5001$). The long-chain differential equation covers radical species of higher chain length.

3.10.2 Simulation Parameters

The same set of rate parameters is used in all calculations unless otherwise stated. These are presented in table 3.3. In this table, all symbols have the same definitions as they do in the differential equations, and in addition t_{sim} the simulation length.

At the start of all simulations the concentrations of all species are set equal to their initial values (zero, unless otherwise indicated) and left to change for the period of the simulation. The values of the error and the concentrations of the living radicals are written to data files periodically throughout the calculations. All simulations were performed on a VAX mainframe

Rate Parameter	Value	Units
k_p	100	L.mol.s^{-1}
M	10	mol.L^{-1}
k_t	1×10^{8}	L.mol.s^{-1}
ρ	1×10^{-6}	mol.L^{-1}
Freq. of Initiation	10	Hz
t_{sim}	2	s
h	1×10^{-4}	s

Table 3.3: Default rate parameters used in all calculations in chapter three. Note that the rate coefficient for termination used in these calculations is different from that used in chapter two.

and monitored through a PC workstation. All computer programs were written in the C programming language and complied with the Borland C++ v. 5 compiler, employing standard C library functions. In these programs, all non-integer variables were declared real. The American convention for termination rate coefficients has been used throughout this thesis (e.g., see equations 3.22 - 3.24).

3.10.3 Constant Step-size Profile

In this section, the Euler method is used with a constant step-size profile. As was mentioned above the step size is the length of time between successive solution values. A step-size profile is a function that describes the size of an integration step at any particular moment in time. Thus, a constant step profile is an example of a time independent step-size profile (TISSP), i.e., the same value is used throughout the simulation. Later, several time dependent step-size profiles (TDSSPs) will be used in conjunction with the Euler method.

Error standard One

The mean error per initiation period has been measured using error standard one. This has been done for a wide range of step sizes and other simulation parameters. The error found by this method has then been plotted against step size and these results are presented in figures 3-2 and 3-3 (note that $(k_p M)^{-1}$equals 1×10^{-3}s for the default rate parameters). To assess whether the error scales with step size in the manner predicted above, i.e., error $\propto h$, the plots

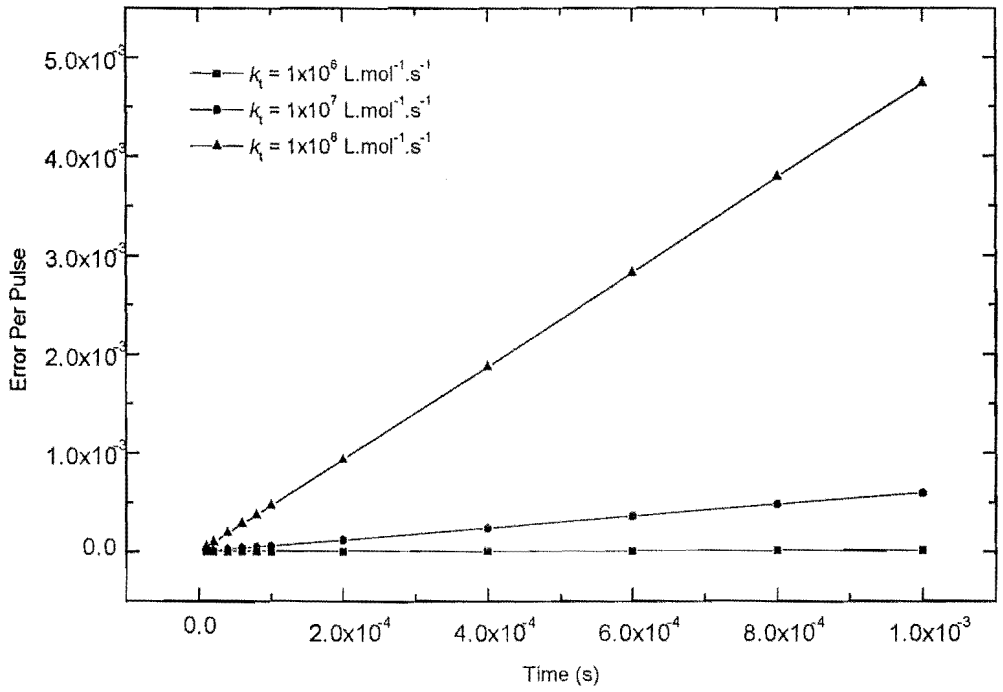

Figure 3-2: Correlation between error per pulse and integration step-size for the Euler method with a constant step-size profile. Rate parameters as per table 3.3.

of error against step size have be fitted with a linear relationship (equation 3.25).

$$E = A + Bh \tag{3.25}$$

The results of this analysis of the data of figure 3-2 is presented in table 3.4.

In this table, A denotes the y-intercept of the fitted line, B the slope of that line and R the correlation coefficient[1]. This data shows three features that will be discussed.

[1] $R = \frac{\sum_i (x_i - \bar{x})(y_i - \bar{y})}{\sqrt{\sum_i (x_i - \bar{x})^2}\sqrt{\sum_i (y_i - \bar{y})^2}}$ In this, expression x_i and y_i are pairs of quantities, in this case, the error per pulse and the step-size, and this test returns a value which is a measure of the correlation between x and y. The value of R lies between -1 and 1 inclusively, where a value of $R = 1$ is known as a complete positive correlation and a value of R = -1 a complete negative correlation. Either of these values suggest that data fits a straight line very well.

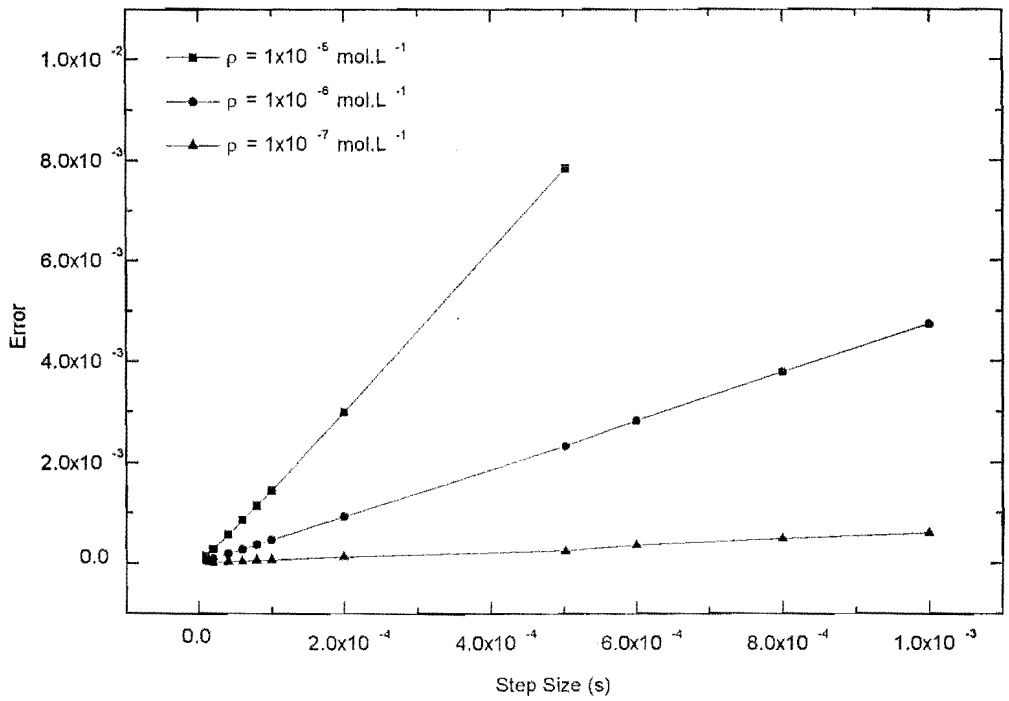

Figure 3-3: The affect of the concentration of radicals added by a burst of initiation upon the correlation between error per pulse and integration step-size for the Euler method with a constant step-size profile. Rate parameters as per table 3.3.

The Magnitude of Error Incurred It is clear from these figures that the error incurred by the Euler method is very low for a wide range of step sizes and rate parameters. The maximum value of the error incurred during these simulations is 0.8% of the total radical concentration. In subsequent analysis (chapter five) it will be shown that although this error causes noticeable effects in the final simulated MWD, even at this level of accuracy the simulated results can be used with confidence.

Dependence of Error on step size There is a strong positive linear correlation between the integration step size and the mean error per pulse. This is shown by the good fits of all data sets to straight lines in figures 3-2 and 3-3 and by the fact that all of the correlation coefficients

k_t (L.mol^{-1}.s^{-1})	A	B	R
1×10^6	$(4 \pm 3) \times 10^{-8}$	$(1620 \pm 6) \times 10^{-5}$	0.999
1×10^7	$(6 \pm 7) \times 10^{-7}$	$(597 \pm 6) \times 10^{-4}$	1.000
1×10^8	$(-9 \pm 4) \times 10^{-6}$	$(474 \pm 9) \times 10^{-3}$	1.000

Table 3.4: Statistical data obtained when the data in figure 3.2 is fitted with equation 3.25

in table 3.4 are equal, or approximately equal, to 1. This proves that the predicted scaling law holds for this system, and that the mean error per pulse is proportional to the step size used. It also indicates that mean error per pulse incurred in the solution of these differential equations can be decreased by lowering the step size. It should be noted that the rate at which the error decreases with step size depends on a number of rate parameters (see below), and that it is not possible to reduce the error to zero by this means (due to round-off error).

Dependence of Rate of Change in Error with step size on Several Rate Parameters
To explore the magnitude, as well as the origin, of the change of the error with step size, a number of simulations has been performed. In these, the mean error per pulse was measured for a range of values of k_t and ρ. These results are presented in figures 3-2 and 3-3. This study indicated that both k_t and ρ affect the correlation between the mean error per pulse and the step size. From figures 3-2 and 3-3 (pay attention to the slope of the lines), and also column B in table 3.4, it is clear that an increase in either k_t or ρ increases the rate of change of the error with step size. This means that if a system of differential equations with a high rate of termination is solved more error will be incurred at a certain integration step size than for the same system with a low value of k_t. Moreover, it means that increasing the step size in a high k_t system rapidly increases the error incurred. Thus, the difficulty of accurately solve the differential equations for a PIP system increases as k_t does. The same line of reasoning follows for system where the value of ρ is high.

Before explaining the reason for this effect it is timely to outline in greater detail the inner workings of the Euler method. Figure 3-1 is a schematic representation of the Euler method solving a hypothetical differential equation. To recap, the Euler method approximates the value of a differential equation during an integration step by the value of that differential equation at the start of the step. It follows from this that the Euler method is sensitive to changes in the differential equation during an integration step. In the example shown in

figure 3-1, the differential equation increases during the integration step. Thus, as the Euler method approximates the value of the differential equation during the step by its value at the start of the step, it underestimates the integral of the differential equation. This means that the estimated solution is lower than the true solution. Note that the opposite occurs if the differential equation decreases during a time step. Moreover, the magnitude of the error that the Euler method introduces is proportional to how much the differential equation changes from its initial value. In general, it can be said that the greater the rate of change in a differential equation, the greater the error incurred by the Euler method. This conclusion agrees with the expression derived for the local truncation error (equation 3.17). This expression says that the local truncation error incurred by the Euler method is proportional to, Φ'', the rate of change in the differential equation.

Given this, how does it help us explain the greater sensitivity to error of systems where k_t or ρ is high? To explore this, an expression for the rate of change in the PIP differential equations has been derived. This is done by observing that the rate of change in the sum of the differential equations for radicals of each chain length is equal to the rate of change in the differential equations for the total radical concentration. To derive an expression for the rate of change in the total radical concentration one begins with the analytic expression for the way that total radical concentration changes with time, equation 3.18. If this expression is twice differentiated with respect to time, it yields equation 3.26.

$$\frac{d^2\mathrm{R}_t}{dt^2} = 8\mathrm{R}_{max}^3 k_t^2 (1 + 2k_t \mathrm{R}_{max} t)^{-3} \tag{3.26}$$

Substituting the expression for the maximum radical concentration derived in chapter one into this expression gives equation 3.27.

$$\frac{d^2\mathrm{R}_t}{dt^2} = \frac{8\rho^3 (\frac{1}{2} + \sqrt{\frac{1}{4} + \frac{1}{2k_t t_0 \rho}})^3 k_t^2}{(1 + 2k_t \rho (\frac{1}{2} + \sqrt{\frac{1}{4} + \frac{1}{k_t t_0 \rho}})t)^3} \tag{3.27}$$

This expression shows that relationship between the rate of change in the differential equations and the values of k_t and ρ is complicated. However, an expansion of this expression reveals

k_t (L.mol^{-1}.s^{-1})	ξ
1×10^6	1.66×10^{-1}
1×10^7	6.03×10^{-1}
1×10^8	4.64

Table 3.5: The efficiency value for the Euler method solving the default kinetic system with a constant step size profile.

that as an crude approximation equation 3.28 holds. This says that:

$$\frac{d^2 R_t}{dt^2} \propto (\frac{k_t \rho}{t})^3 \tag{3.28}$$

It follows from this expression that increasing either ρ or k_t increases the rate of change in the differential equation, and subsequently it increases the error in the solution of equations 3.22 - 3.24. For the sake of brevity and also because both k_t and ρ have similar effects on the phenomena discussed here, only the effects of changes to k_t will be explored from now on. It should also be noted that this expression predicts that the rate of change in differential equations 3.22 - 3.24, and therefore the error in their numerical solution will tend to zero at infinite time.

Solution Efficiency To be able draw conclusions about the applicability of the Euler method, the computational cost of using this method must also be considered. To do this the efficiency will be calculated using equation 3.21. However, before we are able to use this expression we must first find values of n_{steps} and σ_{des}. As constant step-size profile is used in these simulations, n_{steps} is simply the length of time between pulses divided by the size of the integration step, i.e.,

$$n_{steps} = \frac{t_0}{h} \tag{3.29}$$

In addition to this, as the Euler method requires the differential equation to be calculated only once per step, i.e., the value of σ_{des} is equal to one .

As E_{pulse} is linearly dependent on the step size, i.e., $E_{pulse} \propto h$, and n_{steps} is inversely proportional to the step size, i.e., $n_{steps} \propto \frac{1}{h}$, the dependencies of E_{pulse} and n_{steps} cancel each other out and the efficiency value is independent of step size, i.e., it is constant for all step sizes. Table 3.5 contains the efficiency values for the three data sets shown in figure 3-2.

Since the efficiency value is constant for all step sizes, there is no one step size that gives optimal solution efficiency from the Euler method with a constant step size profile. To choose a step size one must consider the maximum error that one is willing to incur and choose the appropriate step size to achieve this. As was noted above, it is harder (more steps must be taken per pulse) to achieve a certain level of error when the values of k_t or ρ are high. For example, if it was decided that the maximum error per pulse period that could be allowed was 1×10^{-5} then one would need to use a step size of 6×10^{-5}s when $k_t = 1 \times 10^6$L.mol^{-1}.s^{-1}, 1.7×10^{-5}s when $k_t = 1 \times 10^7$L.mol^{-1}.s^{-1} and 2.2×10^{-6}s when $k_t = 1 \times 10^8$L.mol^{-1}.s^{-1}. These values show clearly that significantly more effort (more than ten times as many steps per pulse) is required to achieve the same level of error in the solution of these equations when a high rate constant for termination is used.

In fact, there are simple linear relationships between the integration step size that must be used to achieve a certain level of error and k_t and ρ. These relationships are not derived here, as this is only the first attempt at using the Euler method. In the sections that follow refinements will be made that significantly increase the efficiency of the Euler method. In these sections the relationships between step size and numerical error will be derived as then they have practical relevance.

Error Standard Two In this section, error standard two will be used to examine the temporal dependence of the error incurred in the solution of the population-balance differential equations that describe PIP. To date attention has focussed on the mean error per pulse. In contrast to this, here we are interested in how the error added at each integration step depends on the time since the last laser pulse.

Error standard two measures the error in the same manner as error standard one, by taking the difference between the simulated total radical concentration and that predicted by the analytic expression. However, unlike error standard one, error standard two records the value of that error at each time step. Figures 3-4 - 3-6 are the error-time profiles for three simulated systems. All of the simulation parameters used in these simulations are the same as those shown in table 3.3, except for the rate coefficient for termination, which is different in each case.

It is clear from this set of graphs that the error has a complex dependence on the time since

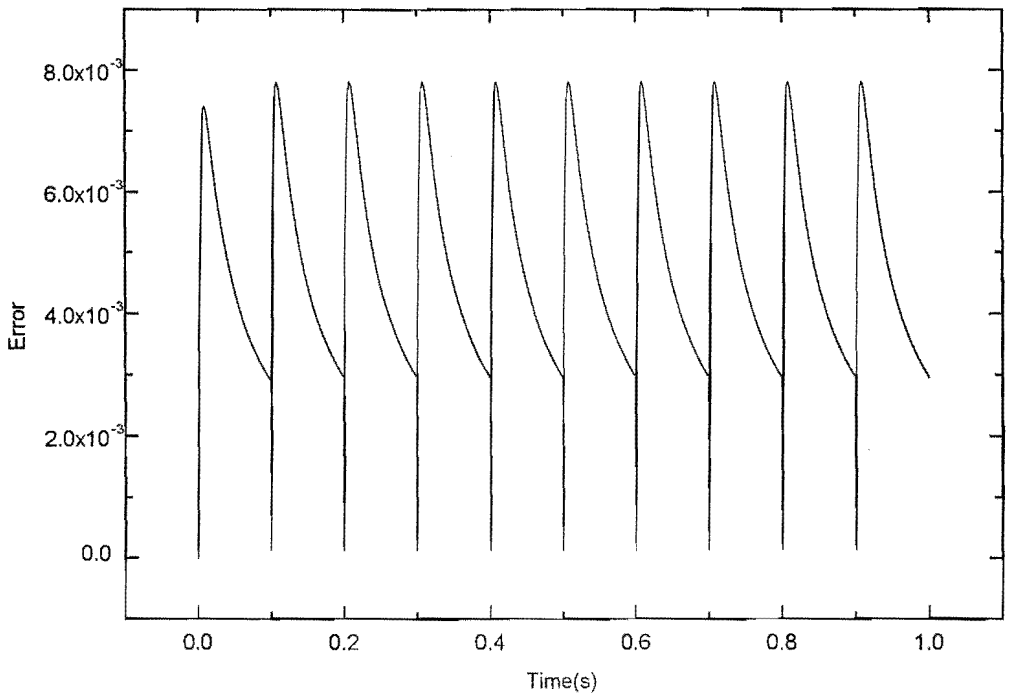

Figure 3-4: Temporal Dependence of Error in the Solution of the Differential Equations. The rate coefficient for termination is equal to 1×10^8 L.mol^{-1}.s^{-1}and all other rate parameters are as per table 3.3.

a burst of initiation. Moreover, the nature of this dependence is strongly influenced by the rate coefficient for termination. Although there are a number of differences between these three plots, there are also several similarities, including: a regular repeating pattern with the same periodicity as the initiation profile (in this case 10 hz); an increase in the amount of error added per pulse followed by a decline and the fact that a pseudo-steady state in error is obtained. In this section, we are going to begin by discussing each of these general features in turn. Having completed this description, we will turn our attention to the effect of the rate constant for termination on the error and the way that it changes with time. The features that we wish to discuss are shown with the greatest clarity in figure 3-5. For this reason, this discussion will be limited to figure 3-5. However, the other two figures do show the same qualitative behavior, a

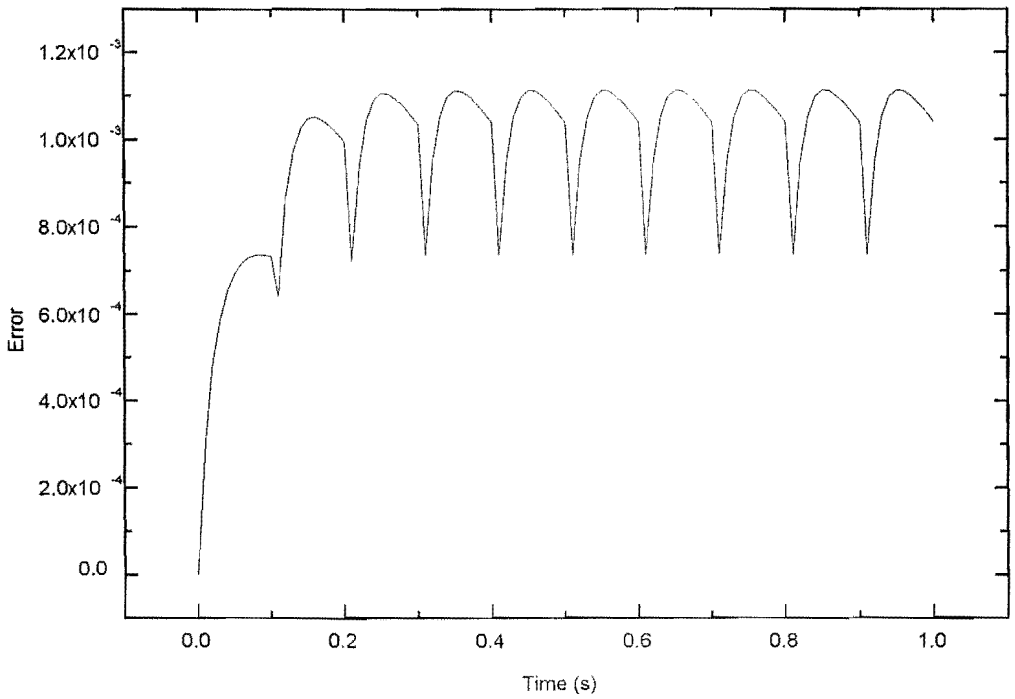

Figure 3-5: Temporal Dependence of Error in the Solution of the Differential Equations. The rate coefficient for termination is equal to 1×10^7 L.mol^{-1}.s^{-1}and all other rate parameters are as per table 3.3.

discussion of the differences between these plots will be given at the end of this section.

General Profile of the Error Between Two Bursts of Initiation The first feature that we will discuss is the general profile of the error between successive initiations. In general, there is an initial increase in the amount of error added followed by slow decline. To explain this phenomenon we need to revisit some ideas pertaining to the nature of the error added by the Euler method.

There are two types of error. The first, known as truncation error, is a result of the approximation of the differential equations during an integration step by the value of those differential equations at the start of that step. This error will always underestimate the total radical con-

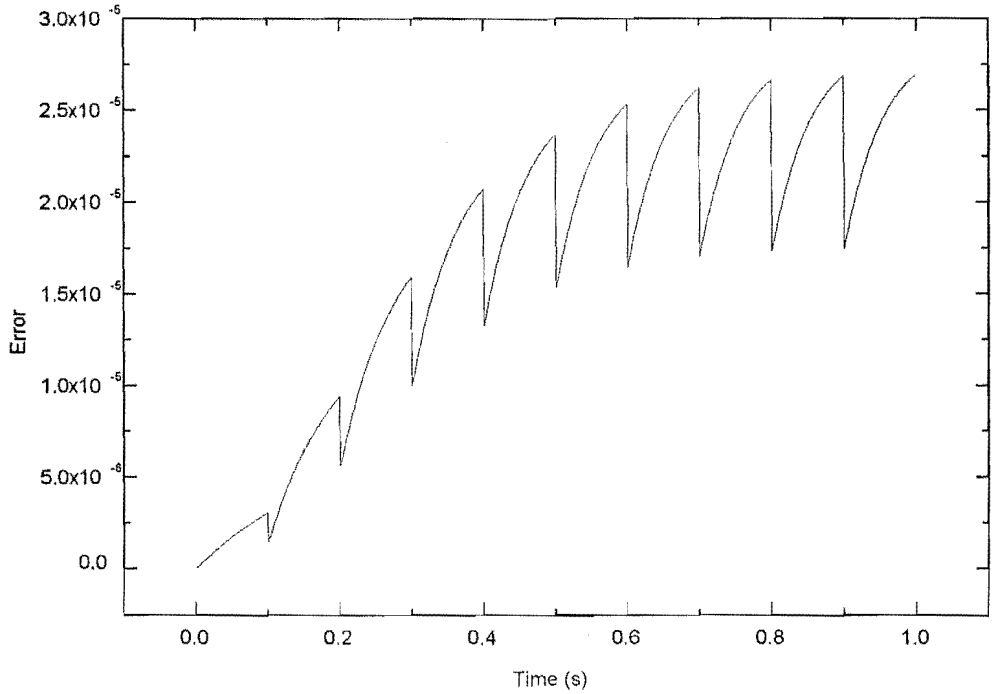

Figure 3-6: Temporal Dependence of Error in the Solution of the Differential Equations. The rate coefficient for termination is equal to 1×10^6 L.mol^{-1}.s^{-1}and all other rate parameters are as per table 3.3.

centration[2], as the differential equation for the total radical concentration is always increasing (becoming less negative). Thus the value of the total radical concentration predicted by the Euler method is always less than the real value. Thus, truncation error is a negative error, i.e., the simulated value is less than the real value. The second type of error, that will be called initial-condition error, is caused by the fact that for all steps, apart from the first, the initial conditions are inexact. The initial conditions for each step are equal to the value of the solution, as calculated by simulation, at end of the last step. As the Euler method underestimates the total radical concentration, the initial conditions used will always be less than the exact initial conditions. Furthermore, as the rate of termination is proportional to the square of the total

[2]Note that truncation error could be positive error if the laser pulsed during an integration step.

radical concentration, the estimated rate of termination is less than the real rate of termination. Hence, initial-condition error leads to an increase in the total radical concentration. It is a positive error. Note that the amount of initial-condition error incurred is proportional to the square of difference between the exact and simulated total radical concentrations. This is because the magnitude of the difference between the inexact and exact total radical concentrations influences the difference between the actual and predicted rates of termination. Hence, a large difference between exact and inexact total radical concentrations causes a large difference between the true and actual termination rates. As this error is proportional to the square of the difference between the two concentrations and opposite in sign to the error present, it is self correcting. The initial-condition error decreases the amount of error present by moving the simulated value closer to the actual value.

Although both of types of error are present at all times, apart from the first step, there are times when one error type is dominant. To understand when this is the case, we will discuss the dependence of both error types upon time.

In general, the amount of truncation error added per step decreases as the time since the periodic initiation increases. This follows from equation 3.28 where the time appears in the denominator. The rate of change and therefore, the amount of truncation error decreases with time. It should be noted that although the truncation error added per integration step decreases with time, error is cumulative, so that if only truncation error was incurred, the error in the numeric solution would increase with time.

Initial-condition error does not have a direct dependence upon time. It depends upon the amount of error already present in the solution. Therefore, as we know that the error in the solution due to truncation error accumulates as time passes, it is reasonable to expect that initial-condition error will also increase with time. In summary, it is expected that truncation error should dominate when the system is effectively error free, such as straight after the arrival of the first laser pulse. However at all other times, initial-condition error should play an important role.

To fully explain the general effect that is observed in the error added per step between two bursts of initiation, the relative importance of two error types will be discussed for a number of times between the two bursts of initiation. Note that these times correspond to figure 3-5.

The first point in time corresponds to straight after a burst of initiation. At this time, the initial conditions are exact, so that all the error is due to truncation error. In addition, a large amount of truncation error is added at this time as the differential equations are changing rapidly.

At some time latter, for example 0.02 s after a burst of initiation, the situation is a little different. The initial conditions are no longer exact, so that the initial-condition error is no longer zero. However, as the difference between the exact and simulated solutions is still small, the amount of initial-condition error incurred is minimal. Nonetheless, the initial-condition error reduces the total error. This effect is accentuated by the decrease in the truncation error that occurs as time passes (see equation 3.28). Overall, the initial-condition error and the decrease in truncation error both contribute to an overall reduction in the total error. This is shown in figure 3-5 by a decrease in the rate at which error increases with time.

At yet a latter time, for example 0.08 s after a pulse, the situation is different again. The difference between the real and simulated total radical concentration is now so great that the dominant effect is the corrective influence of the initial-condition error. This coupled with the greatly decreased truncation error means that the simulated total radical concentration is converging to the exact total radical concentration. Note that although as time passes the simulated total radical concentration will draw closer to the exact radical concentration, they will never actually converge. This is because the truncation error will be non-zero until infinite time has passed, and because of the ongoing effects of round-off error.

In summary, the error added per integration step originates from two cancelling effects. Straight after a pulse a lot of truncation error is added as the rate of change in the differential equations is at its greatest. However, as time goes on this gets corrected by initial-condition error setting in.

The Asymptotic-Like Decrease in Error on the Arrival of the Periodic Initiation
There is an asymptotic-like decrease in the amount of error at the arrival of a burst of initiation. This is an artifact of the way that error is calculated. All error values given here are calculated by taking the difference between the numerical and appropriate analytic solutions and dividing that difference by the analytic solution (in this case equation 3.18). This means that the error is

given relative to the exact solution. The greatest virtue of calculating the error in this manner is that it allows a direct comparison to be made between error values for different times and different conditions. It does mean though that when there is a burst of initiation and a large concentration of radicals are added that a spurious error estimate is given. This is caused by the calculation of the error in a relative manner: a large increase in the radical concentration means that the error appears inordinately small. At this time the difference between the analytic and simulated values stays the same (the numerator) while the magnitude of all values, including the analytic value (the denominator), increases.

The Pseudo-Steady State in Solution Error A pseudo-steady state is established in the solution error, where the period of the error pseudo-steady state is equal to the period of the initiation. By definition, the establishment of a pseudo-steady state means that the error added in the time between two laser pulses is equal to the error lost in the same period. Therefore, the difference between the numerical and analytic solutions at the end of a period must be equal to the difference at the start of the period. This means that for a pseudo-steady state to be established two processes must occur - a process which increases the numerical error, and a process which reduces that error. Error is added as a result of the approximation of the values of the differential equations by their value at the start of the time step, i.e., simple numerical error which is implicit in all numerical solution techniques, and it is lost through the initial-condition error and the asymptotic decrease it error at the arrival of a burst of initiation. There is more to a pseudo-steady state, though, than simply the balance between these two processes. If this was all that was the case, then a pseudo-steady state would be identical to a standard steady state. The other feature of a pseudo-steady state is that the various processes play roles of differing importance at various stages during the period. By this I mean that at one part of the time period the processes which are increasing the value in question dominate, while at other times the processes which are reducing this value are dominant. This is seen in the pseudo-steady state of the total radical population. Here, radical initiation is adding radicals and bimolecular termination is removing them. If both processes occurred continuously at all times, then a steady state would be obtained. However, the radical initiation dominates in the first milliseconds of the time period and termination is the dominant process at all other

times. The situation is more complicated for the error pseudo-steady state. Here, the processes which affect the error in the solution make contributions during the entire period. Also, the relative contribution of these factors is controlled by the nature of the solution. That is, that the solution error accumulates effectively unabated for the first portion of the time period, until the accumulated error is so large that initial-condition error begins to make a significant contribution. It should be noted that the process that adds error does not stop, although because the rate of change in the radical concentration decreases, the magnitude of the error added will decrease. It is just that in the later part of the time period, the initial-condition error is having a greater influence. Nevertheless, while a periodicity is understandable, it is still perhaps surprising that there is no net upward drift in accumulated error.

Although the asymptotic decrease in error upon the arrival of a burst of initiation appears to make a significant contribution to the pseudo-steady state in error, this is merely a result of the way that the error presented. The error shown in these plots is the relative error. The asymptotic decrease in error corrects an overestimate of the error that occurs as the total radical concentration decreases. i.e., as the total radical radical decreases the same amount of absolute error shows up as greater relative error. However, these effects do not affect the real psuedo-steady state in error. This is evident if the absolute rather than relative error is plotted as a function of time.

The Effect of the Rate of Termination on the Error-Time Profiles The rate coefficient for termination has several effects on the error-time profiles shown in figures 3-4 - 3-6. The first of these is upon the magnitude of the error. A high value for the rate coefficient for termination causes there to be more error in the solution of these equations. This correlation was noted and explained above.

The second effect of the magnitude of rate coefficient for termination is to alter the time at which the balance between truncation and initial-condition error shifts. This changeover is shown as a maximum in the error-time plots. In the early stages of the time between bursts of initiation, truncation error is the dominant error type. However, as time passes and the difference between the exact and simulated total radical concentrations increases, initial-condition error plays an increasingly important role. The time at which initial-condition error

overcomes truncation error as the dominant error type is related to the rate coefficient for termination. When the value of k_t is high (1×10^8L.mol^{-1}.s^{-1}) the error added per integration step peaks very early. In contrast to this when the value of k_t is low (1×10^6L.mol^{-1}.s^{-1}) the change in dominance occurs late (if at all). The correlation between the rate coefficient for termination and the changeover in dominant error type is caused by the effect of the value of k_t on the magnitude of truncation error. When the value of k_t is high, as it is figure 3-4, truncation error is added very quickly. This means that the difference between the simulated and analytic total radical concentration is also large soon after a burst of initiation. Therefore, as the magnitude of the initial-condition error is proportional to the square of the difference between the exact and simulated total radical concentrations, the ameliorating influence of initial-condition error is felt early. Hence, a peak in the error in the solution of equations 3.22 - 3.24 is observed early. On the other hand, when the value of k_t is low, as it is figure 3-6, only a small amount of truncation error is added per integration step. Thus, it takes more time for the difference between the exact and simulated total radical concentrations to get large enough that initial-condition error makes a significant impact. This is the case in figure 3-6, where initial-condition error is evident in that it only arrests the increase in truncation error.

The final effect that the termination coefficient has is upon the time taken to reach a pseudo-steady state in error. This phenomenon is closely related to the previous one. A pseudo-steady state in error can only be established when the error added per initiation period (truncation error) is equal to the error lost per truncation period (initial-condition error). When the value of k_t is high, and a lot of truncation error is incurred, this situation is reached very quickly (one or two periods) while when the value of k_t is low this can take up to six periods. This in fact mirrors the obtainment of a pseudo-steady state in error.

Conclusions The magnitude and shape of these error-time profiles have several important ramifications upon practical attempts to solve these differential equations, as well as suggesting a number ways of improving the efficiency of practical strategies for solving these differential equations and therefore for modelling free-radical polymerization.

Firstly, this system of differential equations appears to be significantly more robust than was previously thought. The analysis performed here has shown that this system of differential

equations is self-correcting, so that when error is added, the system acts to reduce that error. This means that less attention needs to be paid to the effects of the accumulation of error. The accumulation of error is a constant worry when employing numerical solution strategies, as it often means that a solution method that incurs only a very small amount of error per integration step can not be used, because this error is quickly amplified. This study has shown us that this is not the case for this system of differential equations that model PIP, so that a simple numerical strategy, such as the Euler method, can be used as practical solution method.

The second feature that has significant practical relevance is the general profile of error between two initiation bursts. The investigation performed in this section has shown that the error in solution to equations 3.22 - 3.24 increases after the arrival of a burst of initiation and then declines as time passes. Moreover, it was clear from the analysis that this pattern is repeated with the same periodicity as the initiation profile. This suggests a method to improve the efficiency of the Euler method could be developed by providing information to the solution algorithm about the regular pattern of the error incurred, so that the algorithm is aware of the times when the system of differential equations is prone to error. Furthermore, the solution algorithm should be given the ability to take more care in solving this system of differential equations at times when the chance of incurring error is high.

Error Standard Three

The chain length of distribution of living radicals is an important product of any simulation of free-radical polymerization, as it is principally this distribution that controls the MWDs (especially when termination occurs through only the disproportionation mechanism). For this reason, it is important that a well developed understanding be gained of the error introduced to this chain-length distribution when it is simulated by a numerical solution strategy. With this aim in mind, error standard three was designed. This analysis attempts to answer several questions, for example: what is the magnitude of this error?, how does it scale with step size?, and how does the error incurred depend upon chain length ?

To provide information that can be used to answer these questions, this error standard employs an analytic expression, equation 3.20. Unfortunately, equation 3.20 is computationally expensive to evaluate, so that it may only be used in a restricted manner.

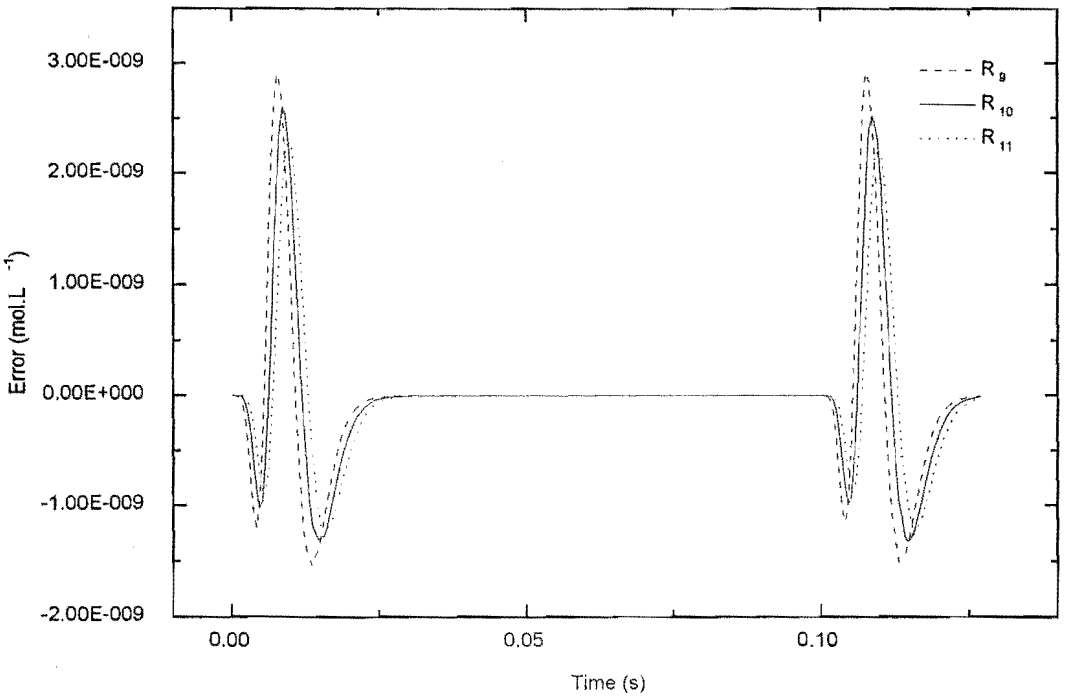

Figure 3-7: The absolute difference between analytic and simulated radical concentrations as a function of time. The error in this figure is equal to $(R_i)_{sim} - (R_i)_{analy}$.

Simulation Results Equation 3.20 was used to predict the concentrations of three radical species, chain lengths $9 - 11$, throughout two initiation periods. Note the only two initiation periods are simulated using this analytic expression - two initiation periods for the polymerization at pseudo-steady state. A normal numerical simulation is then run using the Euler method to solve the differential equations. This simulation is left to run for enough initiation periods so that a pseudo-steady state has been well and truly established (20 initiation periods). During the 21st and 22nd initiation periods, the concentrations of the three radical species (chain lengths $9 - 11$) are written to data files at intervals of 0.005 s (note that times given in these figures are relative to the start of the 21st initiation period). Once both the analytic and simulated data have been calculated it is possible to take the difference between these. This difference is then plotted against time (see figure 3-7). Simulation studies have

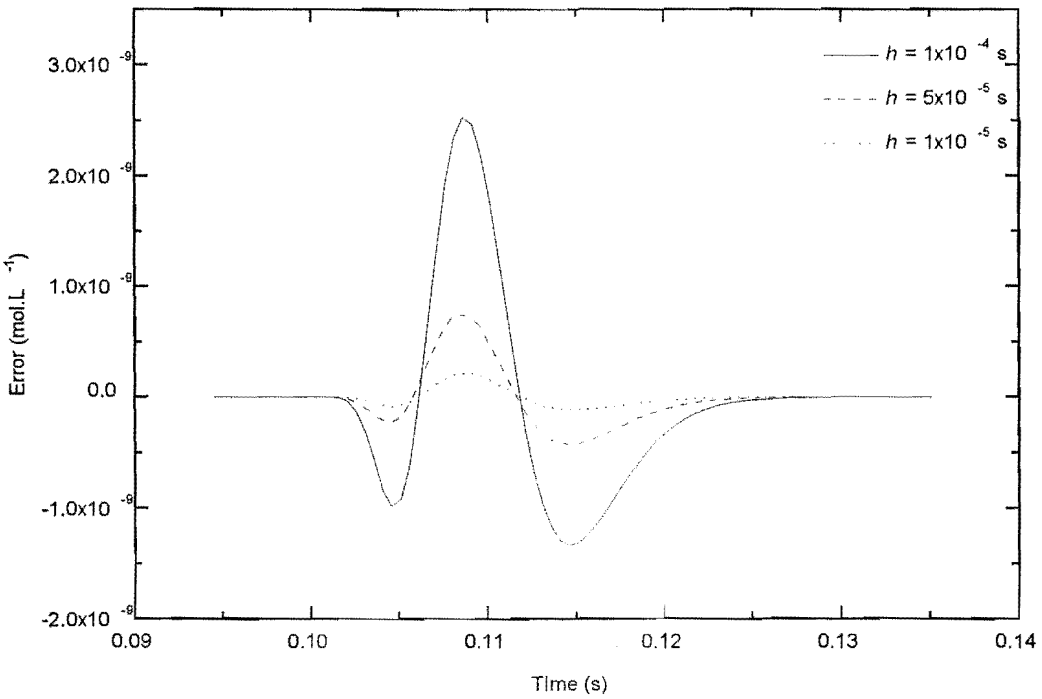

Figure 3-8: The effect of the integration step-size upon the error incurred in the individual radical concentrations. Results are shown for radical species of chain-length 10. The error is the figure is equal to $(R_i)_{analy} - (R_i)_{sim}$.

also been performed that explore how this error depends on the step size used in the numerical solution of the differential equations. This absolute error data is shown in figures 3-7 and 3-8. All simulations have performed with the default rate parameter set (table 3.3).

Note that the relative error has not been presented here. This was calculated, but it was found that nonsensical error values were produced. The reason for this is that values of the actual radical concentrations ($R_9 - R_{11}$) are so low, that even a very small absolute error leads to a large relative error. Thus we confine ourselves to discussing only the absolute error. Note that although the analysis of the affects of error in the concentrations of radicals species of each chain length upon the MWD outlined in chapter five revealed that this type of error usually has only a very small affect upon the final MWD, some time will be spent examining its origin. The

reason for this is twofold. Firstly, there is a special case were this error significantly impacts upon the Euler method. Secondly, this type of error significantly affects some of the numerical strategies used in chapter four.

The error calculated via error standard three shows a complex dependence upon the chain length of the radical species. For example, the difference between the analytically and numerically calculated radical concentrations has a repeating profile with a period of $k_{\mathrm{p}}\mathrm{M}t_0$. The final plot, figure 3-8, shows how the error incurred depends upon the step size used to solve the differential equations.

Model System Figures 3-7 and 3-8 show that the error in the concentration of individual radical chain lengths depends in a complex manner upon both chain length and time. To understand this error, a model has been developed that simplifies the kinetics of this system. This model attempts to develop an expression that describes the rate of change in the differential equations for the individual radical species. To do this it assumes that termination has little effect upon the rate of change in the individual radical concentration (substituting some reasonable values into equation 3.23 confirms this). Moreover, it is assumed that the rate of change in the differential equation for radicals of a certain chain length can be modeled by the movement of a Poisson wave of radicals by it. That is, we ignore all of the other radicals in the system apart from those involved in a single radical wave that is passing by the chain length in question. This allows the concentration of radicals of chain length of i, R_i, at any time t to be described by the expression for a Poisson distribution, i.e.,

$$\mathrm{R}_i \propto \exp(-k_{\mathrm{p}}\mathrm{M}t)\frac{(k_{\mathrm{p}}\mathrm{M}t)^i}{i!} \tag{3.30}$$

This expression can then be used to generate the concentration of radicals of chain length i for a range of times. Here this expression is used to predict the concentration of radicals of chain length $9-11$ at 0.05 s intervals throughout one initiation period. These values can the be numerically differentiated once and then twice to yield the rate of change in radicals of chain length i, as well as the rate of change in the differential equations for radicals of chain length i. The values of R_i, $\frac{d\mathrm{R}_i}{dt}$, and $\frac{d^2\mathrm{R}_i}{dt^2}$ based upon this model system are shown in figures 3-9 – 3-11.

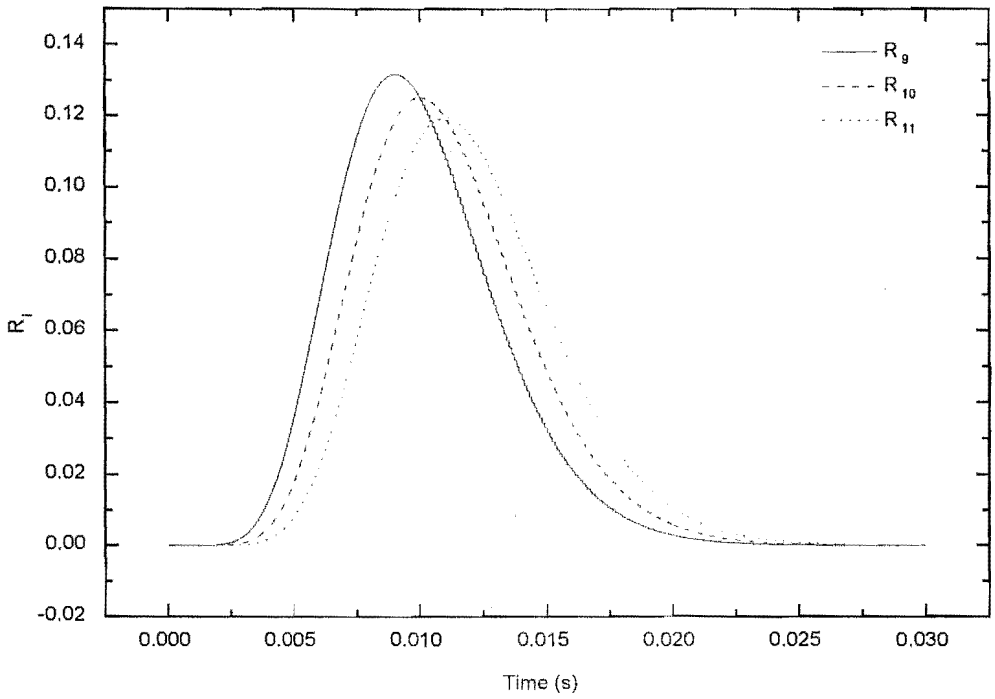

Figure 3-9: Theoretical change in the concentration of radicals of three chain-lengths with time.

Explanation of Error in Radical Chain-Length Distribution Before we can analyze the chain-length dependence of the error shown in figures 3-7 and 3-8 in terms of the model developed above, one last point must be made. This concerns the correlation between the truncation error incurred and the rate of change in the differential equations. It has already been noted that the amount of truncation error incurred by the Euler method is proportional to the rate of change in the differential equations. Moreover, here it has been mentioned that the Euler method overestimates the solution of a differential equation if that differential equation is decreasing and underestimates the solution to a differential equation if that differential equation is increasing. We now have all the tools that are needed to explain the error in these systems. There are three dependencies in the error the must be explained: (1) the dependence of error on time; (2) on chain length; and (3) upon the integration step size.

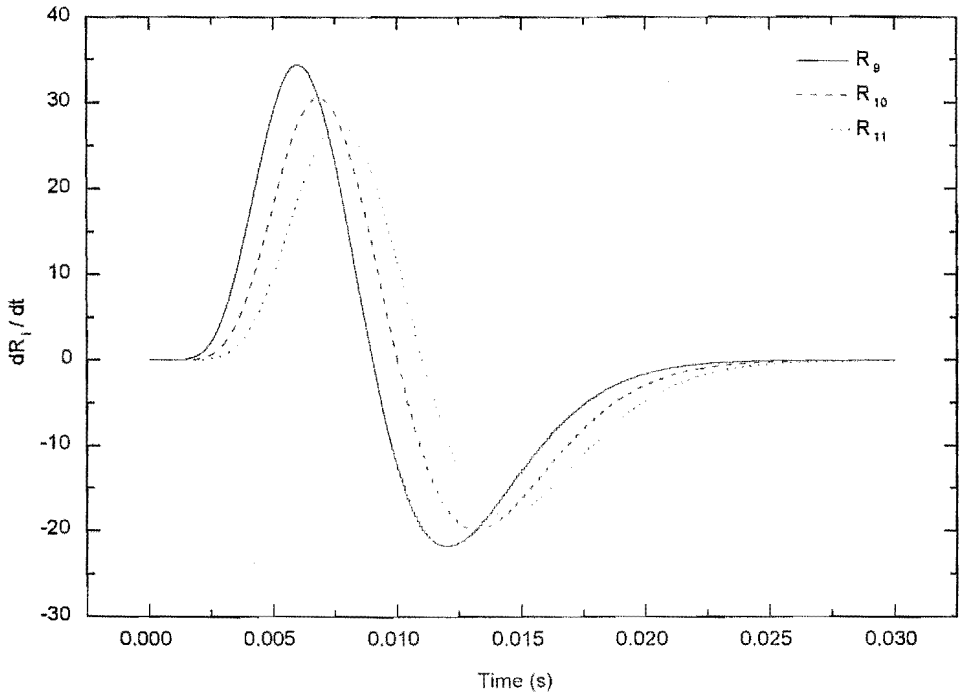

Figure 3-10: Theoretical rate of change in the concentration of radicals of three chain-lengths with respect to time.

The Dependence of Error Upon Time The most striking feature shown in figures 3-7 and 3-8 is the dependence of error upon time. The error in the concentration of a radical of a certain chain length is approximately equal to zero for all times apart from about the time when it has the most probable chain length[3]. Moreover, the next time that chain length is the most probable chain length, i.e., when the next radical wave passes by, the error pattern is repeated. It seems then that the error incurred is related to the wave-like way in which the concentration of radicals of a particular chain length change with time.

As the same error pattern is repeated every time a 'radical wave' passes by a certain chain length it is possible to describe this error profile by dividing it into sections. Each section has

[3]In chapter one, the idea of the most probable chain-length in the radical chain-length distribution was introduced. This is based upon the idea that in time t a radical chain will on average add $k_p M t$ monomer units.

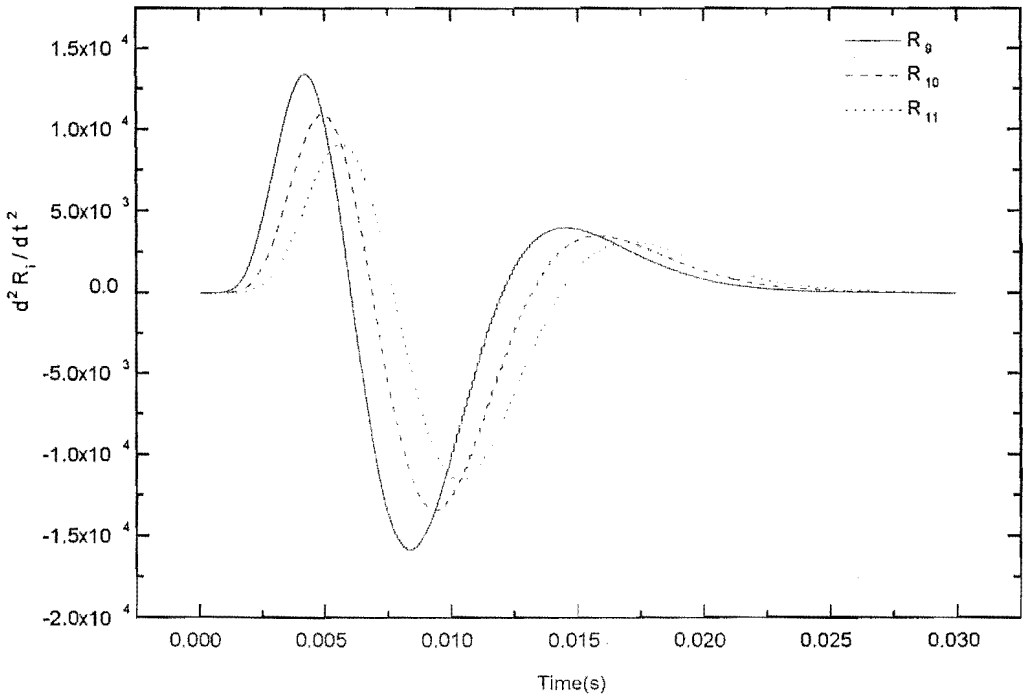

Figure 3-11: Theoretical second derivative of the concentration of radicals of three chain-lengths.

the same length as an initiation period and begins at the point of time when a burst of initiation arrives. Thus, all one needs to do is explain the time dependence of error is to explain the error during one of these sections of time. To do this, the error will be discussed at several critical times.

At time zero, a burst of initiation impinges upon the polymerization system. Here the model (figures 3-9 – 3-11) says that the concentration of radicals of chain length 10 is zero and hardly changing. Thus only a small amount of truncation error should be incurred about this time. This suggestion is borne out by figure 3-7 where the absolute error is approximately zero.

At 0.002 s after the burst of initiation, the concentration of radicals of chain length 10 is beginning to increase. This means that the differential equations are positive, and the rate of change in the differential equations is non-zero. Therefore, negative error is introduced as a

result of the Euler method underestimating the differential equations during a time step. This negative error is shown in figure 3-7.

At 0.005 s after the burst of initiation, the rate of change in the radical concentration of chain length 10 peaks hence at this time the most truncation error is being added, this is shown as a minimum in the absolute error plot (figure 3-7). This point corresponds to the first maximum in the second derivative (figure 3-11).

During the next 0.005 s the differential equations are changing rapidly and they change sign. As the value of the differential equations changes from positive to negative in this period and as the rate of change is large, we expect a large positive peak in the absolute error. This is in fact want is seen (see figure 3-7).

During the last period of time when there is any significant concentration of radicals of chain length ten, 0.01 - 0.02 s, the error incurred is once again negative. This is surprising as the differential equations are decreasing during this period, so one would expect, based on truncation error arguments, that the error should be positive. As this is clearly not the case, we argue that another type of error must play an important role at this time. The most likely candidate is initial-condition error. It was stated above that the magnitude of initial condition error is proportional to the square of the difference between the exact and simulated solutions. Hence, as by this time (0.01 - 0.02 s after a burst of initiation) a lot of numerical error has been added, it is reasonable to argue that initial-condition error is important. As the concentrations of radicals has been overestimated, initial-condition error tends to correct for this by underestimating. The negative error presumably results from this type of overshoot.

The Dependence of Error on Chain Length The amount of error that is added per integration step is less for large radicals than it is for small radicals. This is shown in figures 3-7 and 3-8. This is caused by an increase in the width of the radical wave that occurs as the most probable chain length increases. It is well known that the width at half peak height of a radical wave is proportional to the most probable value of a Poisson distribution. Hence, as the most probable value of a Poisson distribution increases so does the width of that distribution. This means that as radical waves move to higher chain length their width increases.

This is relevant to our discussion of the chain-length dependence of error, because the rate

of change in the differential equations for a broad radical wave is less than that for a sharp radical wave. This is shown in figure 3-11. In this plot it is clear the magnitude of the second derivative is less for large radicals (chain length 11) than for small radicals (chain length 9). As the truncation error is proportional to the rate of change in the differential equations (the second derivative), this means that less error is incurred in solving the differential equations when the radical distribution is broad than when it is narrow. Thus, less error is incurred in solving the differential equations for long radicals than for short radicals.

Not only does the broadening of the radical wave mean that less error is added as the chain length of the radical species increases, but it also means that the error decreases as the time since the last burst of initiation increases. This is because of the linear correlation between time and the most probable chain length. Also, as the most error is incurred in a radical concentration when the chain length of that radical is the most probable chain length, the chain length where most of the error is being incurred increases with time. Hence, as the magnitude of error decreases with increasing chain length, the magnitude of error incurred also decreases with time.

Thus if one wishes to reduce the error incurred in the solution of the differential equations for individual radical species, one is to advised to take more care just after the arrival of a laser pulse. This is a pleasing result as it means that a time-dependent step-size profile can be used to reduce the error incurred in the solution of the differential equations for individual radical chain lengths. Even more pleasing is the fact that the step size profile that is likely to the optimal for reducing the error in the radical chain-length distribution is also that which is optimal for reducing the error in the total radical concentration.

The Dependence of Error on Step Size It is clear from figure 3-8 that the amount of error incurred decreases with increasing step size. This is unsurprising as the analysis performed above suggested that this error is largely due to truncation error. Hence the error in the solution of these equations can be reduced by increasing the integration step size.

Conclusion This analysis has indicated that the magnitude of error added to the concentrations of individual radical concentrations is of the order of 1×10^{-4} and that this error strongly depends on time and chain length. It was clear from this that the most error is incurred around

the time when the chain length of a radical is the most probable chain length. It has also been shown than the argument used to explain the error incurred in the total radical concentration (truncation and initial-condition error) is also applicable to this error system. In addition to this, simulation studies have indicated that the magnitude of the error incurred can be reduced by decreasing the integration step size and potentially decreased with a time-dependent step-size profile.

Of significant practical relevance is the fact that the same type of step size profile could reduce both the error in the radical chain-length distribution and the error in the total radical chain-length distribution. An example of such a step size profile is one which the size of the integration steps increases with time. This means that when, in the following sections, an optimal step size profile is found for reducing the error in total radical concentration, the error in the radical chain-length distribution will also be reduced. Although, such a step size profile might not be the optimal one for reducing the error in the radical chain-length distribution, studies have shown that it is the error in the total radical concentration has the most effect on simulated MWDs (see chapter five). Hence, it is most important to reduce the error in R_t, and the accompanying error reduction is a bonus

An analysis of the effect of this type of error upon the MWD has been performed as a part of this work and the results of this investigation will be given in chapter five. In summary, these results show that error in the total radical concentration has significantly more effect on the simulated MWDs than error in the radical chain-length distribution, such as that outlined above. With this in mind, emphasis will be placed on reducing the error in the total radical concentration rather than on the error in the radical chain-length distribution. It is noted, however, that these two types of error are inextricably linked. As the error in the radical chain-length distribution can not be totally ignored, the following strategy will be implemented. The effect on the error in the radical chain-length distribution will be noted after each successive refinement, so that it is kept below an acceptable level, and the step size will be kept below a certain limit at all times. This requirement is now explained in considering error standard four.

Error Standard Four

The numeric values of the population-balance differential equations and the way that these change with time have a direct influence on the solution that is obtained by a numerical solution algorithm. All of the finite-difference based methods investigated in this study use some function of the values of the differential equations to generate the next value of the solution. Therefore, by developing an understanding of the nature of the differential equations in these systems, we also gain knowledge about how the numeric solution of these differential equations incurs error. With this in mind an analysis of these equations has been performed. In particular, this analysis aims to explore the effect that changes to several of the simulation parameters, including the integration step size, have on the values of these differential equations.

The Shape of the Differential Equation-Time Plot The differential equation-time plots are approximately symmetrical, with a center of symmetry at the time when the chain length of the radical species being described is the most probable chain length. This corresponds to 0.05 s after the last burst of initiation for radicals of chain length 50. Before this time the radical concentration is increasing ($d\mathrm{R}_{50}/dt$ is positive) and after this time the radical concentration is decreasing ($d\mathrm{R}_{50}/dt$ is negative). The rate at which this differential equation changes has already been discussed in detail. To recapitulate, initially the differential equation for fifty-mers increase slowly as radicals of chain length 49 propagate in. At a time that corresponds to 0.035 s in figure 3-12, the rate of change of the differential equation is increasing accelerates. This rate of change peaks at about 0.04 s and slows until the value of the differential equation reaches its positive peak (at approximately 0.045 s). A period of rapid change follows. The value of the differential equation changes from its positive peak to its negative peak value in a short period of time (0.01 s). From the time that corresponds to this negative peak onwards, the way that the differential equations is related by symmetry to way the changed before reaching the positive peak.

Although the shape of the differential equation-time profile is complicated, it can be explained in a simple manner. The shape of this profile is closely related to the form of the differential equation being solved (equation 3.31). All of the features in figure 3-12 can be explained in terms of the difference between the concentration of radicals of chain length 50

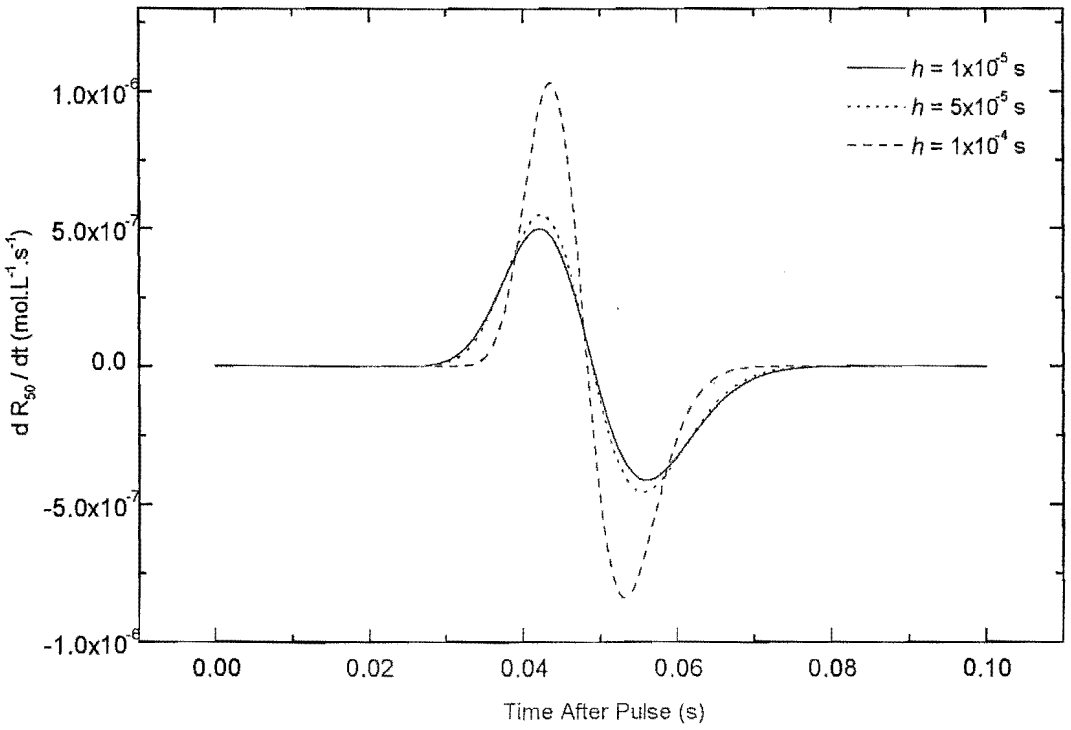

Figure 3-12: The value of the differential equation for the concentration of radical species of chain-length 50 for a range of times and step-sizes.

and 49 and the fact that the rate of production of radicals of chain length 50 is proportional to the concentration of radicals of chain length 49. The shape of the plot of the rate of change in a radical concentration extracted from simulations is the same as that predicted by the model developed above (see figures 3-9 - 3-11). As this model includes only propagation processes, we are justified in ignoring the termination term in this differential equation. Hence, what we are able to argue is that the rate of change in an individual radical concentration is influenced principally by propagation events.

$$\frac{d\mathrm{R}_i}{dt} = k_\mathrm{p}\mathrm{M}(\mathrm{R}_{i-1} - \mathrm{R}_i) - 2k_\mathrm{t}\mathrm{R}_i\sum_{j=0}^{\infty}\mathrm{R}_j \tag{3.31}$$

To explain the shape of the rate of change in the concentrations of radicals of chain length 50, we will imagine a radical wave, i.e., a group of radicals initiation by the same pulse of initiation, propagating towards and passed chain length 50.

Straight after the arrival of a burst of initiation concentration of radicals of chain length 50 and 49 are approximately equal to zero. Hence the value of the differential equation is approximately zero. As time passes the concentration of radicals of chain length 49, and to a lesser degree chain length 50, begin to increase. The concentration of radicals of chain length 49 at this point is greater than those of chain length 50. Thus the differential equation is positive, i.e., $(R_{49} - R_{50}) > 0.0$.

At some latter time, (figure 3-12 $\approx$ 0.04 s) the concentration of radicals of chain length 49 has begun to increase more rapidly. The concentration of radicals of chain length 50 also increases, but at a slower rate. Hence, the net effect is that the difference between the two concentrations and therefore the value of the differential equations has increased. This is shown in figure 3-12 ($\approx$ 0.04 s)

At approximately 0.046 s after the arrival of the initiation burst the differential equation for radicals of chain length 50 reaches its maximum positive value. By definition this means that at this time there exists the greatest positive difference between the concentration of radicals of chain length 49 and 50.

After this time the value of the differential equation changes rapidly in a short period of time, it alters from its maximum positive value to its maximum negative value, and in doing so moves through a point where the concentrations of radicals of chain length 50 and 49 are equal. For radicals of chain length 50, the negative maximum in the differential equations is positioned 0.054 s after a burst of initiation. By definition, at this time difference between the concentrations of radicals of chain length 49 and 50 is at its most negative.

After this time, the differential equation for radicals of chain length 50 is negative and its magnitude is decreasing (approaching zero). This is because the concentration of radicals of chain length 49 and 50 draw closer together as both their concentrations decline. It should be noted that the value of this differential equation is not symmetrical about the time when the concentrations of the two radical chain lengths are equal. The concentration of radicals of chain length 50 decreases more slowly than they increase. This asymmetry is caused by the

asymmetry of the Poisson distribution as the most probable chain length changes with time and because of bimolecular termination.

The rapid change in the value of the differential equations around the time when the chain length of these radicals is the most probable chain length causes a problem for finite-difference numerical methods. I have noted several times that finite-difference based methods have problems dealing with rapidly changing differential equations, and thus incur truncation error under such circumstances. Hence, the solution of the differential equation for radicals when they are close to their maximum values is likely to incur significant amounts of truncation error.

The Effect of Integration step size on the Differential Equation-Time Profile The effect of the step size upon the value of the differential equation for radicals of chain length 50 is shown in figure 3-12. From this figure it is clear that the value of the integration step size affects the value of the differential equations in several ways. This result is unsurprising as it been noted in previous analyses. It is also not surprising that these effects can be explained by the ideas of truncation and initial-condition error. A description of these effects will not be given here as closely related to effects explained above.

However, one final point must be made about the relationship between the error incurred and the step size used. This concerns a situation when the error diverges and the simulation program crashes. Many calculations have shown that the error diverges when a step size is used that is greater than one over the propagation frequency, i.e., the maximum step size that can be used is

$$h_{max} = \frac{1}{k_p \mathrm{M}} \tag{3.32}$$

The value of the differential equation for radicals of chain length 50, for a system where $h \geq h_{\mathbf{max}}$ is shown in figure 3-13. This plot shows what happens if too large a step size is used to solve the differential equations for radical species about the time that it has the most probable chain length. The finite-difference method is unable to describe the value of the differential equation so the error diverges and the program crashes.

This is caused by the stiffness of the differential equations. As described in chapter one, stiffness is the problem that occurs when there are two or more very different scales of indepen-

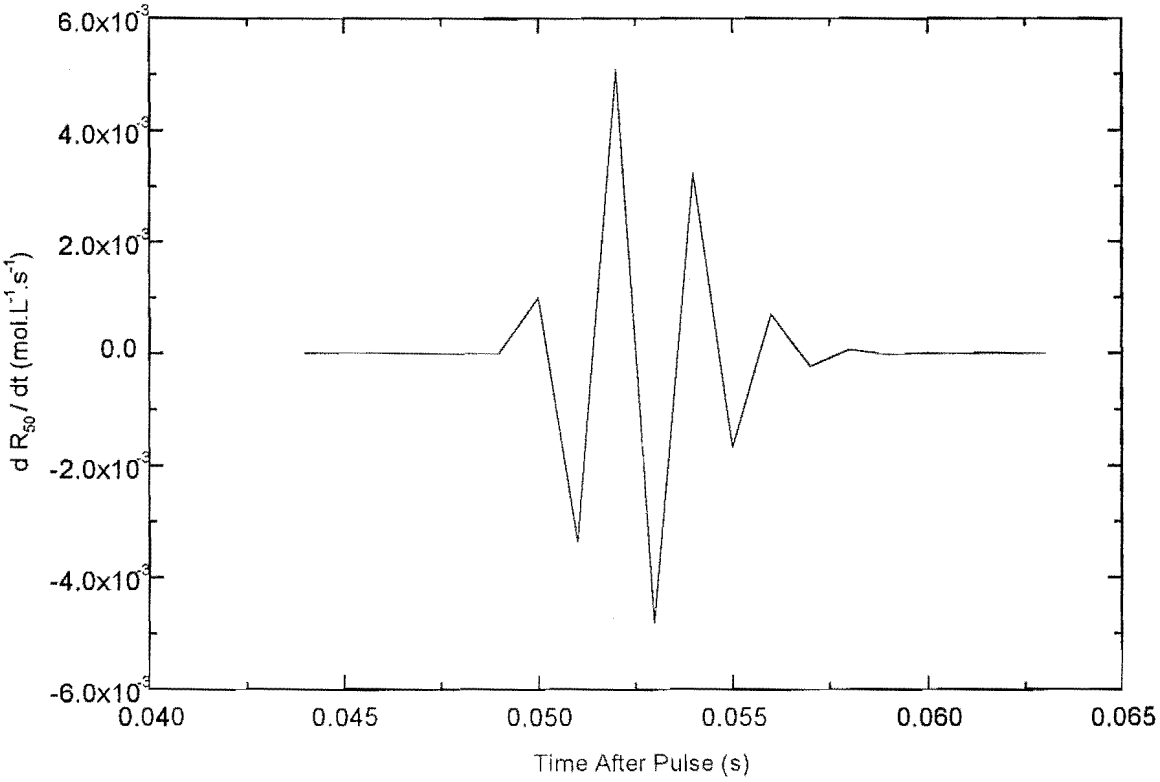

Figure 3-13: The value of the differential equations for radical species of chain-length 50 for a system that has been solved with the Euler method and an integration step-size of $h = 1 \times 10^{-3}$s.

dent variable on which the dependent variables change. In this system of differential equations, the stiffness is caused by propagation terms. One of the effects of stiffness is that when these differential equations are solved by a numerical method there exists a critical step size, such that if a larger step size is used then the solution diverges. There are methods for avoiding this limitation, and by doing so dealing with the stiffness of these equations, one of these methods will used to solve these equations in chapter four.

A detailed explanation of the cause of this convergence will be given in chapter four. This shows that an explicit numerical method, such as the Euler method is only stable for a range of

step sizes, where the largest possible step size is defined as one over the coefficient of the most rapidly changing term, here the propagation terms. This means the differential equations for PIP can only be solved with a step size that is less than one over the propagation frequency. Moreover, in chapter four an explanation will given for the shape of figure 3-13. For the moment it is noted that this plot shows the behavior expected of the solution of the differential equations for a stiff system with a step size that is too large.

3.10.4 The Method of Sections: An Investigation of Time-Dependent step size Profiles

Simulation studies of the error introduced when the Euler method is used to solve the differential equations that characterize intermittently initiated polymerization have shown that this error is time dependent. For example, the error in the simulated total radical concentration depends on the time since the last burst of initiation. In this section a time-dependent method of controlling this error is introduced and tested. It is well known that the error incurred by a finite-difference method can be controlled by varying the step size. As it is a simple procedure to make the size of the integration steps a function of time, a time variant step size appears to be a good way of controlling the variation of error with time. The aim of this section is to explore the effect that using a time-dependent step-size profile has on the error in these systems. It is not altogether clear that using this type of profile will lead to significant increases in efficiency. For example, in section 3.10.3.2 we saw that initial-condition error plays an important role in moderating the amount of error present in the solution of these equations. By changing the step size profile, it is possible that we will also shift the balance between truncation and initial-condition error. To explore the effect that this profile has on the error incurred, a very simple TDSSP will be used and the error incurred analysed.

This step size profile allows the step size to be one of two values; a large step size value ($h = 1 \times 10^{-4}$s) or a small step size value ($h = 1 \times 10^{-5}$s). When this step size profile is used then the time between successive bursts of initiation is divided into ten sections of equal width. All of the time intervals, except one, are given a step size that is equal to the large step size value. The remaining interval has a step size is equal to the small step size value. Hence, a step size profile is created that has the same form as that shown in figure 3-14. In this case,

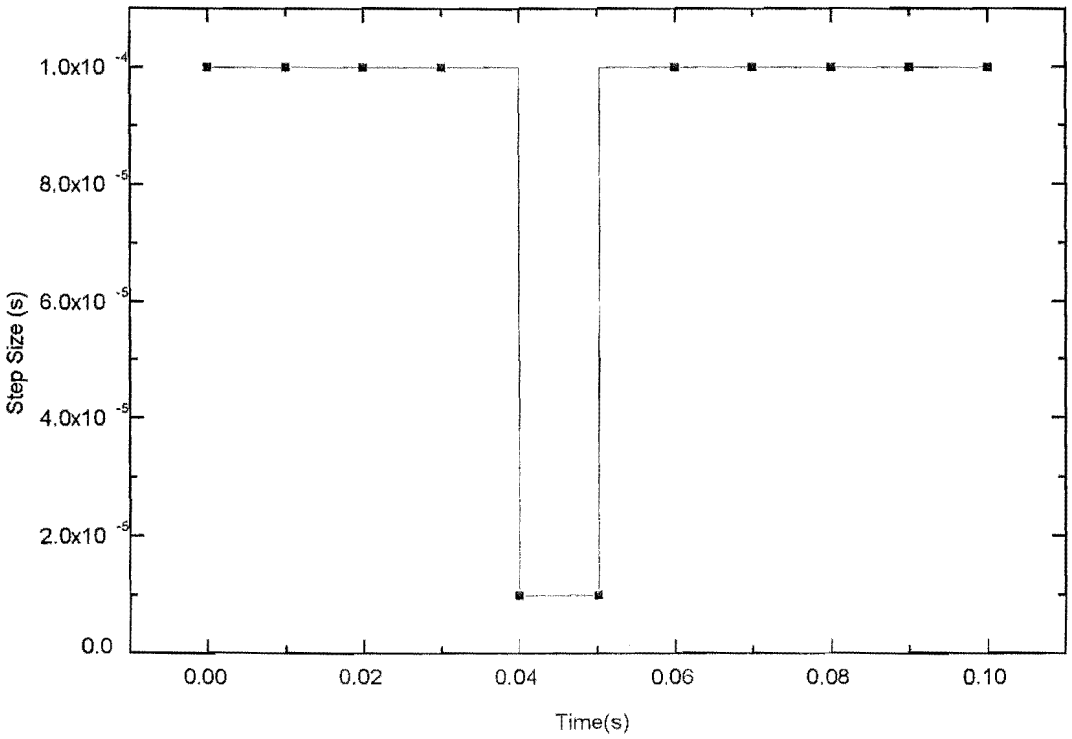

Figure 3-14: An example of the step-size profile used by the Method of Sections.

the fifth interval is the one that has the small step size value.

Error Standard One To explore the effect that this TDSSP has on the error incurred in the solution of these differential equations a series of simulations have been performed. Each simulation uses a step size profile where the interval of small step size begins at a different time, i.e., 0.0, 0.01, 0.02 s and so on. These simulations are run for ten initiation periods and the same step size profile is used for each initiation period. This process is then repeated with a step size profile that has the section of small step size moved forward one section. Ten calculations are run so that the effect of having the interval of small step size at each position is explored. The error is then assessed through error standard one. The data produced by these simulations indicates that the mean error incurred per pulse is strongly dependent of the position of the

small step size interval.

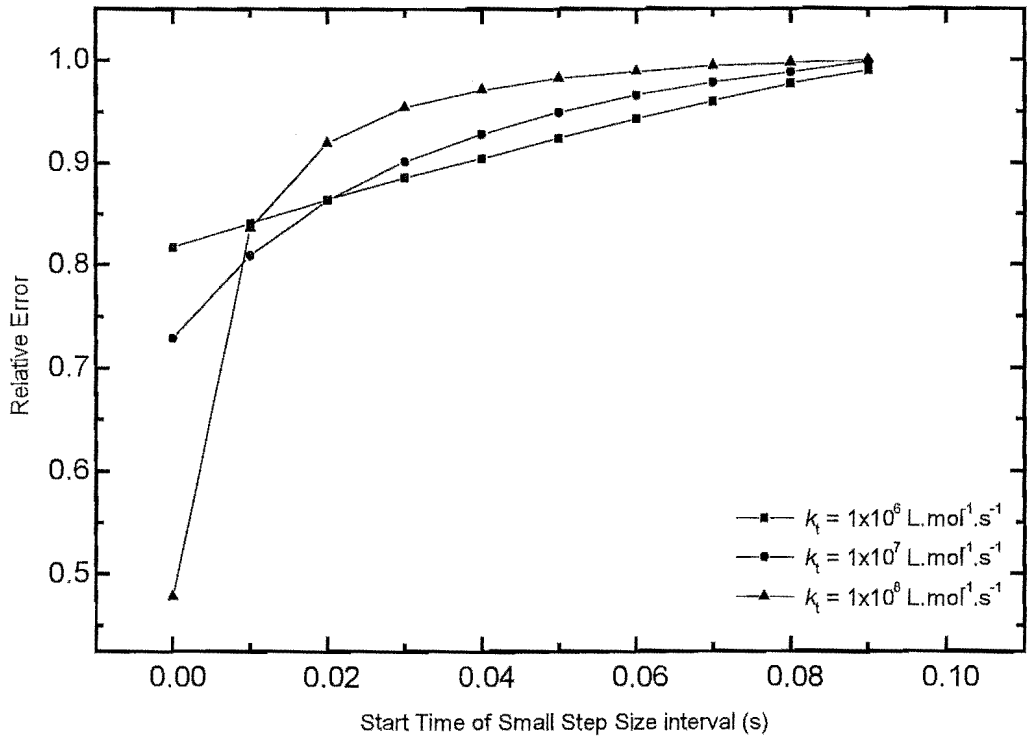

Figure 3-15: The effect of changes in the start time for the small step-size interval on the solution error. Error is shown relative to the error with a constant step-size profile.

Results are shown figure 3-15. This figure contains a plot of the relative mean error per initiation period against the start time for the small step size interval. The mean error per pulse for the interval based step size profile has been divided by the error incurred when a constant step size profile ($h = 1 \times 10^{-4}$s) is used. Figure 3-15 shows that less error is incurred when the interval of small step size is placed early in the initiation period than when it is placed late in that period. For example, when simulations are performed with a $k_t = 1 \times 10^8$L.mol^{-1}.s^{-1} and the small step size interval begins at 0 seconds, the mean error per pulse is 47% of the error when no small step size interval is used. However, if the same simulation is performed and the interval begins at 0.06 s then the error incurred is 99% of the error incurred when no

k_t(L.mol^{-1}.s^{-1})	Error (0.00 s) (%)	Error (0.08 s) (%)
1×10^6	81.7	97.7
1×10^7	72.9	98.8
1×10^8	47.8	99.7

Table 3.6: The effect of the rate coefficient for termination upon the reduction in error caused by the use of a time-dependent step-size profile. Error is given as the percentage of the mean error per pulse period produced with a time-independent step-size profile.

interval is used. Hence, simply by moving the position of the interval of small step size one is able to change the amount of error added by a factor of 2. It should be remembered that the same number of steps are taken per pulse independent of the position of the interval of small step size. The means that the efficiency is directly proportional to the error incurred. Hence, a decrease in error by a factor of 2 causes a two-fold increase in efficiency. This result has significant practical relevance as it means that the efficiency of this solution strategy can be increased by moving the position of the small step size interval. Hence, this study shows that a significant increase in the efficiency of a numerical solution strategy can be made by using a TDSSP. However, it is should be noted that more steps are taken when the TDSSP is used than when a time independent step size profile (TISSP) is used. This has the effect of slightly offsetting the efficiency gains made it using the TDSSP profile.

In this section, we have seen the gains in efficiency that can be made by using a rudimentary step size profile. In the following sections, two more step sizes profile are used, ones where the step size is far less constrained in how it can change with time. Although these profiles are far more complicated, they are based on the same principle as that used in the method of sections. That is, the efficiency of a solution strategy can be increased simply by allowing the size of the integration steps to depend upon time.

The data presented in figure 3-15 shows that the rate coefficient for termination influences the way that error changes with the position of the interval of small step size. If a high value for the rate coefficient for termination ($k_t = 1 \times 10^8$L.mol^{-1}.s^{-1}) is used, less error is incurred when the interval is placed close to the time of the arrival of the intuition burst than if a low value of k_t is used. However, when the same simulations are run but the interval is placed towards the end of the initiation period, the error is reduced by less in a simulation with a high k_t than for a simulation with a low value of k_t. This data is given in table 3.6.

This table shows the percentage reduction in error is greater for a high k_t system (47.8%) than for a low k_t system (81.7%) when the interval is placed at the start of the initiation period (0.00 s), while the reduction in error is greater for a low k_t system (97.7%) than a high k_t system (99.7%) when the interval is placed towards the end of the initiation period (0.08 s).

To explain this we must return to the correlation between the truncation error and the rate of change of the differential equations that was introduced at the start of this chapter. In a system that has a high rate coefficient for termination, the rate of change in total radical concentration is large at the start of the initiation period, but it declines rapidly. The decay of the rate of change is so great that by the end of the pulse period the rate of change of the differential equations in a system with a high k_t is less that for a system with a low k_t. Hence, a system with a high k_t will incur more error than a system with a low k_t straight after the arrival of the initiation pulse but less towards the end of initiation period. Therefore, using a small step size straight after the arrival of an initiation burst will have a greater effect on a system with a high value of k_t than on a system with a low value of k_t. However, using a small step size at the end of the initiation period will have a greater effect on a system with a low k_t than a system with a high k_t.

The practical implication of this is that as the error incurred is a function of the rate constant for termination, the effects of using a time-dependent step-size profile also depend on the value of k_t used. This means that the step size profile used should also depend on the value of k_t used; clearly this is also true for ρ.

Error Standard Two To date we have concentrated on the effect of a time-dependent step-size profile upon the error as measured by error standard one. To fully examine the impact that a TDSSP has on the structure of the error in these systems the remaining error standards must be applied.

Figure 3-16 contains a plot of the error analyzed by error standard two. To allow comparison this figure also includes the error-time profile for these equations when they are solved with a constant step size profile ($h = 1 \times 10^{-4}$s). There are a number of differences in the shape as well as the magnitude of these plots. The most striking difference occurs around the region where the TDSSP uses a smaller step size. In this figure, this corresponds to $0.01 - 0.02$ s after a burst

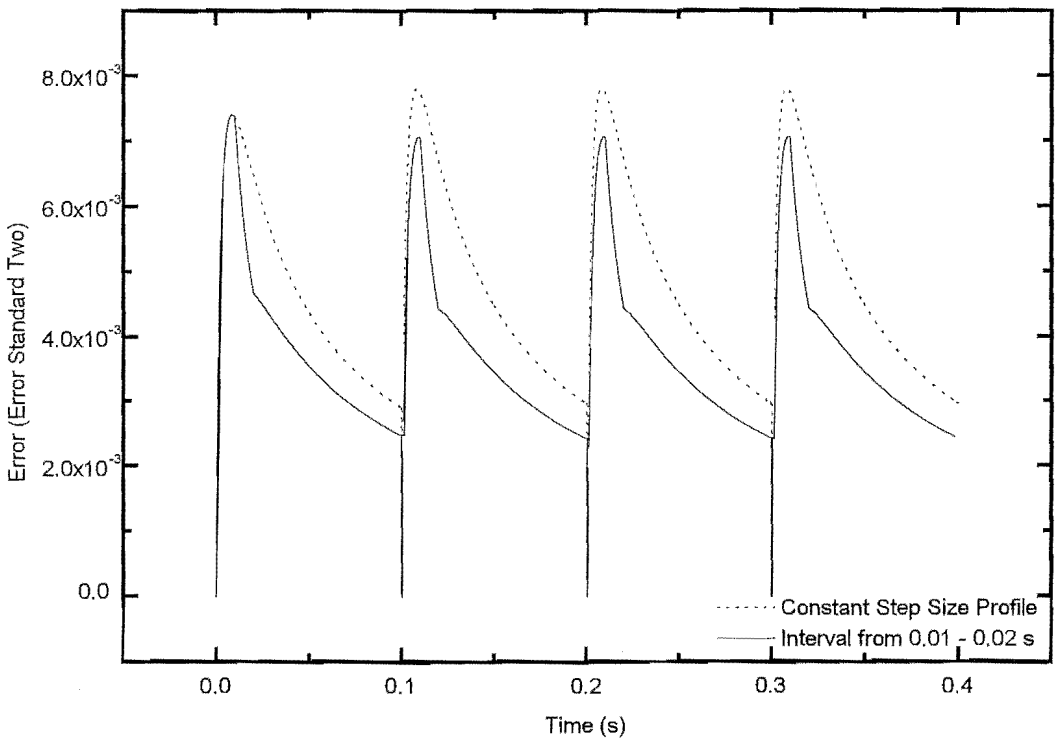

Figure 3-16: The error in the total radical concentration where a time dependent and time independent step-size profile has been used.

of initiation. At this point, the amount of truncation error added per pulse decreases (global truncation error $\propto h$). This has follow-on effects for the rest of the error-time profile. Primarily these are due to initial-condition error. A reduction in truncation error from $0.01 - 0.02$ s means that the difference between the exact and analytic solution is reduced. Thus as the magnitude of initial condition error depends on the square of the difference between the simulated and exact solution, the amount of initial-condition error is also reduced

This has a complicated effect on these error-time profiles. Previous analysis showed that initial-condition error causes the system to self-correct, i.e., the exact and numerical solutions converge. By reducing the amount of the initial-condition error that is added one reduces the amount the system self-corrects. This is shown in figure 3-16 by the fact that the difference

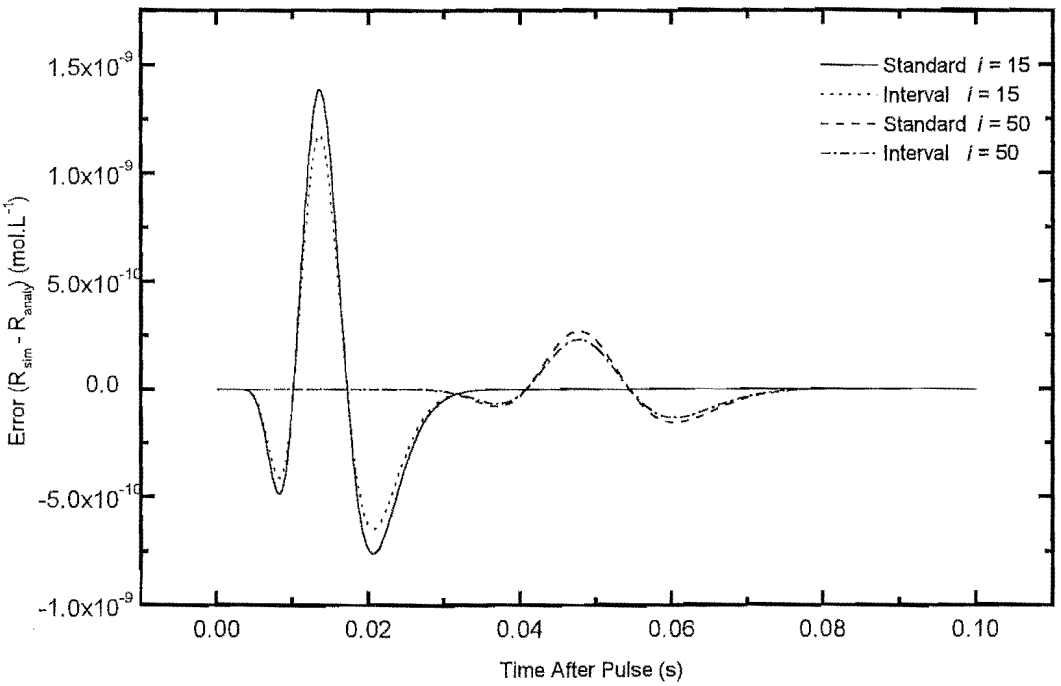

Figure 3-17: The error in the concentration of radicals of chain-length 15 and 50, when the differential equations are solved with and without a time dependent step-size profile.

between the two curves is reduced between 0.02 and 0.1s after the initiation burst. All of the other effects shown in figure 3-16, e.g., the change in the height of the error maximum result from a reduction in the magnitude of error caused by using a smaller step size for $0.01 - 0.02$ s.

In summary, a TDSSP reduces the amount of self-correction in the solution error. This loss is well and truly made up by the overall reduction in the magnitude of error incurred. Therefore, an analysis of the error incurred when this system of differential equations is solved with a time-dependent step-size confirms that this method causes significant gains in accuracy.

Error Standard Three Having examined the effect of a time-dependent step-size profile on the error in the total radical concentration, the error in the radical chain-length distribution must also be explored. To do this error standard three is used. Figure 3-17 is a plot of the difference between the simulated concentration of radicals of chain length 15 and chain length

50 and those same concentrations modeled by equation 3.20. To allow a comparison this plot includes the concentration-time plots for a time-independent as well as a time-dependent step-size profile. The reason that error for the concentration of radicals of two chain lengths is given is that it is important to compare a radical species that has its most probable chain length during the time of reduced step size and one that does not ($i = 15$ is the most probable chain length 0.015 s after the arrival of a pulse).

Figure 3-17 shows that a time-dependent step size reduces the amount of error in both the concentration of radicals of chain length 15 and 50. Hence, allowing the step size to depend upon time increases the accuracy of individual radical concentrations, as well as the total radical concentration.

It was clear from the analysis of the error in the radical concentrations performed when the system was modeled using a constant step-size profile that the most error was added to the concentration of radicals of a certain length when the chain length was the most probable chain length. It follows therefore that a greater gain in accuracy should be made to a chain whose chain length is the most probable chain length during the time when the small step size is used. In this case this means that, as the interval of small step size starts at 0.01 s and continues to 0.02 s, radicals of chain length 10 to 20 should be modeled with greater accuracy; this is in fact the case. If the curves shown in figure 3-17 are integrated and the ratio of the error for constant step size to error for time dependent step is evaluated, it is clear that a greater gain in accuracy is made for the radicals of chain length 15 (error incurred with time dependent step-size profile is 85% of error for constant step-size profile) than for radicals of 50 (98%).

This suggests that the sections of smaller step size should be positioned at times where radicals that are most prone to error pass through their most probable chain length. In the section where the error incurred by a constant step-size profile was studied we saw that the rate of change in these equations, and hence the amount of error incurred, was greatest for radicals of low chain length. This suggests that a step size should be used that takes more care (smaller steps) early in the time between laser pulses. This is a fortunate result as it means that a similar step-size profile can be used to increase the accuracy of the solution of the total radical concentration as well as the radical chain length distribution.

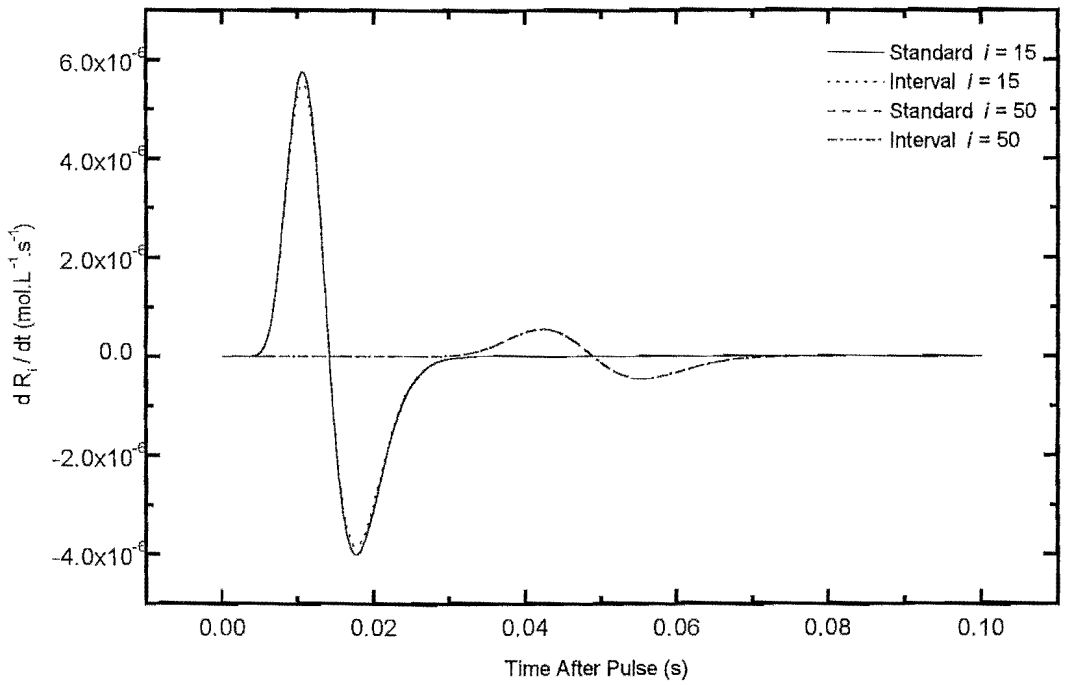

Figure 3-18: The effect of a time-dependent step-size upon the values of the differential equation. Data is presented for radicals of chain-length 15 and 50 where the differential equations have been solved with a time-dependent and time-independent step-size profile. Rate parameters as per table 3.3.

Error Standard Four Error standard three indicated that the error in the radical chain-length distribution decreases when a TDSSP is used. To confirm this and to explore what other effects such a profile has on the error in these systems, error standard four has been applied. The results of this analysis are presented in figure 3-18. Figure 3-18 contains a plot of the rate of change in the concentration of radicals of chain lengths 15 and 50 with a time-dependent and a time-independent step-size profile.

The three previous error analyses indicated that the error in the system of differential equations was reduced by using a TDSSP. Moreover, these analyses indicated that the error was reduced by the greatest amount when the section of small step size was placed early in the interval between two bursts of initiation. Error standard four produces data that supports

these conclusions. It finds that the error in these differential equations is reduced when a TDSSP is used. Furthermore, it indicates that using small steps early in the time between two bursts of initiation leads to the greatest reduction in error. This is shown in figure 3-18, where the greatest reduction of error is achieved when the small step size is used at times when the differential equations are changing by the greatest amount, i.e., at times when the radicals of small chain length are the most probable chain length.

Conclusion This analysis has confirmed that using a time-dependent step size is one method of reducing the error in the solution of these differential equations. Moreover, this analysis suggested that a step-size profile where the size of the integration steps increases with time is the most efficient step-size profile.

However, it is important to point out that the time-dependent step-size profile used in this section decreases the average step size. This means that the error will be reduced simply because the number steps taken per pulse is increased. Thus, to be able to claim that a time-dependent step-size profile should be used, rather than simply a reduction in the step size, one must show that a time-dependent step-size profile reduces the error more than a step size reduction would. That is, one must show that a time-dependent step-size profile increases the solution efficiency. Although a full efficiency analysis will not be performed for this step-size profile, some simple calculations indicate that using a time-dependent step-size profile increases efficiency.

A step-size profile based on the method of sections with a maximum step size of $h_{max} = 1 \times 10^{-4}$s and a minimum step size of $h_{max} = 1 \times 10^{-5}$s causes 1900 steps to be taken per initiation period. If the interval of minimum step size is placed from $0.0 - 0.01$ s after the initiation burst a mean error per pulse of 2.2×10^{-4} is incurred in a system with $k_t = 1 \times 10^{8}$L.mol^{-1}.s^{-1}. To obtain the same level of accuracy with a time-independent step-size profile 2210 steps must be taken per initiation period. Hence, a time-dependent step-size profile leads to an increase in efficiency. It will become clear in the following two sections that greater efficiency can be obtained with more elaborate step-size profiles.

3.10.5 Time-dependent Step-Size Profile Based on the Exponential Function

The step-size profile used above allowed the step size to be one of two values. In this section, a step-profile is introduced that allows the step size to change continuously with time. This step size is based on the exponential function. Thus, the size of a step taken at time t is described by equation 3.33.

$$h_t = h_{max}(1 - ae^{-bt}) \qquad 0 \leq t < t_0 \tag{3.33}$$

Here, h_t is the step size at time t since a burst of initiation, h_{max} is the maximum allowed step size (note that this value maybe varied), t_0 is the length of the initiation period and a and b are values that can be varied according to rate coefficient for termination and R_{max}, the maximum total radical concentration at the start of an initiation period. Clearly $0 \leq a < 1$ and $b \geq 0$. This profile describes how the integration step size will depend on time for one initiation period. At the end of that initiation period, t is set equal to zero and the profile repeats. Figure 3-19 contains a plot of the step-size profile predicted by this expression.

This step-size profile fulfills both of the requirements outlined in the previous sections: it is strongly time-dependent and the step size increases as time passes. The exponential function is used as the basis for this profile because it closely approximates the plot of how the error depends on the start time for the interval of small step size (figure 3-15).

The major problem faced in using this step-size profile is finding the optimal values of a and b, i.e., the shape of the optimal step-size profile. By changing the values a and b one changes the efficiency of the solution strategy, hence to best use this time-dependent step-size profile one must find the values of a and b that minimize the efficiency value, ξ. As was stated above, the efficiency of a solution strategy is defined as the product of the number of steps taken per pulse and the mean error per pulse.

Therefore, to find the optimal values of a and b, one must find expressions for how the number of steps taken per pulse, and the error incurred, depend upon these values.

Equation 3.34 describes the manner that the number of steps taken per pulse period depends on the step-size profile. This expression was derived by performing simulation studies where the values of a, b and h_{max} were systematically varied. There may be an analytic derivation for

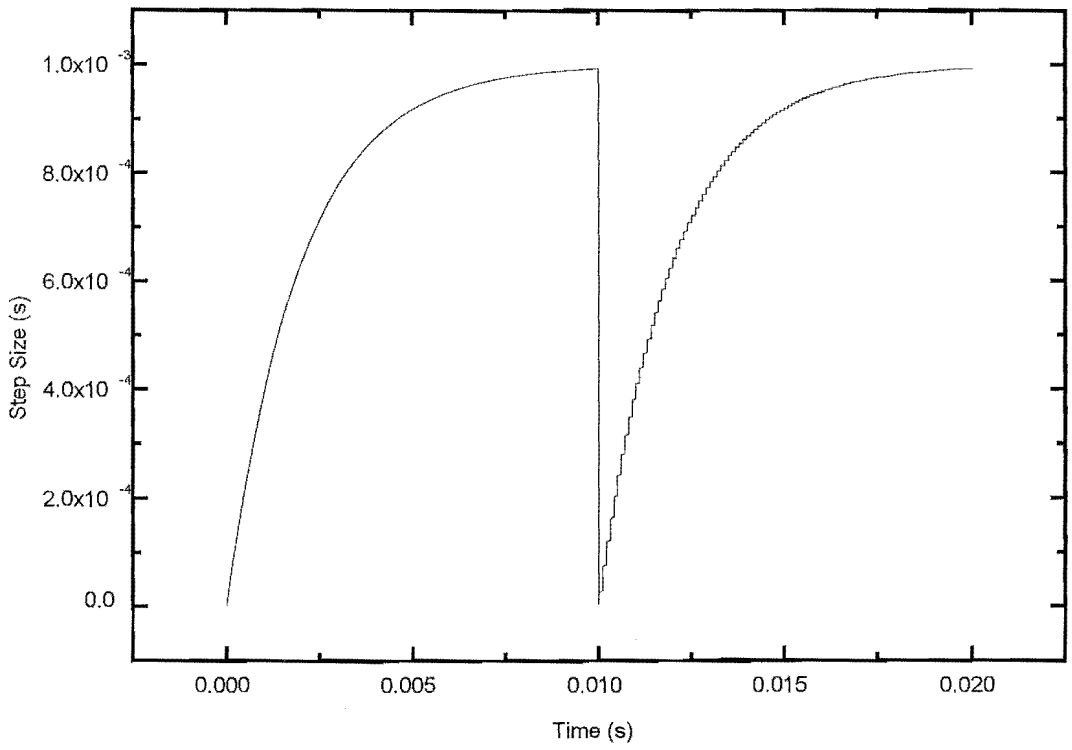

Figure 3-19: Time-dependent step-size profile based upon the exponential function. Parameters: $h_{max} = 1 \times 10^{-3}$s; $a = 0.999$; $b = 500$; and $t_0 = 0.1$s.

this equation, but it was not easily evident.

$$n_{steps} = \frac{t_0}{h_{max}} - \frac{1}{bh_{max}} \ln(1-a) \tag{3.34}$$

In this expression, all symbols have the same definitions as they did in equation 3.33.

An identical procedure is performed to elucidate an expression for how the error depends on these values. This expression is slightly more complicated, as it also depends on the rate constant for termination and radical concentration at the start of an initiation period. Simulation

studies have shown that this expression is:

$$E_{pulse} = \sqrt{k_t R_{max}} h_{max} (0.75 - 5.78 \frac{1-a}{b}) \tag{3.35}$$

Therefore, as the differential equations are evaluated once per integration step the efficiency value is equal to:

$$\xi = E_{pulse} . n_{steps} \tag{3.36}$$

$$\xi = \{\sqrt{k_t R_{max}} h_{max} (0.75 - 5.78 \frac{1-a}{b})\} \{\frac{1}{h_{max}} ((t_0 - \frac{1}{b} \ln(1-a))\} \tag{3.37}$$

As the optimal step size is the one with the minimum efficiency value, it is necessary to solve equations 3.38 and 3.40 for a and b

$$\frac{\partial \xi}{\partial a} = 578 \frac{\sqrt{k_t R_{max}}}{b} (t_0 - \frac{\ln(1-a)}{b}) + \frac{\sqrt{k_t R_{max}} 0.75 - \frac{5.78b}{1-a}}{(1-a)b} = 0 \tag{3.38}$$

$$\frac{\partial \xi}{\partial b} = 78 \sqrt{k_t R_{max}} \frac{1-a}{b^2} (t_0 - \frac{\ln(1-a)}{b}) + \sqrt{k_t R_{max}} (0.75 - 5.78 \frac{1-a}{b}) \frac{\ln(1-a)}{b} = 0 \tag{3.39}$$

$$b = 1156 \ln(1-a) \frac{a-1}{578 a t_0 - 578 t_0 - 75 \ln(1-a)} \tag{3.40}$$

Unfortunately, there are two problems that must be faced when using this method to find the optimal values of a and b. Firstly, as the value of a depends on the value of b and vice versa, these equations must be solved iteratively. Secondly, an analytic expression could not be obtained for the equation for a, so this value had to be found numerically. The Newton-Raphson root finding method was used to achieve this as apart of the iterative solution algorithm.

This method for calculating the optimal values of a and b has been incorporated into a computer program for simulating intermittently-initiated polymerization. This computer program first calculates the maximum radical concentration (the concentration of radicals straight after a burst of initiation) for the pseudo-steady state. This concentration, the rate coefficient for termination and an initial value of a are then used to predict b. This value of b and the Newton-Raphson method are then used to predict a new value for a. This procedure is repeated until a convergence criterion has been satisfied. This criteria required that the relative difference between successive estimates of a and b was less than 0.01%. Typically, three iterations are

k_t(L.mol^{-1}.s^{-1})	a	b	ξ
1×10^6	0.19	22.8	1.98×10^{-2}
1×10^7	0.27	35.2	1.86×10^{-1}
1×10^8	0.85	103.8	5.95×10^{-1}

Table 3.7: Optimal step-size profile parameters for three different termination rate coefficients.

required and the whole procedure is effectively instantaneous.

The values of a and b that were obtained by this method are given in table 3.7 for three termination rate coefficients.

This table also includes the efficiency values for this combination of step-size profile and solution method. All of the efficiency values measured are significantly less than those obtained with a constant step-size profile. For example, whereas it took 16600 steps per pulse to reduce the error in a system with a k_t of 1×10^6L.mol^{-1}.s^{-1} to 1×10^{-5}, when an optimized step-size profile based on the exponential function is used, 1980 steps are required. This is a significant reduction in computational expense. These results provide strong evidence in favor of the use of a time-dependent step-size profile. In the next section, this result will be improved upon further.

It was noted above that the efficiency value obtained for a constant step-size profile is independent of the step size used. A similar result is found when an exponential based step-size profile is used - the efficiency value is independent of the maximum step size. It has also been shown that the optimal values of a and b are independent of the maximum step size (equations 3.38 and 3.40). However, the maximum step size does affect both the mean error per pulse and the number of steps taken per pulse (equations 3.34 and 3.35). This means that one can obtain a required level of accuracy by changing the maximum step size and keeping the optimized a and b parameters constant. In this way one gains greater accuracy, but at commensurate computing cost, and there is no net reduction of the efficiency parameter. However, obviously one is interested in having a certain maximum level of error, and $h_{\max}$ must be chosen accordingly (see equation 3.35).

Figure 3-20 contains a plot of the optimal step-size profile for the solution of the differential equations with three different termination rate coefficients. This plot indicates that the shape of the optimal step-size profile is strongly dependent on the rate coefficient for termination, such

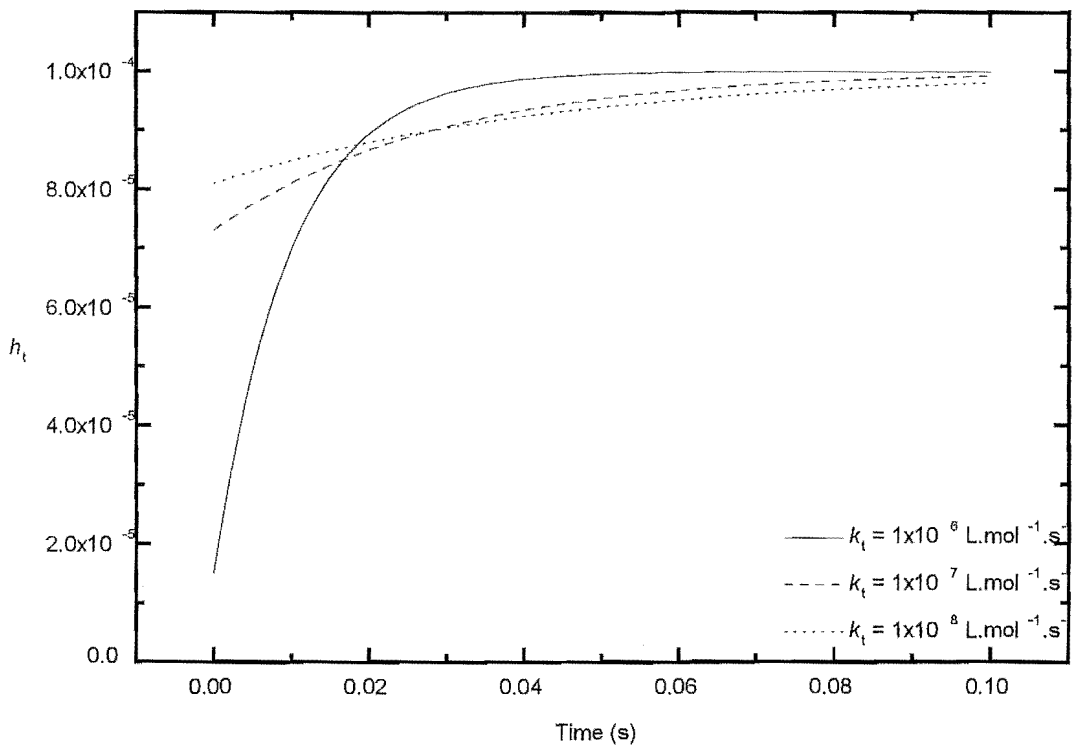

Figure 3-20: Optimal expontential based step-size profiles for three different termination rate coefficients. All rate parameters as per table 3.3 and table 3.17.

that a 'steep' step-size profile is needed when a high value of k_t is used. As has been argued before, this is because the rate of change in the differential equations is dependent on both the rate coefficient for termination and the maximum radical concentration. Hence, as the amount of error incurred, and when most of that error is incurred, is dependent on the rate coefficient for termination and the maximum radical concentration (equation 3.35), it is unsurprising that the method outlined above would yield optimal step-size profiles that dependent on the k_t and R_{max}.

The efficiency values indicate that the use of a time-dependent step-size profile has allowed this system of differential equations to be solved rapidly, while incurring minimal error. However, it is prudent to analyze in detail the error added under these conditions. To do this error

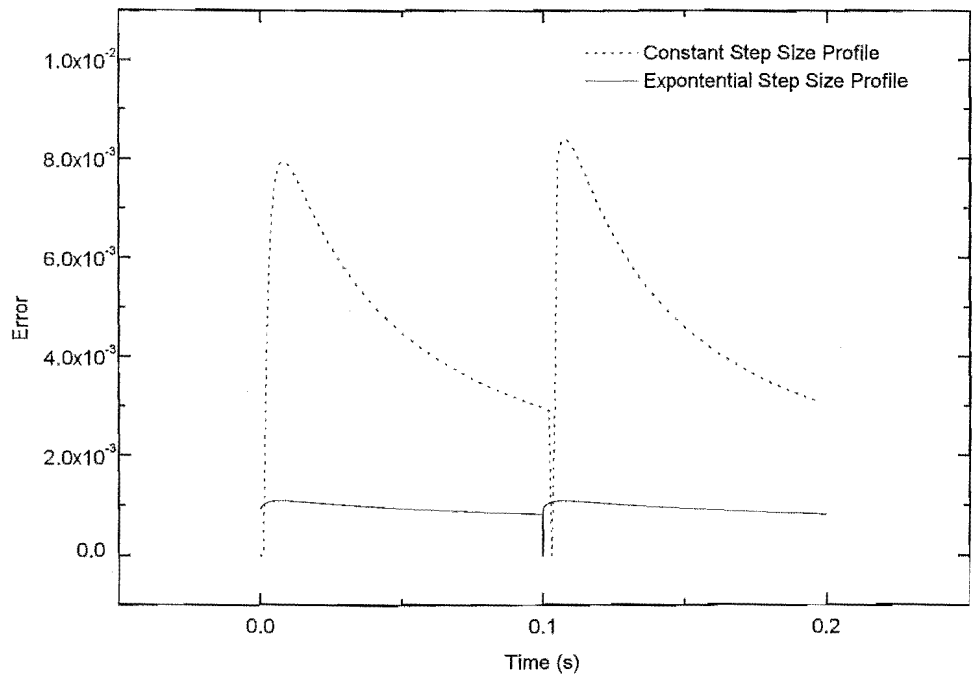

Figure 3-21: The temporal dependence of error when the differential equations are solved with an optimized step-size profile based on the exponential function. Rate parameters are the same as those shown in table 3.3 and $h_{max} = 1 \times 10^{-4}$s. The error-time plot for the differential equations solved with a constant profile is for a step-size $h = 8.5 \times 10^{-5}$s so that the same number of integration steps are taken per pulse in each case

standards two through four will be applied.

Error Standard Two Figure 3-21 contains a plot of the temporal-dependence of error when the differential equations for intermittently initiated polymerization are solved with the optimized step size parameters discussed above. For comparison, the error-time plot for the same differential equations, solved with the Euler method but with a constant step-size profile, are also presented (dotted line).

This plot leaves little doubt that a step-size profile based on the exponential function significantly improves the efficiency of the solution of these differential equations. The magnitude of the error incurred when this profile is used is less than the error incurred by a constant step-size

profile at all times. Moreover, the refined error-time profile is less time dependent than that produced with a time-independent step-size profile.

The shape of the error profile is significant, as it provides an indication of how well the time dependence of error has been accounted for. That is, by taking more care when the system for differential equations are prone to error and less when they are not so, the amount of error incurred has become approximately independent of time. This is yet another indication that the optimized time-dependent step-size profile has been a success. Focussing on the way that the error changes with time when the optimized profile is used suggests that there is further room for improvement. Although the error incurred per step is effectively constant for the majority of the initiation period, there is a small increase in error straight after the arrival of the initiation burst. This failure to completely remove the time dependence of solution error suggests that even an optimized exponential based step-size profile can not completely fit the time-dependence in error. Furthermore, it means that additional gains may be able to be made if a function that fits the temporal dependence of error more closely is used. A function that does this will be introduced in the next section.

Error Standard Three It is now clear that a time-dependent step-size profile based on the exponential function significantly reduces the magnitude the error incurred by accounting for the time dependence in error. However, several questions concerning the effect of this step profile on the error incurred remain unanswered. For example, what effect does this step profile have on the error in the radical chain-length distribution? And how does it affect the values of the differential equations? In this section, attempts will be made to answer the first of these questions.

Figure 3-22 contains a plot of the error in concentration of radicals of chain length 10, when the differential equations are solved using a time-independent and exponential based time-dependent step profile. This plot indicates that the error in the individual radical concentrations is also reduced when this TDSSP is used. Integration of the error incurred in one radical concentration during one initiation period shows that 39.6% as much error is incurred when the exponential step-size profile is used as when a constant step-size profile is used.

A subsequent analysis of the effect upon radicals of chain length 50 showed that the error

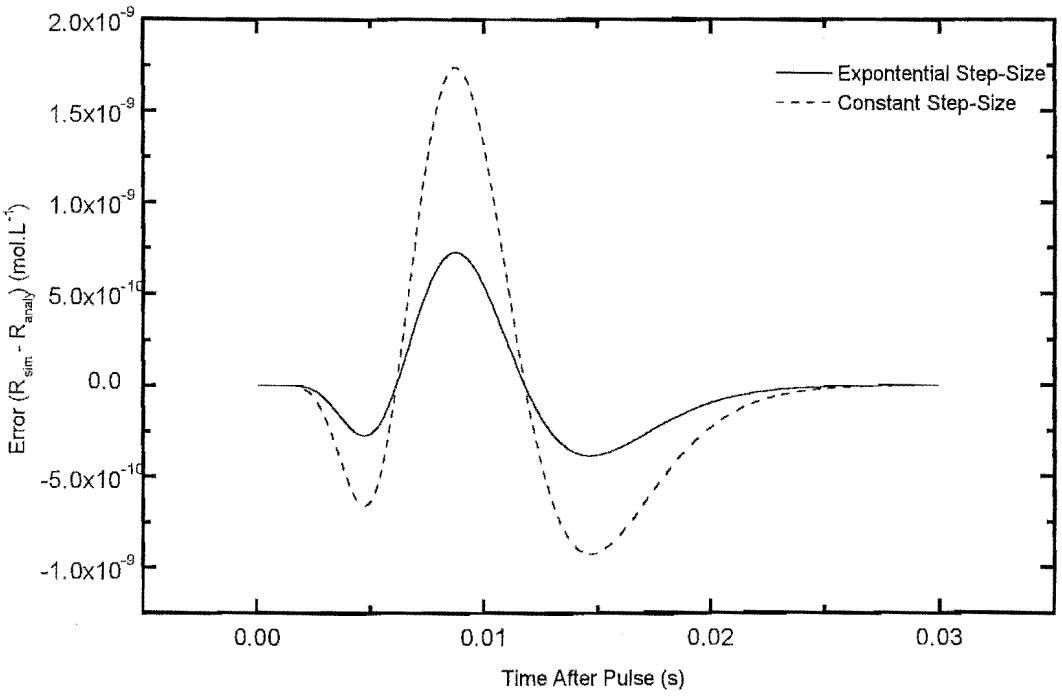

Figure 3-22: Error in the concentration of radicals of chain-length 10 when the differential equations are solved with the constant step-size profile and optimized exponential step profile. Rate parameters as per table 3.3 and in addition $h_{max} = 1 \times 10^{-4}$s. Again the step-size used in the constant step-size profile is chosen so that number of steps taken per pulse is the same in both cases.

in the species had been reduced by a smaller amount (it was 87.5% of its value for a time independent step-size). This is due to the fact this species has its most probable chain length in a period of time when larger integration steps are being taken. This a pleasing result because the magnitude of the error in radicals of chain length fifty is approximately one quarter of that in radicals of chain length 10. So reducing the error in small radicals is an efficient means of reducing the overall error in the radical chain-length distribution. Therefore, this step-size profile significantly reduces the error in the radical chain-length distribution.

Error Standard Four The last method of analyzing the error incurred in the solution of these differential equations shows the same trend as that shown in the three previous error assessments, i.e., the use of a time-dependent step-size profile significantly reduces the error incurred. Using this error standard, two comparisons have been made. Firstly, the value of the differential equations calculated with the exponential based time-dependent step-size profile are compared with those calculated by a constant step-size profile with a very low step size ($h = 1 \times 10^{-8}$s). Secondly, the values of the differential equations predicted by a constant step-size profile ($h = 8.5 \times 10^{-5}$s) are compared with the same very low step-size solution. If it is assumed that the values of the differential equations calculated with the very low step size are the most accurate, then the amount that the other values diverge is an estimate of the error. This analysis indicates that the values of the differential equations obtained with an exponential based step size are significantly closer to the low step-size values than the high step-size values. Hence, as the same number of steps per pulse are taken by the high step-size and exponential based step-size profiles, the exponential based step profile is the most efficient.

Recommendation It is realized that the calculation of the optimal values of a and b is a laborious process. For this reason I recommend that the values for a and b shown in table 3.7 should be used in most modelling studies. The decision about which set of a and b value should be used, i.e., for which value of k_t, should be based on knowledge of the system being study. Otherwise, I recommend that values of $a = 0.85$ and $b = 104$ be used in all other cases.

Conclusion In this section, a step-size profile that allows the integration step size to vary continuously with time has been introduced. A method for optimizing the two unknown parameters in the expression for how the step size changes with time has been developed, and the resulting profiles have been implemented.

An investigation of the error incurred when this profile was used has been performed. This analysis has indicated that an exponential function based TDSSP reduces the amount of error incurred when the error is measured under any one of the four error standards. A full discussion of the implications of these results will be given in concluding this chapter.

3.10.6 The Final Step-Size Based Refinement: A Step-Size Profile Based on the Rate of Change in the Differential Equations.

In this, the penultimate section of this chapter, the final and optimal step-size based refinement for a finite-difference based method acting on the differential equations for intermittently initiated polymerization will be introduced and implemented. In the previous section, an exponential based step-size profile was developed. While this method significantly increased the efficiency of the Euler method, there were several suggestions that step-size profile based refinement could be taken further. For example, although the profile of error incurred against time was almost time-independent, it was not completely so. This is likely to be the result of an incomplete fit of the exponential function to the hypothetical optimal step-size profile. Therefore, it may be possible to achieve even greater efficiency using a function that will fit more closely to the hypothetical optimal step-size profile.

Previously, when explaining the origin of truncation error frequent use was made of the idea that the error in the solution of the differential equations is proportional to the rate of change in the differential equations. The step-size profile used in this section is based upon this concept. This step profile takes small steps when the differential equations are changing rapidly and large steps when they are changing slowly. Equation 3.26 describes the way that the rate of change in the differential equations depends upon the time since the laser pulse. It says that the rate of change is proportional to one over the time cubed or

$$\frac{d^2\mathrm{R}}{dt^2} = \frac{A}{(1+Bt)^3} \tag{3.41}$$

In this expression, A and B are values which depend on a combination of rate parameters (see equation 3.26). A function for the step-size profile based on this function is:

$$h_t = h_{max}(1 - \frac{a}{(1+bt)^3}) \tag{3.42}$$

In equation 3.42, h_t is defined as the size of the integration step at time t, h_{max} is the maximum step size and a and b are values that the depend on the rate coefficient for termination and the maximum radical concentration (note that these are different values of a and b from those used

with the exponential step-size function).

To find the values of a and b that define the step-size profile that gives the most efficient solution to these differential equation the procedure used to find the optimal step-size profile based on the exponential function will again be used here. This involves finding expressions for how the error and the number of steps per pulse depend on a and b, then combining these expressions to give an expression for how the efficiency of the solution depends on a and b. The next step in this procedure is to evaluate the partial differentials of this expression, and solving these for a and b.

The first part of this procedure involves finding an expression that describes the way the number of steps taken per pulse depends on a and b. Unfortunately, it is more difficult to find this expression than it was to find equation 3.34. An expression has been found that works under certain conditions:

$$n_{steps} = \frac{t_0}{h_{max}}(1 - 4.04\frac{\ln(1-a)}{1+b}) \qquad \text{for } b > 1 \times 10^{-4} \tag{3.43}$$

If a value of b less than 1×10^{-4} is used, then this expression does not hold. However, as such values of b produce a step-size profile that increases linearly with time – a step-size profile that is far from optimal – this limitation does not severely restrict this method.

The second stage in this procedure is the elucidation of a function that describes the dependence of error upon a and b. This function has been found via a number of simulation studies.

$$E_{pulse} = h_{max}\sqrt{k_t R_{max}}(0.76 - 8.68\frac{(1-a)}{b}) \tag{3.44}$$

Using these two expressions, a function for the efficiency of the solution in terms of a and b, as well as several other parameters can be found.

$$\xi = E_{pulse}.n_{steps} \tag{3.45}$$

$$\xi = \sqrt{k_t R_{max}}(0.76 - 8.68\frac{(1-a)}{b})t_0(1 - 4.04\frac{\ln(1-a)}{1+b}) \tag{3.46}$$

The partial differentials of this expression with respect to a and b can then be evaluated and

k_t(L.mol^{-1}.s^{-1})	a	b	ξ
1×10^6	0.55	0.45	1.974×10^{-2}
1×10^7	0.75	0.85	1.586×10^{-1}
1×10^8	0.95	1.67	5.318×10^{-1}

Table 3.8: Optimized step-size profile parameters and efficiency values for three values of the termination rate coefficient.

set equal to zero and solved.

$$\frac{\partial \xi}{\partial a} = 8.68\sqrt{k_t R_{max}} b^3 t_0 (1 - 4.04\frac{\ln(1-a)}{1+b}) 4.04\sqrt{k_t R_{max}}(0.76 - 8.68\frac{1-a}{b^3})\frac{t_0}{(1-a)(1+b)} = 0 \tag{3.47}$$

$$\frac{\partial \xi}{\partial b} = 26.04\sqrt{k_t R_{max}}\frac{1-a}{b^4}(1-4.04\frac{\ln(1-a)}{1+b}) + 4.04\sqrt{k_t R_{max}}(0.76-8.68\frac{1-a}{b^3})t_0\frac{\ln(1-a)}{(1+b)^2} = 0 \tag{3.48}$$

Both of these expressions are solved by the Newton-Raphson method and iterated until there is an insignificant change in the values of a and b. Table 3.8 contains the optimal values of a and b for three termination rate coefficients. If the efficiency values obtained with this step-size profile are compared to with those for the previous step-size profile, it is clear that there is refinement increases the solution efficiency. For example, the efficiency value for the solution of these equations for termination rate coefficient of 1×10^8 L.mol^{-1}.s^{-1} is 10% less than the efficiency value of the same system when an exponential based step-size profile is used. Furthermore, the extent of this refinement depends upon the rate constant for termination. For example, there is a negligible increase in efficiency of the solution of differential equations with a $k_t = 1 \times 10^6$L.mol^{-1}.s^{-1}.

This suggests that the problems the exponential based step-size profile faced in fitting the hypothetical optimal step-size profile were most dramatic for high k_t systems. The step-size profile based on equation 3.42 provides the best means to date for obtaining efficient solution to the PIP differential equations with the Euler method.

Again, to be able to argue with the utmost confidence that this new step-size profile does in fact reduce the error incurred with the same amount of computational expense, the error

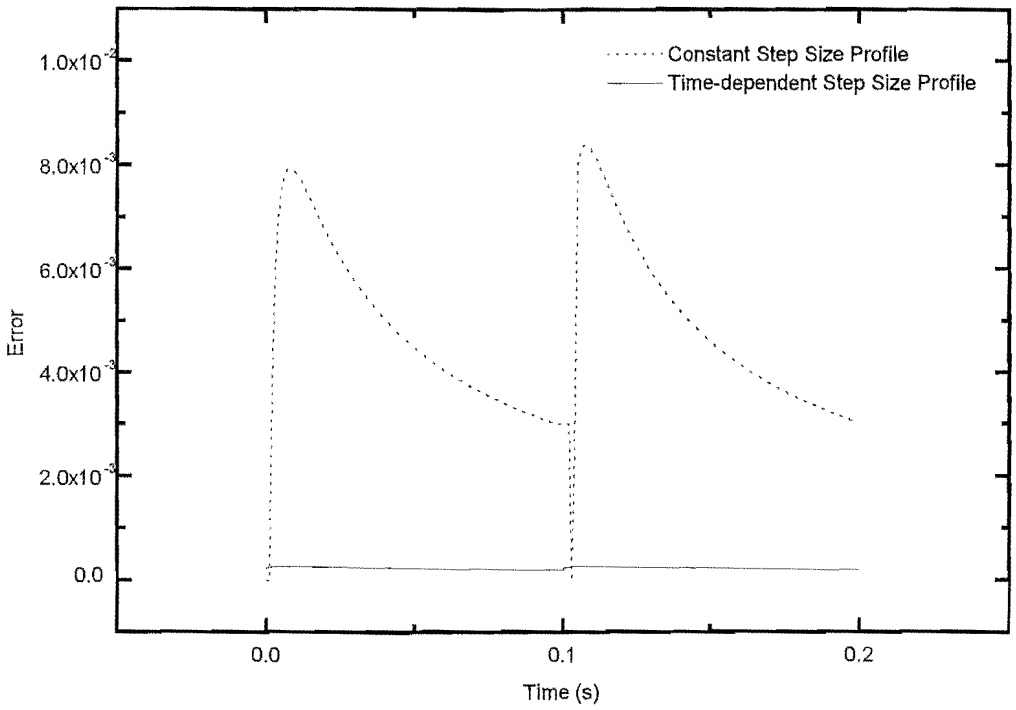

Figure 3-23: A comparison of the error-time profiles for the Euler method with and without a time-dependent step size profile. Error measured via error standard two.

must be analyzed in detail. To do this the error will be examined as it was above, via error standards two, three and four.

Error Standard Two Figure 3-23 contains a plot of the time-dependence of the error incurred when the system of differential equations is solved with the rate of change based time-dependent step-size profile and a constant step-size profile. The constant step-size profile is adjusted so that both methods take the same number of integration steps per pulse. A maximum step size of $h = 1 \times 10^{-3}$s is used with the time-dependent profile for a $k_t = 1 \times 10^{8}$L.mol^{-1}.s^{-1} system and a time-independent step-size profile with $h = 1.77 \times 10^{-4}$s was used. Figure 3-23 shows clearly the reduction in error that occurs when a TDSSP is used. The amount of error incurred is significantly less than that when a TISSP is used. Moreover, the error-time profile

is significantly flatter for the TDSSP than for the TISSP. The error profile produced by this time-dependent step-size profile shows even less dependence on the time since the arrival of the initiation burst than the error-time profile contained in figure 3-21. However, there is still some residual time dependence. This can be attributed to slight numerical errors in the optimization procedure; in particular, the Newton-Raphson procedure frequently had trouble obtaining the value of b. To ascertain the cause of this problem, the efficiency value was plotted for several values of b about the optimal value. This indicated that the efficiency value was very sensitive to changes in the value of b, so that a small change in the value of b caused significant changes in the efficiency of the solution. Hence, I attributed the time dependence shown in figure 3-23 to a slight error in the value of b.

This aside, a step-size profile based on the rate of change in the differential equations is more effective than the one based on the exponential function in accounting for the time-dependence of error. Because of this, this solution strategy incurs less error.

Error Standards Three and Four The last error standards investigate the error in the individual radical concentrations and their corresponding differential equations. Plots of the error produced by these analyses are not given here as they are very similar to those outlined previously (section 3.10.5). A time-dependent step-size function based on the rate of change in the differential equations has the same effect on the individual radical concentrations and the values of the differential equations as the exponential based step-size function did; most importantly, it reduces the error incurred. Hence, we are able to conclude that this step-size profile can be used with some confidence.

Recommendation I recommend that the values of a and b shown in the table 3.8 should be used along with the time-dependent step-size profile developed above. Moreover, I recommend that if there is any doubt about which values of a and b should be used, then a should be set equal to 0.95 and b to 1.67.

3.11 Conclusion

In this chapter, finite-difference based numerical methods have been introduced and a set of standards for measuring the error in the solutions generated when these methods are used to solve equations 3.22 – 3.24 has been developed. In addition to this, the efficiency of these solution strategies has been defined and an expression that allows a numeric value for the efficiency to be calculated has been established.

The simplest finite-difference based numeric solution strategy - the Euler method - has been used to solve these differential equations and the error thoroughly studied. This analysis has shown that the Euler method is effective at generating efficient solutions to this system of differential equations. Moreover, this analysis revealed a number of trends in the error incurred. In general, the error measured by all of the standards is strongly dependent upon time and upon the radical chain length distribution in these systems.

The concept of a time-dependent step-size profile has been introduced and number of these profiles have been implemented and the resulting error assessed. This analysis has shown that the optimal step-size profile is one based on the time-dependence of the rate of change in the differential equations for the total radical concentration. In particular, using this TDSSP significantly increased the efficiency of the Euler method. On average, the refinement outlined here decreased the efficiency values by one order of magnitude. This means that when this step-size profile is used in conjunction with the Euler method that one tenth the number of integration steps per pulse are need to achieve the same level of accuracy. Practically, this means that detailed kinetic studies can be performed on complicated polymerization systems in reasonable lengths of computer time.

Moreover, the analysis of the error incurred with error standard two indicated that this step-size profile has drastically reduced the temporal dependence of the error. These results suggest that the profile used almost achieved the aim of making the error time independent.

Finally, an analysis of the error in the radical chain-length distribution showed that this refinement also decreased the error in the concentrations of individual radical species. Furthermore, the error in small radical species, those most prone to error, is reduced by a greater degree than that for larger radical species.

Therefore, overall this refinement is a simple method for significantly increasing the efficiency

of the simple Euler numerical solution strategy by providing that strategy information about the nature of error in intermittently initiated polymerization systems.

The most significant discovery made in this chapter is in fact one of the simplest. This is that a simple FDB method – the Euler method – can be used to solve this system of differential equations. It is accepted wisdom that explicit methods, of which the Euler method is an example (see chapter four), can not be used to solve stiff differential equations. Here we have seen that this is not the case. A simple explicit method can be used to successfully solve a stiff system. As was explained in chapter one, stiffness is a result of the solution to a differential equation containing two components, ones that change at very different rates. This means that when solving stiff differential equations one is forced to use a step size that accounts for the most rapidly changing part of the solution, even if that part of the solution is not important in terms of the final results. It does not mean however that an explicit method can not be used – all that is required is the step size used is small enough so that it does not incur significant error in the rapidly changing component of the solution. This is what we have seen here. A simple explicit method can be used to solve a set of complex differential equations as long as the step size used is less than $\frac{1}{k_p M}$. The real effect of stiffness is that by forcing one to use a small step size, a step size that can model the rapidly changing solution component, it drastically increases the cost of obtaining the solution. That is, it does not mean that an explicit method can not be used; rather it means that frequently the cost of using an explicit method is high. This is where implicit methods come into their own. Implicit methods circumvent the limitations imposed by the rapidly changing solution component, and by doing so generally reduce the cost of obtaining the solution. However, this is not always the case. We will see in the next chapter that the gains an implicit method allows are well and truly outweighed by the costs they incur.

Chapter 4

Numerical Solution Techniques: The Approximation Function

4.1 Introduction

In the previous chapter, a differential equation solver was introduced, implemented and refined. This method, a finite-difference based (FDB) numerical approach, was used to solve the system of differential equations that describe intermittently initiated free-radical polymerization with some success. The analysis of this method revealed that this complex system of differential equations can be solved accurately, in a short period of time, by a simple method: the Euler method. Moreover, a refinement of this solution strategy was developed that significantly increased the efficiency of the Euler method. This investigation proved that even the simplest finite-difference based solution strategy can be successfully used as the core of a kinetic study of this type of polymerization.

In this chapter, a selection of more complex differential equation solution methods will be applied and assessed. The majority of these solution methods differ only in the approximation function that they use. As has been described previously, the approximation function is at the core of all finite-difference based numerical strategies. An approximation function is a function that uses several pieces of information to model the value of a differential equation during a time step. For example, the approximation function used by the Euler method is simply the value of the differential equations at the start of the time step. However, the

apparent simplicity of the task can be deceptive. Estimating the values of a complex system of differential equations can be a difficult task indeed, a task that is often akin to taking a step in the dark. A large number of approximation functions has been developed that can be used to solve differential equations. These approximation functions use a diverse range of approaches. As the methods based upon different approximation functions vary in how successful they are at solving a particular differential equation system, it is not always obvious which method should be applied. This then, is the question that I will attempt to answer in this chapter: which approximation function is best suited to solving the differential equations that characterize intermittently initiated free-radical polymerization?

To obtain information that can be used to answer this question, we will use the methodology developed in the previous chapter. This will allow us to measure the error incurred, and subsequently to assess the efficiency of a wide range of approximation functions. Those methods that appear to be the most proficient at solving these differential equations will then be used in conjunction with the time-dependent step-size profile developed in chapter three.

From this analysis, a series of recommendations about when a particular approximation function should or should not be used will be made. It will become clear that the decision about which approximation function is likely to give optimal efficiency is dependent upon several rate parameters, including the rate coefficient for termination and the truncation chain length.

4.2 Approximation Functions

There are two major types of approach used to derive approximation functions. The first approach works by expanding a hypothetical exact solution to a differential equation as an infinite series, for example a Taylor series (see equation 4.1). This expansion is then truncated, and the remaining terms approximated numerically. Two of the families of methods used in this thesis are derived in this manner, these being Taylor series and Runge-Kutta methods. The second approach produces methods that are known as extrapolation or multistep methods. This approach relies on that fact that if a function is able to describe previous values of the differential equations (for example their values at the last three integration steps), then it is likely that the same function will describe the differential equations during the next time step.

Extrapolation methods work by fitting a simple mathematical function, for example a second-order polynomial, to previous values of the differential equations and then extrapolating this function through the next time step.

These two approaches to deriving approximation functions yield two groups of methods. The first group combines values of the differential equations calculated at a number of points during an integration step to generate the next value of the solution. The second type, for instance multistep methods, uses the values of the differential equations from previous steps as the basis for predicting the next value of the solution.

In general, methods like the Runge-Kutta method (see section 4.4) are particularly suited to solving differential equations that are difficult to solve, for example, differential equations that are rapidly changing. These methods are normally thought of as being robust, but computationally expensive to use. On the other hand, multistep methods, for example the Predictor-Corrector method (see section 4.5), are known to be suited to solving differential equations that change slowly. These methods are normally thought of as being fast but unstable. In this sense, these two types of method can be thought of as opposites. Runge-Kutta or Taylor series methods are slow but robust, while multistep methods are fast but unstable.

The rationale behind applying both types of methods is as follows. The Euler method is a Taylor series method, and as this method met with some success, it reasonable to hypothesize that more complex Taylor series and Runge-Kutta methods will do as well, if not better. Secondly, it was surprising that such a rudimentary method (the Euler method) could be so successful. As this suggests that equations 1.18 – 1.21 may not be as unstable to numerical approximation as previously thought, methods that are renowned for their speed rather than their stability might prosper. Thus predictor-corrector and extrapolation methods were applied.

In this thesis one method will be used that is a hybrid of these two approaches. This method is known as Richardson's Extrapolation and the Bulirsch-Stoer method (see section 4.6).

Two other approaches, an implicit and a stochastic method, are used in this thesis, but these methods will not be introduced until just before they are implemented (see sections 4.7 and 4.8). For a more detailed introduction to approximation theory, see for example [20][6][13][53].

4.2.1 Taylor Series Methods

Taylor series methods are based on the Taylor series expansion of the exact solution to a general differential equation. For example, if $\Phi(t_n)$ is the exact solution at t_n, then the exact solution at $t_n + h$ is given by the Taylor series expansion given in equation 4.1.

$$\Phi(t_n + h) = \Phi(t_n) + h\Phi'(t_n) + \frac{h^2\Phi''(t_n)}{2!} + ... \tag{4.1}$$

Note that $\Phi'(t_n)$ denotes the first derivative of the exact solution with respect to time and that the m^{th} derivative is denoted by m accents. To convert expression 4.1 into a form that is useful as a numerical solution strategy two assumptions must be made. The first is that expression 4.1 can be truncated after a set number of terms without introducing significant error (truncation error). The second is that the exact solution and its derivatives can be replaced by the numerical solution and its derivatives (initial-condition error). The use of these assumptions produces expressions that can be used to numerically solve differential equations. As was noted above, if the Taylor series is truncated after two terms then the resulting expression is the equation for the Euler method (equation 4.2).

$$y(t_n + h) = y(t_n) + hf(t_n, y(t_n)) \tag{4.2}$$

Here the function $f(t_n, y(t_n))$ is the value of differential equation that is to be solved at time t_n. The Euler method solves a differential equation by using the last value of the solution and the value of the difference equation at that point to predict the next value of the solution. Other Taylor series methods can be derived by truncating the Taylor series after three or more terms.

4.2.2 Runge-Kutta Methods

One of the failings of Taylor series methods is the asymmetric way that they calculate and use derivative information; they advance the solution through an interval h, but only use derivative information from the start of a step. To overcome this limitation, a series of methods were developed that use derivative information more productively; these methods are known as Runge-Kutta methods. Runge-Kutta methods do this by taking trial steps. A trial step is a

small step, some fraction of h in length. Typically, a Taylor series method, i.e., Euler method, is then used to predict the solution after this trial step. Once the trial solution has been calculated, the value of the differential equations can also be evaluated. The final value of the solution for a whole step of length h is then calculated based on the value of the differential equations at the mid and end points. Some Runge-Kutta methods use more that one trial step. To illustrate how a Runge-Kutta method works we will consider the midpoint method. The midpoint method is a second-order Runge-Kutta method which takes one trial step of length $h/2$ per h sized integration step.

The equations for the midpoint method are:

$$k_1 = hf(t_n, y(t_n)) \tag{4.3a}$$

$$k_2 = hf(t_n + \frac{1}{2}h, y(t_n) + \frac{1}{2}k_1) \tag{4.3b}$$

$$y(t_{n+1}) = y(t_n) + k_2 \tag{4.3c}$$

In this equation, $y(t_n)$ is the old value of the solution at time t_n, and $y(t_{n+1})$ is the new value of the solution at t_{n+1},where $t_{n+1} = t_n + h$. First, a trial step of length $\frac{h}{2}$ is taken and a Taylor series method is used to predict the value of the solution. The differential equations are then evaluated at this point. This allows the final step to be taken using the value of the differential equation from the middle of the step, as predicted using the value of the differential equations at the start of the step. Note that this is not the same as using the simple Euler method with time step of $h/2$. This process is also shown mathematically by equation 4.3a - c. The first term, k_1, is the increase in the value of the solution over a whole, h sized, step. The second term, k_2, recalculates the change in the value of the solution based upon the value of the differential equations at the midpoint.

Two different orders of Runge-Kutta methods have been used in this study. The order of a Runge-Kutta method is related to the number of trial steps that it takes for each whole step. The most widely used Runge-Kutta method is the fourth-order Runge-Kutta. This method takes three trial steps and evaluates the differential equation four times per whole step. The fourth-order Runge-Kutta is a popular method because for most differential equation systems it has the right balance in accuracy and computational cost. The other Runge-Kutta method

used is the Modified Euler method, which is another second-order Runge-Kutta method (see section 4.3).

4.2.3 Multistep Methods

Both of the methods outlined above use information from the previous step only. However, once approximate values have been obtained for a few integration steps it is natural to ask whether better use can be made of this information. Methods that use information from more that just the last step are known as multistep methods.

One of the most popular multistep methods is the Adams-Bashforth-Moulton predictor-corrector method. This method takes information from the previous four steps, t_n, t_{n-1}, t_{n-2} and t_{n-3} to calculate the value of the solution at t_{n+1}. Before this method can work, three steps must have been taken. These initial steps are normally taken by a Runge-Kutta or Taylor series method.

There are two stages to operation of the Adams-Bashforth-Moulton method: a predictor and a corrector. The first stage, the Adams-Bashforth predictor, approximates the value of the differential equations from t_n to t_{n+1} by fitting a polynomial of degree three to the last four values of the differential equations. It can be shown that this can always be done and that this polynomial, known as the 'interpolation polynomial', is always unique. This polynomial is then substituted into equation 4.4.

$$y(t_{n+1}) - y(t_n) = \int_{t_n}^{t_{n+1}} y'(t)dt \tag{4.4}$$

In this expression $y'(t)$ is the polynomial approximation for the differential equations during the interval of t_n to t_{n+1}. Evaluating this integral gives the Adams-Bashforth predictor formula (equation 4.5).

$$y(t_{n+1}) = y(t_n) + \frac{h}{24}(55y'(t_n) - 59y'(t_{n-1}) + 37y'(t_{n-2}) - 9y'(t_{n-3})) \tag{4.5}$$

The second stage of the Adams-Bashforth-Moulton predictor-corrector is the Adams-Moulton corrector. This improves upon the value of $y(t_{n+1})$ calculated by equation 4.5. The expression for the corrector is derived in a similar manner to the predictor. This derivation involves fitting

a polynomial of degree three to the last four values of the differential equations, these being $y'(t_n)$, $y'(t_{n-1})$, and $y'(t_{n-2})$ and to the value of the differential equation based the value of the solution estimated by the predictor. The expression for the corrector is:

$$y(t_{n+1}) = y(t_n) + \frac{h}{24}(9y'(t_{n+1}) + 19y'(t_n) - 5y'(t_{n-1}) + y'(t_{n-2})) \tag{4.6}$$

In summary, multistep methods use information from previous integration steps to better approximate the value of the differential equations during the current integration step. Note that one is not limited to using the corrector only once; normally the corrector algorithm is reapplied until a convergence criteria has been satisfied.

4.2.4 The Hybrid Method: Richardson Extrapolation and the Bulirsch Stoer Method

This hybrid method approaches the solution of initial-value differential equations in quite a different manner to the methods outlined above. Central to its operation is the idea of Richardson's deferred approach to a limit. This involves considering the final solution of a numerical calculation as itself being an analytic function (if a complicated one) of an adjustable parameter, such as the step size. The form of the analytic function can be probed by performing numerical calculations with values of the step size that are higher than would normally be used in typical calculations. By performing a series of such probing calculations information is gained about how the final solution at the end of an interval, H, is affected by the size of the integration steps taken over that interval. When enough is known about the way that this final solution, i.e., $y(H)$, depends on the size of h used across that interval, an analytic function can be fitted to that data. The strength of this method is that the information gained by performing inexpensive (high h) calculations can be used to obtain the solution which would be obtained with a small step size (a potentially expensive calculation). This is done by extrapolating the analytic function to zero step size, i.e., taking the limit $h \to 0$. This method allows us to infer from numerical calculations the solution after a certain interval size (H) as if that solution had been acquired with an infinitely small step size. Extrapolation methods vary in the number of numerical calculations and the size of the steps that are used in those numerical calculations

to provide the data for the function fitting. They also vary in the type of function that is used in this fitting. In this study only one hybrid method has been used, this being Richardson's Extrapolation and the Bulirsch-Stoer method. This method uses rational analytic functions as the fitting functions and performs up to eight numerical calculations with large step sizes. These eight numerical calculations divide the size of the actual interval (H) into 2, 4, 6, 8, 10, 12, 16 and 24 intervals successively.

Richardson Extrapolation and the Bulirsch-Stoer method is a hybrid of the Multistep and Taylor series methods in the sense that it combines both of these approaches. A Taylor series method is used to perform the calculations that gather the information for the second phase of this method, and then rational function extrapolation is used.

4.3 The Modified Euler Method

The first numerical method that will be studied in this chapter is closely related to the Euler method. Note that it the remainder of this chapter if the Euler method is referred to this means the standard Euler method, that studied in chapter three. The modified Euler (ME) method is, as its name suggests, a refinement of the standard Euler method. It is a refinement that attempts to deal with the major failing of the Euler method – the difficulty it has in dealing with changes in the value of the differential equations during an integration step. To do this, the ME method evaluates the differential equations at the start, and at end of every integration step. It then evaluates the average of these two values and uses this as the approximate value of the differential equations. As an average is usually a better approximation of the actual rate of change than the initial value, the ME method normally incurs less error than the Euler method. However, this increase in accuracy does come at a cost. The ME method evaluates the differential equation twice per integration step. This means that the ME method must incur less than one half as much error as the Euler method to be a more efficient solution strategy. The expression that is at the core of the ME method is equation 4.7.

$$y(t_{n+1}) = y(t_n) + \frac{f(t_n, y(t_n)) + f(t_{n+1}, y(t_{n+1}))}{2} h \tag{4.7}$$

Equation 4.7 is the expression that the ME method uses to predict the value of the solution $y(t_{n+1})$ at time t_{n+1}. In this expression, $f(t_n, y(t_n))$ is defined as the value of the differential equations at time t_n when the value of the solution is equal to $y(t_n)$. There is one problem that must be overcome before this method can be implemented. This originates from the fact that the right-hand side of equation 4.7 contains an unknown, $f(t_{n+1}, y(t_{n+1}))$, the value of the differential equations at time t_{n+1}. As the value of the differential equations at the end of the time step can not be calculated until the solution $y(t_{n+1})$ has been found, an approximate value of $y(t_{n+1})$ must be found before equation 4.7 can be used. Typically, the Euler method is used calculate this approximate value of $y(t_{n+1})$ and this value is then used to calculate the differential equations $(f(t_{n+1}, y(t_{n+1})))$, allowing equations 4.7 to be evaluated. This means that the ME method is constrained by the accuracy of the Euler method. Nonetheless, the ME is normally an improvement upon the Euler method. The use of the Euler method to approximate the final value of the solution can be expressed as

$$f(t_{n+1}, y(t_{n+1})) \simeq f(t_n + h, y(t_n) + hy'(t_n)) \tag{4.8}$$

Note that the ME method is similar but slightly distinct from the second-order Runge-Kutta method outlined earlier. The latter uses an estimate of the differential equations at the midpoint of the interval, see equation 4.3.

4.3.1 Order of Error in the Modified Euler Method

In the previous chapter the order of the local truncation error in the Euler method was derived and a rule of thumb used to infer the order of the global truncation error. Subsequent simulations showed that this scaling law held when solving the population-balance differential equations for PIP. Here the order of the local truncation error in the ME method will be derived.

To establish the order of the local truncation error, the exact solution, Φ, is expanded as a Taylor series (see equation 4.1). The difference between this exact and ME-based solutions is then evaluated. Note that equation 4.10 is obtained by assuming that $\Phi'(t_n) = y'(t_n)$, i.e., that the lack of initial-condition error ensures that the rate of change for exact and numerical

solutions are equal for the first step.

$$e_{n+1} = \Phi(t_{n+1}) - y(t_{n+1}) \tag{4.9}$$

$$= \frac{\Phi''(t_n)h - \{f[t_n + h, y(t_n) + hf(t_n, y(t_n))] - f(t_n, y(t_n))\}}{2!}h + \tag{4.10}$$

$$\frac{\Phi'''(t_n)h^3}{3!} + ... \tag{4.11}$$

It can then be shown that both the first and second terms in this expression are proportional to h^3. Moreover this means that if the differential equations being solved satisfy certain requirements then equation 4.12 holds for the local truncation error (for an explanation of these requirements see for example [6]).

$$e_{n+1} = \frac{\Phi'''(t_n)h^3}{6} \tag{4.12}$$

This expression says that the local truncation error in the ME method is proportional to the h^3. Thus the global truncation error is proportional to the step size squared (h^2). However, equation 4.12 contains more information than just how the error depends on the step size. Equation 4.12 indicates the error is proportional to $\Phi'''(t_n)$, the third derivative of the exact solution. This means that the local truncation error is related to the rate of change in the differential equations in a similar, but not identical manner to that seen in chapter three with the Euler method. In chapter three, we saw that the Euler method depends on the $\Phi''(t_n)$. Furthermore, in that chapter we were able to derive a simple expression for how the error depended on the values of k_t, ρ and t. Unfortunately, the third derivative of the exact solution is significantly more complicated than the second derivative. Because of this, an expression will not be derived for $\Phi'''(t_n)$. However, it is reasonable to expect, and simulations have confirmed this, that the error incurred by the ME method will also depend on k_t, ρ and t.

4.3.2 Application of Modified Euler Method

The ME method will now be applied to the solution of the differential equations that characterize PIP. The system of equations studied in this chapter is the same as those used in chapter three (equations 3.22 – 3.24). Furthermore, all of the rate parameters used here are identical to those used in chapter three (these parameters are summarized in table 4.1). The

Parameter	Value	Units
k_t	1.0×10^8	$L.mol^{-1}.s^{-1}$
k_p	100.0	$L.mol^{-1}.s^{-1}$
M	10.0	$mol.L^{-1}$
ρ	1×10^{-6}	$mol.L^{-1}$
freq	10.0	Hz
h	1×10^{-4}	s
t_{sim}	2.0	s

Table 4.1: Default Rate Parameters for calculations performed in chapter four.

ME method will be initially applied with a constant step-size profile. Once this assessment has been completed, a time-dependent step-size profile will be utilized. In every other way, apart from the approximation function used, this assessment is the same as that performed on the Euler method.

Constant Step Size

Error Standard One Figure 4-1 contains a plot of the error incurred for a range of step sizes and three values of the termination rate coefficient, where this error has been calculated with error standard one, i.e., it is the periodic average of the relative difference between the simulated and analytical total radical concentrations.

Figure 4-2 contains the same data as figure 4-1 except that the square root of the error per initiation period is plotted against the step size. The data in figure 4-1 has been fitted with a linear relationship (equation 4.13) and the summary data for this fit are shown in table 4.2. Note that if the concentration of radicals added at an initiation burst is varied instead of the value of k_t, the same effect is observed, i.e., an increase in the value of ρ increases the rate of change in error with step size. The data in these two figures and in table 4.2 display three important features: (1) the magnitude of the error is significantly less than error incurred by the Euler method; (2) the error is proportional to the step size squared, and (3) the rate that the error increases with step size depends on the magnitude of the termination rate coefficient. A brief explanation is now given for each of these features.

$$\sqrt{\text{Error per pulse}} = A + Bh \tag{4.13}$$

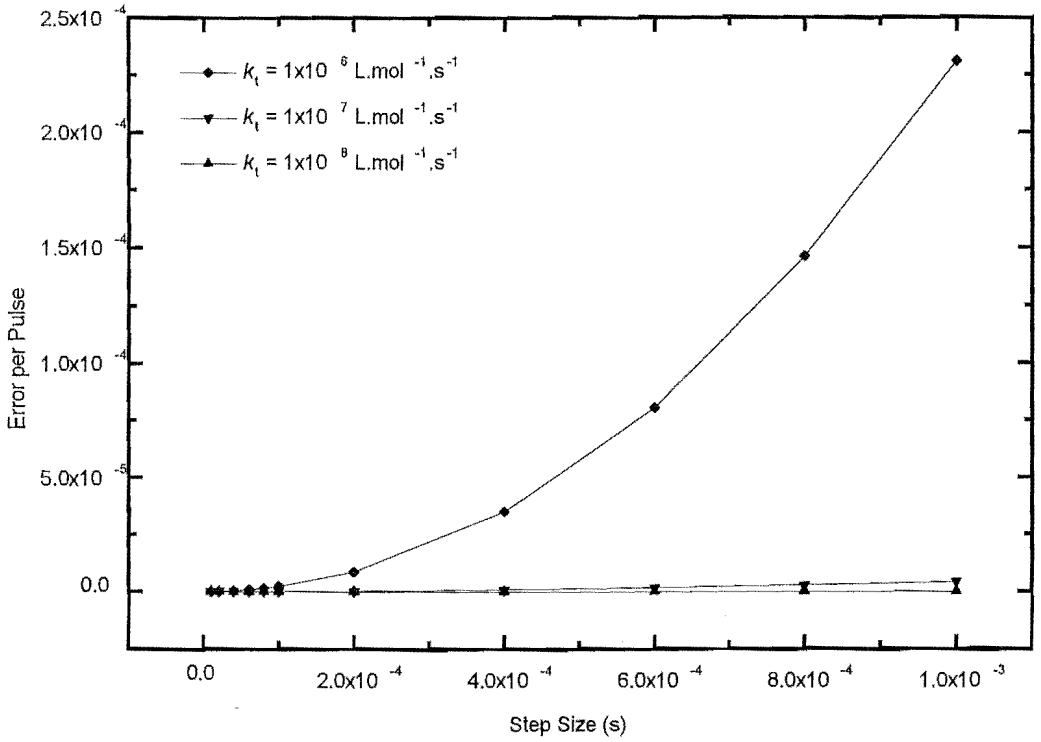

Figure 4-1: Correlation between error per pulse and integration step-size for the Modified Euler method with a constant step-size profile. Rate parameters are as per table 4.1. Note that the error in this plot has been measured by error standard one employing equation 3.9.

The Magnitude of the Error Incurred. It is clear from figures 4-1 and 3-2 that the use of the average of the value of the differential equations at the start and end of an integration step better approximates the actual average value of these equations than simply using their value at the start of the time step. Thus, using the ME method significantly reduces the error in the solution of these differential equations. For example, when the differential equations were solved with the Euler method with $k_t = 1 \times 10^8 \text{L.mol}^{-1}.\text{s}^{-1}$ and $h = 1 \times 10^{-4}\text{s}$, the error incurred was 4.6×10^{-4}. In contrast to this, when the ME method is used with the same parameter set the error is 2.12×10^{-6}. This represents a reduction in error of more than two

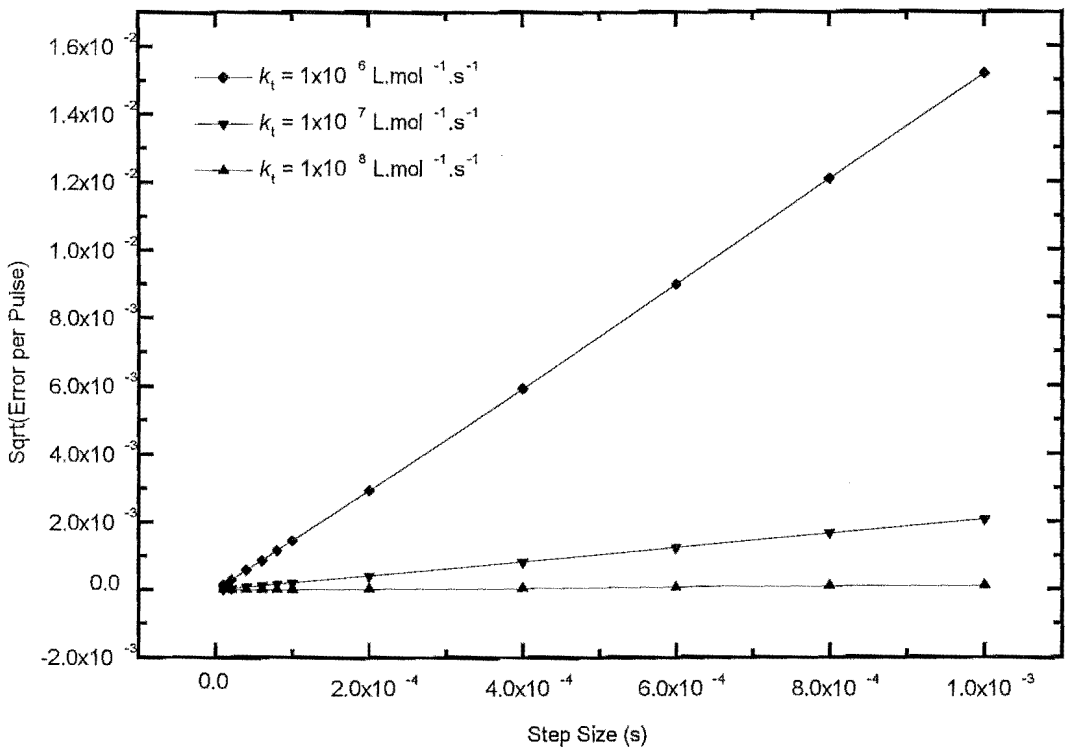

Figure 4-2: Correlation between the square root of the error per pulse and integration step-size for the Modified Euler method with a constant step-size profile. Rate parameters are as per table 4.1. Note that the error in this plot has been measured via error standard one employing equation 3.9.

orders of magnitude while the computational cost only doubles. The added cost of evaluating the differential equations twice instead of once per integration is more than balanced by the gain in accuracy.

The Dependence of the Error Upon Step Size The linearity of all of the curves contained in figure 4-2 (all have $R = 1.0$ when fitted with equation 4.13) confirms that the global truncation error is proportional to the step size squared. Therefore, these results agree with the order of error predicted in section 4.3.1. This means we can have confidence the ME method is working as it should be in this system.

k_t (L.mol^{-1}.s^{-1})	A	B	R
1×10^6	$(1 \pm 1) \times 10^{-7}$	$(1235 \pm 3) \times 10^{-4}$	1.000
1×10^7	$(4 \pm 8) \times 10^{-7}$	$(2076 \pm 1) \times 10^{-3}$	1.000
1×10^8	$(-5 \pm 2) \times 10^{-7}$	$(1516 \pm 2) \times 10^{-2}$	1.000

Table 4.2: Statistical data obtained when the data in figure 4.3 is fitted with equation 4.11.

The way that the error depends on the integration step size is important, as it affects how easy it is to achieve a certain level of accuracy by altering h. Whereas when the Euler method was used one had to halve the step size to halve the error, with the ME method halving the step size gives a 75% reduction in error. However, the reverse is also true, if one is forced to double the step size used with the ME, then the error is increased fourfold.

The Dependence of $\frac{dError}{dh}$ Upon the Rate Coefficient for Termination It is clear from figures 4-1 and 4-2 and table 4.2 that more error is incurred, and that error is more dependent on step size, for systems with higher values of k_t. More error is incurred at all values of h when $k_t = 1 \times 10^8$L.mol^{-1}.s^{-1}than when $k_t = 1 \times 10^6$L.mol^{-1}.s^{-1}. Moreover, the slope of the square root of the error per pulse against h plots (column B of table 4.2) is significantly greater for a kinetic system with high values of k_t than for those with low values of k_t.

These dependencies are expected for two reasons: (1) because of the precedent set by the analysis of the Euler method (both of these trends were observed in chapter three), and (2) because of the local truncation error scaling law (equation 4.13). It is clear from this equation that the local truncation error of the ME method is dependent on the third derivative of the analytic solution to a differential equation. Although an analytic expression will not be derived for the third derivative (as it was for the second derivative in chapter three), an empirical study has been performed. This study explored the way that the global truncation error depends upon the values of k_t and ρ. This indicated that the global truncation error is proportional to $k_t\rho$. Thus as the values of k_t and/or ρ increase the global truncation error should increase.

In the previous chapter, it was shown that increasing the values of k_t and ρ increased the rate of change in the differential equations. Moreover, this observation was used to rationalize the increase in the error with increases in these values. Such an argument said that the approximation function of, in that case, the Euler method was unable to describe the actual value of the differential equations accurately when these differential equations where changing rapidly,

i.e., when the value of k_t and/or ρ was large. This appears to be a problem also faced by the ME method: it incurs more error when the differential equations are changing rapidly.

There are two ways of reducing the error in a system where the values of k_t and/or ρ are large. The first is to use a smaller step size; this of course also increases the computational cost of obtaining the solution (see below for an efficiency analysis). The second is to use a better approximation function. The fourth-order Runge-Kutta, used in the next section, is known to better model rapidly changing differential equations.

Solution efficiency Having shown that the magnitude of error incurred by the ME method is less than the Euler method and that the error is proportional to the step size squared, it is important to consider the efficiency of this solution strategy. To do this, the formula that was developed and used in chapter three is used here. The solution efficiency is equal to the mean error per initiation period multiplied by the number of steps taken per pulse and by the number of evaluations of the differential equations per integration step, i.e., for the ME method $\xi = 2E_{pulse}.n_{steps}$. Results are presented in figure 4-3.

The most striking feature of this plot is the dependence of the efficiency value upon the integration step size. The efficiency value increases linearly with step size. This means that a more efficient solution is obtained at lower step size.

The efficiency value is proportional to the step size because it is a product of one term, the error, which is proportional to the step size squared, and another term, the steps per pulse, that is proportional to h^{-1}. The dependence of the efficiency value on the step size suggests that one should use as small a step size as possible to improve the efficiency of the solution obtained. While this is indeed true, the absolute values of the number of steps per pulse and the mean error per pulse must also be considered. It advisable when using this method to use as small a step size as possible because this increases the efficiency of the solution obtained, but not such a low step size as to make the method so computationally expensive that it is infeasible to use. Again this analysis indicates that the solution of these differential equations is less efficient when a high value of k_t is used.

Error Standard Two To explore the time dependence of the error incurred by the ME method, the relative error in the total radical concentration has been plotted against time.

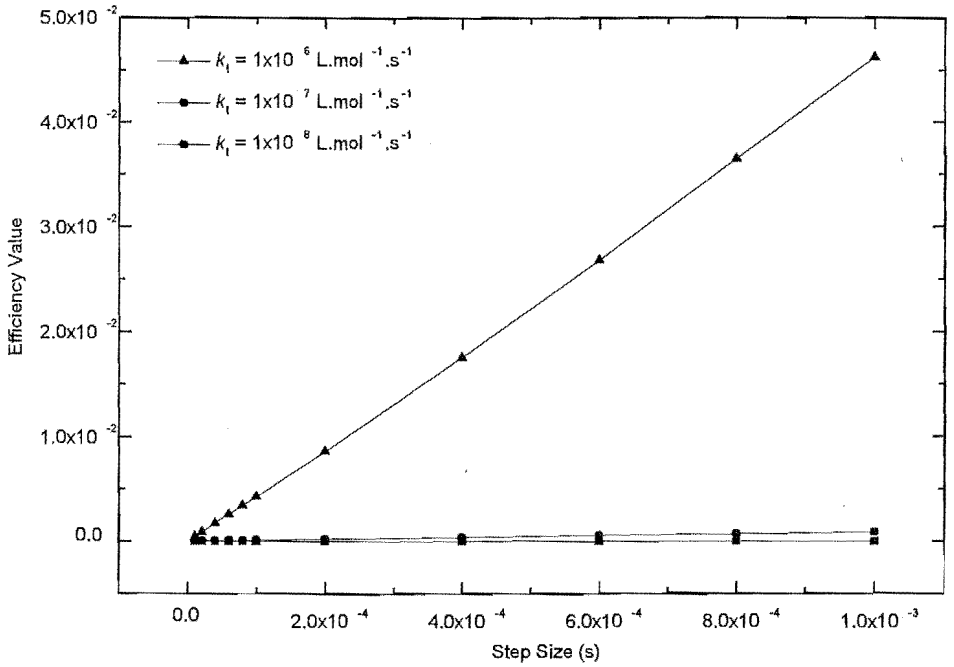

Figure 4-3: A plot of the dependence of the efficiency value upon the integration step-size.

This data is presented in figure 4-4 and 4-5. Figure 4-4 contains data for the error incurred by the Euler and ME methods. This figure makes it very clear that the use of the ME method does reduce the error at all times. Error-time plots for the same data as well as for two other values of k_t are shown in figure 4-5. The data of figure 4-4 is presented again to show a facet of the error that was obscured because of scale in figure 4-4. Figure 4-5 indicates that there is a rapid initial rise in error followed by a slow decay and confirms that the error incurred has the same time profile for the ME method as it did when the Euler method was used. It follows from figure 4-5 that the ME method incurs more error when the differential equations are rapidly changing, i.e., at the start of the initiation period, and when the value of $k_t$or ρ is high. This suggests that if the ME method was used with a treatment that 'understands'

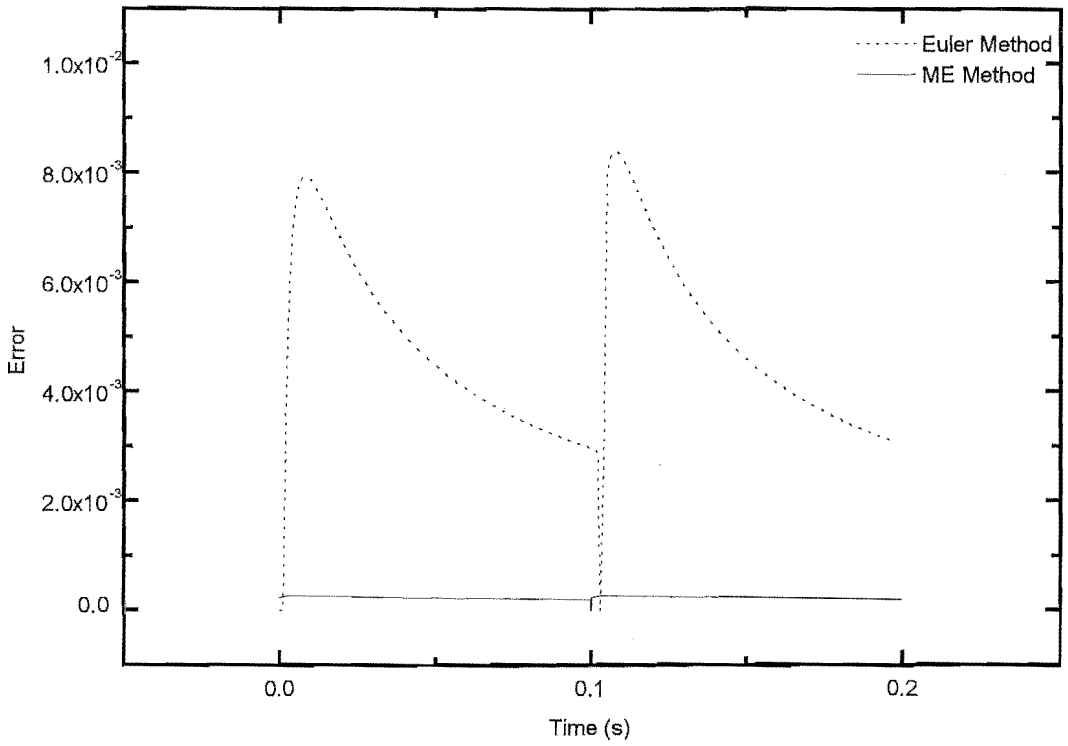

Figure 4-4: A comparison of the time-dependence of the error in the solution of the population-balance differential equations by the Euler and ME methods. Default rate parameters are used in both calculations. Note that the error in this plot has been measured via error standard two.

when the system was prone to error – a method that knows how to reduce that error – then the efficiency of this method would be increased.

Error Standard Three To confirm that the ME method does not incur significant amounts of error in the individual radical concentrations, the difference between the simulated and analytic concentration of R_{10} has been calculated. These results are presented in figure 4-6. Also included in this figure is the error in R_{10} when the Euler method is used. The step size used with the Euler method has been adjusted so that the ME and Euler methods evaluate the differential equations the same number of times per integration step. As $h = 1 \times 10^{-4}$s for the

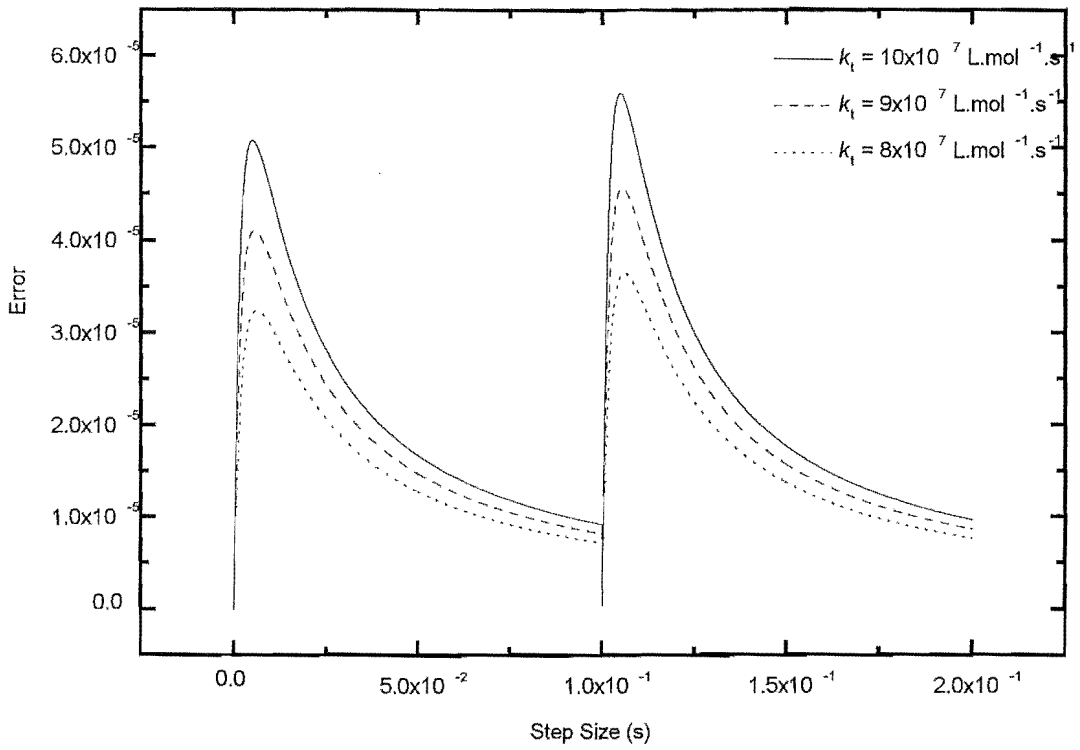

Figure 4-5: The time-dependence of error when the population-balance differential equations are solved with the ME method. Default rate parameters are used in calculations. Note that the error in this plot has been measured via error standard two.

ME method, a step size of $h = 5 \times 10^{-5}$s is used with the Euler method. This plot shows that the ME method decreases the error in the concentrations of the individual radicals species.

Hence, although the ME method incurs error in the individual radical concentrations that is qualitatively the same as that incurred by the Euler method, the magnitude of that error is significantly reduced.

In summary, the ME method reduces the error in total radical concentration. Moreover, this method reduces the error incurred in solution of the differential equations for individual radical concentrations. It can be concluded then that the ME method incurs error which is typically two orders of magnitude less than that incurred by the Euler method. This means

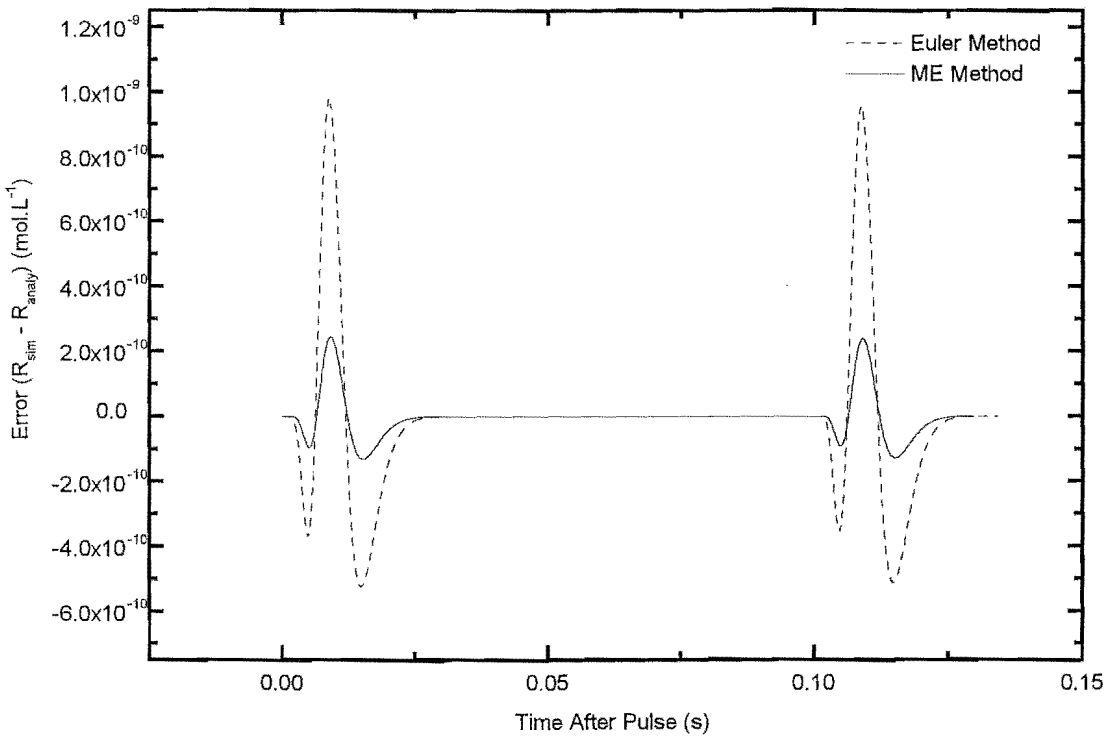

Figure 4-6: Error in the concentrations of radicals of chain-length 10 for the Euler and ME methods. Default rate parameters used. The step-size of the ME method is $h = 1 \times 10^{-4}$s while a step-size of 5×10^{-5}s is used with the Euler method.

that the ME is the best solution method to date for solving the differential equations for PIP.

Time-dependent Step-size Profile

The ME method has been tested with the time dependent step-size profile based on the rate of change of the differential equations developed in chapter three. This step-size profile uses integration steps of width h that depend on the length of time since that last burst of initiation, i.e.,

$$h_t = h_{max}(1 - \frac{a}{(1+bt)^3}) \tag{4.14}$$

$k_t(L.mol^{-1}.s^{-1})$	a	b	ξ
1×10^6	0.999	1.21×10^{-3}	1.57×10^{-8}
1×10^7	0.997	0.11	3.84×10^{-7}
1×10^8	0.993	7.03	1.82×10^{-4}

Table 4.3: Optimal step-size parameters and efficiency values. All rate parameters are as per table 3.3 and $h_{max} = 1x10^{-4}s$.

To use this step-size profile relationships must be established for the dependence of the error per pulse period and the number of steps taken per pulse upon the parameters a and b. Fortunately, the relationship used to describe how the number of steps taken per pulse depends on the values of a and b (equation 3.43) is the same as that derived for the Euler method. However, the relationship presented in chapter three for how the error incurred per pulse depends on values of a and b does not hold for the ME method, and must be re-derived here. To do this a series of simulations have been performed. These simulations have indicated that the error in the total radical concentration per pulse period is described by equation 4.15.

$$E_{pulse} = h_{max}^2 k_t R_{max}(4.15 - 8.27\frac{(1-a)}{b}) \tag{4.15}$$

From this expression, relationships can be derived for $\frac{\partial \xi}{\partial a}$ and $\frac{\partial \xi}{\partial b}$ and these expressions numerically solved (by the Newton-Raphson method) for the optimal values of a and b. Table 4.3 contains the values of a and b that define the optimal step-size profiles for three values of k_t.

A quick comparison between the efficiency of the ME method using a time-dependent and time-independent step size reveals that a time-dependent step-size profile improves the efficiency of this technique. For example, if one wishes to obtain a solution for a system of differential equations with $k_t = 1 \times 10^8$ L.mol$^{-1}s^{-1}$ than contains 1×10^{-6} error, then 4230 steps need be taken when a time-independent step-size profile is used, while only 182 steps per initiation period need be taken with a time-dependent step-size profile. Hence, the use of a time-dependent step-size profile decreases the number of steps that need be taken per initiation period by more than an order of magnitude. Thus, the use of this refinement allows the ME method to be used to solve the population-balance differential equations for this complex kinetic system in a much shorter period of time.

4.3.3 Conclusion

This analysis has shown that the ME method is well suited to solving the differential equations that characterize PIP. Although this method incurs less error than the Euler method, it does so in a very similar way. A superficial comparison of the ME and Euler methods shows that in all regards the ME method is better suited to solving these differential equations.

4.4 The Fourth-Order Runge-Kutta Method

The next solution technique to be assessed is also a Runge-Kutta method. Whereas the modified Euler method is a second-order Runge-Kutta that takes one trial step per h-sized step, the fourth-order Runge-Kutta (RK4) method takes three trial steps per full sized integration step. In a manner reminiscent of the ME method, the RK4 method uses a weighted average of the initial, two midpoint and one final value of the differential equations to approximate the actual value of the differential equations during a time step. The fourth-order Runge-Kutta is a widely used solution algorithm that is well-known to provide a good balance between accuracy and speed for a wide range of differential equations.

The RK4 method works by using the Euler method to take a trial step to the midpoint in the integration step, i.e., $h/2$. At this point it calculates the value of the differential equations. Another trial step is then taken, again from the start of the step to the midpoint, however, unlike the first trial step this one uses derivative information from the start as well as the middle of the whole h-sized time step. Finally, a trial step is taken from the beginning to end of the whole h-sized integration step using the information gained by the previous two trial steps. These four values of the differential equations can then be combined to yield a final value of the solution, $y(t_{n+1})$. The mathematical expression for the RK4 method is

$$k_1 = hf(t_n, y(t_n)) \tag{4.16a}$$

$$k_2 = hf(t_n + \frac{h}{2}, y(t_n) + \frac{k_1}{2}) \tag{4.16b}$$

$$k_3 = hf(t_n + \frac{h}{2}, y(t_n) + \frac{k_2}{2}) \tag{4.16c}$$

$$k_4 = hf(t_n + h, y(t_n) + k_3) \tag{4.16d}$$

$$y(t_{n+1}) = y(t_n) + \frac{k_1}{6} + \frac{k_2}{3} + \frac{k_3}{3} + \frac{k_4}{6} \tag{4.16e}$$

It is clear that the RK4 method requires the differential equations to be evaluated four times per integration step. This means that the error incurred must be one quarter of that of the Euler for the RK4 to be the more efficient method. However, it also means that the RK4 method should be more accurate.

4.4.1 Order of Error in the Fourth-Order Runge-Kutta Method

While in principle it is not difficult to show that equations 4.16a - e differ from the Taylor series expansion of the exact solution, Φ, by terms that are proportional to h^5, the algebra is rather lengthy. Hence the relationship for the local truncation error will simply be stated here (equation 4.17) (for the complete derivation see for example Boyce and DiPrima[6]).

$$e_t = \frac{\Phi^{(5)}(t_n)h^5}{120} \tag{4.17}$$

Hence, the global truncation error is proportional to h^4. In this expression, $\Phi^{(5)}(t_n)$ denotes the fifth derivative of the exact solution with respect to time. The fact that the local truncation error is proportional to $\Phi^{(5)}(t_n)$ suggests that it will also depend upon some combination of k_t, ρ and t. The analytic expression for $\Phi^{(5)}(t_n)$ is not given here as it is non-trivial. However, simulations have shown that the global truncation error is proportional to $(k_t\rho)^3$(see equation 4.19).

4.4.2 The Application of the Fourth-Order Runge-Kutta Method

To assess the nature of the error incurred by the RK4 method, this method has used in conjunction with a constant and a time-dependent step-size profile. In every other way, apart from the method used, this assessment is identical to that performed on the Euler and ME methods.

Constant Step-size Profile

The error incurred by the RK4 method and how that error depends on step size as well as the termination rate coefficient are shown in figure 4-7. Note that this figure contains

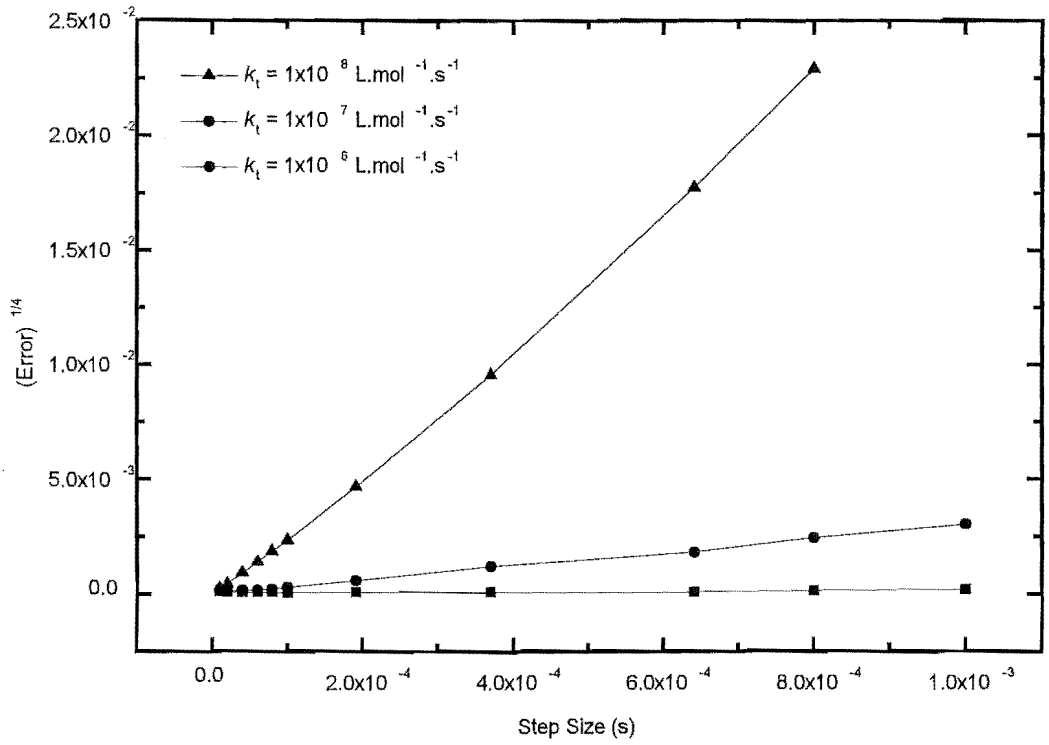

Figure 4-7: Correlation between the error per pulse and integration step-size for the RK4 method with a constant step-size profile. Default rate parameters are used. The lines shown simply connect points (they are not the lines of best fit).

$\sqrt[4]{\text{Error per Pulse}}$ plotted against the step size. Table 4.4 contains the statistical data for the fit of equation 4.18 to the data shown in figure 4-7

$$\sqrt[4]{\text{Error per Pulse}} = A + Bh \tag{4.18}$$

The fact that these plots are reasonably straight lines (R $\approx$ 1.0) suggests that the global truncation error is well modeled by the predicted scaling relationship. Moreover, all of the features shown by the error incurred by the ME method are shown here. Namely, there is a significant decrease in the magnitude of the error, a strong dependence of the error on the value

k_t(L.mol^{-1}.s^{-1})	A	B	R
1×10^6	$(10 \pm 1) \times 10^{-5}$	$(7 \pm 2) \times 10^{-2}$	0.9547
1×10^7	$(5 \pm 20) \times 10^{-5}$	$(298 \pm 5) \times 10^{-2}$	0.9859
1×10^8	$(-4 \pm 2) \times 10^{-4}$	$(2970 \pm 3) \times 10^{-2}$	0.9979

Table 4.4: Statistical data obtained when the data in figure 4.7 are fitted with equation 4.16.

of k_t (and ρ) and the expected relationship between error and step size.

An effect not shown by the ME method is the dependence of the R-value on the magnitude of k_t. As the value of k_t increases so does the goodness of fit. This is due to round-off error. The error incurred when the RK4 method is used to solve the population-balance differential equations with $k_t = 1 \times 10^6$ L.mol^{-1}.s^{-1} and $h = 1 \times 10^{-4}$s is so low (1×10^{-16}) that round-off error makes a significant contribution to the total error. As has been noted previously, the amount of round-off error incurred is proportional to the number of calculations performed. Thus, as the number of calculations performed in an initiation period increases when the step size is decreased, the magnitude of the roundoff error increases. This causes both the error and efficiency value against step size plots to diverge from their expected relationships at small step size. While the presence of round-off error is interesting in its own right, the real significance of observing it here is that it indicates that the RK4 method has been very successful in solving the differential equations that model this kinetic system.

The effect of round-off error on the error-time plot is shown in figure 4-8. The rate parameters for this calculation are the same as the those shown in table 4.1 except for $k_t = 1 \times 10^6$L.mol^{-1}.s^{-1}and $h = 1 \times 10^{-4}$s. The plot presented in figure 4-8 shows that the error incurred is very low and that it increases with time. Note also that error has the appearance of random noise, a typical feature of roundoff error. As has been already noted, round-off error is caused by the limitations of the way that a computer performs mathematical calculations. As the magnitude of this error is unrelated, at least for our purposes, to the concentrations of the species present, it is effectively random. It should be noted that this error is always present, it is just that normally it is obscured by truncation error. Figure 4-8 indicates that the amount of error present increases with time. This is consistent with the effects of round-off error, as round-off error is known to accumulate as the number of calculations performed increases.

No attempt will be made to reduce the amount of round-off error in this system - a range of

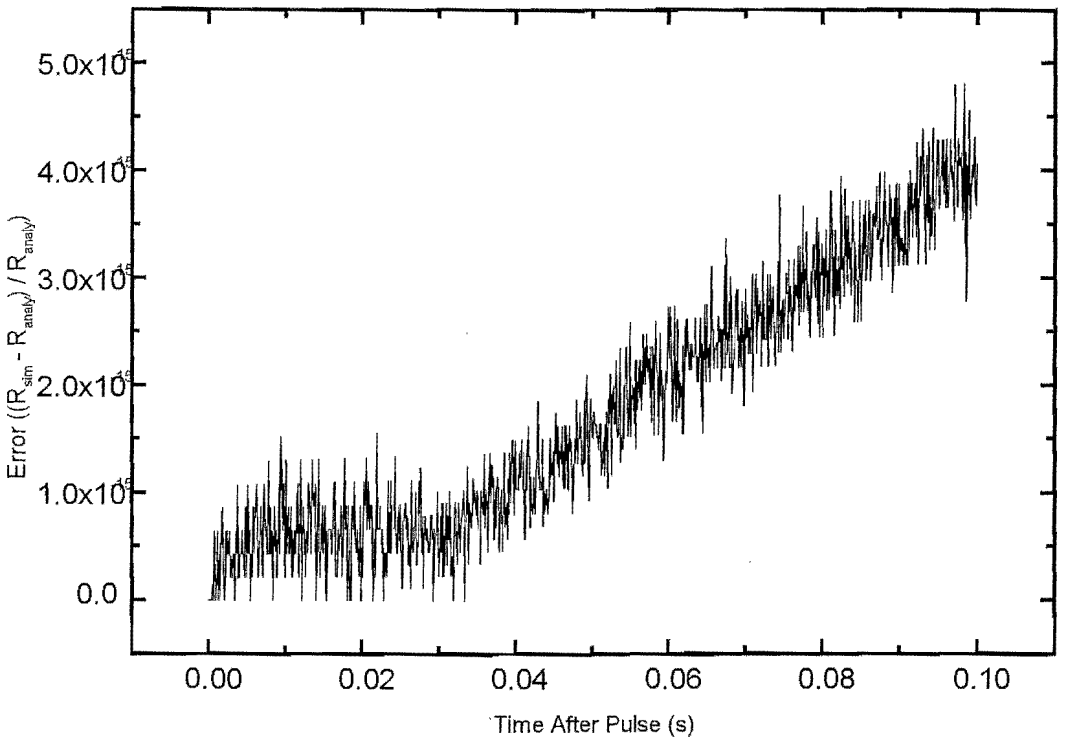

Figure 4-8: Error-time plot for a system of differential equations solved by the RK4. For rate parameters see text.

procedures do exist - for the magnitude of this error is so low that it has no significant effect on the kinetics and/or MWDs for these systems. This has been confirmed by simulations outlined in chapter five.

The efficiency values for the RK4 method are shown in figure 4-9. These have been calculated using $\sigma_{des} = 4$. We know that $E_{pulse} \propto h^4$ and $n_{steps} \propto h$. Hence, it should be observed that $\xi \propto h^3$. This is in fact the case, even if it is not immediately evident from figure 4-9, for all cases except when $k_t = 1 \times 10^{-6}$L.mol^{-1}.s^{-1}. The error incurred in a system with a low value of k_t (1×10^{-6}L.mol^{-1}s^{-1}) does not follow the expected scaling law because the error is dominated by roundoff error and the predicted scaling law only holds for truncation error. The efficiency values shown in this plot are significantly lower that those for the ME method. For example, if

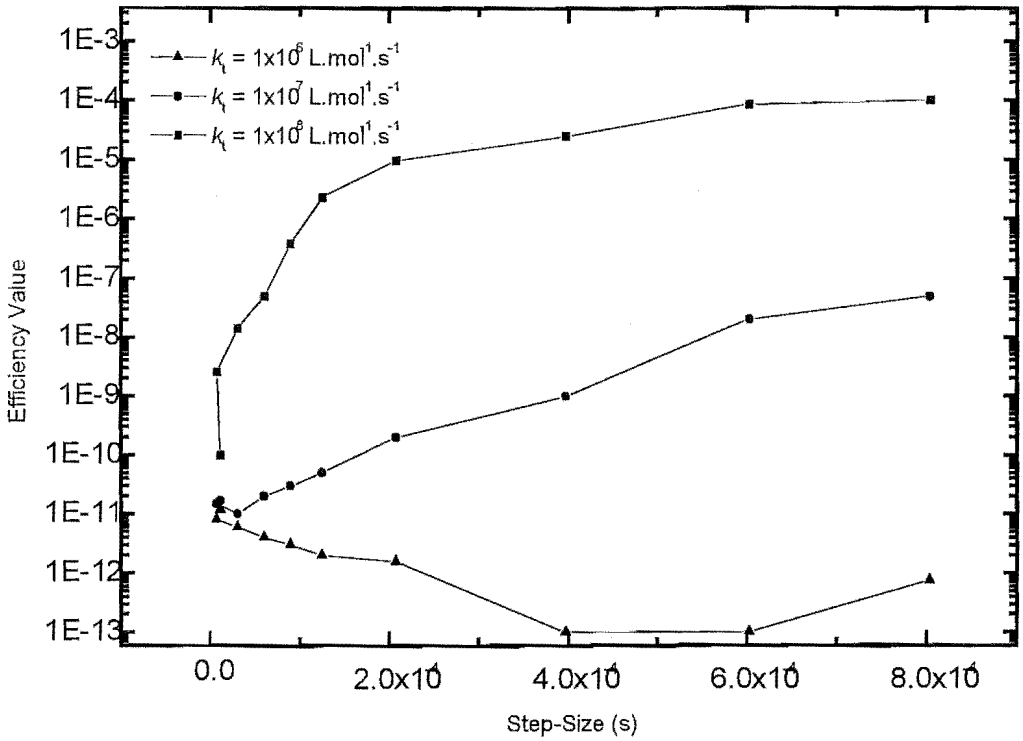

Figure 4-9: The efficiency values for the RK4 method. Note that this is a log-linear plot. The data has been presented in this manner as it varies over several orders of magnitude.

$k_t = 1 \times 10^8$ L.mol^{-1}.s^{-1} and $h = 1 \times 10^{-4}s$, then the efficiency value for the RK4 method is a staggering 1×10^4 times smaller than that for the ME method. Therefore, for all of the step sizes that would be used in a normal simulation the RK4 is a more efficient method.

Error standard two The error time plots acquired when the RK4 method is used are qualitatively the same as those for all of the methods used so far. Figure 4-10 contains a plot of this type for $k_t = 1 \times 10^8$ L.mol^{-1}.s^{-1} and $h = 1 \times 10^{-4}$s. This plot shows that the error incurred by the RK4 method is strongly dependent on time. However, figure 4-8 is also a plot of the temporal dependence of error incurred by the RK4 method (this time with $k_t = 1 \times 10^6$L.mol^{-1}.s^{-1}). The shape of this figure is dramatically different from figure 4-10, and indeed from all of the

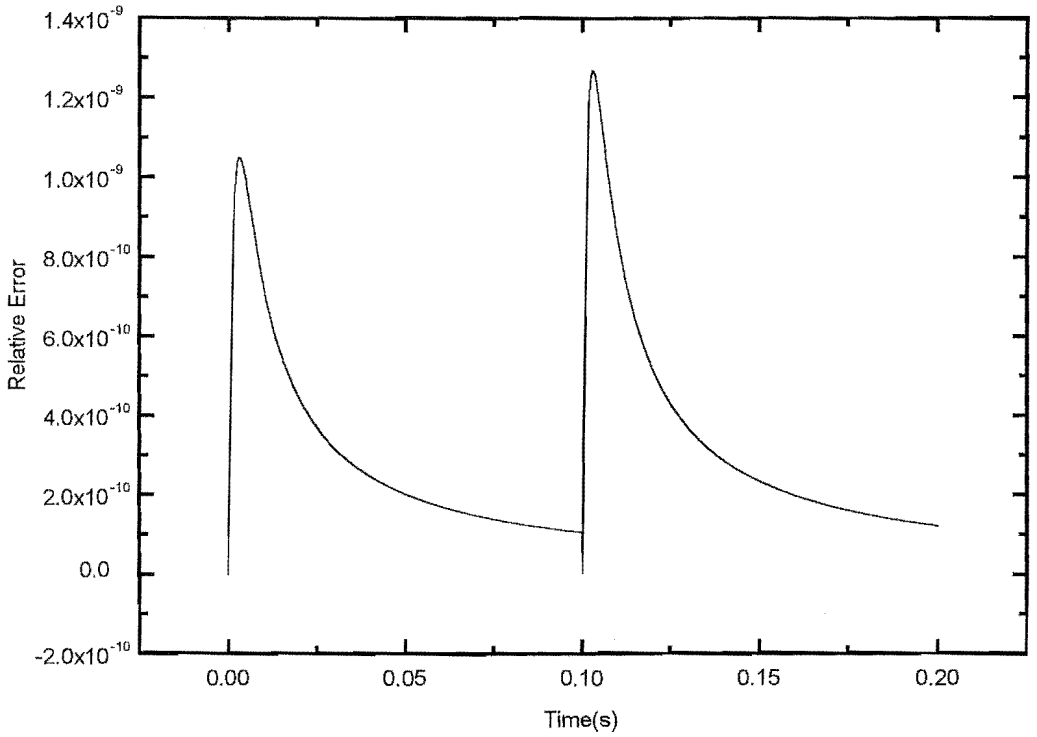

Figure 4-10: A plot of the temporal dependence of error when the RK4 method is used. Rate parameters are as per table 4.1. Error is measured using error standard two employing equation 3.9.

error standard two plots presented in this thesis so far. Moreover, although the error shown in figure 4-8 does increase slightly with time, the error incurred is far less dependent on time then any of the others shown so far. This suggests that when the k_t for a system of these population-balance differential equations is low, the RK4 method is able to approximate the change in the differential equations exceedingly well. However, if a high k_t is used, as in figure 4-10, then although the RK4 method incurs minimal error, this error does depend strongly upon the time since the last burst of initiation . This suggests that a time-dependent step-size profile can be used to improve the efficiency of this solution technique for systems where the value of $k_t\rho$ is high.

Error standard three The final analysis that has to be performed here interrogates the error in the concentrations of individual radical species. To do this, the difference between the simulated and analytic concentrations of R_{10} is plotted against time. This error is shown in figure 4-11. The error incurred in the radicals of chain length 10 by the Euler method has also been included. The step size used with the Euler method has been adjusted so that this method evaluates the differential equations the same number of times per initiation period as the RK4 method, i.e., so that the computational cost is the same. As the step size used with the RK4 method is $h = 1 \times 10^{-4}$s, a step size $h = 2.5 \times 10^{-5}$s is used with the Euler method. Note that $k_t = 1 \times 10^8$ L.mol^{-1}.s^{-1}. Figure 4-11 shows that the RK4 method significantly reduces the error in the concentration of radicals of chain length ten. Therefore, not only is the RK4 method the most efficient method used to date (error assessed by error standard 1), but it incurs the least error in the radical chain-length distribution. Note that the initial decrease in error that is expected in the RK4 method data shown in figure 4-11 is present but difficult to see.

Time-dependent Step-size Profile

The RK4 method has been tested with the time-dependent step-size profile developed in chapter three (section 3.10.6). To use this method an expression for how the mean error per pulse depends upon the values of a and b must be derived. The resulting expression is given as equation 4.19.

$$E_{pulse} = h_{max}^4 (k_t R_{max})^3 (0.25 - 4.32\frac{(1-a)}{b}) \tag{4.19}$$

This expression has all of the expected dependencies, for example E_{pulse} is proportional to h^4 and to $(k_t R_{max})^3$. Note that if a is set equal to zero then this expression describes the error incurred by a constant step-size profile. To obtain the values of a and b that define the optimal step-size profile the partial derivatives of a and b with respect to ξ are evaluated. These expressions are then set equal to zero and solved. Table 4.5 contains the optimal values of a and b for the default rate parameters and three values of k_t. Also included in this table is the optimal efficiency value.

The use of a time-dependent step-size profile increases the efficiency of the RK4 method. For example, if a system of differential equations with a $k_t = 1 \times 10^8$L.mol^{-1}.s^{-1} is solved by

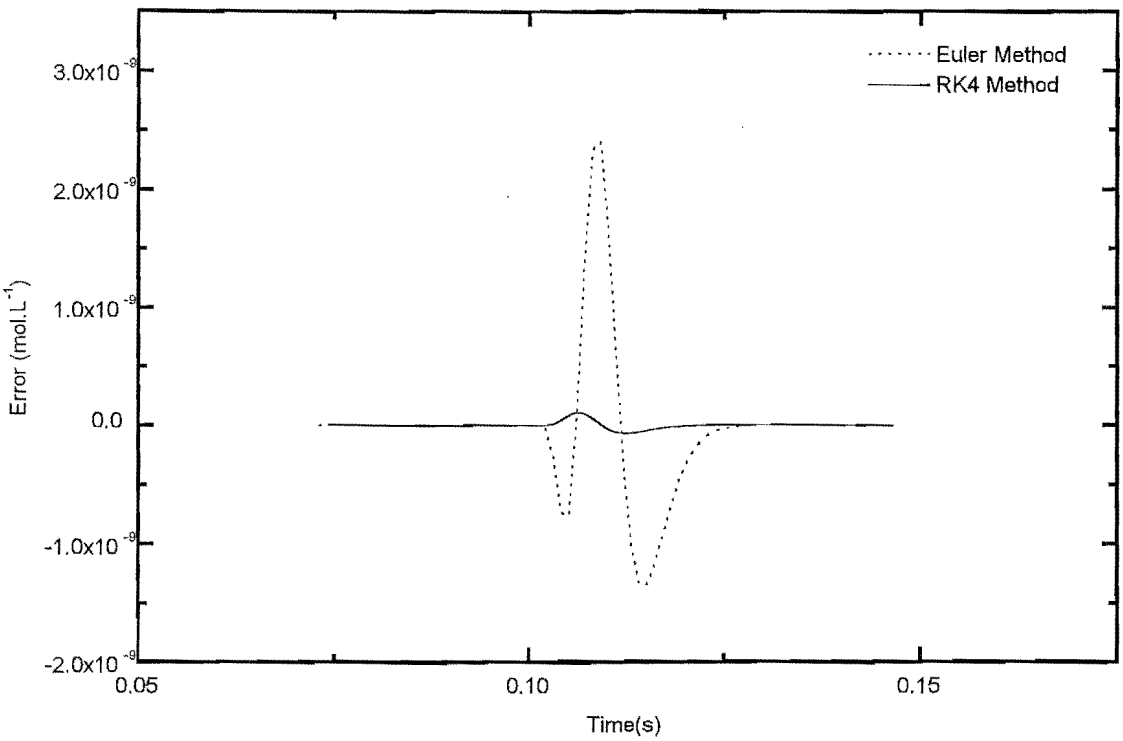

Figure 4-11: Error in the concentration of radical of chain-length 10 when the differential equations are solved by the RK4 and Euler methods. Default rate parameters are used and an integration step-size of $h = 1 \times 10^{-4}$s is used with the RK4 method and a step-size of $h = 2.5 \times 10^{-5}$s with the Euler method. The error in equal to $(\mathrm{R}_{10})_{sim} - (\mathrm{R}_{10})_{analy.}$

the RK4 method with a time-independent step-size profile then $\xi = 1.2 \times 10^{-7}$ is optimum while if a time-dependent step-size profile is used then $\xi = 2.24 \times 10^{-11}$is optimum. Thus, the RK4 in conjunction with a time-dependent step-size profile is a very efficient means of simulation this system of differential equations; in fact it is the best to date.

The results in this analysis of the RK4 method indicate that it can be used to solve the differential equations that characterize PIP with an extraordinary degree of accuracy. Even when a large step size ($h = 1 \times 10^{-3}$s) is used to model a kinetic system with a high value of k_t (1×10^8 L.mol^{-1}.s^{-1}) the error incurred is very low (2.73×10^{-7}). In fact, the error incurred

$k_t(L.mol^{-1}.s^{-1})$	a	b	ξ
1×10^6	0.99	14.98	9.67×10^{-14}
1×10^7	0.97	11.31	7.63×10^{-13}
1×10^8	0.97	7.00	2.24×10^{-11}

Table 4.5: Optimal step-size parameters and efficiency values for the RK4 method.

was so low that it was decided that there was little point in studying higher order methods of this type, i.e., a fifth- or sixth-order Runge-Kutta method. Instead, attention was focussed on methods that used intelligent techniques to reduce the computational cost of acquiring a solution.

4.5 The Adams-Bashforth-Moulton Predictor-Corrector Method

The Adams-Bashforth-Moulton Predictor-Corrector (ABMPC) method is an extremely popular differential equation solution method that is used widely throughout science and engineering. It is a multistep method, and as such uses information gained in previous integration steps to predict the values of the differential equations during the next integration step. Multistep methods do this by fitting a mathematical function to the previous values of the differential equations. For example, the Adams-Bashforth predictor fits a third-order polynomial to the values of the differential equations from the four previous evaluations of the differential equation. This function is then extrapolated to predict the differential equation during the next time step.

One of the advantages of methods of this type is that they reduce the computational cost of calculating the solution. Whereas the RK4 method evaluates the differential equations four times per integration step, a typical predictor-corrector method calculates them only once. Although this means that methods of this type can generate solutions with minimal computational cost, it does mean that they are prone to error.

Significant amounts of error will be introduced if the extrapolation based on the fit of a function to previous values of the differential equations does not agree with the actual values of the differential equations. Frequently this failure can be caused by two reasons. The first way that error can incurred is if an inappropriate fitting function is used. For example, fitting a linear relationship to the previous values of a non-linear differential equation will usually introduce error. Secondly, error can be introduced if there is an abrupt change in the values of the

differential equations, for example, at the arrival of a burst of initiation. In this circumstance, a multistep method predicts the slow decline in the radical concentration typical of the end of an initiation period, rather than the rapid decline that normally occurs straight after the arrival of a laser pulse.

The ABMPC method is made up of two parts: an Adams-Moulton predictor (AMP) and an Adams-Bashforth corrector (ABC). One of the analyses performed here will explore the effect on the solution error of applying the AMP algorithm and then repeatedly improving upon the solution through the use of the ABC algorithm.

The ABMPC method requires three values of the differential equations to be known before it can operate. As these values are not known at the start of a simulation, another method must be used to generate them. In this study the RK4 method is used to do this. Moreover, the RK4 method is used to calculate the first three values of the solution at the start of every initiation period. This is done to avoid the error that is incurred when the ABMPC method attempts to predict the value of the differential equations just after the arrival of the laser pulse (see above). Simulation studies indicated using the ABCMPC method just after the arrival of a pulse resulted in unacceptable amounts of error.

4.5.1 Error in the Adams-Bashforth-Moulton Predictor-Corrector Method

The local truncation error in the ABMPC method is of the same order as that in the fourth-order Runge-Kutta method, i.e., it is proportional to h^5 . Furthermore, both the ABC and AMP components of this method incur the same order of error. However, the ABC and AMP components differ in the value of the constant of proportionality between error and step size. For example, the AMP routine incurs local truncation error (e_t) that is described by this relationship[6]:

$$e_t \propto \frac{251}{720} h^5 y^{(5)}(t_n) \tag{4.20}$$

while the ABC routine incurs local truncation error that is described by equation 4.21 [6]:

$$e_t \propto \frac{9}{720} h^5 y^{(5)}(t_n) \tag{4.21}$$

Thus, the application of the corrector routine decreases the amount of error in the system, bringing the numerical solution closer to the analytic solution. The error is diminished further by repeatedly recalculating the differential equations and reapplying the corrector formula. Nonetheless, the global truncation error for both the AMP and the ABC components should always be proportional to h^4.

A system of nomenclature is used to define the number of times the AMP (denoted P) and the ABC (denoted C) algorithms are applied. Note that an evaluation of the differential equations is denoted E. $P(EC)^m$ indicates how many times each of these procedures is carried out per integration step, where here $0 \leq m \leq 3$. For example, if $m = 2$ then the P algorithm is applied (AMP) followed by two cycles of differential equation evaluation and correction (ABC).

4.5.2 The Application of the Adams-Bashforth-Moulton Predictor-Corrector Method

Before we are able to draw conclusions about how well this method solves this system of differential equations, we must establish the optimal value of m. To do this a series of simulations are performed where the differential equations are solved with the $P(EC)^m$ method for a range of values of m ($0 \leq m \leq 3$). In these calculations the default rate parameter set is used (see table 4.1). Figure 4-12 contains a plot of the error incurred (error standard one) when the ABMPC algorithm is used. In this plot, the different lines correspond to different combinations of the AMP and ABC routines. This plot shows that this method incurs significant amounts of error, and in an erratic manner, when solving these differential equations. The error incurred by a single predictor step ($P(EC)^0$) (solid line obscured by the $P(EC)^1$ line) diverges causing the simulation code to crash at low step size ($h = 1 \times 10^{-4}s$). The error incurred with step sizes greater than $h = 1 \times 10^{-4}s$ is not shown on this plot, as it is very high (1×10^3). If the predictor algorithm is followed by a corrector algorithm ($P(EC)^1$) the error does not diverge until the step size used is higher ($h = 6 \times 10^{-4}s$). If the corrector routine is applied one ($P(EC)^2$) and then two ($P(EC)^3$) more times per integration step, the differential equations can be solved at higher step size, but more error is incurred at all step sizes. An explanation of the increase of error with successive applications of the corrector algorithm will be given below. A plot of $\sqrt[4]{\text{Error per initiation Period}}$ against step size is not presented here as there is little

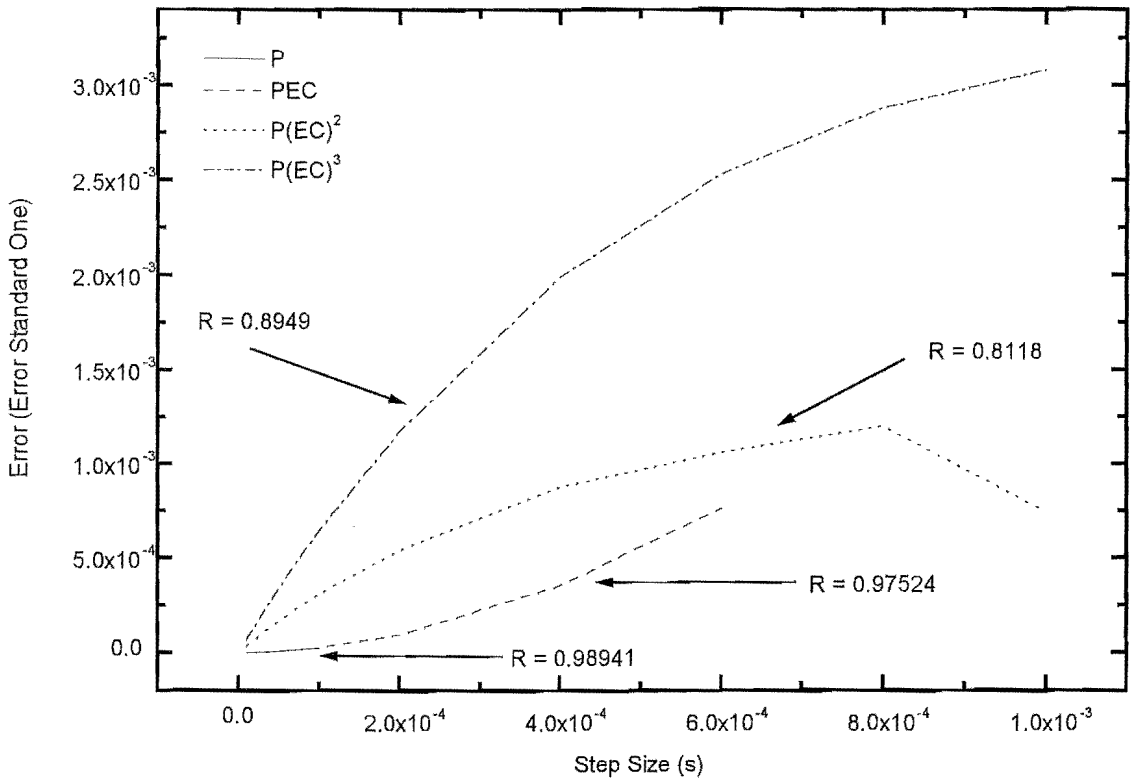

Figure 4-12: A plot of error against step-size for the ABMPC solution method of type P(EC)^m for $0 \leq m \leq 3$. All calculations were performed with the default rate parameters.

correlation between this value and step size. However, the correlation coefficients for the plot of $\sqrt[4]{\text{Error per initiation Period}}$ against step size are included in figure 4-12. Calculations were performed where the rate coefficient for termination was altered. Although the error incurred did decrease with the k_t, this effect was slight, and the same erratic behavior was observed.

It is important that the reasons why this method failed are understood, as they inform us whether the problems faced by this method are symptomatic of this approach in general. To explore the origin of this error, error standards two and three have been employed. Figures 4-13 and 4-14 contain plots of the error incurred (measured by error standards two and three) against time for the P(EC)^2 variant of the ABMPC method. Figure 4-13 indicates that the

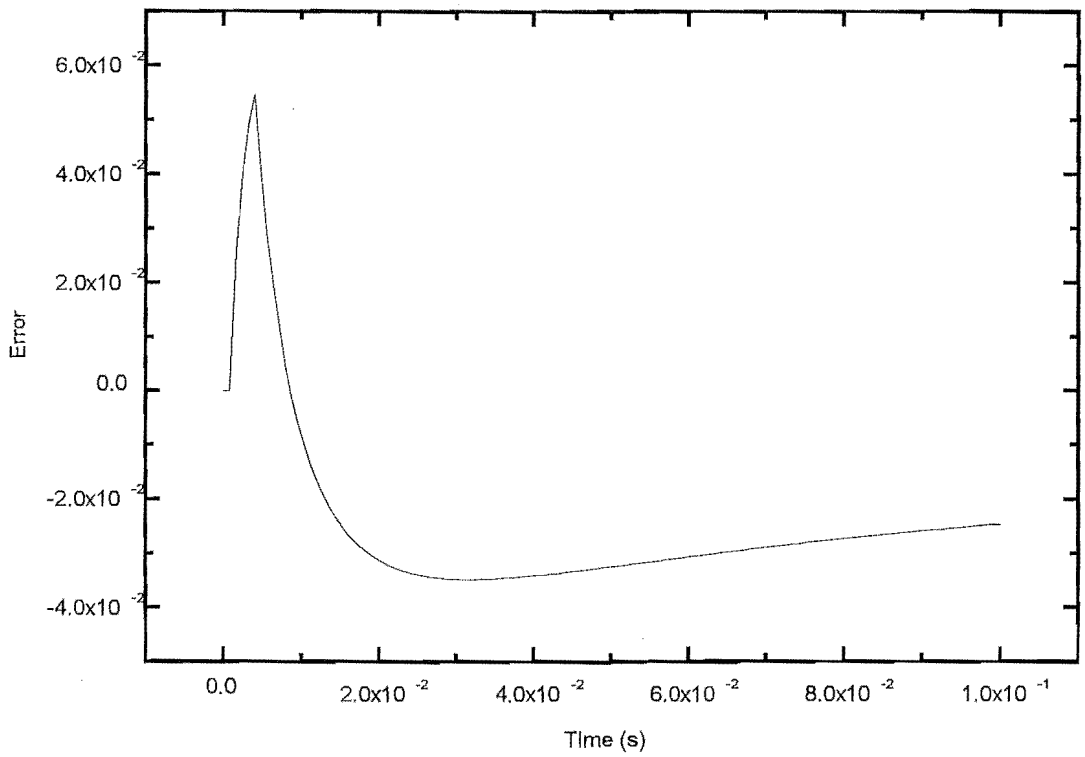

Figure 4-13: The temporal dependence of error for the ABMPC method ($P(EC)^1$) and the default rate parameters (see table 4.1). The error shown in this plot is the difference (not the absolute difference!) between the simulated and analytic total radical concentrations, i.e., $R_{sim}-R_{analy}$.

error in the total radical concentration is initially ($t < 1 \times 10^{-4}$ s) very low. This corresponds to the period when the RK4 method is used to solve the differential equations. From this time onwards, the magnitude and sign of the error show a complex dependence upon time. It is not obvious how the behavior of the error in the total radical concentration displayed in 4-13 can be explained. However, we will see that it is not necessary to do so, as this error is a result of the inability of the ABMPC method to accurately solve the differential equations for the individual radical species. The error in the concentration of radicals of chain length 10 (figure 4-14) is even more complex and is reminiscent of the error incurred when a step size of greater

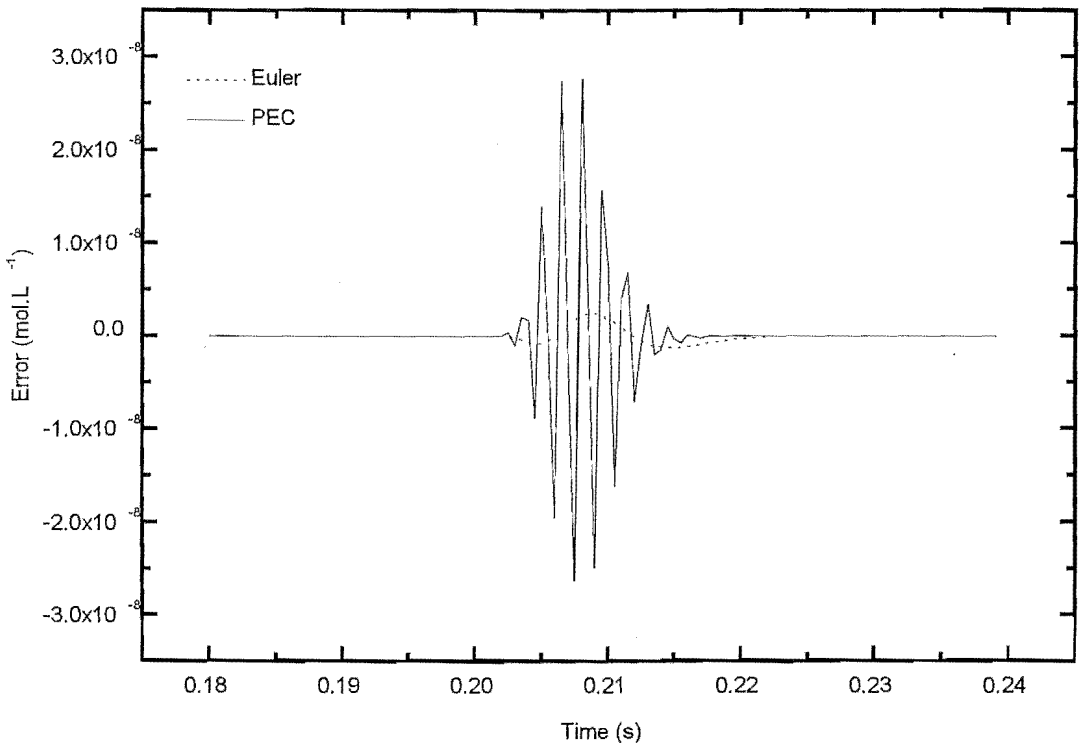

Figure 4-14: The temporal dependence of error in the concentration of radicals of chain-length 10 for the ABMPC method ($P(EC)^1$) with the default rate parameter set. The error in this plot has been calculated in the same way as the error in the previous plot.

than $\frac{1}{k_p M}$ was used with a single step Euler method in chapter three. Note the error is greatest about the time when chain length 10 is the most probable chain length (0.01s after an initiation burst). This suggests that the error originates from an inability of the ABMPC to solve the differential equation for the radicals species that has the most probable chain length. Moreover, it suggests that the erratic error revealed by error standards one and two is a reflection of this underlying error.

The ABMPC has difficulty solving the differential equations for the radical species when their chain length is the most probable chain length because at this point the differential equations diverge from the values predicted by the polynomial fit to the previous values of

the differential equations. This method depends upon the differential equations changing in a manner that can be well modeled by a third-order polynomial fit to the last four values of the differential equations. If this fit does not well model the next value of the differential equations, as when the chain length of a radical species is the most probable chain length, then this method introduces significant error. To recapitulate, the AMP predicts a value of the differential equation at the end of the integration step based upon their previous values. Hence, if there is a change in the value of the differential equations that is not well modeled by an extrapolation of a polynomial fit, then the estimate of the differential equations based upon the previous value will be erroneous.

To explain the failure of the ABMPC method, a discussion will be given of the error introduced in the solution of the differential equations for radical species of chain length as a radical 'wave' passes by that chain length. In figure 4-14, it is clear that in the time between radical waves, negligible error is introduced. As the radical wave draws closer to chain length 10, the value of the differential equations begins to increase. Now suppose for the moment that we can ignore the contribution of the propagation of 9-mers in the differential equation for radicals of chain length 10, i.e., we ignore the term $+k_p MR_9$. This means that the AMP method predicts a value of the differential equation that underestimates the magnitude of this rate of change, and by doing so underestimates the concentration of radicals of chain length 10. This is shown as negative error that is shown in figure 4-14 at 0.202 s. The differential equations are then evaluated and the actual value of the differential equations is calculated based on the current radical concentrations. As the concentration of radicals is lower than expected the value, the calculated value of the differential equations is higher than expected[1]. This causes the next value of the differential equations predicted by the AMP is higher than is expected, hence the positive error at 0.204 s. Of course while this argument holds for the artificial case where the propagation of 9-mers can be ignored, this is not really the case. The inclusion of the $+k_p MR_9$ term means that the behavior of radicals of chain length ten is coupled to those of radicals of chain length nine. Hence, the oscillations observed in the differential equations for radicals of chain length nine affect the differential equations of chain length ten. This means that the

[1] Remember that the concentration of radicals of chain-length 10 is only included in the loss terms of the differential equation for $i = 10$.

oscillations that begin with the erroneous solution of the differential equation for primary radicals move up the chain-length distribution adding error to the solution of the equations of all species. Thus this error is caused by two factors. The first being the error transferred from radicals of length $i-1$ and secondly the error incurred in solving the differential equations for radicals of chain length i. This oscillation has been seen for a range of chain lengths and it continues until the radical wave has passed. Note that a larger step size accentuates this effect.

The oscillation between overestimating and underestimating the value of the differential equations, and therefore the radical concentration, means that the ABC algorithm does not improve the value of the solution significantly. This is shown in figure 4-12 where increasing the number of cycles of correction does allow this method to be used at higher step size but also increases the error. The corrector routine uses the predicted solution of the differential equations to calculate the actual value of the differential equations at the end of an integration step. It then uses this value to define another polynomial and then recalculate the solution. As the value of the differential equations which is calculated by the corrector depends upon the predicted value of the solution, we have a problem analogous to that faced when taking successive steps. The error in the previous value of the solution introduces error of the opposite sign in differential equations. This means that successive applications of the corrector causes oscillations. This is not seen in figure 4-12 as only the absolute, i.e., always positive, value of the error is presented.

In summary, the ABMPC method introduces significant amounts of error when solving the differential equations for PIP. This method is unable to treat the rapid change in the differential equation for a radical species about the time that the chain length of that species is the most probable chain length. Hence, although this method approaches the solution of these equations in an intelligent manner and has the potential to solve less complex differential equation systems efficiently, it is of little use here.

This method was also implemented with a time-dependent step-size profile, but this refinement did not significantly increase the efficiency of this solution strategy.

4.6 Richardson Extrapolation and the Bulirsch-Stoer Method

The next finite-difference based method used in this study is the most complicated – the Richardson Extrapolation and the Bulirsch-Stoer Method. This method is widely used to solve a diverse range of differential equations system[43]. To reiterate some of what was said in the introduction, the Richardson Extrapolation and Bulirsch-Stoer (REBS) method involves two ideas. The first is the concept of Richardson's deferred approach to a limit. This states that the final answer of a numerical calculation can be thought of as an analytic function of, for example, the integration step size. If one is able to find this function, then it can be used to extrapolate to zero step size. It can be used to give the value of the solution that would be obtained if infinitely small steps were taken across an interval. The virtue of this is that, if it is assumed that the error in the solution decreases with step size, then this method should produce an error free solution. To find this analytic function a series of calculations are performed. These calculations attempt to find the value of the solution after a large integration step, H, by taking a series of smaller integration steps h across that interval. In this study, successive calculations are performed where H is divided into 2, 4, 6, 8, 10, 12, 16, and 24 smaller steps. This yields a set of data that corresponds to the size of the steps (h) taken across the interval H and the value of the solution at $t+H$, i.e., $y(t+H)$. This data is then fitted with an analytic function and extrapolated to $h = 0$. In this study, the Euler method has been used to generate the value of the solutions that are fitted by the analytic function, i.e., the Euler method is the method that solves the differential equations for each small integration step (h).

The second idea concerns the fitting function that is used in this procedure. In this study, the rational functions recommend by Bulirsch and Stoer[53] are used. The rational function that fits a set of data with $m+1$ data points with the form $(x_i, y_i)(x_{i+1}, y_{i+1})...(x_{i+m}, y_{i+m})$ is

$$y = \frac{p_0 + p_1 x + ... + p_\mu x^\mu}{q_0 + q_1 x + ... + q_\nu x^\nu} \tag{4.22}$$

Note that in this study y is equal to the solution at the end of the H-sized interval, i.e., $y(t+H)$ and x is equal to the step size which is taken across than interval, i.e., h.

A routine for fitting a rational function to a data set has been developed by Bulirsch and Stoer[53], and this works in a similar manner to the well-known recursive functions that are

used when fitting polynomial functions. Rational, rather than polynomial, functions are used to fit this data because rational functions are better at dealing with singularities. While there are no real singularities in this system, the change in the concentration of radicals upon the arrival of a laser pulse can be thought of as a quasi-singularity. Hence, it was hypothesized that rational functions might be better suited to the task of fitting around the time that corresponds to the arrival of a burst of initiation.

4.6.1 Error in the Richardson Extrapolation and the Bulirsch-Stoer Method

For all of the methods introduced so far, we have been able to give expressions that describe how the local truncation error depends upon the integration step size used. This cannot be done for the REBS method for several reasons. Firstly, the whole idea of the order of the error, i.e., of the local truncation error being modeled by an expression similar to equation 4.21, does not neatly apply to the REBS method. The size of the integration step used, H, is often so large as to render it completely meaningless. Furthermore, the error incurred depends upon not only H but also the number of trial calculations performed, i.e., how many data points are used in the function fitting, and therefore upon the size of the small integration steps (h) used.

In fact, the way that the error incurred depends upon the H as well as the size of the small integration steps (h) that should be used is still poorly understood. However, several things can be stated about the error incurred by this method. Firstly, the order of the error in the REBS method should be greater than or equal to the error incurred by the Euler method, i.e., greater than or equal than one. Secondly, the error should decrease as the number of data points used in the function fitting (i.e., number of divisions of H) increases.

To analyze the error incurred by this method when it is used to solved the population-balance differential equations for PIP, the same computer experiments that have played an integral role in the assessment of the previous four methods will be performed.

4.6.2 The Application of the Richardson Extrapolation and the Bulirsch-Stoer Method

The REBS method will now be assessed in the same way as the previous solution methods have been. Figure 4-15 contains a plot of the error incurred when a system of differential equations

with $k_t = 1 \times 10^8$ L.mol^{-1}.s^{-1} is solved with a series of REBS methods. In this figure, the error that is incurred when different numbers of trial calculations are performed per H step are plotted against step size. The number of trial calculations is defined as the number of times the solution at $t + H$ is calculated. For example, if two trial calculations are performed then the solution at $t + H$ is calculated twice, once where $h = H/2$ is used and once where $h = H/4$ is used.

To use the REBS a series of preliminary calculations have to be performed to find the optimal number of trial calculations. The number of trial calculations is closely related to the efficiency of this technique. For example, if three trial calculations are performed per H step, then the differential equations must be evaluated $(2 + 4 + 6) = 12$ times per step, i.e., for $h = H/2$, $h = H/4$, and $H/6$. In contrast to this, if five trial calculations are used per H step then the differential equations must be evaluated $(2 + 4 + 6 + 8 + 10) = 30$ times. Thus, unless the amount of error incurred is reduced three-fold by using five instead of three trial calculations per step, then the more efficient solution strategy is that which takes three trial calculations per step. This means that it is imperative that a study be performed to assess the optimal number of trial calculations that must be used per H step. In figure 4-15, methods are denoted REBS$_i$, where i indicates the number of trial calculations that are undertaken per H step. For example if $i = 4$ (REBS$_4$) trial calculations are performed to calculated $y(t+H)$ with step sizes: $h/2$, $h/4$, $h/6$, and $h/8$ and if $i = 5$ (REBS$_5$) with step sizes: $h/2$, $h/4$, $h/6$, $h/8$, and $h/10$. Data is not presented for simulations that take less than four trial calculations per step, as the rational function extrapolation failed in these cases. From this plot, it is clear that the number of trial calculations undertaken per H step does affect the amount of error incurred. This plot shows that the mean error per pulse converges as the number of trial calculations taken per step increases. Calculations show that no gain in accuracy is made by using more that six trial calculations per step. In addition to this, this plot indicates that the error incurred is proportional to H for RESB$_6$.

There are a number of notable features shown in this plot. Firstly, once the error has converged ($i \geq 6$), the mean error per pulse is directly proportional to the step size (H) used. This is a surprising result as the numerical technique used as the basis for these calculations,

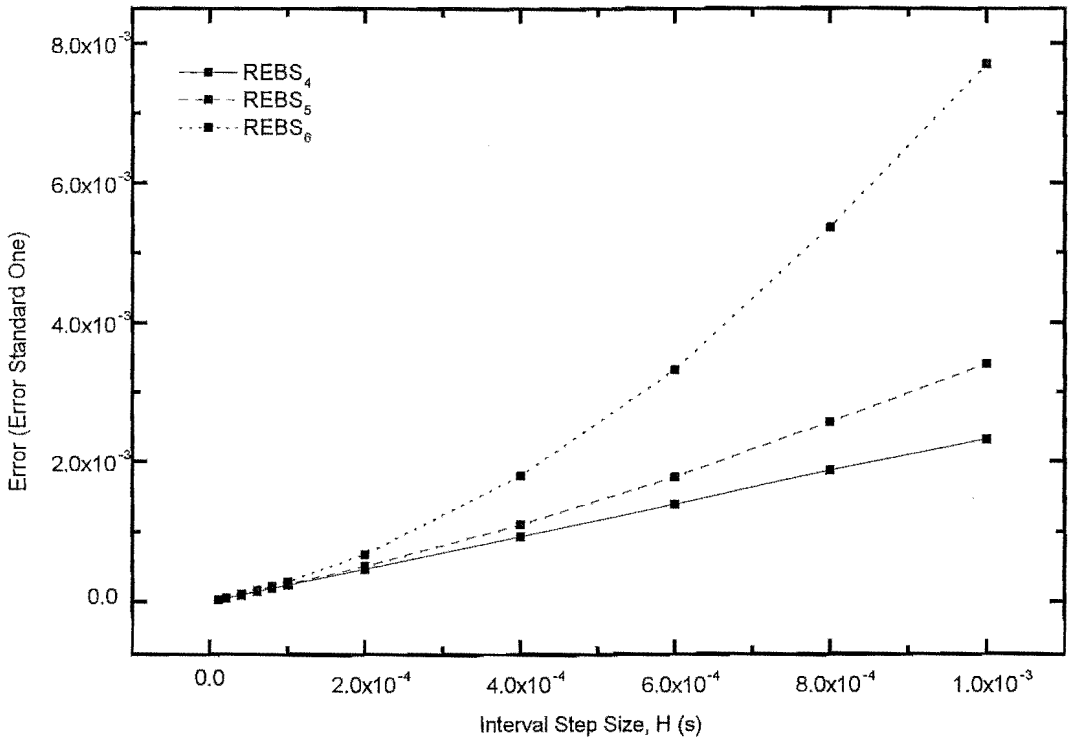

Figure 4-15: A plot that illustrates effect of increasing the number of trial calculations that are used to provide data for rational function extrapolation. All rate data as table 4.1.

the Euler method, also incurs error[2] that is proportional to the H. Moreover, and this brings us to the second point, the magnitude of the error incurred is greater than that incurred by the simple Euler method of step size H. This means that all the extra computational effort spent performing trial calculations and then the rational function extrapolation produces no increase in accuracy. This is exemplified by the efficiency analysis performed below. To explore the effect of the rate coefficient for termination upon error incurred by this method a series of simulations have been performed where the rate coefficient for termination is varied. The results of these simulations are given in figure 4-16.

[2]Note that the h used with the Euler method is equal to H in the REBS method.

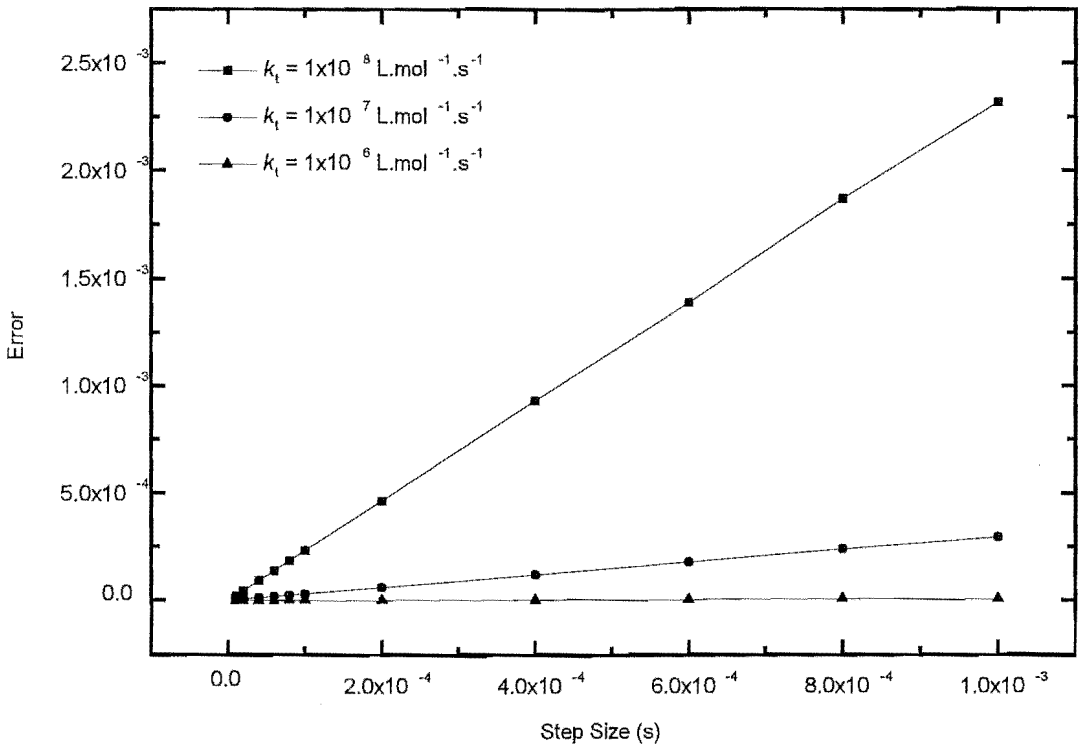

Figure 4-16: The effect of the rate coefficient for termination upon the error incurred by the $REBS_6$. All other simulation parameters are the same as those shown in table 4.1. Note that the error presented here has been assessed via error standard one and that the step-size corresponds to H not h.

This study indicates the mean error per pulse incurred by this method depends upon this rate coefficient in the same way as the error incurred by methods such as the RK4 and ME methods. Hence, more error is incurred in a system where the value of k_t is high.

To assess the efficiency of this method the mean error per initiation period has been multiplied by the number of steps taken per pulse. The number of steps taken per pulse for the $REBS_6$ is defined as

$$n_{steps} = \frac{42t_0}{H} \tag{4.23}$$

This expression is essentially the same as that for a constant step size profile multiplied by the

k_t(L.mol^{-1}.s^{-1})	ξ
1×10^6	3.99×10^{-2}
1×10^7	1.45
1×10^8	11.1

Table 4.6: The efficiency value for the optimum REBS method (i = 6).

number of trial steps that are taken. Note that as the Euler method is used as the basis for these calculations, the differential equations must be evaluated once per trial integration step.

The efficiency values for the $REBS_6$ method are presented in table 4.6. The efficiency values for the $REBS_6$ method are presented as a table rather than a plot, as they are independent of the integration step size used. This is because $E_{pulse} \propto H$ and $n_{steps} \propto H$. A comparison of the efficiency of the $REBS_6$ with those for Euler method reveals that in general the REBS method is less efficient. For example, the efficiency value for the Euler method solving a system of differential equations with a $k_t = 1 \times 10^8$ L.mol^{-1}.$s^{-1}$is 4.64 while the efficiency value for the $REBS_6$ method for the same system is 11.1. Hence, if the $REBS_6$ method is used 2.4 times as many steps must be taken per integration step to obtain the same level of accuracy. In contrast to this, when a system of differential equations with a $k_t = 1 \times 10^6$ L.mol^{-1}.s^{-1} are solved by the REBS method the efficiency value (3.99×10^{-2}) is lower than that for the Euler method (0.166). Thus, the REBS method is more efficient than the Euler method at solving the differential equations for low k_t system but less efficient for a high k_t system.

For this method to be successful, the data produced by the trial calculations must be able to be fitted by a rational function, and the extrapolation of that function must produce a low error solution. The results of the study outlined above suggest this extrapolation is performed with greater success for a low k_t than for a system with a high value of k_t. While there appears to be no obvious explanation for this, it is likely to be a result of the dependence of the rate of change in the error upon the k_t. In chapter three, it was shown that a large value of the termination rate coefficient causes the differential equations to change at a greater rate than when a small value of k_t is used. Therefore, a high k_t will mean that the solutions predicted by the trial calculations will change more rapidly with the number of steps taken in the interval H. Rational function extrapolation appears to be more successful when the rate of change is low.

The problem with high k_t solutions is probably related to the chosen rational function being a poor fit to the trial data. A better choice of rational function should remedy this problem. However this was not tried. It principle it should be impossible for the REBS method with a particular H to be less accurate than the Euler method with same H, so the high k_t results are surprising. The possibility of the NAG library routine used for rational function fitting malfunctioning can not be discounted.

Although there are cases when the $REBS_6$ method is more efficient than the Euler method there are no cases when the REBS the method is more efficient that the RK4 or even the ME method. For this reason, the REBS method must be ruled out as a potential practical solution strategy. It will not be studied further in this thesis.

4.7 The Implicit Euler Method

The last finite-difference based numerical solution strategy used in this thesis is a method designed for solving stiff differential equation systems. As has been described previously (chapter one), numerical solution strategies have difficulty solving stiff differential equations as the solution of these equations contains two or more terms that change at very different rates. For example, the solution of the differential equations for intermittently initiated free-radical polymerization contains a slowly changing term, the termination term, and a transient term, the propagation term. The presence of these two terms in the solution limits the step size that can be used in explicit methods for solving these differential equations. It forces the solution algorithm to use a step size that is small enough so that little error is introduced to the transient part of the solution, a step size that is significantly less than that which could be used to solve the slowly changing part of the solution without incurring a lot of error. Hence, even if the transient part of the solution is of little interest, one is forced to use a step size small enough to correctly describe it, or else one incurs significant amounts of error in the entire solution. The effects of stiffness were shown in the error analysis performed in chapter three by the fact that a step size of less than the reciprocal of the propagation frequency had to be used at all times. The solution of equations 3.22 - 3.24 was limited by the transient or propagation term. This is the generic disease of stiff equations: we are required to follow the variation in the solution

on the time scale of the transient term in order to maintain the stability of the integration, even though accuracy requirements allow a much larger step size. It seems then, that if a technique could be developed that removes this limitation, then these differential equations could be solved with as yet unrivalled efficiency. Although methods that deal with stiffness do exist, it will become clear that they do no greatly increase the solution efficiency.

4.7.1 Implicit Finite-difference Methods[20]

To see how we might cure the problem of stiffness, consider a simple differential equation

$$y'(t_n) = -Cy(t_n) \tag{4.24}$$

where $C > 0$ is a constant. The explicit, or forward, Euler method for the integration of this equation with step size h is

$$\begin{aligned} y(t_{n+1}) &= y(t_n) + hy'(t_n) && (4.25) \\ &= (1 - Ch)y(t_n) && (4.26) \end{aligned}$$

This method is not stable for all h, i.e., there are some values of h where this method diverges. For example, if $h > 2/C$ then $y \to \pm\infty$ as $t \to \infty$ giving an incorrect solution to equation 4.24.

It is timely to now consider the way that these ideas relate to free-radical polymerization systems. In these systems it is well known that it is the propagation terms in the living radical differential equations that produces the transients in the solution. Thus if we ignore the termination term in these differential equations, they can be rewritten as:

$$\frac{d\mathrm{R}_i}{dt} \approx C(\mathrm{R}_{i-1} - \mathrm{R}_i) \qquad \text{where } C = k_\mathrm{p}\mathrm{M} \tag{4.27}$$

Hence based on the analysis of equation 4.24, the numerical solution of these differential equation should be stable for step sizes less than $\frac{2}{k_\mathrm{p}\mathrm{M}}$. However, the analysis of equation 4.24 only holds for a simple differential equation of that form. It is unsurprising that slightly different behavior is observed when solving the system of complex differential equations that model the living radical chain-length distribution. Numerical calculations have shown that for these systems,

one must use a step size of less than $\frac{1}{k_p M}$ to ensure that explicit methods do not produce solutions which diverge from the actual value of the solution.

Finally, these ideas can be used to explain the shape of figure 3-13. This is plot presented in chapter three that showed the shape of the differential equations predicted when the Euler method is used with step size greater than $\frac{1}{k_p M}$. In this plot there are large oscillations in the value of the differential equations about the time when the radical species in question has the most probable chain length. A simple explanation of these oscillations can be given by considering what happens when differential equation 4.24 is solved by an explicit method with a step size greater than $\frac{2}{C}$. In this case the expression for this numerical method, i.e., equation 4.26 reduces to

$$y(t_{n+1}) > -y(t_n) \qquad \text{where } h > \frac{2}{C} \tag{4.28}$$

This means that no matter what the initial value of $y(t_{n+1})$, the new value predicted by an explicit method will be greater in magnitude and opposite in sign. It is clear that this means that value of solution will oscillate in value and diverge. Note that again this explanation does not quite carry over to free-radical polymerization systems where other effects are involved, i.e., the coupling of the differential equations. A full mathematical analysis of the stability of the differential equations for PIP has not been performed in this thesis.

The simplest way of remedying the problem of stiffness is to resort to implicit differentiation, where the differential equations are evaluated at t_{n+1} rather than t_n. In this case, we get the implicit, or backward, Euler method:

$$y(t_{n+1}) = y(t_n) + hy'(t_{n+1}) \tag{4.29}$$

$$= \frac{y(t_n)}{1 + Ch} \tag{4.30}$$

For this differential equation, this method is absolutely stable: even as $h \rightarrow \infty$, we still get $y \rightarrow 0$, the correct solution. For non-trivial differential equations, i.e., equations when C is not simply a constant, this method is not absolutely stable, but it is normally more stable than an explicit method.

If we consider the situation when a differential equation is solved that has a non-constant

C value, then the implicit form of the Euler method is represented by equation 4.31.

$$y(t_{n+1}) = y(t_n) + hf(t_{n+1}, y(t_{n+1})) \tag{4.31}$$

To convert this expression into a form where it depends only on the values of $y(t_n)$ and $y(t_{n+1})$, $f(t_{n+1}, y(t_{n+1}))$ must be expressed in terms of $y(t_n)$ and $y(t_{n+1})$. In general, this can only be done by iteratively solving a set of non-linear equations. However, $f(t_{n+1}, y(t_{n+1}))$ may be linearized, i.e., expanded as a Taylor series, to give equation 4.32. This method is called an 'semi-implicit' method, and is not guaranteed to be stable.

$$y(t_{n+1}) = y(t_n) + h\left[f(t_{n+1}, y(t_n)) + \left(\frac{\partial f}{dy}\right)_{y(t_n)} (y(t_{n+1}) - y(t_n))\right] \tag{4.32}$$

Here $\frac{\partial f}{dy}$ is the matrix of partial derivatives at t_n known as the Jacobian (the partial differentials of the differential equations) and $f(t_{n+1}, y(t_n))$ is the value of the differential equations at t_{n+1} based on the solution at t_n, $y(t_n)$. Thus, to use this method one must invert the matrix that is the identity matrix less the integration step size multiplied by the Jacobian, i.e., equation 4.33.

$$I - h\frac{\partial f}{dy} \tag{4.33}$$

The Application of the Implicit Euler Method

The implicit Euler (IE) method has been used in this thesis to solve equations 3.22 - 3.24. To implement this method a computer program was written to solve equation 4.32. As a part of this program the NAG library routine F01ADF was used to invert the matrix defined by equation 4.33. Some of the results of this study are shown in figure 4-17 (note the high values of this error and see later for an explanation of this).

It follows from this figure that there are many similarities as well as several differences between the error incurred by the IE and explicit Euler (EE) methods. The first difference is the shape of the error-h plots. A linear relationship was found between the error incurred by the EE method and the integration step size. In contrast to this figure 4-17 indicates that the error incurred by the IE method is approximately proportional to$\sqrt{h}$. However, the most significant difference between the two methods is the range of the step sizes that the IE method

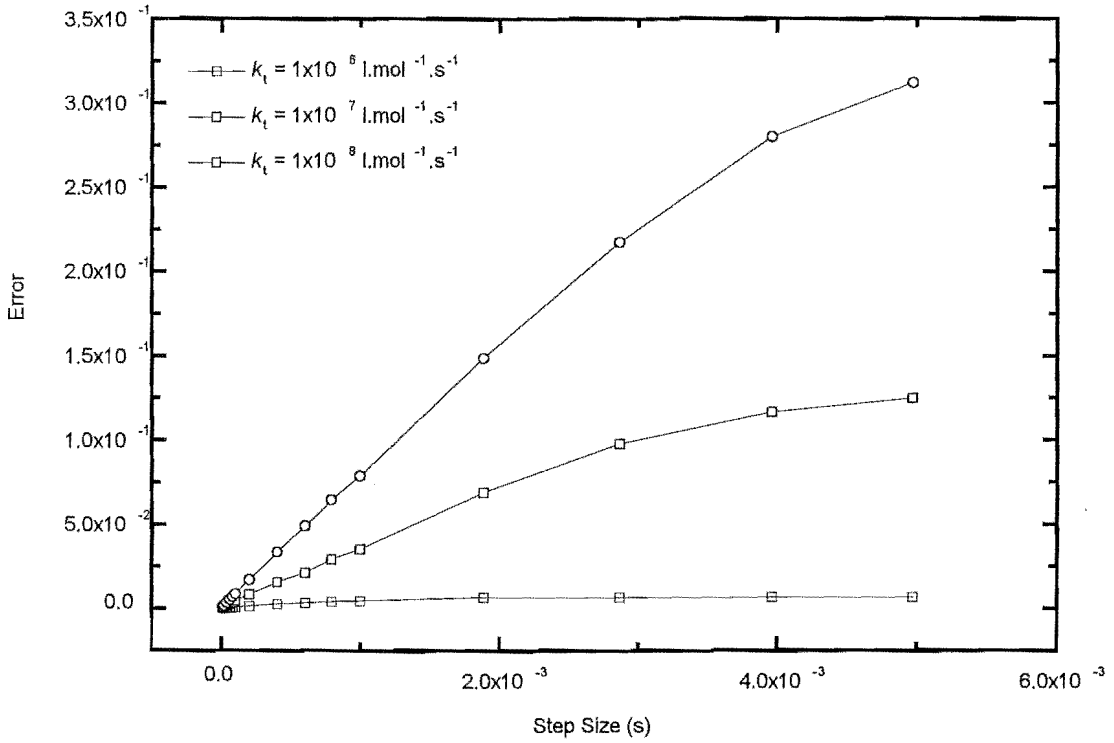

Figure 4-17: The dependence of error upon step-size for the Implicit Euler Method. All rate parameters are as per table 4.1. The error in this plot has been assessed via error standard one.

can be used over. Whereas the EE method was limited to using step sizes below one over the propagation frequency ($\frac{1}{k_p \mathrm{M}}$), the IE method is not limited in this way. This means that larger step sizes can be used, and therefore less computational effort can be spent solving these differential equations.

Factors Which Limit the Gains Made From Using an Implicit Method

Although the use of implicit methods allows larger step sizes to be used, three additional considerations mean that this freedom does not always result in an implicit method being the most efficient method for solving these differential equations. Firstly, the computational cost of taking an integration step with the implicit method is significantly greater than for

the explicit method. This is because a further computationally expensive task, in addition to the evaluation of the differential equations, must be performed every integration step when an implicit method is used. This task is the inversion of the matrix defined by equation 4.33. The matrix inversion method used in this study incurs a cost that is proportional to N^3 for a N by N matrix. Remember that N is large for PIP systems, e.g., $N = 5000$ was used in simulations here. Hence, although we are normally able to use larger step sizes with a implicit method, the cost of taking these steps is significantly greater.

The next consideration imposes a further limitation on the step size that can be used. Although we need no longer limit the size of integration steps to values less than one over the propagation frequency, the value of the pulse frequency limits the maximum value of h. Simulation studies have shown that a significant amount of error is introduced if a step size greater than half the time between bursts of initiation is used with an implicit method, i.e., if $h > \frac{t_0}{2}$. Although this means that for the default rate parameter set (table 4.1) that the maximum step size that can be used is fifty times what it was when an explicit method was used, i.e., $h_{\max} \leq \frac{50}{k_{\mathrm{p}}\mathrm{M}}$, this will not always be the case. Specifically, as $k_{\mathrm{p}}\mathrm{M}t_0$ is reduced, there is little scope for an implicit method to increase the value of h that can be used, so the advantage of using an implicit method is completely lost.

The last consideration involves the error that is incurred by increasing the step size. Figure 4-17 shows that the error incurred by the IE method continues to increase (although at a slower rate) as the step size is increased. So if a step size of $h = 2 \times 10^{-3}$s is used, then a significant amount of error is incurred (at least for systems where $k_{\mathrm{t}} \geq 1 \times 10^{7}\mathrm{L.mol}^{-1}.s^{-1}$). Again this reduces the gain in efficiency that the use of an implicit method can bring. Although the IE method allows the differential equations to be solved at a higher step size, these three factors combine to minimize the increase in efficiency that this could otherwise cause.

In summary, implicit methods allow the use of step sizes greater than $\frac{1}{k_{\mathrm{p}}\mathrm{M}}$. However, the computational cost of using these methods, the error incurred by the use of higher step sizes, and the additional limitations imposed by the initiation frequency mean that frequently there is no gain in efficiency.

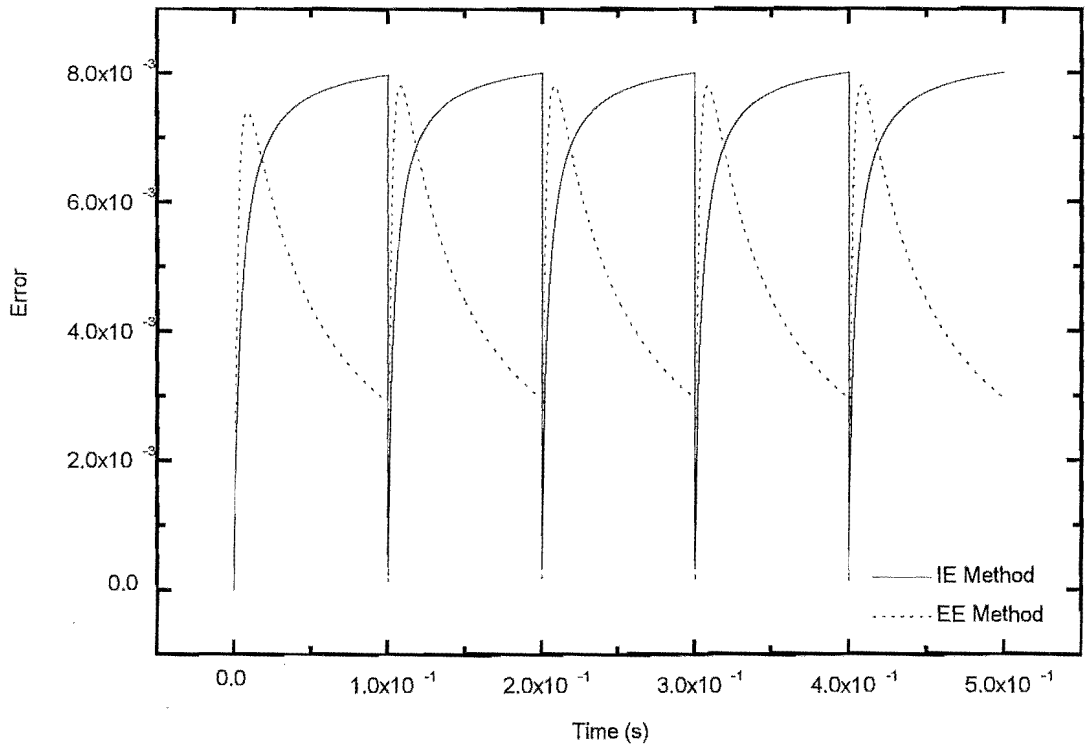

Figure 4-18: The temporal dependence of the error incurred by the IE and EE methods. All rate parameters are as in table 4.1. Note that the error in this plot has been via error standard two, i.e., $(R_{sim}-R_{analy})/R_{analy}$.

Error Standard Two As there appear to be situations where the IE method has advantages over all of the other methods presented so far, a thorough analysis of the error incurred will be performed. Figure 4-18 contains a plot that illustrates how the error incurred by the IE method depends upon time.

Figure 4-18 contains a plot of the error in the total radical concentration incurred by the IE and EE methods. Although this plot shows that a comparable amount of error (with the IE method incurring more error) is incurred, it is clear that the shape of the error-time profiles is different for each method. For example, while the error in the solution obtained by the EE method peaks early and then decays, the error in the solution obtained by the IE method

increases through out the initiation period. This difference in shape is a direct result of the way that these methods work.

In summary, explicit methods use the value of the differential equations at the start of a step, while implicit methods use the value at the end of the step. This means that whereas the EE method normally incurred negative truncation error, the IE method incurs positive truncation error (note the absolute - always positive - value of the error is given in these plots). In addition to this, the self-correcting influence of initial-condition error does not appear to play the same role in the error of the IE method as it did in the EE method. The error in the EE method declines rapidly after an initial peak, because the underestimation of the total radical concentration leads to an underestimation of the rate of termination, and hence a increase in the total radical concentration. This does not appear to occur in the IE method. It is possible that this is due to a cancellation of the effects that this has on the value of the differential equations by the effect that it has upon the Jacobian. Finally, an inspection of the derivative of error incurred against time reveals that the rate at which error is added decreases with time. This is in agreement with ideas developed previously that suggest that the error in the Euler method is proportional to the rate of change in the differential equations.

Finally, the error has been analyzed with error standard three. This has shown that the error in the radical chain-length distribution is essentially the same as that incurred by the EE method except that it has the opposite sign. This is consistent with difference between the truncation error that the EE and IE methods incur.

Other Implicit Methods Several other implicit methods have been investigated in this study. These include: an implicit ME method; an implicit RK4 method commonly used in the DASSL program; a variant of the implicit predictor-corrector method commonly known as the Gear method; and an implicit REBS method. Although a detailed study of these methods is not presented here, some comments will made on each of the methods.

- **The Implicit ME and RK4 methods** Both these methods give very similar results to the IE method. The use of an implicit, rather than explicit, version of the method allows step sizes greater than $\frac{1}{k_p M}$ to be used. However, the same three limitations restrict the efficiency of these methods. Firstly, the computational cost of obtaining a solution

by an implicit method is significantly greater than for an explicit method. In fact, this effect is more pronounced for the ME and RK4 method than it was for the IE method. This is because the computationally expensive task of inverting the Jacobian matrix must performed after every trial step. Hence, as the ME and RK4 methods take two and four times as many trial steps respectively per integration step as the IE method does, having to invert the Jacobian every step has a greater effect upon these methods. Moreover, time step gains are limited by the pulsing of the laser, i.e., one cannot possibly use a time step greater than $\frac{t_0}{2}$. Nonetheless, there are circumstance where these methods are of practical use.

- **The Implicit Predictor-Corrector Method** A widely used variant of the implicit predictor-corrector method is the Gear algorithm. In section 4.5, it was shown that the AMBPC method was poorly suited to solving the differential equations for this sort of polymerization. Moreover, error standard three revealed that this was a result of the difficulty this method has in dealing with the differential equations for the radical species that has the most probable chain length. As this is the exact problem that an implicit method attempts to deal with, one would expect that an implicit predictor-corrector would be a significant improvement upon an explicit predictor-corrector; this is partly the case. While the semi-implicit ABMPC method introduce significantly less error than the explicit ABMPC method it does still does not rival the simple Runge-Kutta methods in terms of overall efficiency and stability.

- **The Implicit REBS Method** Using an implicit, rather than an explicit, method to calculate the data that is used in the rational function extrapolation does not appear to remedy the problems of the REBS. Essentially, the same problems are found. The implicit REBS method still incurs more error than the IE method for high k_t systems, while requiring a lot more computational effort.

4.8 The Monte Carlo Solution Method

The Monte Carlo (MC) method is the last, and only non-finite-difference based, method used in this study. The MC method is a stochastic method that models the kinetics of a reaction system

using random numbers. This method creates a hypothetical reaction vessel that contains a large collection of molecules. Based upon the numbers of the various species in this vessel, as well as rate coefficients for all possible reactions, this method decides when and what type of reaction should take place. To do this, it uses an appropriately weighted random number to decide the length of time between reaction and the types of reaction. The MC method then alters the number of molecules contained within the reaction vessel to reflect the reaction that has taken place. By repeatedly applying this simple procedure the MC method is able to describe the time evolution of all chemical species in the hypothetical vessel.

One of the advantages of a MC approach is that it is not necessary to have an expression for all of the types of chemical species that can be present in the reaction vessel before modelling that system. This is not true of a differential equation based approach. To describe a chemical system using any differential equation based method, one must have a differential equation for every species or group[3] of chemical species present. Thus, MC methods have an advantage over differential equation based treatments in chemical systems that contain a very large number of different species. Consider, for example, a system where the long chain branching produced by transfer to polymer is important. If one allows the radical activity to be transferred to a dead polymer chain more than once, then there are a vast number of possible species. This means that an impracticable number of differential equations must be used to describe these systems. In contrast to this, a MC method must include only one more reaction and have some method of recording all of the species produced.[50]

To describe a chemical system using the MC method one defines a series of so-called transition rates. A transition rate is the rate of change of the state of the reaction vessel to another particular state, where the state of the vessel is defined by the numbers of all the chemical species present. For example, for the system that has been modeled in this thesis, three transition rates are needed. These are shown in table 4.7. In table 4.7, N_A is Avogadro's number and V is the volume of the simulated vessel. Note that populations are now in terms of the number rather than the concentration of molecules in the hypothetical reaction vessel, i.e., in

[3]Lumping treatments such as 'coarse-graining' treat a group of species as if they were one species. Therefore, they do not transcend this limitation.

Reaction	Transition Rate
$R_i + M \xrightarrow{k_p} R_{i+1}$	$\frac{k_p M R_i}{N_A V}$
$R_i + R_j \xrightarrow{k_{td}} D_i + D_j$	$\frac{2k_{td} R_i R_j}{N_A V}$ $i \neq j$
	$\frac{k_{td} R_i (R_i - 1)}{N_A V}$ $i = j$
$R_i + R_j \xrightarrow{k_{tc}} D_{i+j}$	$\frac{2k_{tc} R_i R_j}{N_A V}$ $i \neq j$
	$\frac{k_{tc} R_i (R_i - 1)}{N_A V}$ $i = j$

Table 4.7: Transition probabilities for the MC simulation of intermittently initiated free-radical polymerization

these transition rates

$$R_i = N_A V R_i \qquad M = N_A V M \tag{4.34}$$

If R is defined as the total number of living radicals, i.e., $R = \sum_{i=0}^{\infty} R_i$, then the transition rate due to all possible propagation reactions is equal to

$$W_{prop} = \frac{k_p M R}{N_A V} \tag{4.35}$$

Similarly, transition rates for all termination by combination and by disproportionation reactions are defined as[50]

$$W_{td} = \frac{k_{td} R(R-1)}{N_A V} \tag{4.36}$$

$$W_{tc} = \frac{k_{tc} R(R-1)}{N_A V} \tag{4.37}$$

Hence, the total transition rate for all reactions is equal to

$$W_{total} = W_{prop} + W_{td} + W_{tc} \tag{4.38}$$

Note that a transition rate is not included for initiation, as this process is assumed to occur instantaneously and only at the time corresponding to periodic initiation by, for example, a pulsing laser.

This allows us to define the length of time between successive reactions. This is determined

by the total transition rate and a uniformly distributed random number, $\alpha \in]0,1]$.[50]

$$\Delta t = \frac{-\ln \alpha}{W_{total}} \tag{4.39}$$

Once the time that the next reaction will occur has been decided, a second random number is used to choose which reaction takes place. Each reaction is chosen according to its probability, e.g., W_{prop}/W_{total}. If the random number falls in the interval corresponding to the probability of a reaction occurs, e.g., $]0, W_{prop}/W_{total}]$ for propagation. The radical species participating in that reaction is then randomly chosen (1 species if it is propagation, 2 species if it is termination) and the species in the vessel altered to reflect the reaction.

Summarizing, the algorithm works as follows:

1. Choose a volume at the start of the reaction and calculate the particle numbers. Set the particle numbers for living and dead polymer species equal to zero, apart from R_0 which is set equal to $N_A V \rho$.
2. Decide whether a burst of initiation has just arrived, and if it has then increase the value of R_0 by $N_A V \rho$.
3. Calculate the transition rates and probabilities for all reactions.
4. Determine the time (Δt; using equation 4.39) after which the next reaction occurs and increment time by that value.
5. Determine which reaction and which species reacts.
6. Alter the state of the system to reflect the reaction chosen in step 5.
7. Continue with step 2 if the simulation time is less than the final simulation time.

This algorithm has been used to model the kinetics and MWDs of a PIP with the standard kinetic model described above. All of the rate parameters used in these simulations are shown in table 4.1. In addition to this, the default simulation volume used in all simulations is $V = 1 \times 10^{-12}$ L and $k_t = 5 \times 10^7 \text{L.mol}^{-1}.\text{s}^{-1}$. This is the volume of the hypothetical reaction vessel. Hence it can be used in conjunction with the concentration of the various species to define the number of molecules in the system. Note that the integration step size h has no meaning in these calculations. Moreover, the maximum chain length is now not limited to 5000. The

program which implements the MC algorithm increases the value of the maximum chain length as required (based on the current longest chain); typically the required value never exceeded 5000. The MC simulations outlined here took a significantly greater amount of time than any of the FDB simulations presented above. For example when the default rate parameters where used a simulation took 10 hours of computer time.

Preliminary calculations showed that the majority of the time spent implementing this algorithm was taken up modeling propagation reactions. To understand the reason for this one need only look at the events that have to occur to make a dead polymer chain containing 100 monomer units. If that chain was terminated by the disproportionation termination mechanism, then the ratio of propagation to termination events is 100 : 1. Thus, the efficiency of the MC method could be increased if some treatment was developed that decreased the amount of time spent describing propagation events.

For this reason a distribution based treatment of the propagation reaction has been developed. This treatment is similar to that used by Seeβelberg et. al.[50] for MC simulations of a continuously-initiated free-radical polymerization. This idea is based on the well-known idea that the propagation of free-radical polymer chains is a Poisson process. This means that the number of monomer units that a radical chain adds in a period of time can be described by a Poisson distribution. The Poisson distribution for the probability $P(i,t)$ that a chain will add i monomer units in t seconds is given by equation 4.40.

$$P(i,t) = \exp(-k_{\mathrm{p}}\mathrm{M}t)\frac{(k_{\mathrm{p}}\mathrm{M}t)^i}{i!} \tag{4.40}$$

For example, if we consider a time of $\frac{1}{k_p\mathrm{M}}$ seconds, on average a chain will grow one monomer unit. However, there is a $1 - \frac{1}{e}$ probability that a chain will not grow at all. To use this distribution to model propagation steps it is necessary to model the Poisson distribution by a Normal distribution (4.41). This is because it is difficult and computationally expensive to evaluate the Poisson distribution on a computer for high values of i or $k_{\mathrm{p}}\mathrm{M}t$. To avoid this difficulty the Poisson distribution has been approximated by the Normal distribution. This

gives equation 4.41, which a good approximation for equation 4.40 when $k_p M t \geq 20$.

$$P(i,t) \approx \frac{1}{\sqrt{k_p M t}} \exp\left(\frac{-(i - k_p M t)^2}{2 k_p M t}\right) \tag{4.41}$$

The advantage of treatment this way can be seen by considering the time between reactions. The time between reaction events is proportional to $\frac{1}{W_{total}}$. Thus when propagation is treated as a distribution, the transition rate for propagation is effectively being removed from the calculation of the total transition rate, i.e., $W_{total} = W_{td} + W_{tc}$, so that the average length of time between reactions increases. This means that a PIP simulation takes a shorter amount of computer time.

To use this improved method one begins, as before, by calculating the length of time until the next reaction using equation 4.39. Then one chooses one of the two termination reactions and the two reacting radicals species. To determine the chain length of those radicals, the difference between the current time and the time when these radical species were created is taken. This time generates a probability distribution of chain lengths according to equation 4.41. A random number is then used to select a chain length from that distribution. Effectively what this process does is randomly pick a chain length from the Normal distribution centered about the most probable chain length for a radical species of that age. This allows us to model the stochastic nature of propagation events without having to treat every event individually. This refinement decreases the computational cost by a factor of one hundred. Simulation studies that compare the standard and improved MC algorithms indicate that the difference in the two predicted MWDs is negligible when the default parameter set is used.

4.8.1 Error Standard One

The error in the MC method is assessed in the same way as it was when FDB methods were used. Figure 4-19 contains the mean error per initiation period for ten initiation periods, where error is defined as the difference between the analytic and simulated total radical concentrations. All simulations were repeated ten times and the error shown in this plot is the average of those ten simulations. Note that error is defined here as being an absolute value, and so there can be no cancellation of positive and negative values from 10 simulations. Note that error is plotted

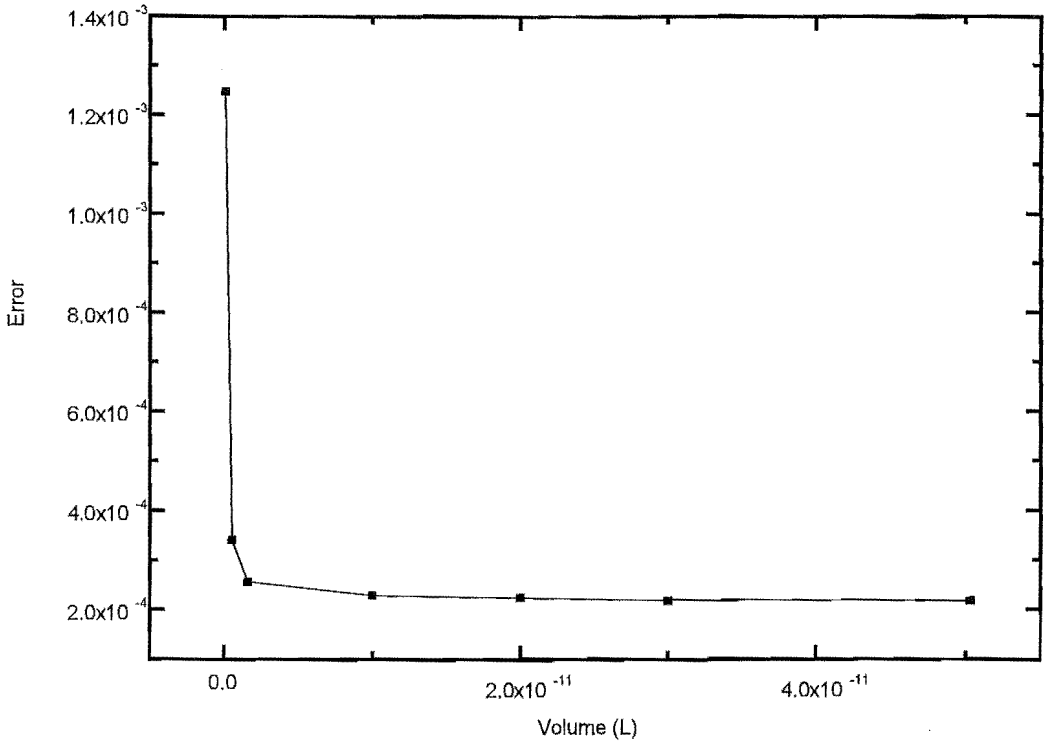

Figure 4-19: The error incurred by the modified MC method for a range of simulation volumes. The error in this figure has been assessed via error standard one.

against simulation volume rather step size in figure 4-19. It is clear from figure 4-19 that the error incurred by the MC method is correlated with the simulated volume, so that when the volume is decreased the error increases. The volume used in a MC simulation is the independent variable that can be changed to alter the accuracy of the simulation. The relationship between V and the error incurred can be understood in terms of the statistical principle that accuracy of a result is proportional to the sample size. As the volume defines the number of molecules contained in the reaction vessel, increasing the volume increases the sample size and therefore the accuracy. Note that increasing the simulated volume also increases the computational cost of obtaining the solution. This is because the size of the time steps, Δt, is inversely proportional to the total transitional rate, which is increases as more molecules are added to the system.

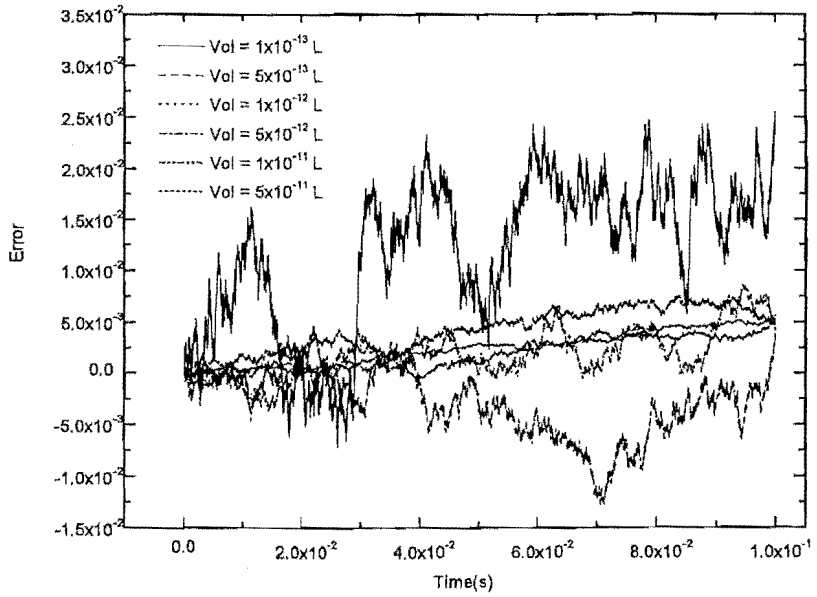

Figure 4-20: The temporal dependence of error incurred by a Monte Carlo Simulation. Note that the error in this plot is the difference between (not the absolute difference) the between the analytic and simulated total radical concentrations.

The effects of the random error mentioned above are shown with greater clarity in figure 4-20. This figure contains a plot of the error incurred per integration step throughout an initiation period and for a range of simulated volumes. Note that whereas figure 4-19 contained error values that where averaged over ten runs, figure 4-20 contains data for a single run. Although the most striking feature shown in this plot is the random scatter of the error values, there are, nonetheless, two additional trends. Firstly, the error decreases as the size of the volume increases. This trend is in keeping with the ideas outlined above about the need for a large sample size to reduce the effect of random fluctuations. Secondly, this plot shows that the error increases as time passes. This trend is clearer for the simulation where the greatest simulated volume was used (5×10^{-11}L), i.e., the simulation in which we should have the greatest confidence. To confirm the authenticity of this trend additional simulation runs were performed. These showed that this trend is a result of random fluctuations. The opposite trend, a decrease of error (becoming more negative) with time was observed in several runs. This suggests that this trend is merely a statistical effect, rather than systematic error introduced by the MC

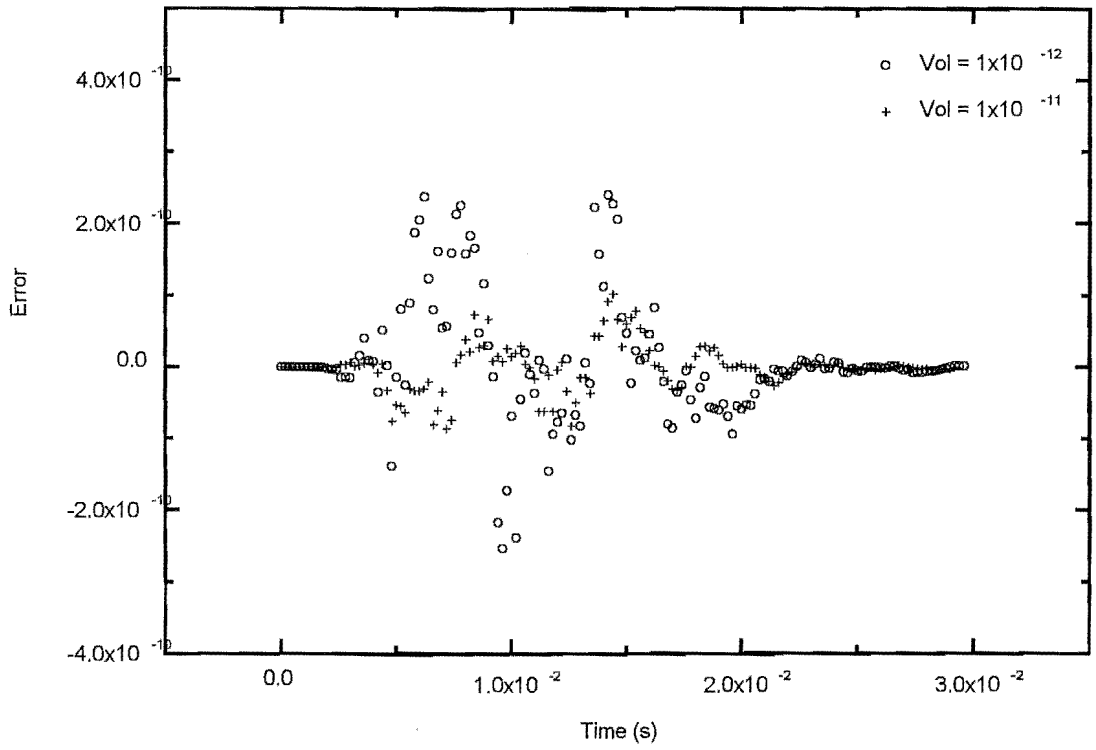

Figure 4-21: The error in the concentration of radicals of chain-length 10 incurred when the standard MC method is used. Default rate parameters used in both simulations. The error shown in this plot is the difference between simulated and analytic radical concetrations of radicals of chain-length 10, i.e., error is equal to $(\mathrm{R}_{10})_{sim} - (\mathrm{R}_{10})_{analy}$.

method.

The final error analysis performed in the solution produced by the MC method is error standard three. Note that for this analysis the simulations obviously has to be performed with the standard simulation algorithm (the treatment of individual propagation steps). Figure 4-21 contains a plot of the error incurred in the concentration of radicals of chain length 10 as a function of time. This plot shows the same trend that has been seen throughout this thesis: the error is greatest around the time when the chain length of the radical species is the most probable chain length. Although MC methods do not incur error in the same manner as FDB

methods do, a similar line of reasoning can be used to explain this effect. About the time when a radical species has the most probable chain length its concentration changes by the greatest amount. Thus, at this time MC must describe more propagation events concerning this radical species. This means that at the time when a radical species is the most probable species statistical fluctuations can have the greatest effect upon its concentration. It is clear from this plot that an increase in the simulation volume decreases the error incurred.

4.9 Conclusion

In this chapter and the proceeding one, seven solution methods have been introduced and applied. The error incurred by, and the efficiency of, each of these methods has been examined in some detail. This analysis has shown that some of these methods are far more suited to solving the system of differential equations that characterize PIP. In this section, the results obtained by each method are compared and a set of recommendations made. Each method is judged in terms of the error it incurred and efficiency at which it operates. Based upon this assessment a decision is made about the usefulness of each method for solving the model system of differential equations used in this chapter and the general system of differential equations that characterize this type of polymerization. This discussion is divided into three parts: (1) the advantages and disadvantages of each method; (2) the optimal numerical method for the model system; and (3) the optimal method for modelling PIP in general.

It should be noted that this discussion will focus on the error incurred by each method relative to the other methods used in this study. A discussion of the error incurred in the final MWD is left to chapter five.

4.9.1 An Assessment of the Tested Methods

Table 4.8 contains summary information for the numerical methods used in this study. It includes the predicted (or observed) scaling law, the efficiency of the method with and without a time dependent step-size profile and the number of differential equation evaluations required per time step. If these methods are ranked in terms of efficiency the order is: (1) TDSSP RK4 method; (2) TISSP RK4 method; (3) TDSSP ME method; (4) TISSP ME method; (4) ABMPC

Method	Scaling Law	Efficiency with TISSP	Efficiency with TDSSP	σ_{des}
Euler	$\propto h$	4.64	5.31×10^{-1}	1
ME	$\propto h^2$	4.23×10^{-3}	4.82×10^{-4}	2
RK4	$\propto h^4$	1.20×10^{-7}	2.24×10^{-11}	4
ABMPC	$\propto h^4$	2.37×10^{-1}	–	1
$REBS_6$	$\propto h$	1.11×10^{1}	–	42
IE	$\propto h$	5.78	–	1+ Inversion
MC	–	$E_{pulse} = 2.2 \times 10^{-4}$ $V = 5 \times 10^{-12}$L 10 hrs computer time	–	–

Table 4.8: Summary of Results when calculations are performed with default rate parameters. Note the standard MC algorithm is included in this table and the ABMPC variant is that with i = 1.

method (P(EC)^1 variant); (5) TDSSP Euler method; (6) TISSP Euler method; (7) IE method (excluding the cost of inverting the Jacobian); (8) REBS^{6}method; (9) Standard MC method

The Euler, Modified Euler and Fourth-Order Runge-Kutta Methods

- **Advantages** These methods produce the solutions that contain the least error in the shortest period of computer time. This is reflected in the efficiency values of these methods which are on average the lowest obtained. Moreover, the error incurred by these methods can be further reduced if a time-dependent step-size profile is used. The approach that these methods take is well suited to this system of differential equations. These methods are efficient, simple to use and robust.

- **Disadvantages** The ME and RK4 methods require the differential equations to be calculated twice and four times per initiation period respectively. This can mean that these methods are computationally expensive to use if either a larger number of differential equations have to be solved, or the simulations have to be carried out for a long period of time. The second disadvantage is derived from the $\frac{1}{k_p M}$ limit on the step size. If the propagation frequency is high then these methods are forced to use step sizes that are less than those that implicit methods can use.

The Adams-Bashforth-Moulton Predictor-Corrector Method

- **Disadvantages** The ABMPC method is poorly suited to solving the differential equations that characterize PIP. This study has revealed that there are no circumstances when the ABMPC $(P(EC)^i \quad 0 \leq i \leq 3)$ is the method of choice for solving this systems of differential equations. The ABMPC method introduces significant amounts of error in an erratic fashion. It appears that these differential equations are simply too sensitive to error to be solved by this method.

The Richardson Extrapolation and Bulirsch-Stoer Method

- **Disadvantages** The REBS method incurs more error than the ME and RK4 for all the combinations of rate parameters used in this study. Moreover, this method requires significantly more computational effort. There are no possible situations where the REBS method is not bettered by one, if not all, of the Taylor series / Runge-Kutta methods used in this study.

Implicit Methods

- **Advantages** The only advantage that implicit methods have is their ability to transcend the limitations imposed by the stiffness of the differential equations. Implicit methods are able to use integration step sizes greater than $\frac{1}{k_{\mathrm{p}}\mathrm{M}}$. This means that there are circumstances when implicit methods are the most efficient methods for solving the differential equations for PIP (see below).

- **Disadvantages** The most obvious disadvantage is the added cost that using a implicit method incurs. At every time step these methods require a matrix to be inverted, or a system of non-linear equations to be solved. This means that before using these methods one must consider whether the gain in efficiency made by using a time step greater than $\frac{1}{k_{\mathrm{p}}\mathrm{M}}$ outweighs the extra computational cost incurred.

The Monte Carlo Methods

- **Advantages** The MC algorithm should be used if a very large number of different types of chemical species are present, for example, in a system where transfer to polymer is an important process and a full resolution of the species created is required.

- **Disadvantages** Modelling PIP with a MC algorithm, even the improved algorithm (see above), is a computationally expensive task. Even though the MC method does not lend itself to the efficiency assessment developed in this thesis, a simple comparison based upon the computer time can be made. This shows that even a low accuracy MC calculation ($V = 1 \times 10^{-12}$ L) using the improved algorithm takes approximately twice as much computer time as a high accuracy FDB calculation (e.g. TDSSP RK4).

Analytic Methods

- **Advantages** In chapter two it became clear that the only advantage that analytic methods afford over numerical methods is that the solution they produce is error-free. However, if the step size and approximation function used with a numerical method are chosen appropriately, then there is little difference in the accuracy of the final solutions.

- **Disadvantages** There are a number of ways that analytic methods are inferior to numerical methods. For example, they are inflexible to changes in the kinetic model as they are difficult to re-derive to reflect those changes and they take more computing time than most of the numerical methods.

4.9.2 The Optimal Method for the Tested System

It is clear from table 4.8 and from the analysis performed in this chapter and the previous one that the best method for solving this model system of differential equations, i.e., the default rate parameter set, is the fourth-order Runge-Kutta method with a TDSSP. This method incurs a minute amount of error in both the total and individual radical concentrations, while generating a solution to these equations in a short period of time, typically 2 minutes of computer time per pulse period ($h = 1 \times 10^{-4}$ s). Hence, we recommend that the RK4 should be used to solve the differential equations for the model conditions detailed in this chapter. There is no reason

for using a method such as Gear, which is often favored for kinetic simulations. In fact there are good reasons for not using the Gear method.

4.9.3 Extending These Methods to Other Pulse Initiated Polymerization Systems

Unfortunately (or maybe fortunately!), not all PIPs can be modeled with the same rate parameter set. Thus if the techniques described here are to be useful for the simulation of real-world PIPs, they must be able to solve these differential equations, and others similar to them, for a wide range of rate parameters. These methods must work efficiently for systems with higher and lower truncation chain lengths and systems where the rate coefficients depend on the chain length(s) of the reacting species. Fortunately, the information gained in this study can be used to infer how well these methods will work in a variety of different situations. Here we will discuss eight different changes that can be made to the kinetic model or rate parameter set and the way that these affect the numerical solution method that should be used.

The Rate Constant for Termination and the Concentration of Radicals Added by a Burst of Initiation

As the rate constant for termination and the value of ρ affect the MWD and kinetics of any intermittently initiated free-radical polymerization, it is not surprising that they also affect the error incurred in solving the differential equations that describe this type of polymerization. In this chapter, and also in chapter three, it emerged over and over again that there is a strong correlation between the value of $k_t\rho$ and the error incurred. For example, the analysis performed in section 4.4.2 revealed that the error incurred by the RK4 is proportional to $(k_t\rho)^3$. Given this strong dependence it is easy to imagine that the value of $k_t p$ could affect the optimal numerical solution technique. For example, it is possible that either the ME or the RK4 could be the optimal solution strategy depending on the value of $k_t\rho$. However, this is not generally the case. All of the methods investigated in this study are affected in the same way by changing the value of $k_t\rho$, i.e., increasing $k_t\rho$ increases the error incurred. However, one caveat must be placed on this. The rate at which the error changes with the values of $k_t\rho$ depends on the method used. For example, the global truncation error incurred by the Euler method is proportional

to$\sqrt{k_t\rho}$, while the same error for the ME is proportional to $k_t\rho$, and as was stated above the same error incurred by the RK4 method is proportional to $(k_t\rho)^3$. Hence, it is possible that there are values of $k_t$and ρ where the RK4 incurs more error than the Euler method. However, trial calculations indicate that this crossover occurs when the values of $k_t$and ρ are physically impossible.

The Effect of the Termination Mechanism

Although the effects of allowing termination to occur by the combination mechanism will not be fully examined until chapter five, a few comments will be made here. When evaluating the dead chain differential equations where termination by the combination mechanism occurs at all one is forced to evaluate the sum:

$$\sum_{j=0}^{i} \mathrm{R}_{i-j}\mathrm{R}_j \tag{4.42}$$

for all chain lengths i. For long chains a double sum must also be calculated (see equation 1.23), taking even more computer time. In contrast to this, the sum $\sum \mathrm{R}_j$ needs to be evaluated only once when termination occurs exclusively by the disproportionation mechanism. Hence, allowing termination to occur by combination can affect the computational effort. This in turn affects which method is the optimal solution strategy. Any termination by combination can mean that a PIP solution takes so much computer time that one is forced to use a method that reduces the number of differential equation evaluations per integration step, e.g., the Euler instead of the RK4 method. Hence, then termination mechanism can affect the optimal solution strategy.

Systems That Require Higher Truncation Chain Lengths

In principle it is possible for a radical to grow to any chain length. However, when a differential equation based approach is used to model the kinetics of free-radical polymerization it is assumed that the radical chain-length distribution can be truncated at a certain low chain length. While this approach means that differential equations are not included for all radical species, the error incurred by making this assumption is minimized by (1) choosing a high enough trun-

cation chain length and (2) including a 'long chain' differential equation for radical species for chain length higher than the truncation chain length. Nonetheless, some systems do require a higher truncation chain length than others. Thus, any method for solving the differential equations for PIP must be able to work efficiently for a large range of truncation chain lengths. The effect that increasing the truncation chain length has upon any numerical method is to increase the cost of evaluating the differential equations. This is simply because more time is taken to evaluate a larger number of differential equations. Moreover, not all solution methods are equally affected by this. For example, as the RK4 method requires the differential equations to be evaluated four times per integration step, increasing the truncation chain length has a greater effect upon it than upon the Euler method, which requires the differential equations to be evaluated only once per integration step. This can mean that the RK4 method might no longer be the most efficient solution strategy.

Increasing the truncation chain length has a more dramatic effect upon implicit methods. It was noted that the cost of matrix inversion that can be a part of the process of calculating a solution to a differential equation by an implicit method is proportional to N^3. Hence, the cost of using an implicit method increases rapidly as the truncation chain length increases. This can mean that the gain allowed by using an implicit method, i.e., $h > \frac{1}{k_{\mathrm{p}}\mathrm{M}}$, is outweighed by the cost of obtaining that solution.

An Explicit or Implicit Method

We now know that the major advantage of using an implicit rather than an explicit numerical technique is that it means that step size greater than $\frac{1}{k_{\mathrm{p}}\mathrm{M}}$ can be used to solve the differential equations for PIP. However, in section 4.7 it became clear than there is an additional limitation on the step size that can be used in these calculations. The step size must be less than $\frac{t_0}{2}$. Thus, when deciding whether or not to use an implicit method we must consider, among other things, the value of $\frac{k_{\mathrm{p}}\mathrm{M}t_0}{2}$. This value calculates how many times greater than $\frac{1}{k_{\mathrm{p}}\mathrm{M}}$ a step size can be used before the initiation profile limits the size of the steps that can be taken. For example, if $\frac{k_{\mathrm{p}}\mathrm{M}t_0}{2} \leq 1$ then an implicit method does not allow a bigger step size to be used. i.e., the limitation imposed by the initiation profile is as stringent as that imposed by the equation stiffness. Based on the simulations conducted in this study I recommend that a implicit method

should not be used unless $\frac{k_p M t_0}{2} \geq 100$, i.e., an implicit method allows a step size one hundred times greater than $\frac{1}{k_p M}$ to be used. For systems of this type the gain in efficiency made by using a larger step size can outweigh the cost of the matrix inversion. Nevertheless, this will depend upon (1) the required truncation chain length and (2) the error incurred by using a greater chain length. Generally the error incurred by using a larger step size is so much greater than the error of an explicit method that it isn't worthwhile using an implicit method.

Chain-Length Dependent Termination

Allowing the rate coefficient for termination to depend upon the chain-length of the terminating radicals changes the form of the differential equations. Although this is likely to change some of the mathematical characteristics of these systems, most of the results obtained in this thesis will still hold true. For example, the differential equations for living radical species will still change rapidly just after the arrival of the laser pulse, so the numerical solution of these differential equations should still be prone to error at this time.

One of the effects that chain-length dependent does have on the solution of these differential equations is to alter the cost of their evaluation. If the simple model for termination used in chapter six is assumed, then an additional sum, $\left(\sum_{j=0}^{\infty} k_t^{j,j} R_j\right)$ has to be calculated every integration step. Hence, including chain-length dependent termination increase the computing time required to generate a solution. Moreover, allowing a chain-length dependent model for termination also affects the relative costs of evaluating the terms for termination by combination and disproportionation (see chapter five). However, these differences aside I recommended that same solution strategy used for systems where k_t is independent of chain-length should be used for systems where it does depend on the chain-length of the terminating radicals.

Continuously-Initiated Polymerization

While no investigations of continuously-initiated polymerization have been presented in this thesis, the fact that there are many similarities (as well as some important differences) between continuously-initiated and PIP systems means that some of the results outlined here may be relevant to these systems. In particular, these results could be relevant for the initial stages of a continuously-initiated polymerization. At times when continuously-initiated systems are

far from steady-state (such as right at the start of these polymerization), the values of the differential equations for the living radical species are known to change rapidly. As I have shown here this normally means that these differential equations are difficult to solve numerically and susceptible to error, it could be that these initial time regions could be solved efficiently with the RK4 method and a TDSSP profile. This remains to be investigated. Note that this would only be important if one wished to model this non-steady-state stage of a continuously-initiated polymerization rather than just assuming that the steady-state had been obtained.

Other Model Systems

In the second to last chapter of this thesis two modeling studies of experimental PIPs are outlined. Both of these studies required the solution of a system of differential equations that are similar but not identical to those studied in this chapter. In both of these studies differential equations more complicated than those based upon the standard reaction scheme (see chapter one) are solved; this will frequently be the case. The major difference between the differential equations solved in chapter six and those solved here is their number. Almost all of the minor modifications that are likely to be made to the standard kinetic scheme are unlikely to significantly affect the error structure. Thus solving the equations for more complex systems is similar to increasing the truncation chain-length - it increases the cost of evaluating the differential equations. Again, this can mean that it is better to use a method such as the ME method, which does not require the differential equations to be evaluated as many times per integration step.

4.9.4 Concluding Remarks

In general the RK4 method is recommended, as it is simple, robust and accurate. There may be situations where an implicit method is more computationally efficient in a strict sense, but the longer time steps (and hence faster computing times) come at the expense of accuracy. Besides, the RK4 method is quite quick enough, e.g. model simulations of this chapter ran at less than two minutes of CPU time per pulse (on a VAX mainframe). Hence the RK4 method is recommended. Nevertheless, it is advisable to assess the error incurred by using error standard one. This provides a simple, inexpensive way of measuring the error. Also, in situations where

expressing a model system as a set of differential equations requires an extraordinary number of differential equations, consider using the improved MC method.

Further computational gains can be made by using a time-dependent step-size profile. In particular, a profile with a small h for highly non-steady-state periods is advisable, while a longer step size can be used when rates are more steady. An advantage of writing one's own differential equation solving routine is that a TDSSP can be employed (as opposed to using a package program). In this respect, note that algorithms for the RK4 and ME methods are very easy to write.

Chapter 5

Numerical Solution Techniques: The Dead Polymer Chains

5.1 Introduction

In the two previous chapters, several methods for numerically solving the differential equations for living radical species in a pulse initiated polymerization (PIP) were examined. A significant amount of effort was spent studying these differential equations because they are thought to be difficult to solve. Moreover, it was realized that a method that could solve these differential equations well would be able to form the heart of a simulation strategy for PIP. Now that we know which techniques can be used to solve these equations and the error these methods incur, it is time to focus on the differential equations for dead polymer chains.

The differential equations for dead and living species relate to each other in an interesting way. Under the kinetic model used in this thesis, the living radical differential equations are independent of the dead polymer differential equations, while the dead chain differential equations are coupled to the living radical differential equations. Moreover, clearly the differential equations for living radical species are far more complicated than those for dead polymer species. This means that it is likely that the differential equations for living radicals will be more difficult to solve accurately, and solving them will incur more error than the solution of the dead chain differential equations. However, it is only very rarely that the concentration of radicals are compared directly with experiment. Normally, the experimental data compared

with simulation are the dead polymer chain length distribution and occasionally the monomer concentration. This means that the dead polymer chain length distribution can be thought of as the final product of a PIP; so a PIP simulation strategy should be judged by how well it predicts the dead polymer MWD. Thus, we are placed in an odd situation when simulating PIP. We know that a lot of error is incurred in solving the living radical differential equations, but we have to judge this error by how it affects the dead chain MWD.

For these reasons it is imperative that an understanding be gained of the solution of the differential equations for dead polymer chains. Here we will try to develop such an understanding. This analysis is divided into two parts. Firstly, the error incurred in the solution of the differential equations for dead polymer chains is investigated. This investigation will examine the error incurred in solving differential equations 1.22 – 1.25. As the radical chain length distribution must be known before these differential equations can be solved, some way of calculating it has to be found. Here the analytic expression derived in chapter two is used (equation 2.34). This expression can be used to predict the radical distribution without incurring error. Thus any error in the dead chain MWD must have been introduced in the solution of the dead chain differential equations. In the second section, the error incurred in solving the dead chain differential equations is ignored. Here the effects of error in the living radical chain-length distribution upon the dead chain MWD will be investigated. From this we will be able to say how much error we can allow in the living radical chain-length distribution before the dead chain MWD is badly compromised.

The Model System

The model system that has been used throughout this thesis is used in this investigation. This is based upon the reaction scheme presented in chapter one that leads to differential equations 1.18 – 1.25. Two assumptions are made to reduce the complexity of these differential equations. It is assumed that all rate coefficients are independent of the chain length of the reacting species and chain transfer is ignored. Almost the same set of rate parameters as those used in chapters three and four is used here. There are two notable exceptions. Firstly, the rate coefficient for termination is reduced by one order magnitude. This change proved necessary to ensure the highest possible resolution of the PIP features, i.e., to ensure that the simulated MWD

displayed several clear overtones. It is desirable that the model system yield as resolved a PIP MWD as possible as this means that the error in the MWD will be as clear as possible. Also in these simulations the default value of λ is 1.0, i.e., termination only via disproportionation.

5.2 The Error Introduced in Solving the Differential Equations for Dead Polymer Chains

In the section, we will assess how much error is incurred in the numerical solution of the dead chain differential equations (equations 1.22 – 1.25). To do this we begin with the analytic expression for the living radical chain-length distribution. This expression (see chapter two) is used because it is error free (note that this not the dead chain analytic expression which must be integrated). This means that we can have confidence that all of the error present in the final MWD is incurred in the numerical solution of the differential equations for dead polymer chains. If this approach was not used, and the differential equations for the living radical chains were also solved numerically, then it would be difficult to separate the two sources of error, i.e., that from solving the dead chain and living radical differential equations respectively.

A computer program has been written to perform these calculations. This program emulates the numerical solution of the living radical differential equations by evaluating the living radical analytic expression at the start of every integration step, i.e., every time we want to solve the dead chain differential equations. The concentration of all living radicals is then substituted into the dead chain differential equations and these are solved numerically. To illustrate how this procedure works, consider the solution of differential equations 1.22 – 1.25 with the Euler method and a constant step size of $h = 1 \times 10^{-4}$s. To do this, the computer program would evaluate the analytic expression for living radical species and solve the dead polymer chain differential equations every 1×10^{-4} seconds. This simulation would be run for the same length of time as a normal PIP simulation, i.e., for 2 seconds of simulated polymerization time, and the concentration of dead polymer chains would accumulate throughout the simulation. Also a truncation chain length of 5000 was used at all times. Note this is a computationally expensive procedure as the analytic expression for the living radical chain-length distribution takes a lot of time to evaluate.

In this study of the dead chain differential equations, this procedure has been repeated where the Euler, Modified Euler (ME) and fourth-order Runge-Kutta (RK4) methods are used to solve equations 1.22 – 1.25. Note that calculations are performed where termination occurs either by exclusively disproportionation ($\lambda = 1$) or exclusively combination ($\lambda = 0$).

To calculate the error incurred by numerically solving differential equations 1.22 – 1.25, we compare the MWD obtained numerically with that predicted by the semi-analytic dead polymer chain-length distribution derived using the method of integrating factors (see chapter two). The difference between these two distributions is evaluated and this is used as an estimate of the error incurred in solving equations 1.22 – 1.25. Note that although this method provides a useful estimate of the numerical error it does not provide an absolute estimate of the error. In chapter two we saw that an analytic expression for the dead polymer chain-length distribution could not be derived. The dead polymer chain-length distribution had to be calculated by numerically evaluating an integral (the numerical evaluation of an expression for the dead chain MWD should not be confused with the numerical solution of the differential equations). Thus any 'analytic' dead polymer chain-length distribution contains error. This means that the difference between the numerical and 'analytic' MWD includes error incurred in evaluation of the analytic expression. Nonetheless, this 'analytic' MWD has been used as if it was error free. To ensure that this has as little effect as possible on the measurement of error, an extremely low error bound has been used with the numerical integration of the analytic expression. The relative error in each 'analytic' dead chain concentration was not allowed to exceed $1 \times 10^{-4}\%$ at any stage.

5.2.1 Error in the Dead Polymer Chain MWD: A Comparison of the Euler, Modified Euler, and Fourth-order Runge-Kutta Methods

Figure 5-1 contains four simulated PIP MWDs: one MWD calculated via the analytic expression for the dead chain MWD and three via the numerical solution of equations 1.22 – 1.25. The three numerically simulated MWDs have been obtained by different numerical solution techniques: the Euler, ME and RK4 methods. Each of these methods was used with a step size of $h = 1 \times 10^{-4}$s and a TISSP. In each case, the procedure outlined above was used where the analytic expression for the living radical chain-length distribution was evaluated. The

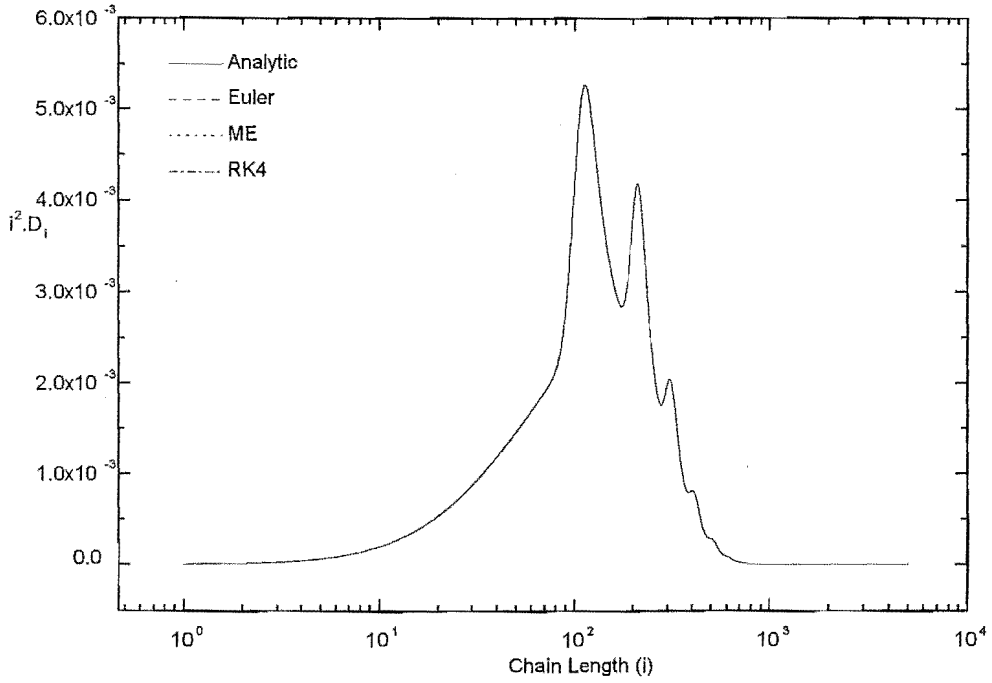

Figure 5-1: A plot of four MWDs: three have been calculated by FDB numerical solution strategies ($h = 1 \times 10^{-4}$s) while one has been calculated by evaulating the analytically derived expression based upon the method of integrating factors.

'analytic' MWD included in this plot was predicted using equation 2.36. Figure 5-1 shows that only a minuscule amount of error is incurred by the numerical solution of differential equations for dead polymer species. The three numerically simulated MWDs lie on top of the analytic MWD. In all cases, the magnitude of the error incurred is very low (typically less than 0.01%). This confirms the hypothesis that the numerical solution of the differential equations for dead polymer chains incurs little error. This means that far more error is incurred in the numerical solution of the living radical differential equations than of those for dead chains. Moreover, as there is little difference between the MWDs predicted by each of the numerical solution methods, i.e., Euler, ME and RK4, it seems that a low level of treatment, i.e., the Euler method, can be used to minimize the computational cost of obtaining the solution while hardly increasing the error incurred (see below). Figure 5-2 is a plot of the relative error in the numerically

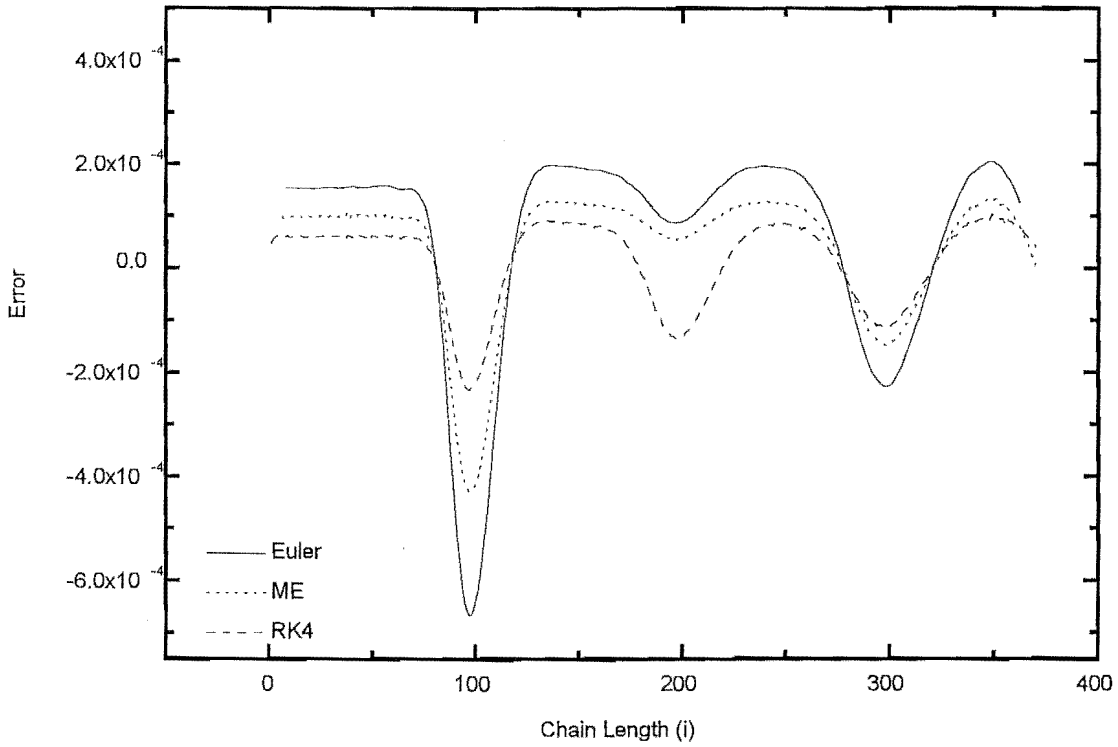

Figure 5-2: The relative difference between the analytic and numerically obtained MWDs for three numerical methods.

simulated MWD. This error is calculated by dividing the absolute error (figure 5-1) by the value of the analytic solution, i.e., the error in figure 5-2 is equal to $\frac{(\mathrm{D}_i)_{sim}-(\mathrm{D}_i)_{analy}}{(\mathrm{D}_i)_{analy}}$. Furthermore, note that the error in this plot is calculated for the D_i, rather than the $\mathrm{D}_i i^2$ distribution. This plot indicates that there is a correlation between the dead polymer chain length and the amount of error incurred. The relative difference between the analytic and numerical solutions is greatest about chain lengths that are multiples of $k_\mathrm{p}\mathrm{M}t_0$, i.e., the peaks in the MWD. This correlation can be explained by the ideas developed in the two previous chapters. We know that finite difference based (FDB) numerical solution strategies incur error when the actual value of the differential equation changes from the value predicted by that numerical method. Moreover, it is known that the difference between actual and predicted values is greatest when the value of

the differential equation changes rapidly during an integration step, i.e., when the rate of change in the differential equations is high. This argument suggests that the differential equations for dead polymer species that have chain lengths approximately equal to $k_p M t_0$ change at the greatest rate.

Before explaining the results in figure 5-2, a background point must be made. This is that the error shown in these plots is the error accumulated during the entire course of the simulation, i.e., 20 initiation periods. Thus the error incurred in the differential equations for dead polymer species of chain lengths approximately equal to $k_p M t_0$ does not have to be greater at all times than the error incurred in all other chains lengths, e.g., halfway through a dark period the error incurred dead polymer chains of chain length $\frac{k_p[M]t_0}{2}$ might be greater than the error incurred for dead-chains of chain length $k_p M t_0$. However, figure 5-2 suggests that the sum of the error incurred when solving the dead polymer chains of chain length $k_p M t_0$ must be greater than the sum of the error incurred in other chain lengths.

With this in mind it can be argued that the correlation between error and chain length is due to the rapid changes in the rate of termination straight after the arrival of a burst of initiation. The frequency of this periodic initiation is $1/t_0$, thus the most probable chain length for living radical species upon the arrival of an initiation burst is $k_p M t_0$. Therefore if termination occurs exclusively via the disproportionation termination mechanism, the dead polymer chains that are most likely to be formed when the rate of termination is changing at the greatest rate are approximately equal to multiples of $k_p M t_0$. Hence, as more error is incurred when the value of the differential equations are changing rapidly, i.e., in this case when the rate of termination is high, it is the solution of the dead polymer differential equations for chain lengths of approximately $k_p M t_0$ where the most error is incurred. Two additional points must be made concerning this argument. Firstly, the solution of dead polymer differential equations for chain lengths other than those which are close to multiples of $k_p M t_0$ will also introduce error straight after the arrival of an initiation burst. However, as the concentration of these species is very low at this time, the magnitude of the error incurred is small compared to the total concentration of these dead polymer species. Secondly, contrary to what the description given above implies, the numerical solution of the differential equations for dead polymers of chain length around multiples of $k_p M t_0$ can contain large amounts of error. This is because the

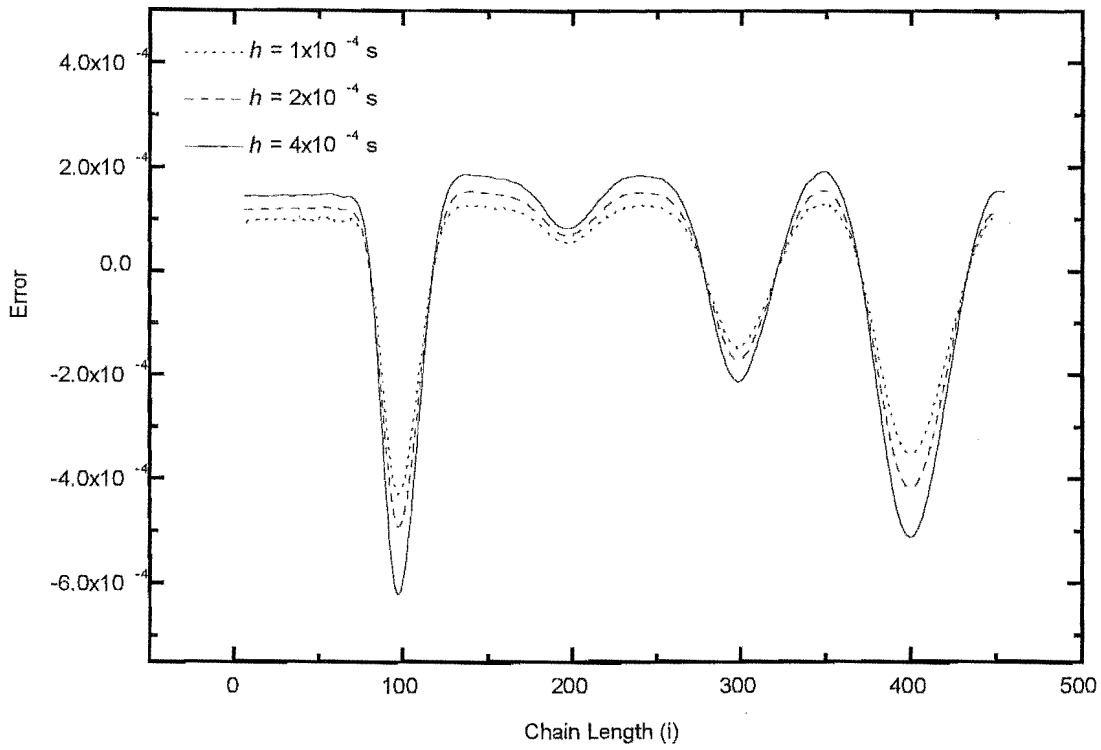

Figure 5-3: The effect of the integration step size upon the error incurred in the solution of the differential equations for dead polymer chains. This solution has been obtained through the use of the fourth-order Runge-Kutta algorithm.

distribution of living chains at time t_0 is a Poisson distribution about the chain length $k_p M t_0$, i.e., some chains have chain lengths less than and some more than $k_p M t_0$. Hence, at the time when the rate of termination is high there exists significant numbers of living radical chains that have chain lengths around $k_p M t_0$, so that at this time the solution of the differential equations for these species incurs error (see figure 5-2).

Figure 5-3 illustrates the effect that changes to the integration step size have on the relative error in the dead chain MWD. It is clear from this that the error incurred in solving these differential equations can be reduced by decreasing the step size. Such a reduction in step size decreases the size of the interval over which the values of the differential equations must

be approximated. Thus it reduces the magnitude of the error. This plot also indicates that these differential equations are relatively insensitive to changes in h: surprisingly there is not a fourfold increase in error when the step size is increased fourfold. Note that it is possible to use step sizes greater than $\frac{1}{k_p M}$ (the maximum step size that can be used to solve the living radical differential equations) to solve the dead chain differential equations. Importantly, this is because the dead chain differential equations are not mathematically stiff like the living radical differential equations.

An analysis of the error in the dead chain MWD has also been performed for a kinetic system where termination occurs exclusively via the combination mechanism. The error incurred in these differential equations shows trends similar to those shown when termination took place only by disproportionation: the amount of error incurred was small and correlated to the chain length of the dead polymer chains. Figure 5-4 contains the simulated MWDs for a kinetic system where $k_{tc} = k_t$ and $k_{td} = 0$, as obtained by three numerical solution strategies: the Euler, ME and RK4 methods using a TISSP and an integration step size of $h = 1 \times 10^{-4}$s. It is clear from this figure that there is little difference between the MWD predicted by each numerical method. Note also that the same results are obtained by the 'analytic' solution.

There are, however, several differences between the error incurred when termination occurs by the disproportionation mechanism and when termination occurs via the combination mechanism. However, as this error does not have a significant effect upon the final MWD it will not be discussed in detail here. It should be noted that all of the differences between the error incurred when termination occurs by the disproportionation mechanism as compared to the combination mechanism are caused by the fact that disproportionation produces two chains of length equal to the termination radical species while combination produces one dead polymer chain that has a chain length equal to the sum of the chain lengths of the two radical species.

Finally, three other features can be noted from figures 5-2 and 5-3. Firstly, the values of the error shown in this figure oscillate between being positive and negative. Secondly, there is only a small amount error present for very small radical species, yet from the discussion given above it was clear that error for small radical species should be large, e.g. $i = 1$. Finally, the amount of error present in chain lengths close the peaks of primary peak and overtones decreases from $i = 100$ to $i = 200$, but is increases from chain length $i = 200$ to $i = 300$. I will not attempt to

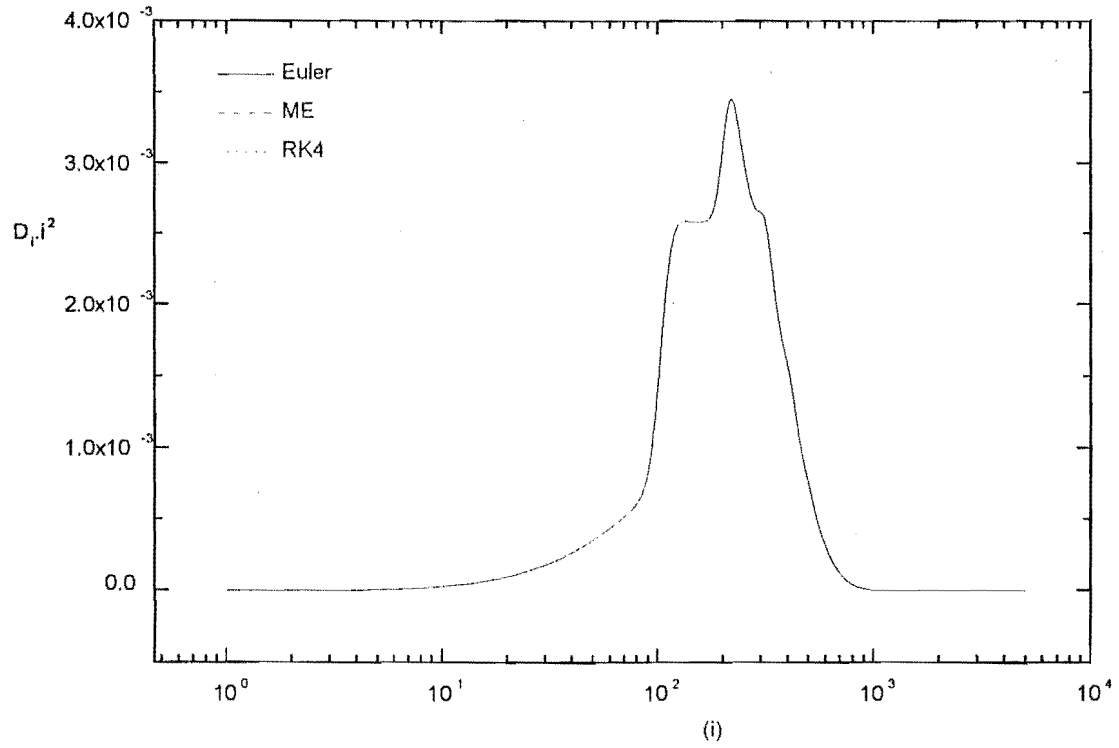

Figure 5-4: The simulated molecular weight distribution for a PIP. Each of the three simulated distribution have been obtained by a different solution algorithm. The default rate parameter set and a step-size of $h = 1 \times 10^{-5}$s was used in each case.

give a complete description of these features as it is clear that the error in solution of the dead chain differential equations has little affect on the simulation results. However, these effects could have been caused by the way the error was measured, i.e., relative to dead chain-length distribution, or because the 'analytic' dead polymer chain-length distribution will contain some residual error.

5.2.2 The Effect of the Error Incurred in Solving the Differential Equations for Dead Polymer Chains on Parameters Meriting Special Attention

There are a several features of the dead polymer MWD that deserve special attention. These are the low molecular weight side point of inflection and peak maximum of the primary peak as well as the number and weight average chain lengths. These values merit special attention as methods have been developed that use them to calculate the rate coefficients for propagation[37] and termination (see chapter one).[38][39] Here I judge a simulation strategy on how well it reproduced these values. It should be noted, however, that if the difference between the analytically and numerically calculated MWDs is small, then this will usually mean that the simulation will accurately reproduced these average and characteristic chain lengths. Nonetheless, here and in the next section these values will used as an additional means of assessing the effects of numerical error.

Arguably the most important of these four values is the chain length that corresponds to the low molecular weight side inflection point. A well known and widely used method uses this chain length to obtain a value for the rate coefficient for propagation (see chapter one). It should be noted, however, that the failure of simulation to reproduce the position of the inflection point at exactly $k_p M t_0$ is not necessarily due to numerical error. Many authors[37][47] have noted that approximately 5% error is introduced in taking the point of inflection to be equal to $k_p M t_0$. For example, when the default rate parameter set is used in the simulation of the MWD the point of inflection is positioned at a chain length of 97, i.e., not exactly at $k_p M t_0 = 100$. Therefore, to measure the effect of numerical error upon the point of inflection we extract the position of the point of inflection from an analytic calculation. Numerical simulations are then performed and the point of inflection is extracted from these MWDs. The difference between the analytic and numerical based inflection point positions is a measure of the effects of numerical error. In all of the simulations performed above with three different numerical methods, numerical error had a small effect upon the position of the inflection point, i.e., all of the inflection points occurred at a chain length of approximately 97. This is further confirmation that the numerical error incurred in solving the dead polymer chain differential equations has a negligible effect on the MWD.

Although the position of the point of inflection is routinely taken to provide the best estimate

of $k_p M t_0$ it has been shown that for some sets of rate parameters, ones that produce the so called high termination limit, the position of the peak maximum provides a better estimate of $k_p M t_0$ (again, see chapter one).[47] Hence, here we use the position of the peak maximum as another means of measuring the effect of numerical error on the final MWD. However, again there is no direct correspondence between $k_p M t_0$ and the position of the peak maximum. The position of the peak maximum extracted from an analytically calculated MWD is used as if it was error-free. The position of the peak maximum can then be taken from a numerically calculated MWD and the difference between the analytic and numeric-based values evaluated. Again this means of estimating the error indicated that the solution of the differential equations for dead polymer chains incurs little error. The maximum of the primary peak is positioned at a chain length of 113 in the analytic and all numerical MWDs.

The final values that are used as a measure of the error in the MWD is the number and weight average chain length, i.e.,

$$P_n = \frac{\sum_{i=0}^{\infty} i D_i}{\sum_{i=0}^{\infty} D_i} \qquad P_w = \frac{\sum_{i=0}^{\infty} i^2 D_i}{\sum_{i=0}^{\infty} i D_i} \tag{5.1}$$

Here D_i is the concentration of dead polymer chains of chain length i. Although a wide range of moments and ratios of moments can be defined, special attention is payed to these two. The average chain lengths taken from the analytic and numerically predicted MWDs are in close agreement, i.e., in all cases $P_n = (2.12 \pm 0.01) \times 10^2$ and $P_w = (4.77 \pm 0.01) \times 10^2$. Again this suggests that little error is incurred in the solution of the differential equations for dead polymer species.

5.2.3 Conclusion

This investigation has shown that the error incurred in the numerical solution of the differential equations for dead polymer chains is low and insensitive to both the integration step size and approximation function used. This study has indicated that almost the same amount of error is incurred when a fast but error-prone numerical solution is used, i.e., the Euler method, as when a slower but more accurate numerical solution strategy, i.e., fourth-order Runge-Kutta method, is used.

Although the dead chain differential equations only contain gain terms, the evaluation of the term derived from termination by the combination mechanism can be time consuming. For example, suppose we wished to calculate the termination by combination term in the differential equations for radicals of chain length k, i.e.,

$$k_{\mathrm{tc}} \sum_{j=0}^{k} \mathrm{R}_j \mathrm{R}_{k-j} \tag{5.2}$$

This 'combination sum' counts all of the possible ways that two radicals can combine to form a dead polymer chain of chain length k. As this sum is different for each dead polymer chain length, and as the R_i change with time, this sum must be calculated every time the differential equations are evaluated. This is in contrast to the term for termination by disproportionation, that only needs to be evaluated once every differential equation evaluation, because $\sum_{j=0}^{\infty} \mathrm{R}_j$ is independent of k. Moreover, the number of terms in the above sum (equation 5.2) increases as k increases. Thus more effort is spent evaluating the rate of dead polymer production due to termination by combination as the truncation chain length increases. To illustrate the effect that allowing termination to take place via the combination termination mechanism has, consider a simulation with a truncation chain length of 5000. If this simulation allows termination to occur via the combination mechanism then the required CPU time is 10 times greater than a simulation where termination occurs exclusively via the disproportionation termination mechanism (solving the differential equations for dead and living species numerically). This means that when combination occurs, any method that can increase the speed at which the dead chain differential equations can be solved will significantly increase the overall speed of the simulation of PIP. Note the argument given above only holds for chain-length independent termination, if termination is allowed to depend upon the chain-length of the terminating radicals the situation will change slightly. From a cursory analysis it appears that there will less of a difference between the computer time need to evaluate the combination and disproportionation terms under these conditions.

In this section we have seen that the differential equations for dead polymer species are far less sensitive to error than those for living radical chains. This suggests that different solution strategies should be used to solve the differential equations for living and dead species

respectively.

Therefore I recommend that it could be profitable to use a different numerical method or integration step size to solve the differential equations for dead polymer species than to solve the differential equations for living radical species. For example, for a particular system it might be necessary to use a high level numerical solution strategy, such as the fourth order Runge-Kutta, to solve the differential equations for living radical species. This does not mean, however, that the same solution strategy should be used to solve differential equations for dead polymer chains. The analysis performed here has indicated that to do so, especially when termination occurs via combination, would be a gross waste of resources, requiring computational effort to be expended for little gain in accuracy.

5.3 The Effect of Error Generated in the Concentrations of Living Radical Species Upon the Dead Polymer Chain Molecular Weight Distribution

In the second part of this chapter, the problem of how the error incurred in solving the living radical differential equations affects the final MWD will be addressed. The relevance of error in the final MWD has been already been noted several times. The MWD is the final product of a simulation: it is the data that is compared with experiment, a comparison that allows mechanistic conclusions to be drawn. Hence the whole process of simulation stands or falls upon its ability to produce an MWD that does not contain significant amounts of error. In this section, we will explore the effect that the numerical error incurred in the solution of the differential equations for living radical species has upon the final dead chain MWD. Based on this information we will establish guidelines for the maximum amount of error that can be incurred in the solution of the differential equations before the quality of the dead polymer chain MWD is adversely compromised. For example, in chapters three and four studies showed that the solution of the living radical differential equations incurs large amounts of error straight after the arrival of a burst of initiation. Here we will explore how this systematic error affects the MWD; does it lead to an misestimation the concentrations of high molecular weight species or alter the position of the inflection point?

To be able to assess the affects of numerical error, a means of separating and quantifying that error must be established. This proved to be a difficult task as the numerical solution of a system of differential equations always introduces a range of types of error at the same time. For example, the numerical solution of the living radical differential equations introduces error associated with changes in the total radical population as well as changes in the individual radical concentrations, i.e., error as measured by error standards one and three. Moreover, it is also difficult to separate the error associated with the solution of the differential equations for living and dead species respectively. To get around this problem an assumption is made and a procedure similar to that used above is developed.

The study outlined in the previous section indicated, as was expected, that the solution of the differential equations for dead polymer chains introduces minimal error, and that this error has little effect upon the MWD. Here the error associated with the solution of these differential equations will be ignored altogether. In this section we explore the effect of error incurred in solution of the differential equations for living species only. To do this we make use of the analytic expression for the living radical chain-length distribution developed in chapter two (section 2.1), i.e., the same expression that was used in section 5.2. In the same way as this expression was used above, here it is used to emulate the numerical simulation of the differential equations for living radical species. The expression is evaluated before every 'integration step'. However, in contrast to the treatment used above the concentrations of living radicals are modified before they are substituted into the dead polymer chain differential equations (equations 1.22 – 1.25). These differential equations are then solved, the time updated, and this cycle repeated until the simulation has finished.

The analytic expression for the concentration of living radical species is error-free. This means that the effect of one type of error can be studied by altering the living radical concentrations to emulate the effects of that error and only that error. For example, suppose we wish to explore the effects of random error in the concentration of living radicals upon the MWD, i.e., roundoff type error. To do this we calculate the error-free living radical chain-length distribution after every integration step. The concentration of these radicals is then modified to reflect the effects of the error being investigated. For random error the living radical chain-length distribution is multiplied by a uniformly distributed random number α, where alpha takes a

value between $-\beta \leq \alpha \leq \beta$, where β is the maximum error, positive or negative, that can be added. Note that α is the percentage of error that will be added.

$$R_i^e = (1 + \frac{\alpha}{100})R_i^{ne} \tag{5.3}$$

In this expression, R_i^e is the modified, error-containing living radical concentration, α the random number and R_i^{ne} the error-free radical concentration as calculated by the analytic expression. Note that the same value of α has been used for all radical chain lengths, i.e., α systematically affects R_i but randomly affects R. This modified living radical chain-length distribution is then substituted into the dead polymer chain differential equations and these equations solved by the RK4 method with a TISSP and a step size of $h = 1 \times 10^{-4}$s. This procedure of calculating the living radical chain-length distribution every integration step, generating a new value of α, modifying those concentrations to reflect error, and solving the dead polymer chain different equations is repeated until the simulation has run for two seconds of simulated polymerization time. The cumulative MWD is then analyzed for error in the same way that it was above, i.e., by comparing it to an 'analytic' MWD. To explore the effect of different amounts of error, the maximum magnitude of the error (β) added at each integration step is changed and the entire simulation procedure repeated. Comparing the 'analytic' and error-containing dead polymer MWD for a range of β values allows conclusions to be drawn on the effects of random error upon the MWD. Moreover, this analysis allows conclusions to be drawn about the maximum amount of error that can be tolerated in the solution of the differential equations for living radical species without adversely compromising the accuracy of the dead polymer MWD.

Several other error types have been analyzed in addition to random error. These include: (1) time dependent error; (2) error in the concentration of radicals that are the most probable chain length; and (3) chain-length dependent error.

5.3.1 Random Error

By definition, random error is error that is not correlated to any facet of the polymerization – it does not depend upon the time since the last burst of initiation, the chain length of reacting radical species or upon any of the other rate parameters. In chapter four it was

shown that there are circumstances when random error is the dominant error type (it has the greatest magnitude). In that chapter it became clear that when the RK4 method is used to solve the differential equations for a system with a low rate coefficient for termination, e.g. $k_t = 1 \times 10^6 \text{L.mol}^{-1}.\text{s}^{-1}$ then truncation error is almost completely removed. The error in the total radical concentration then had the appearance of random noise and was very small in magnitude. In the numerical solution of differential equations random error originates from roundoff effects. In chapter three, we saw that roundoff error is introduced when a computer truncates a number as a part of a numerical calculation, for example representing 1 / 3 as 0.3333.

The procedure for emulating random error (see above) has been used for a range of values of β (1×10^{-5} to 1×10^{-2}). This analysis indicates that random error, even with a large value of β, has little affect on the dead polymer chain MWD. Moreover, if random error is of the same magnitude as that found in the numerical solution of the living radical differential equations, i.e. $\beta = 1 \times 10^{-15}$, then the MWD is unaffected. Thus, it is unlikely that random error will ever significantly affect the dead polymer MWD. This is an expected result.

Note that while in this section β was the upper bound for a randomly generated number, in the remaining sections it represents a fixed number.

5.3.2 Error in the Total Radical Concentration – Time Dependent Error

In chapters three and four it became clear that the numerical solution of the differential equations for living radical species introduces error into the total radical concentration, error that is a result of inability of finite difference based methods to deal with changes in the value of the differential equations during an integration step. Moreover, it became clear that the magnitude of this error depended on the time since the arrival of the last burst of initiation. Here error of this type is added to the total concentration of radicals and the effect that this error has on the dead polymer MWD is analyzed. To do this a simple model is used to emulate the error in the total radical concentration. This model is similar to the method of sections that was used in chapter three to give a time dependent step size profile. To use this method we divide the time between bursts of initiations, i.e., t_0 seconds, into ten intervals of equal width. A series of calculations are then performed where a PIP is simulated for 2.0 seconds. These

simulations differ in the way that error is added to the total radical concentration. In the first simulation of each series error of magnitude β is added to the total radical concentration after each integration step for the first interval, i.e., the first $\frac{t_0}{10}$ seconds after each burst of initiation.

$$R^e = (1 + \frac{\beta}{100})R^{ne} \qquad \text{for } \frac{(j-1)t_0}{10} \leq t < \frac{jt_0}{10} \qquad \text{where } j \in [1, 10] \tag{5.4}$$

In the remaining nine intervals no error is added. In other words, $j = 1$ in equation 5.4. This process of adding error in the first interval is repeated for 20 initiation periods or 2 seconds worth of simulated polymerization. At the end of that period the dead polymer chain MWD is written to a data file. The next calculation in series performs essentially the same task, however this time error is added in the second of the ten intervals, i.e., $j = 2$ in equation 5.4. This process of performing calculations where error is added in one of the ten intervals is repeated until error has been added to all of the ten intervals. The entire process is then repeated for a different value of β. This analysis allows the effects of adding error of different magnitudes as well as at different times to be explored. The final MWDs have been analyzed in the same manner as for the random error (see above).

The impact of this type of error is shown in figure 5-5. This figure illustrates the effect of error in the total radical concentration upon the position of the low molecular weight point of inflection and peak maximum of the primary peak, as well as the values of P_n and P_w. In these plots all values are shown relative to their error-free equivalents. Note that a value of $\beta = 1 \times 10^{-2}$ means that error of magnitude 1×10^{-4} has been added.

It follows from figure 5-5 that as the magnitude of the added error decreases (β), the difference between the values derived from error-containing and error-free distributions decreases. It is also clear that if the magnitude of the error added is less than or equal to $\beta = 0.01$, i.e., error of 1×10^{-4}, then the added error has no discernible effect upon any of these four values (in all cases the value for a distribution containing error is equal to that without error). Furthermore, this analysis shows that it does matter at what time the error is added to the total radical concentration. Consider for example the position of the low molecular weight point of inflection when error of magnitude $\beta = 0.1$ is added. Error added straight after the arrival of the laser pulse causes the greatest change in this value. This is because the majority of the dead

polymer of chain lengths close to the position of the point of inflection are formed around the time when a laser pulse arrives. Thus, error added at this time has more effect on the position of the point of inflection. This is also true of the position of the peak maximum. The weight and number weight averages also show a dependence upon the time when the error is added. This reflects that the rate of dead polymer formation is greatest straight after the arrival of the laser pulse. Figure 5-6 contains three MWDs for the solution of the dead polymer chain differential equations based on the living radical distribution where error has been added in the first time interval. It is clear that as the magnitude of the error added increases so does the effect upon the MWD. In this way these MWDs mirror the results shown in figure 5-5.
It is unfortunate that the solution of the dead polymer differential equations is most sensitive to error in the total radical concentration at times when the greatest amount of this error is incurred, i.e., a lot of error is added straight after the arrival of a laser pulse and the dead polymer differential equations are most sensitive to error at this time. However, the analysis performed here indicates that the effects of this error can be removed simply by reducing the error incurred in the solution of the living radical differential equations to below $\beta = 0.01$ at all times. To ensure that the error in the total radical concentration is always less than $\beta = 0.01$ we must use the results gained in chapters three and four. These results tell us how much error is introduced into the total radical concentration by a certain numerical technique and step size combination. An inspection of these results reveals that the error incurred by the three methods of choice (Euler, ME and RK4) is always less than $\beta = 0.01$. This means that a method can be chosen that minimizes the time spent solving the differential equations, i.e., in this case the Euler method with a step-size close to $h = 1 \times 10^{-3}$s. However, although this is the case for the default rate parameter set, it will not be the case for all rate parameter sets. In some cases it may prove necessary to use a smaller step-size to ensure the integrity of the final MWD. To ensure that $\beta < 0.01$, the error in the total radical concentration should always be included in the output of the numerical solution and steps taken to reduce that error when necessary. It is noted that this is not always possible especially where simulations are performed where chain-length dependent rate coefficients are used. In these cases, all efforts should be made to minimize the error incurred.

Also note that even though the error added here is always positive, this does not have to

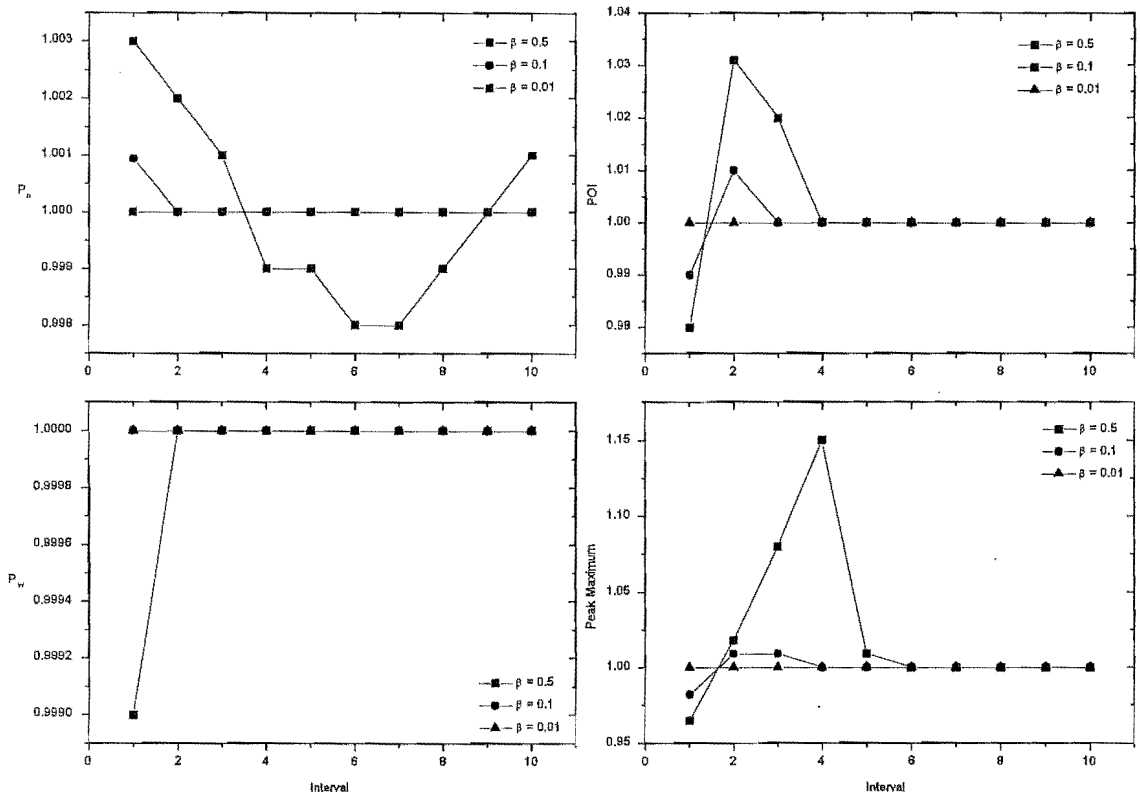

Figure 5-5: The effect of time dependent error in the total radical concentration. All values are shown relative to the corresponding error-free values.

mean that this error will always causes the parameters being measured to increase. For example, error which increases the total radical concentration will cause the rate of termination to be higher, hence the number average chain length to decrease. Moreover, note that this may also be the case it the following sections.

5.3.3 Error in the Most Probable Radical Chain Length

The next type of error studied is the error incurred in solving the living radical differential equations for a species that has one of the most probable chain lengths. The most probable

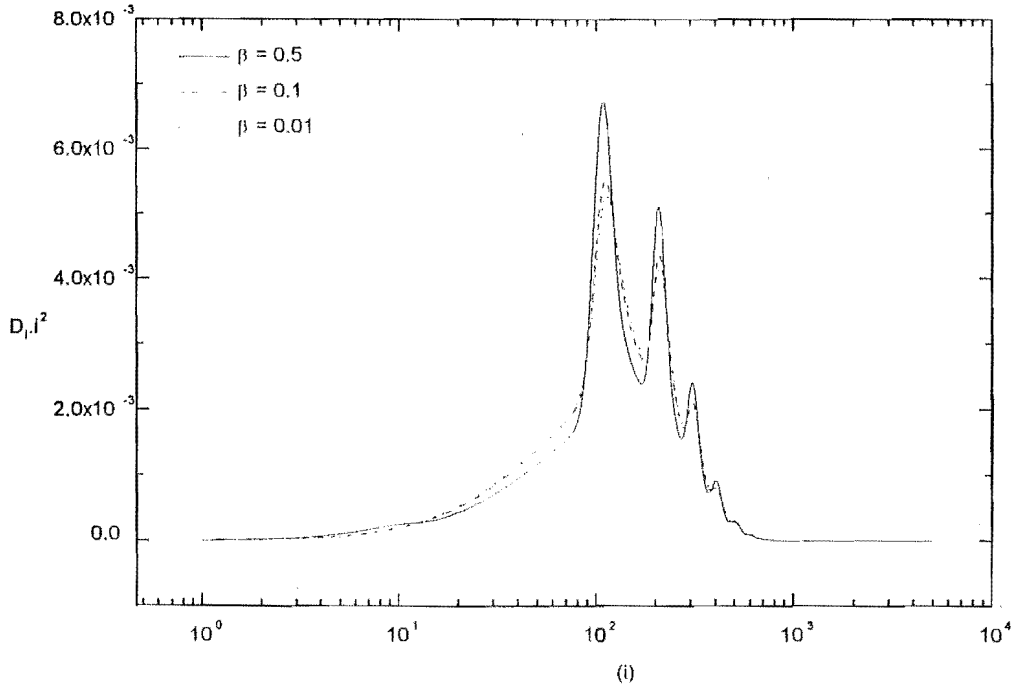

Figure 5-6: The effect of time dependent error upon the dead polymer chain-length distribution. The distributions are shown here are for a range of values of β where the error has been added in the first interval.

chain-lengths are given by

$$L_{\mathrm{mp}} = k_{\mathrm{p}}\mathrm{M}t + jk_{\mathrm{p}}\mathrm{M}t_0 \qquad \text{for } j \geq 0 \tag{5.5}$$

The error incurred in the solution of these differential equations is a result of the rapid change in the concentration of radicals about the time that they have the most probable chain length, a rapid change that numerical solution techniques have a hard time modeling. To study the effects of this type of error a procedure similar to that used above is implemented. The numerical solution of the living radical differential equations is emulated by evaluating the value of an analytic solution at time steps of h. Error is then added to the living radical chain-length distribution. However, whereas above error was added to all radical species, here error is only

added to those radicals with chain lengths given by equation 5.5. The magnitude of error added is defined by the constant β, such that

$$R^{e}_{mp} = (1 + \frac{\beta}{100})R^{ne}_{mp} \tag{5.6}$$

In this expression, R_{mp} are the concentration of radicals with the most probable chain lengths (note that there will be more than one). The results obtained from this series of calculations are shown in figures 5-7 and 5-8. Figure 5-7 contains plots that display the effect of this type of error upon the position of the point of inflection and peak maximum as well as the number and weight chain-length averages. Moreover, figure 5-8 contains the full MWD when error of three different magnitudes is added. It is clear from both these figures that error in the most probable chain length has little effect upon the final MWD. Even when a lucridiously high value of $\beta = 1$, i.e., 1% error is used the effect upon the MWD (figure 5-8) and certain features of the MWD (figure 5-7) is negligible. Therefore, as the values of β found in the actual solution of the differential equations for living radicals ($\beta = 1 \times 10^{-2}$) is significantly less than a value that affects the MWD, this error can be ignored. There is of course one notable exception, which is when step sizes greater than $\frac{1}{k_p M}$ are used with explicit methods. Then the error in the living radical concentrations explodes, and there are large errors in the dead chain MWD.

5.3.4 Error That is Dependent on Chain Length

The final type of error that will be investigated is error that depends on the chain length of the radical species. Error of this type can originate from effects such as the Poisson broadening of the radical waves, which leads to a decrease in the error incurred in solving the differential equations for the most probable radical species as the distribution becomes broader with increasing i (see chapter three). To model this type of error a simple model is used. This says that the error incurred in solving radical species of chain length i is proportional to chain length, i.e.,

$$e_i \propto 1 - \frac{\beta i}{100} \qquad \text{if } 1 - \frac{\beta i}{100} \leq 0 \text{ then } e_i = 0. \tag{5.7}$$

Therefore,

$$R^{e}_{i} = (2 - \frac{\beta i}{100})R^{ne}_{i} \tag{5.8}$$

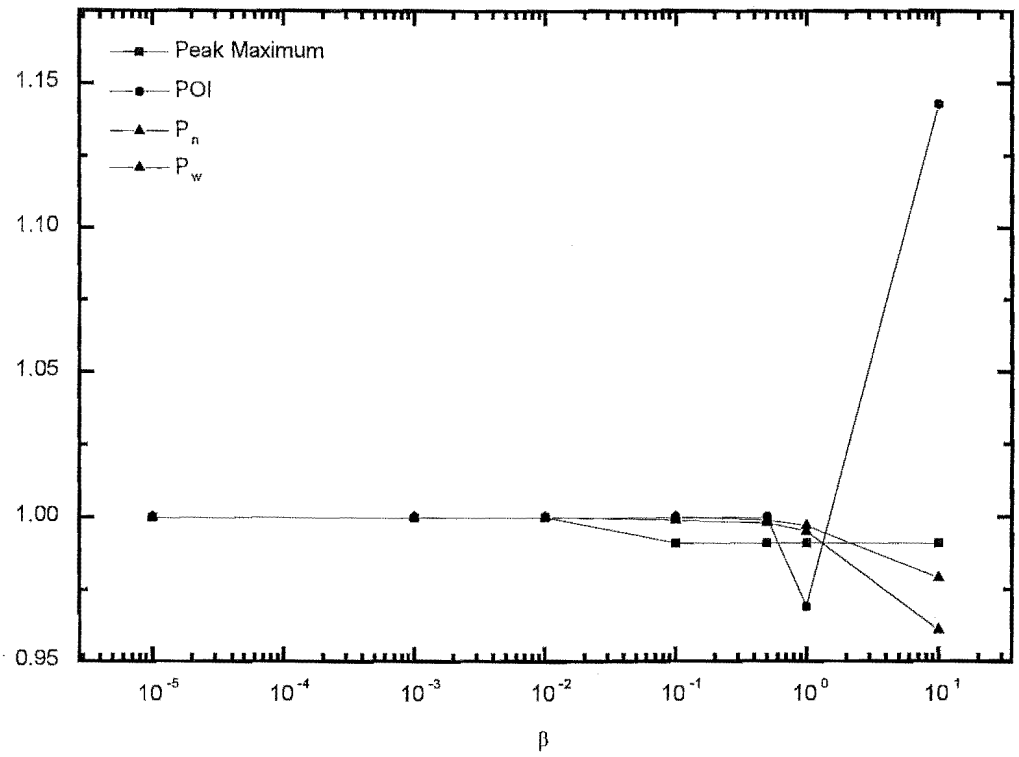

Figure 5-7: The effect of error in the most probable radical chain length on various dead polymer chain-lengths.

To study the impact of such error, the procedure used above is used here. Calculations have been performed for a range of values of β. These results are shown in figures 5-9 and 5-10. These plots show that this type of error has little effect upon the MWD or the features extracted from it unless $\beta \geq 0.01$, which for $i > 10$ leads to error far greater than any encountered in real numerical solution. Hence it is concluded that the chain-length dependent error incurred in the solution of the living radical differential equations is far less than that which significantly affects the dead polymer chain-length distribution.

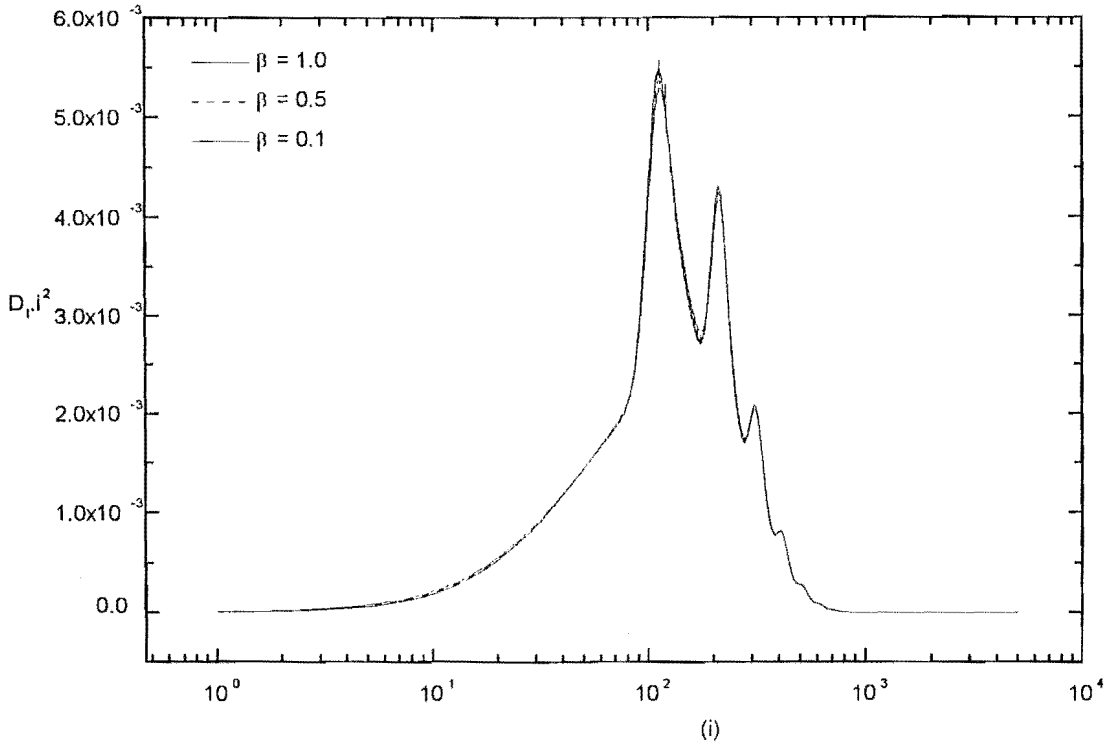

Figure 5-8: The effect of error in the most probable radical chain-length upon the full dead chain MWD.

5.3.5 Conclusion

In summary, the dead polymer MWD is insensitive to error in the concentration of living radicals. Typically, the error in the concentrations of radicals from numerical simulation is at least one order of magnitude less than that which would significantly affect the dead polymer chain MWD. The type of error that has the greatest effect is error in the total radical concentration. This is partly because this error has the greatest affect upon the dead chain MWD, but also because more of this type of error is incurred in the solution of the living radical differential equations than any other type of error. Although the magnitude of this type of error incurred in the normal solution of living radical differential equations for the default rate parameter set

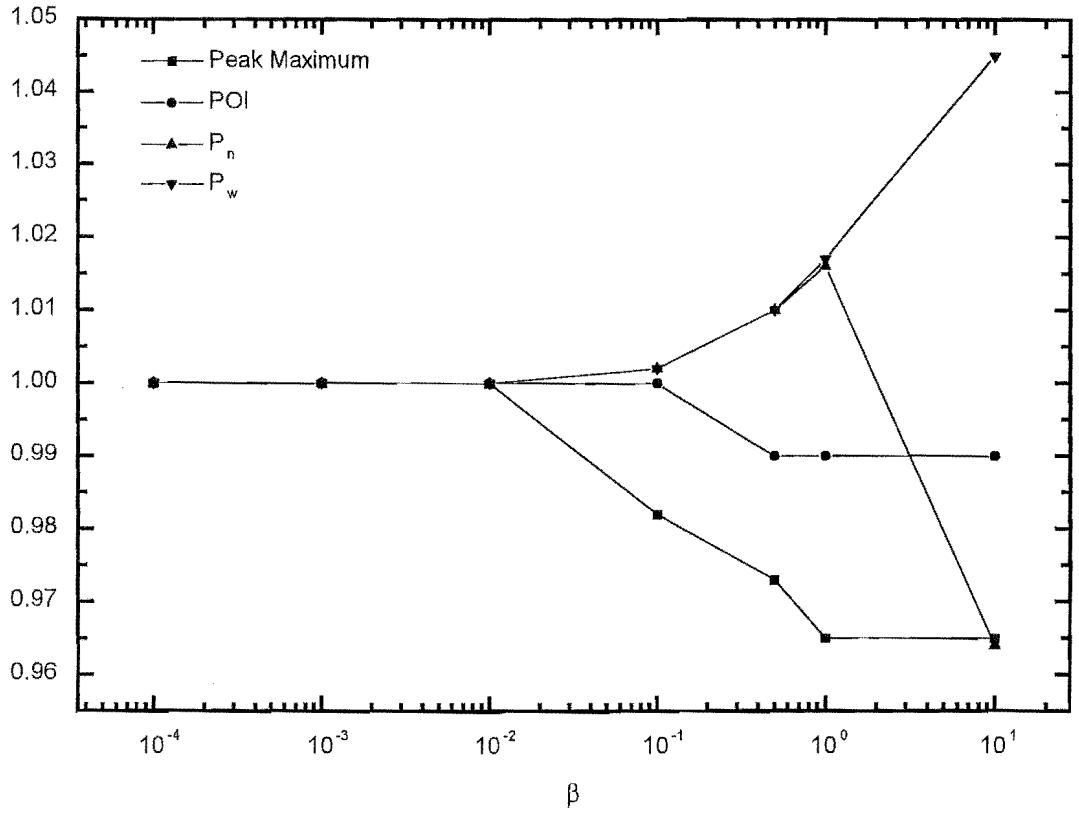

Figure 5-9: A plot of the impact of chain-length dependent error upon features of the dead polymer chain MWD.

is less than that which significantly affects the MWD, there is the possibility that this will not always be the case. To ensure that β is always less than 0.01 it is recommended that where possible the error in the total radical concentration is calculated as part of a normal simulation. The solution strategy (numerical method and step size) can then be altered to ensure that the numerical error in the total radical concentration is not so high that the MWD is affected.

Finally, the work of this chapter has indicated that what is most important for a PIP simulation is the solution of the living radical differential equations. Small timesteps and/or high-level approximation functions should be used to ensure accuracy in the simulated R_i.

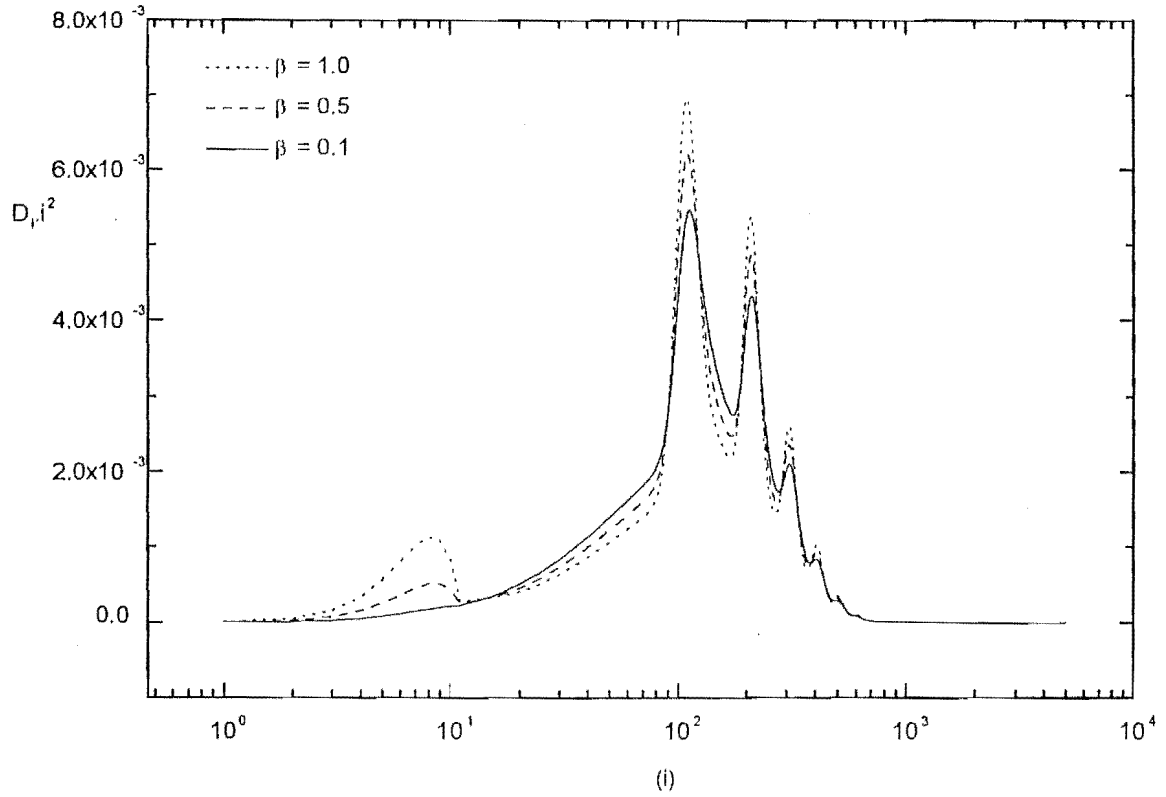

Figure 5-10: The MWD distribution for PIP systems where chain-length dependent error has been added.

Once this is done, longer timesteps and/or lower-level approximation functions can be used to simulate the resulting D_i. This should give significant savings in computing time without a loss of accuracy. There is every reason to suspect that such a solution strategy should work well for other types of free-radical polymerization simulations, e.g., continuously initiated ones. This is because the underlying reasons should hold for all polymerizations: the dR_i/dt are always stiff, always contain gain and loss terms, and always change in value quickly, while dD_i/dt are normally not stiff, always contain only gain terms, and do not change in value so quickly.

Chapter 6

The Application of Numerical Solution Techniques

6.1 Introduction

In this thesis a lot of effort has been expended developing techniques to efficiently solve the differential equations that characterize pulse initiated polymerization (PIP). This study has produced a suite of methods that can be used to solve these differential equations accurately and in a short period of time. In this chapter, these numerical techniques are used to model two real-world polymerizations. The simulation studies outlined in this chapter highlight the ease by which these strategies can be used to model complex kinetic systems. Moreover, the work outlined in chapters three to five has established a set of guidelines that ensure that error incurred in solving these differential equations will not blight the final MWD. Hence we can have confidence that the simulations presented here will not be unduly affected by numerical error.

The experimental data presented in this chapter has been obtained by the research group of Dr. Thomas Davis of the University of New South Wales, Sydney, Australia. The majority of experimental data modeled here were obtained by Dr. Michael Zammit as a part of his PhD thesis studies.

The first simulation study models MWDs measured by two different techniques and uses this data to extract information about the mechanism of termination in methyl methacrylate

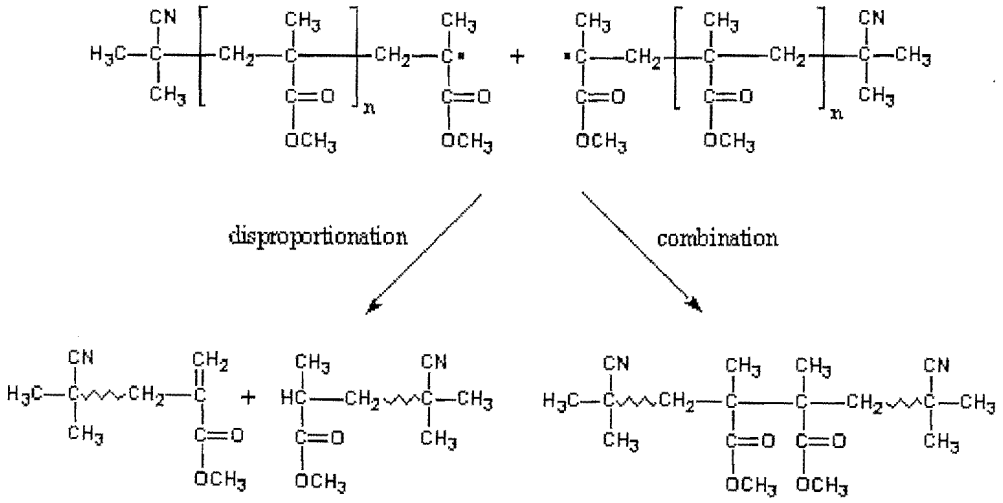

Figure 6-1: A reaction scheme for the termination in the polymerization of MMA.

(MMA). The second simulation study models the MWDs obtained when a novel photoinitiator is used to initiate PIP.

6.2 The Mechanism of Termination in the Free-Radical Polymerization of Methyl Methacrylate

It has long been known that the termination reaction of free-radical polymerization can occur via the disproportionation or combination mechanism. For the polymerization of methyl methacrylate (MMA) initiated by $2,2'-$ azobis(isobutyronitrile) (AIBN), these two reaction mechanisms are as shown in figure 6-1.

This scheme indicates how disproportionation gives two 'dead' polymer molecules, each with one initiator-derived endgroup (a cyanoisopropyl group in the case of AIBN), while combination gives a single dead polymer molecule with an initiator residue at each end. It is therefore clear that the prevailing termination mechanism influences both the number of initiator-derived endgroups per polymer molecule and the average molecular weight of product dead polymer (combination obviously leading to higher average molecular weights than disproportionation). Several methods have been developed to use the difference in the molecular weight (MWT) of the

products of these two mechanisms as a means of obtaining information about the termination mechanism. Such methods have been reviewed by Moad and Solomon[33][34] who point out that all these polymerization-based methods are compromised by neglect of other pathways by which dead chains may be formed. The most notable such reaction is transfer, which, for example, acts to reduce molecular weights and to reduce the number of initiator-derived endgroups per polymer molecule. So results which suggest that disproportionation is the prevailing termination mechanism may in fact really be evidencing no more than that transfer is occurring.

With the advent of better and better analytic techniques, increasingly more information can be extracted about the kinetics of polymerization. The work outlined here is based on a new analytic technique that can be used to measure the number of initiator-derived endgroups attached to dead polymer chains. This method, known as Matrix-Assisted-Laser-Desorption-Ionization Mass-Spectroscopy (MALDI-MS) can be used to measure the dead polymer chain-length distribution. The strength of MALDI-MS is its high resolution. A MALDI-MS dead polymer chain-length distribution contains separate peaks for species that differ in mass by as little as three Daltons. This is important for this study, as it means that MALDI-MS can separate chains that differ only in the number of cyanoisopropyl endgroups they contain. A MWD measured by MALDI-MS provides the raw data needed for a study of the termination mechanism.

One of the advantages that MALDI-MS affords over other, typically spectroscopic, techniques for counting the number of initiator-derived endgroups attached to a dead polymer chain is that it can resolve the number of initiator-derived endgroups attached to polymer of a particular chain length. Whereas standard spectroscopic techniques give information about the total number of chains with one or two endgroups, MALDI-MS allows the ratio of chains with one cyanoisopropyl endgroup N_1 to those with two endgroups N_2 to be calculated for a wide range of chain lengths.

The technique at the core of this study – MALDI-MS – is a new and somewhat untested technique (at least for the measurement of dead polymer MWDs). Thus, before we use information extracted from MALDI-MS MWDs, we wish to establish the reliability of this data. This is can be done by comparing MALDI-MS MWDs with those obtained by gel permeation chromatography (GPC) (a well established method of measuring MWDs) and also simulated

MWDs. From this comparison the region of the MWD where there is the best agreement between GPC and MALDI-MS is found; this region can be used for rate parameter extraction.

The idea at the core of this study is that the proportion of termination that occurs by the disproportionation mechanism ($\lambda = k_{td}/(k_{td}+k_{tc})$) can be extracted from the ratio of N_1/N_2 as a function of chain length. Unfortunately, the ratio N_1/N_2 is not simply equal to λ; several other rate parameters and a number of kinetic effects also affect this ratio (see below). This means two things. Firstly, to obtain the value of λ we must fit a kinetic simulation to the ratio of $N_1$to N_2. Secondly, it means that we have to extract the values of several other rate parameters before these simulations can be (see the section on GPC modelling). To extract these rate constants we compare simulated and experimental GPC MWDs for a pulsed laser polymerization (PLP) obtained in the same conditions as the MALDI-MS MWDs. The experimental MWDs used here have been published previously by Zammit et. al.[56]

6.2.1 Experimental Molecular Weight Distributions

Molecular weight distributions are an important source of information about the kinetics of free-radical polymerization. In this study, information about the mechanism of termination in MMA has been extracted from a MWD measured by MALDI-MS. As the rectitude of any mechanistic conclusion drawn from a MWD depends strongly on the quality of that distribution, we first investigate the quality of the MWD. This is done in two ways: firstly, by comparing the MWD measured by GPC with that measured by MALDI-MS, and secondly by comparing experimental and simulated MWDs. In this section of this chapter, we focus on the first part of this comparison: MALDI-MS and GPC. A detailed account of the fit of a simulated MWD to the experimental distributions is left to a later section.

The first part of this comparison of the MWDs measured by GPC with those measured by MALDI-MS is a detailed description of the GPC MWD. The second part is a similar description of the MALDI-MS MWD, and finally a comparison of the two types of MWD is given.

The Experimental MWD from GPC.

The GPC analysis of the laser-polymerized polymer is shown in figure 6-2 with a derivative inlay. The derivative and $w(log_{10}M)$ plots indicate that there are a number of peaks in the

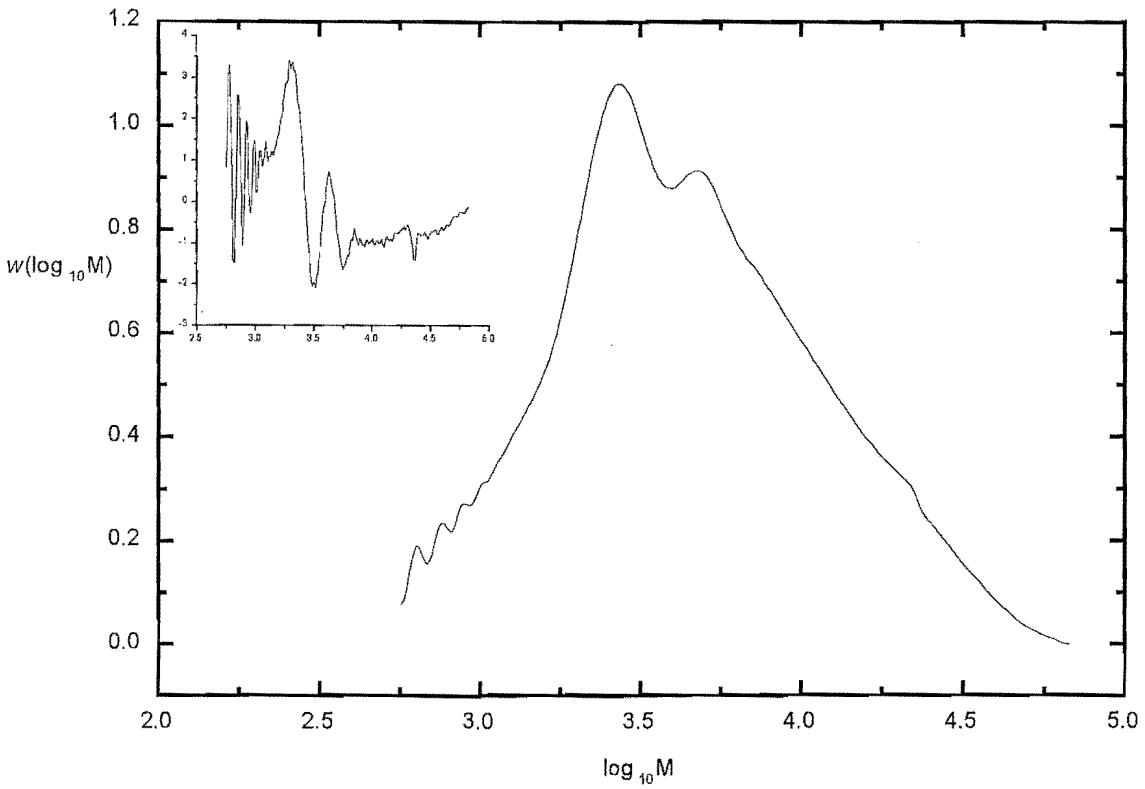

Figure 6-2: MWD for the pulsed laser polymerization of methyl methacrylate as measured by GPC. The inlay shows the derivative of the MWD.

GPC distribution, as is expected for a MWD from an intermittently-initiated polymerization. The inflection point on the low molecular weight side of the lowest molecular weight (or 'primary' peak) corresponds to a MWT of 2000, or approximately 20 kinetic chain units of MMA.

Several other peaks (or overtones) are shown by the derivative and $w(log_{10}M)$ plots. The presence and the positions of these peaks confirm that pulsed-laser polymerization conditions were obtained.[8] These overtones have low molecular weight inflection points, most clearly seen in the derivative plot, positioned at MWT of 4000 and 6000, or at molecular weights corresponding to $2L_0$ and $3L_0$, where L_0 is equal to $k_p M t_0$, M is the concentration of monomer ($mol.L^{-1}$), and t_0 the length of time between laser pulses. There is some suggestion of a shoulder

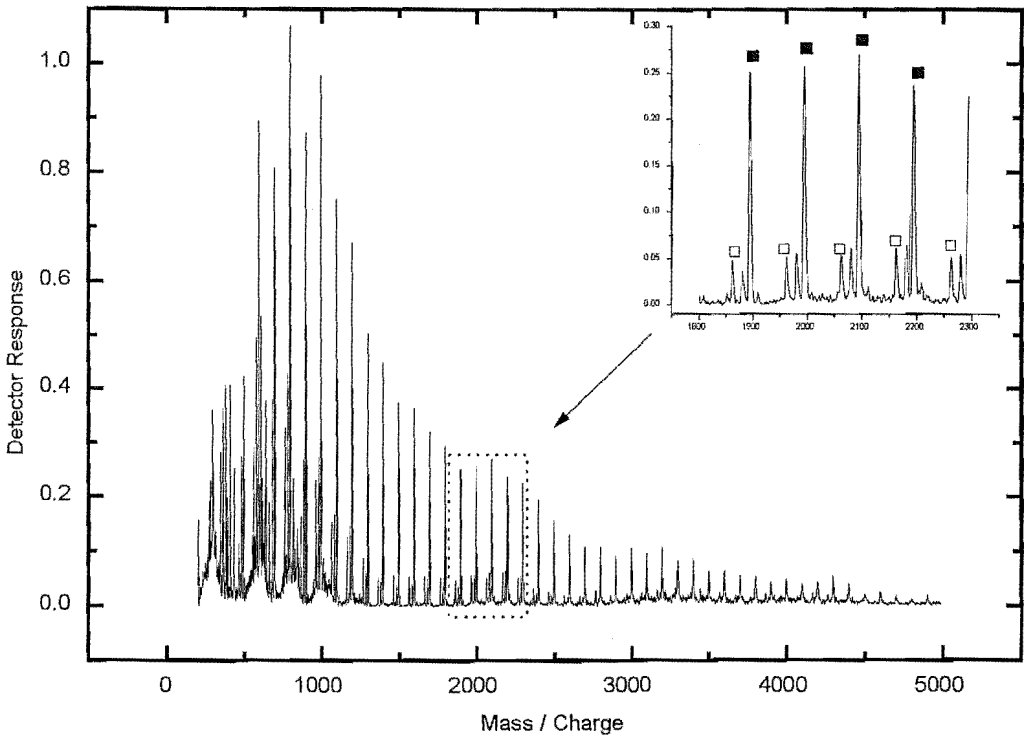

Figure 6-3: MALDI-MS MWD with an inlay of an expanded section of the MWD. The black squares denote dead polymer chains that contain one initiator-derived endgroup, the white squares those dead polymer chains with two initiator-derived endgroups.

at MWT 20000. I believe that this is an experimental artifact. This conclusion is confirmed by attempts to fit the experimental MWD with a simulation. A discussion of this apparent overtone and the region of the MWD around it are given in section 6.2.3.

The Experimental MWD from MALDI-MS

An example of an MWD obtained by MALDI-MS analysis is shown in figure 6-3. In contrast to GPC, MALDI-MS produces a discrete distribution where different polymeric products give rise to resolved peaks. This difference in the appearance of the two types of distribution is due to a fundamental difference in the way these techniques separate polymer species: GPC is a size

exclusion technique, while MALDI-MS is a mass spectrometry technique. Fundamental to any size exclusion technique is an effect known as chromatographic broadening. Chromatographic broadening causes polymer of a particular chain length to emerge from the GPC column as approximately a Gaussian distribution which is so wide that it overlaps with the distributions for polymer of adjacent chain lengths. Thus the GPC MWD is the sum of these overlapping Gaussian distributions. The measurement of a MALDI-MS does not cause chromatographic broadening and the signal for dead polymer chains of a particular chain length emerges as a separate peak.

The ability of MALDI-MS to resolve dead polymer chains that differ in mass by as little as three Daltons is the key advantage that MALDI-MS has over GPC. This greater resolution means that a MALDI-MS MWD contains significantly more kinetic information. The expansion of the MALDI-MS MWD shown in the inlay to figure 6-3 illustrates the form that this extra kinetic information takes. MALDI-MS produces a distribution that has separate peaks for polymer with two initiator-derived endgroups (white squares) and for polymer with one initiator-derived endgroup (black squares).

It is clear from the MALDI-MS number distribution shown in figure 6-3 that there are many more peaks in this distribution than there are possible polymer species. These peaks correspond to the adducts of the cations of sodium, potassium and lithium to each polymer species. Thus, the raw MALDI-MS is a number distribution that contains three copies of the number distribution, one for each cation. The sodium cation series has been used in this study, because it gives by far the strongest signals. The choice of one cation series rather than the sum of all three involves an assumption. We assume that the MALDI-MS response is not sensitive to the cation. This assumption seems justifiable as the number molecular weight distribution that is produced is a reasonable fit to GPC and simulated MWDs.

Although MWDs measured by MALDI-MS are not affected by chromatographic broadening, these distributions are broadened in two other ways. In general, this broadening is caused by the presence of species of very similar mass, species that MALDI-MS is unable to resolve. The first type of broadening is caused by termination by disproportionation. The two products of termination by disproportionation (see figure 6-1) have a very similar mass (they differ by 2 Dalton). As the MALDI-MS apparatus used in this study can only resolve species that

differ in mass by more than 3 Daltons, MALDI-MS is unable to resolve the saturated and unsaturated products of disproportionation. Therefore, the peaks for polymer produced by the disproportionation termination mechanism are really two unresolved peaks of slightly different mass. In contrast to this, the combination termination mechanism produces one product (again see figure 6-1), hence the peaks in the MALDI-MS MWD for this material are not broadened in the same way. This has an important ramification. It means that one should not use the ratio of the peak heights for polymer produced by disproportionation to polymer produced by combination as an estimate of N_1 to N_2. Rather, one should use the peaks areas as it is these areas that reflect the numbers of chains of a particular chain length. The peak areas are used here.

The second type of broadening is known as isotopic broadening. This occurs when a dead polymer species contains atoms that have several isotopes with reasonably high natural abundances. The most obvious example of such an atom is carbon-12 and its isotope carbon-13. The natural abundance of carbon-13 is approximately 1%. Thus a dead polymer chain length distribution will contain some polymer where one or more carbon atoms are carbon-13. For example, consider a dead polymer chain of chain length 20. These chains contain 100 carbon atoms (each monomer unit contains five). Based on the natural abundance of carbon-13 we would expect that there will be on average one carbon-13 per chain. However, the distribution of carbon-13 atoms is random, so that some chains will contain no carbon-13, while others will contain more than one. As isotopes have different masses, there are several possible signals for dead polymer of each chain length. Moreover, as these signals are so close together in mass, MALDI-MS is unable to resolve them and each peak will be broadened. Note that the extent of this broadening is chain-length dependent. As the chain length of a polymer chain increases, so does the likelihood of it containing more than one carbon-13 isotope. Hence, peaks for high molecular weight species have greater absolute broadness than those for low molecular weight species. It is clear that isotopic broadening will dominate disproportionation broadening - which is a constant 2 Daltons, independent of chain length - at high i say $i \geq 40$ (see $i = 20$ example above).

The chain-length dependence of isotopic broadening does not affect the ratio of N_1 and N_2. This is because N_1 and N_2 are calculated from peak areas, and a given peak will include all

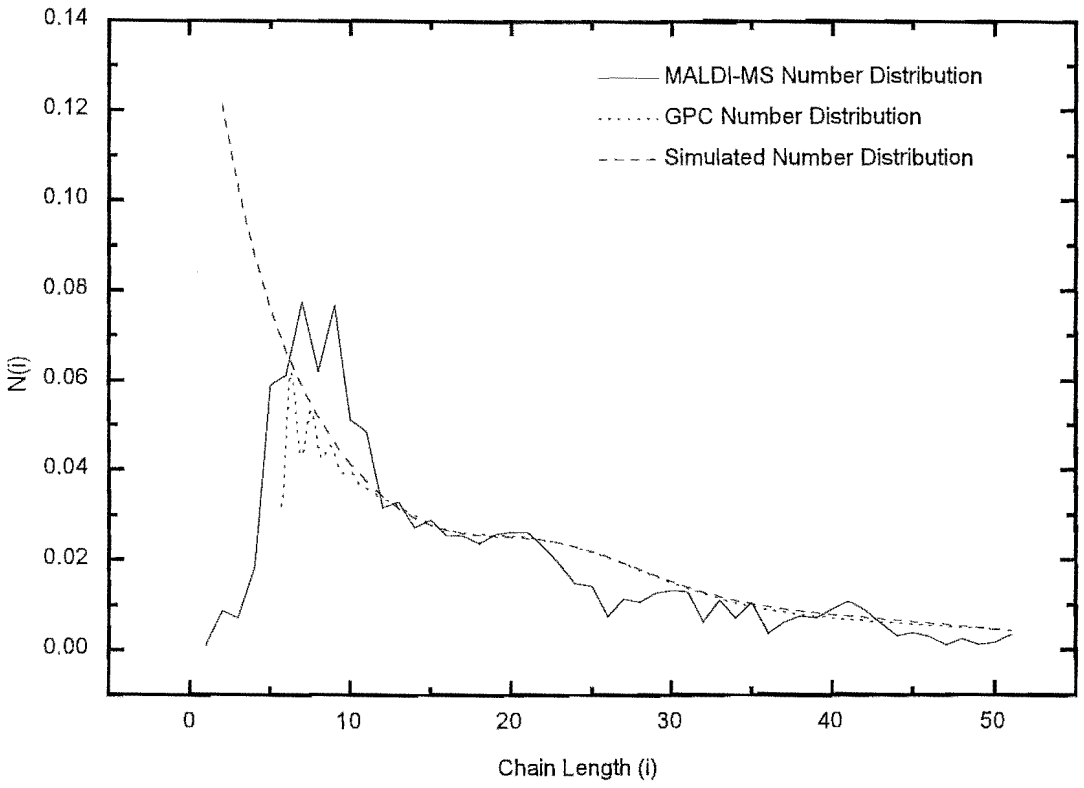

Figure 6-4: A comparison of three number distributions: a simulated number distribution, that obtained by MALDI-MS and that extracted by GPC data. For the simulated distribution, best fit parameters have been used.

isotopes of a particular chain length. Hence values of N_1 and N_2 reflect all polymer of that chain length.

The Comparison of GPC and MALDI-MS MWDs

Figure 6-4 contains three number molecular weight distributions (NWD): a simulated NWD for the best fit parameters (see below for these parameters and how they were obtained), a NWD transformed from an MWD measured by GPC and a NWD measured by MALDI-MS, where the peaks have been integrated and the contribution of chains formed by disproportionation and by combination summed. The agreement between all three distributions is good, especially in the

central region of the NWD. The quality of this agreement means that we can have confidence in the quality of the MALDI-MS NWD, and because of this, have confidence that data will not lead to false mechanistic conclusions being drawn.

It is in the low MWT region (MWT < 1000) of the NWD that the agreement between the MALDI-MS and GPC NWDs is poorest. Moreover, it also this region where the difference between the simulated distribution and the two experimental NWDs is greatest. There are a number of mechanistic and experimental reasons why this might be the case. The simulated NWD in this plot is based on a model that does not include chain-length dependent propagation. One of the effects of a chain-length dependent k_p upon the NMD is that it reduces the amount of low MWT polymer (assuming the standard model for chain-length dependent k_p, see below). Thus a model that allows k_p to depend on chain length is likely to give a better agreement with experiment. Another possible reason for the differences between these distributions comes from the way that the GPC is measured and transformed. The low as well as the high MWT regions of the MWD measured by GPC are known to have a high signal to noise ratio. Thus error is greatest in these regions. Further, the transformation of the GPC MWD to a NMD accentuates the error in the low MWT region, so little confidence can be placed in this region of the GPC NMD. Finally, although it has been shown here and in other studies[49] that MALDI-MS gives a good fit to the GPC MWD, less confidence should be placed in the low and high MWT regions of the MALDI-MS NMD. Thus in this study we focus on the central region (MWT $1000-4000$) of the NMD for all fitting and rate parameter extraction studies.

In conclusion, there is good agreement between the NMDs measured by GPC and those measured by MALDI-MS, especially in the central region of the NMDs. As a result of this, the central region of these NMDs will be used with some confidence to draw mechanistic conclusions.

6.2.2 Kinetic Modeling

Here a kinetic model and system of population-balance differential equations that can be used to describe the kinetics and MWDs of these systems is developed. The primary aim of this modeling is the extraction of rate parameters, foremost the ratio λ, but also the rate constants for propagation and termination, as well as the concentration of radicals added by a laser pulse. However, the comparison of simulated and experimental MWDs also provides a test for the

kinetic model used as a basis of these simulations.

Reaction Scheme

The first step that must be taken when modeling the kinetics of a free-radical polymerization system is to propose a kinetic scheme, one that includes all the processes that are believed to influence the kinetics (and thus the MWD) of the system being studied. The kinetic scheme used in this work is a modified version of the standard kinetic model. This reaction scheme (see below), includes, as does the standard kinetic model, five kinetic processes: chain initiation; chain propagation; chain transfer; and bimolecular termination by the disproportionation and combination mechanisms. The model used in this study differs from the standard kinetic model as it keeps track of species that contain different numbers of initiator-derived endgroups. Whereas in the standard model all radicals of chain-length ten, for example, are treated equivalently, in this model radicals of chain length ten are divided into two types. The first type contains all radicals that contain one initiator-derived endgroup and the second type radicals with no initiator-derived endgroups. The same system of classification is used for the dead polymer chains. However, dead polymer chains may contain none, one or two initiator-derived endgroups. To allow for this increase in resolution a new system of nomenclature is used. Here R_i^k denotes a radical of chain length i that contains k initiator-derived endgroups, while D_i^k is a dead polymer chain of chain length i that contains k initiator-derived endgroups. Hence, the model reaction scheme is:

$$\text{Initiator} \longrightarrow 2R_0^1 \tag{6.1}$$

$$R_i^k + M \xrightarrow{k_p^i} R_{i+1}^k \qquad k = 0 \text{ or } 1;\ \ i \geq 1 \tag{6.2}$$

$$R_i^k + M \xrightarrow{k_{tr,m}} D_i^k + R_1^0 \qquad k = 0 \text{ or } 1;\ \ i \geq 1 \tag{6.3}$$

$$R_i^k + R_j^m \xrightarrow{k_{td}^{i,j}} D_i^k + D_j^m \qquad k, m = 0 \text{ or } 1;\ \ i \text{ and } j \geq 1 \tag{6.4}$$

$$R_i^k + R_j^m \xrightarrow{k_{tc}^{i,j}} D_{i+j}^{k+m} \qquad k, m = 0 \text{ or } 1;\ \ i \text{ and } j \geq 1 \tag{6.5}$$

Here 'Initiator' denotes a molecule of initiator, M a molecule of monomer, and R_0^1 a primary radical that is the direct product of initiator decomposition (whether it photo- or thermally-induced). The rate coefficients k are subscripted to indicate which of the above reactions

they correspond to, and superscripted according to their chain-length dependence. Note that it is assumed that none of the rate coefficients depend upon the number of initiator-derived endgroups present. This assumption seems justifiable based on standard chemical arguments: the radical center is distant from the chain end for all but the smallest of radical species. Simulation studies have shown that allowing the reactivities of small radical species to depend upon the number of initiator-derived endgroups they contain does not significantly affect the kinetics or MWDs.

Population Balance Differential Equations

From the above model, it is possible to write down the population-balance differential equations that describe how the concentration of all species change with time t. These are as follows.

Living Radicals:

$$\frac{d\mathrm{R}_0^0}{dt} = 0 \tag{6.6}$$

$$\frac{d\mathrm{R}_0^1}{dt} = R_{init} - k_\mathrm{p}^0 \mathrm{M}\mathrm{R}_0^1 - k_{\mathrm{tr,m}}\mathrm{M}\mathrm{R}_0^1 - 2\mathrm{R}_0^1 \sum_{j=0}^{\infty} k_\mathrm{t}^{0,j}(\mathrm{R}_j^0 + \mathrm{R}_j^1) \tag{6.7}$$

$$\frac{d\mathrm{R}_1^0}{dt} = \mathrm{M}k_{\mathrm{tr,m}} \sum_{j=0}^{\infty}(\mathrm{R}_j^0 + \mathrm{R}_j^1) - k_\mathrm{p}^1 \mathrm{M}\mathrm{R}_1^1 - k_{\mathrm{tr,m}}\mathrm{M}\mathrm{R}_1^1 - 2\mathrm{R}_1^0 \sum_{j=0}^{\infty} k_\mathrm{t}^{1,j}(\mathrm{R}_j^0 + \mathrm{R}_j^1) \tag{6.8}$$

$$\frac{d\mathrm{R}_1^1}{dt} = k_\mathrm{p}^0 \mathrm{M}\mathrm{R}_0^1 - k_\mathrm{p}^1 \mathrm{M}\mathrm{R}_1^1 - k_{\mathrm{tr,m}}\mathrm{M}\mathrm{R}_1^1 - 2\mathrm{R}_1^1 \sum_{j=0}^{\infty} k_\mathrm{t}^{1,j}(\mathrm{R}_j^0 + \mathrm{R}_j^1) \tag{6.9}$$

$$\frac{d\mathrm{R}_i^k}{dt} = k_\mathrm{p}^{i-1}\mathrm{M}\mathrm{R}_{i-1}^k - k_\mathrm{p}^i \mathrm{M}\mathrm{R}_i^k - k_{\mathrm{tr,m}}\mathrm{M}\mathrm{R}_i^k - 2\mathrm{R}_i^k \sum_{j=0}^{\infty} k_\mathrm{t}^{i,j}(\mathrm{R}_j^0 + \mathrm{R}_j^1) \qquad k = 0 \text{ or } 1;\ i \geq 2 \tag{6.10}$$

Dead Polymer Chains:

$$\frac{d\mathrm{D}_0^0}{dt} = 0 \tag{6.11}$$

$$\frac{d\mathrm{D}_0^1}{dt} = k_{\mathrm{tr,m}}[\mathrm{M}]\mathrm{R}_0^1 + 2\mathrm{R}_0^1 \sum_{j=0}^{\infty} k_{\mathrm{td}}^{0,j}(\mathrm{R}_j^0 + \mathrm{R}_j^1) \tag{6.12}$$

$$\frac{d\mathrm{D}_0^2}{dt} = k_{\mathrm{tc}}^{0,0}\mathrm{R}_0^1\mathrm{R}_0^1 \tag{6.13}$$

$$\frac{d\mathrm{D}_i^0}{dt} = k_{\mathrm{tr,m}}\mathrm{M}\mathrm{R}_i^0 + 2\mathrm{R}_i^0 \sum_{j=0}^{\infty} k_{\mathrm{td}}^{i,j}(\mathrm{R}_j^0 + \mathrm{R}_j^1) + \sum_{j=0}^{i} k_{\mathrm{tc}}^{i-j,j}\mathrm{R}_{i-j}^0\mathrm{R}_j^0 \qquad i \geq 1 \tag{6.14}$$

$$\frac{dD_i^1}{dt} = k_{tr,m} M R_i^1 + 2R_i^1 \sum_{j=0}^{\infty} k_{td}^{i,j} (R_j^0 + R_j^1) + 2 \sum_{j=0}^{i} k_{tc}^{i-j,j} R_{i-j}^0 R_j^1 \qquad i \geq 1 \qquad (6.15)$$

$$\frac{dD_i^2}{dt} = \sum_{j=0}^{i} k_{tc}^{i-j,j} R_{i-j}^1 R_j^1 \qquad i \geq 1 \qquad (6.16)$$

Note that although the symbols used in these differential equations stand for the same type of species as they did in the reaction scheme, their meaning has changed slightly. Whereas in the reaction scheme the symbol M denoted a single molecule of monomer, in the population balance differential equation this symbol corresponds to the concentration of monomer. Note that a differential equations is not included for the rate of change in the concentration of monomer, as it is assumed that monomer consumption is negligible (this is a standard PLP assumption). Moreover, differential equations for D_0^0 and R_0^0 are included only for the sake of completeness (these species are not formed).

Two assumptions may be made that reduce the complexity of these differential equations. The first of these relates to chain transfer. Several authors have measured the rate coefficient for transfer to monomer, including a recent study by Kukulj et. al.[28] and a definitive study by Stickler et. al.[52] that showed that $k_{tr,m}/k_p = 2.1 \times 10^{-5}$ for MMA at 25°C. This is a very low value, and at 0°C, the temperature of the experiments under discussion, $k_{tr,m}/k_p$ will be even lower. So it seems reasonable to assume that transfer to monomer does not affect the kinetics and MWDs in this system. Definitive evidence in support of this assumption comes from the MALDI-MS data (see figure 6-3). As has already been stated, MALDI-MS has the ability to resolve dead polymer chains according to endgroup. This means that MALDI-MS can provide information about the contribution of the chain transfer process. Dead polymer chains that contain no initiator-derived endgroups can only be produced, and therefore potentially be present in MALDI-MS data, if chain transfer is occurring. The reason for this is illustrated by the population-balance differential equations given above. Equation 6.14 models the concentration of dead polymer chains with no initiator-derived endgroups. It is clear that equation 6.14 is only non-zero when the concentration of R_i^0 is non-zero. As the only way that R_1^0 can be produced is by chain transfer (see equation 6.8), the lack of peaks for dead polymer chains with no initiator-derived endgroups in the MALDI-MS MWD proves that chain transfer is an insignificant process. Therefore we exclude chain transfer from the reaction scheme used in this

study. The population-balance differential equations that reflect this change are as follows:

Modified Population Balance Differential Equations

Living Radicals:

$$\frac{d\mathrm{R}_0^1}{dt} = R_{init} - k_\mathrm{p}^0 \mathrm{M}\mathrm{R}_0^1 - 2\mathrm{R}_0^1 \sum_{j=0}^{\infty} k_\mathrm{t}^{0,j} \mathrm{R}_j^1 \tag{6.17}$$

$$\frac{d\mathrm{R}_i^1}{dt} = k_\mathrm{p}^{i-1} \mathrm{M}\mathrm{R}_{i-1}^1 - k_\mathrm{p}^i \mathrm{M}\mathrm{R}_i^1 - 2\mathrm{R}_i^1 \sum_{j=0}^{\infty} k_\mathrm{t}^{i,j} \mathrm{R}_j^1 \qquad i \geq 1 \tag{6.18}$$

Dead Polymer Chains:

$$\frac{d\mathrm{D}_0^1}{dt} = 2\mathrm{R}_0^1 \sum_{j=0}^{\infty} k_\mathrm{td}^{0,j} \mathrm{R}_j^1 \tag{6.19}$$

$$\frac{d\mathrm{D}_0^2}{dt} = k_\mathrm{tc}^{0,0} 2\mathrm{R}_0^1 \mathrm{R}_0^1 \tag{6.20}$$

$$\frac{d\mathrm{D}_i^1}{dt} = 2\mathrm{R}_i^1 \sum_{j=1}^{\infty} k_\mathrm{td}^{i,j} \mathrm{R}_j^1 \qquad i \geq 1 \tag{6.21}$$

$$\frac{d\mathrm{D}_i^2}{dt} = \sum_{j=0}^{i} k_\mathrm{tc}^{i-j,j} \mathrm{R}_{i-j}^1 \mathrm{R}_j^1 \qquad i \geq 1 \tag{6.22}$$

These differential equations are less complicated than differential equations 6.6 – 6.16. One of the important features of these new differential equations is that each termination mechanism produces a distinct type of dead chain species. Whereas, under the previous model, the inclusion of chain transfer meant the dead polymer chain containing one initiator-derived endgroup could be produced by any one of the three dead chain formation mechanisms (transfer, disproportionation and combination), the exclusion of chain transfer means that chains containing one initiator-derived endgroup are produced exclusively by the disproportionation mechanism, while as always those containing two endgroups are a product of the combination mechanism.

The second assumption concerns the importance of chain-length dependence effects. The model given above allows the rate coefficients of termination and propagation to depend upon the chain length of the relevant reacting species. For chain propagation, this involves increasing the rate coefficient for small radicals, i.e., chain lengths zero to three. For example, $k_\mathrm{p}^0 = k_\mathrm{p}^1 = 10k_\mathrm{p}^\infty$; $k_\mathrm{p}^2 = 5k_\mathrm{p}^\infty$; $k_\mathrm{p}^3 = 2k_\mathrm{p}^\infty$ where k_p^∞ is the rate coefficient for long radicals is a chain-length

dependence which is consistent with several investigations.[24][19][34]

It is well-known that the rate constant for termination depends upon the chain length of both of the terminating radicals, where longer radicals terminate at a slower rate. Chain-length dependent termination has been discussed in a number studies, e.g.,[3][45]. The majority of simulations presented here assume that the rate constants for propagation and termination are independent of chain length of the reacting molecule(s), i.e., for chain propagation it is assumed that

$$k_{\mathrm{p}}^{i} = k_{\mathrm{p}}^{\infty} \qquad \text{for } i \geq 0 \tag{6.23}$$

and for termination

$$k_{\mathrm{t}}^{i,j} = k_{\mathrm{t}}^{1,1} \qquad \text{for } i,j \geq 1;\ k_{\mathrm{t}}^{0,i} = 0 \tag{6.24}$$

Again, these assumptions reduce the complexity of the differential equations. Ignoring primary radical termination is an additional assumption, later shown to have negligible effect on results. These differential equations are not given here as they follow simply from equations 6.17 – 6.22. The real rewards of making these two assumptions are reaped when one comes to solve these differential equations. The population-balance differential equations for a system that ignores chain transfer and where the rate coefficients for k_{p} and k_{t} are independent of chain length take much less time to solve than those for a kinetic system where these processes are included.

Having established the differential equations that model the way that the concentrations of all species change with time, they must be solved. Trial calculations indicated that the modified Euler method was best suited to solving these differential equations (this was established using the criteria described at the end of chapter four). These calculations were performed on a VAX mainframe, where simulation took three hours of CPU time for a typical run. As has been noted previously, the time taken to complete a simulation depends upon the termination mechanism (see chapter five). If termination occurs exclusively by the disproportionation mechanism, then a simulation took 30 minutes of CPU time, but the inclusion of any termination by combination increased the time taken six-fold. In all simulations, differential equations for individual chains-lengths up to and including $i = 2,000$ were solved, with a single differential equation for all species of greater chain length being used (a truncation chain length of $2,000$ was found to cover the entire MWD in all cases). All R_i^1 were initially set equal to zero and allowed to build up to

their pseudo-steady-state profile. Simulations were carried out for ten pulses of polymerization, this being long enough for a pseudo-steady-state to be well and truly established. In the present simulations, a pseudo-steady-state was always reached within $2-3$ pulses, so for most of the time the simulation was in a pseudo-steady-state. Thus the cumulative MWD for the entire simulation is effectively equivalent to the MWD one would obtain from a PLP. Simulation results are presented as normalized cumulative (from the entire simulation) MWDs with the number MWD ($D_i^1 + D_i^2$) being transformed as appropriate. Through careful monitoring it was ensured that the error from numerical solution of the system of differential equations remained negligible at all times (less then 1%).

6.2.3 Gel Permeation Chromatography Modeling

The modeling of the GPC MWD is an essential part of the process of obtaining a value for λ from N_1 / $2N_2$. The ratio N_1 / $2N_2$ depends on a number of rate constants in addition to the ratio λ, i.e., k_p and $k_t \rho t_0$. Fortunately, these rate parameters can be found unambiguously by fitting simulated MWDs to the experimental GPC MWD. The evaluation of these rate parameters from the GPC MWD is outlined here.

In addition to this, a number of other effects - chain-length dependent termination and propagation, and chromatographic broadening - are also studied. It is hoped their inclusion will improve the agreement between theory and experiment.

GPC Modeling: The Rate Constant for Propagation.

A method for calculating the rate constant for propagation from the GPC MWD for an intermittently-initiated polymerization[37] is now well established and widely used. This method involves measuring the position of the inflection point on the low molecular weight side of the lowest molecular weight peak (the primary peak) of the GPC MWD and then rearranging equation 6.25 to solve for the value of $<k_p>$, where $<k_p>$ is a chain-length averaged value of k_p.

$$L_0 = <k_p> \mathrm{M}\ t_0 \tag{6.25}$$

Here L_0 is the chain length of the inflection point, M the concentration of monomer, and t_0 the time between laser pulses. The rate constant for propagation evaluated in this manner from the data for figure 6-2 is equal to 170 $L^{-1}mol^{-1}.s^{-1}$. To confirm this value, and to check the model used, a series of simulations were performed. In these simulations the value of the rate constant for propagation was varied until the best fit between the simulated and experimental MWDs was obtained. Figure 6-5 contains three simulated MWDs; the dashed line is the best fit to experiment. The rate parameters used in this calculation are: $k_t = 1 \times 10^7 L.mol^{-1}.s^{-1}$; M= $1.191 mol.L^{-1}$; $\rho = 9 \times 10^{-7} mol.L^{-1}$; $\lambda = 0.78$; $t_0 = 0.1s$; a step-size of $h = 1 \times 10^{-5}s$ was used. From this figure it is clear that the best fit between theory and experiment is obtained when k_p is 170 ± 5 $L.mol^{-1}.s^{-1}$. This is confirmed by the derivative plot (figure 6-6), where the derivatives of the $w(log_{10}M)$ distributions – experimental and simulated – are compared. The value of the k_p for MMA at 0°C which is predicted by the Arrenhius equation from the IUPAC working party[5] is 143 $L.mol^{-1}.s^{-1}$. Although there is a significant difference between the value measured here and the IUPAC average value, there are several plausible explanations for this. For example, the fact that this polymerization was performed at low temperature conditions means that only a small quantity of polymer was produced. Thus polymer produced before or after the actual PLP experiment could significantly affect this MWD (see below). It is also possible the processes, such as the abstraction from polymer due to photoinitiation, might be responsible for the difference between the theoretical and experimental MWDs.

The calculations outlined above assume that the value of the rate constant for propagation does not depend on the chain length of the propagating radical. A number of studies have shown that this assumption is not always valid.[24] To explore the effect that chain-length dependence in k_p has on the shape of the MWD, simulations have been performed. Figure 6-7 is an example of this type of simulation; rate parameters were: as per figure 6.5 but with $k_p^0 = k_p^1 = 10k_p^\infty$; $k_p^2 = 5k_p^\infty$; $k_p^3 = 2k_p^\infty$; $k_p^i = k_p^\infty$ for $i \geq 4$ where $k_p^\infty = 170$ $L.mol^{-1}.s^{-1}$.

The inclusion of a chain-length dependent model for the propagation rate coefficients has three effects on the MWD. Firstly, it moves the whole distribution, including the position of the inflection point, to higher MWT. This is not a surprising result, as using a chain-length dependent model for k_p increases the average rate of propagation, and hence the average chain length that a newly-formed radical will grow in a certain period of time. As the position

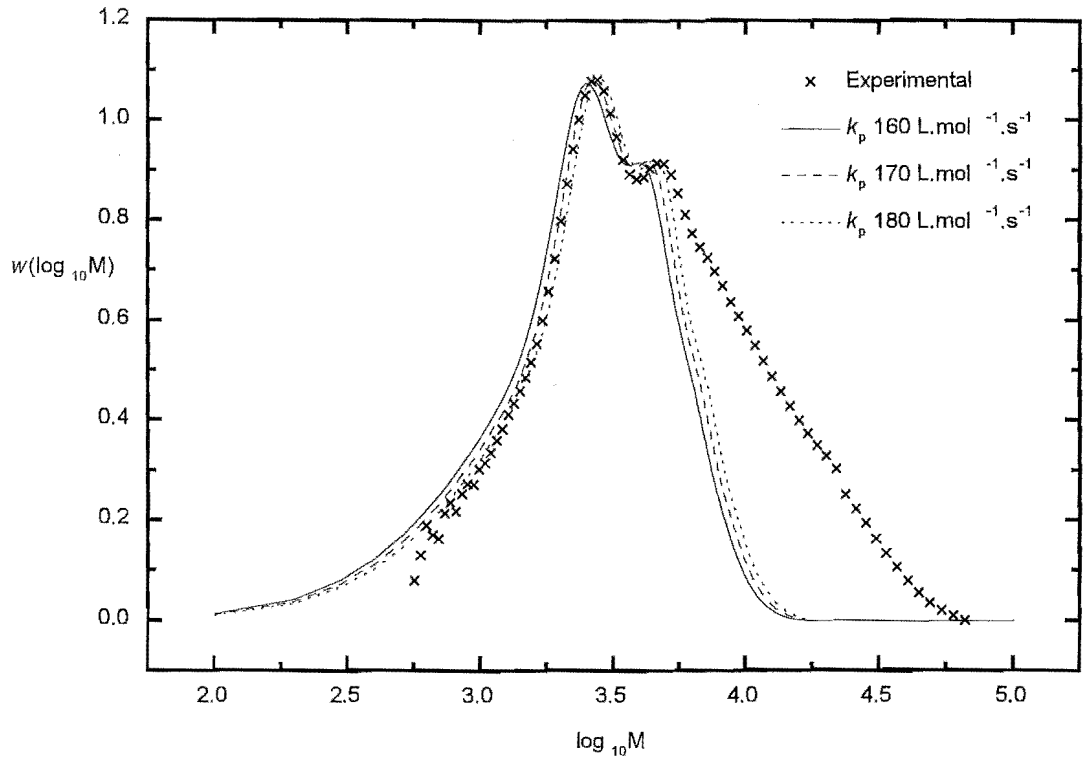

Figure 6-5: Fitting the rate constant for propagation to the GPC MWD.

of the inflection point is sensitive to the model used for k_p, the value of k_p obtained by the inflection point method will have a similar sensitivity. The error introduced to k_p can be estimated by evaluating k_p from the inflection point of the MWD in figure 6-7. The value of k_p from a chain-length independent model is 170 L.mol^{-1}.s^{-1}, as already seen, while the k_p from the chain-length dependent simulation is 180 L.mol^{-1}.s^{-1}. This constitutes a difference of approximately 5%. Therefore, under the conditions of this experiment, ignoring the effects of chain-length dependence in the propagation rate constant has a small but significant effect on the value of k_p extracted from the position of the inflection point. In particular, it is estimated that $k_p^{\infty} = 160$ L^{-1}.mol^{-1}.s^{-1} is probably a better estimate from the experimental data, once the chain-length dependence of propagation is taken into account. This value is closer to the

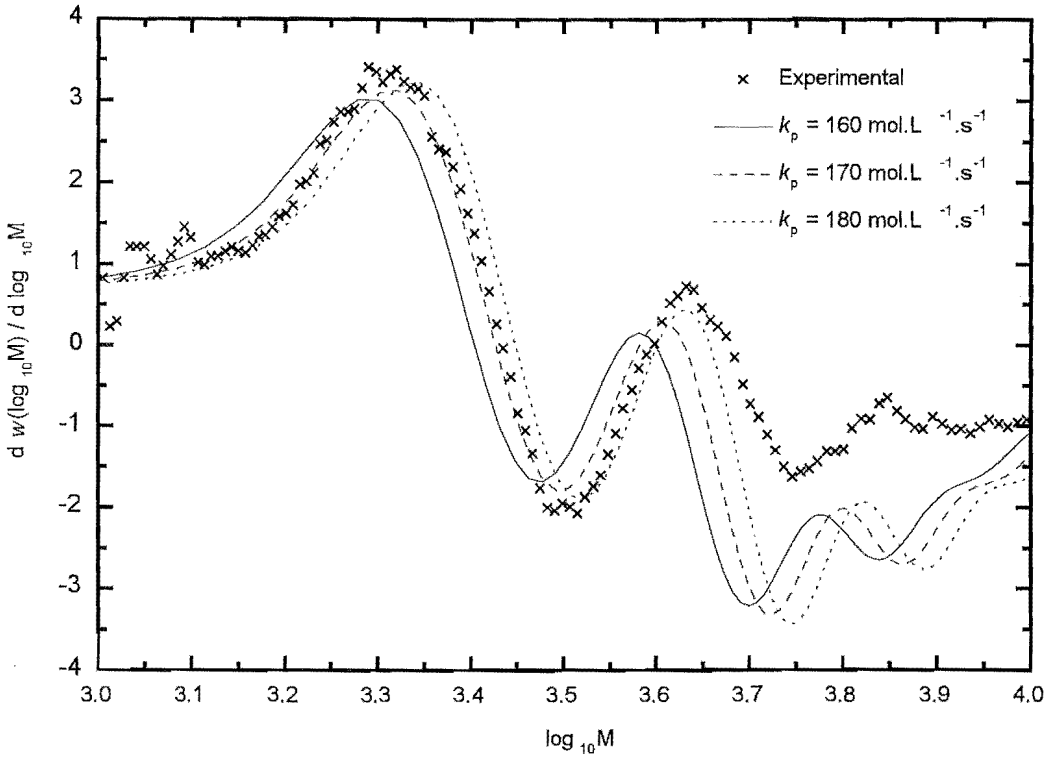

Figure 6-6: Fitting the rate constant for propagation to the derivative of the GPC MWD.

IUPAC recommended value for 0°C, which is encouraging.

Secondly, chain-length dependent propagation reduces the amount of low molecular weight dead polymer (dead polymer chains with less than five monomer units) present in the MWD. This can be understood in the following way. It is well known that the radical chain-length distribution in an intermittently-initiated polymerization consists of a series of Poisson distributions. The distance between these Poisson distributions is $L_0 = <k_p>[\mathrm{M}]t_0$, and they move, that is increase in MWT, at a rate that is proportional to the rate constant for propagation. Thus a radical wave will move (grow) faster when the rate constant for propagation is large. Thus, when a chain-length dependent model for propagation is used, the radical wave will move faster at low chain lengths than at higher chain lengths, i.e., faster for chain lengths

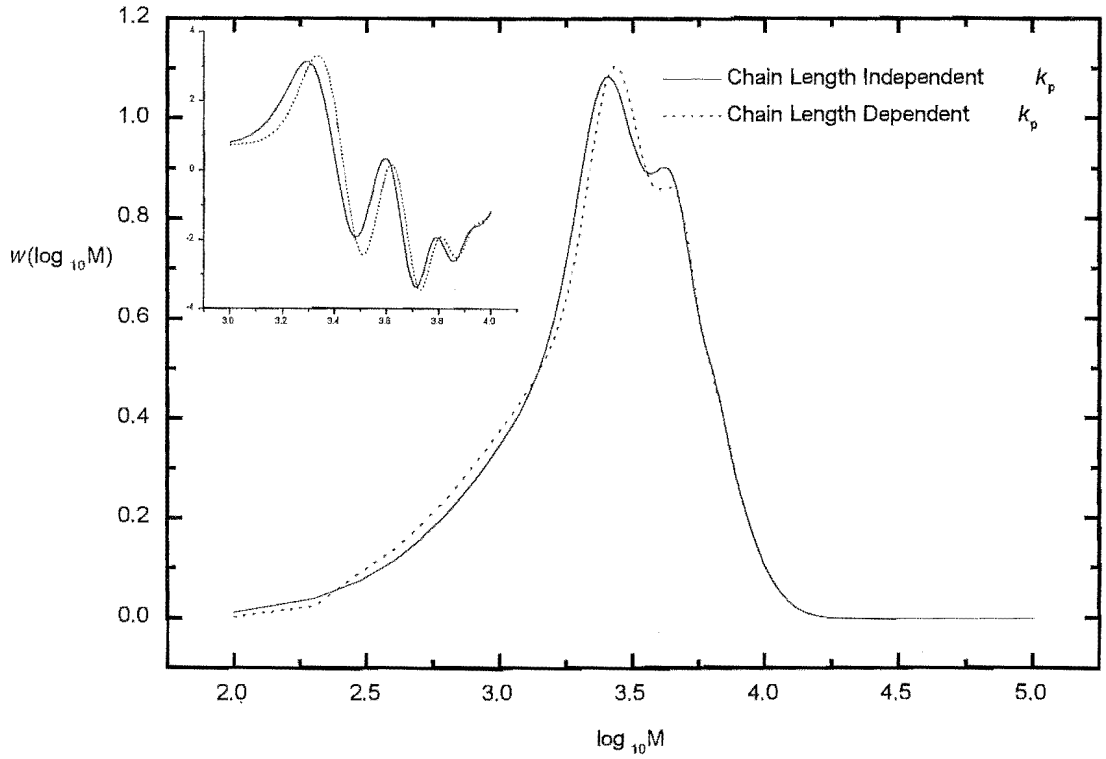

Figure 6-7: The effect of allowing the rate coefficient for propagation to depend on the chain-length of the growing species. A derivative inlay has been included.

where $k_{\mathrm{p}}^{i} > k_{\mathrm{p}}^{\infty}$. If radicals propagate rapidly through a chain length then they are less likely to terminate at that chain length, hence less polymer of that (or twice that chain length for combination) will be produced. This effect can be seen in figure 6-7.

The last comment relates to the separation of peaks in the dead chain distribution. The use of a chain-length dependent model for k_{p} affects the separation of successive low molecular weight side inflection points, i.e., L_0, L_1, L_2. If a chain-length independent model is used for propagation, the separation of these inflection points is a constant $k_{\mathrm{p}}\mathrm{M}t_0$. In contrast to this, when a chain-length dependent model is used for propagation then the separation between inflection points varies. For example, if the chain-length dependent model for k_{p} described

above is used, then $L_0 > k_p^\infty M t_0$ (as discussed), while $L_2 - L_1 = L_1 - L_0 = k_p^\infty M t_0$. This means that $<k_p>$ decreases as L increases. Also, it suggests that a manifestation of chain length-dependent would be $L_1 - L_0 < L_0$, i.e., a smaller than expected gap between the primary and secondary inflection points. Referring to figure 6-6, it is evident that if anything the present experimental data shows the opposite trend. However there is no reason to regard this as a significant result, because (1) GPC is not precise enough (e.g., broadening, calibration), and (2) inflection points does not give exact values of $<k_p>$.

GPC Modeling: The Rate Coefficient for Termination

In this section a series of simulations are outlined that fit the value of the product of $k_t \rho t_0$ to the GPC MWD. The simulations performed here confirmed that it is the product of these rate constants that determines the shape of the MWD, rather than their individual values.[37] For example, if the rate constant for termination is doubled, and the value of ρ halved, the MWD remains exactly the same. This means that when trying to fit a simulated MWD to an experimental MWD it necessary to try and overcome the problem of having one piece of information (the shape of MWD) and two variables (k_t and ρ). Note that the value of t_0 is known independently. As a result of this is it is not possible to obtain the individual values of the rate constant for termination and ρ by fitting a MWD in this manner.

Figure 6-8 shows the three simulated MWDs that are the best fit to experiment. By best fit I mean the closest agreement in the primary peak region of the MWD; this will be justified in the next section. It is clear that $k_t \rho t_0 = 0.9 \pm 0.05$ gives the best fit to the MWD. Given $t_0 = 0.1$ s, this means that if $k_t = 1 \times 10^7$ L.mol^{-1}.s^{-1}, ρ would be equal to 9×10^{-7} mol.L^{-1}. Unfortunately no independent estimate of either k_t or ρ is possible for the present experimental system, so nothing further can be said about the actual values of these parameters.

At first the shape of the theoretical MWDs may seem surprising. They do not contain the multiple, well defined overtones that are normally present in simulated PLP MWDs. Instead, only two overtones are present and these are broad. An explanation of this is given in section 6.2.8. However, for the moment it is important to note that it was not possible to simultaneously fit both the peaks and higher MWT regions of the experimental MWD by varying $k_t \rho t_0$. Figure 6-9 illustrates this point. In this plot, the MWD for the best-fit value of $k_t \rho t_0$ (0.9) is plotted

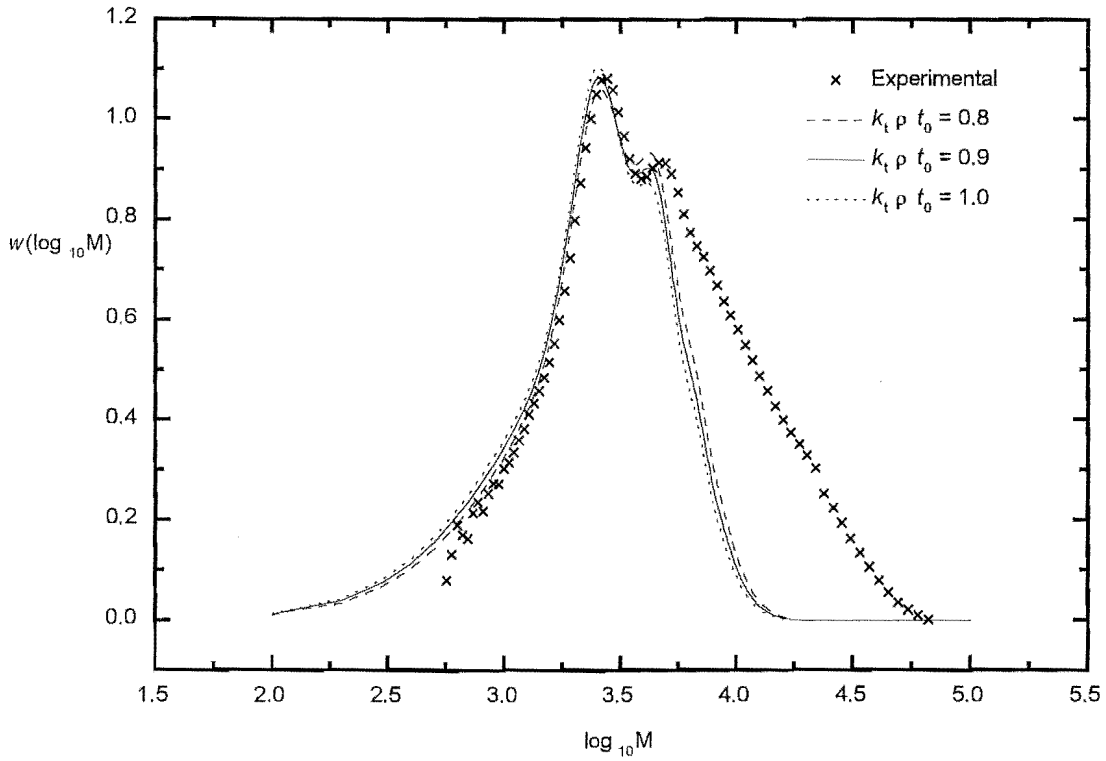

Figure 6-8: Simulations that provided the best fit value for the product of the rate coefficient for termination, concentration of radicals added by a pulse and the time between pulses (see text).

along with MWDs for a high and low value of $k_t\rho t_0$. This shows that although a lower value gives a better fit to the high MWT region of the MWD, this is at the cost of the peak region. Therefore, deciding which value of $k_t\rho t_0$ to take as the best fit value is equivalent to deciding in which part of the MWD to place more confidence, the low-middle MWT region or the high MWT. In section 6.2.1 several reasons were given for why the greatest confidence should be placed in the low-middle (peak) MWT region.

A number of simulations have been performed that include a chain-length dependent model for termination. In these simulations a simple model is used, where the termination rate

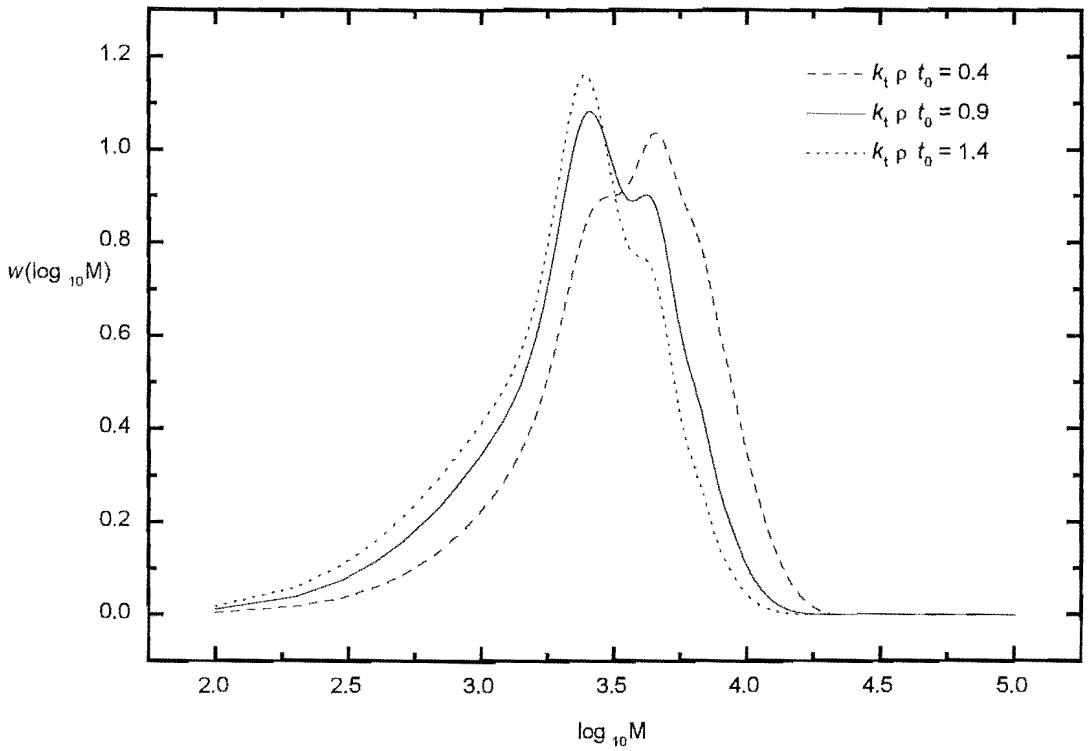

Figure 6-9: The effect of varying the product of the rate coefficient for termination, concentration of radicals added by a pulse and the time between pulses (see text) has on the shape of the MWD.

coefficient for a radical of chain length i and a radical of chain length j, $k_t^{i,j}$, is equal to

$$k_t^{i,j} = \frac{1}{2}(k_t^{i,i} + k_t^{j,j}) \tag{6.26}$$

where

$$k_t^{i,i} = k_t^{1,1} i^{-\alpha} \tag{6.27}$$

In this expression, $k_t^{1,1}$ is the rate of termination of two radicals containing one monomer unit each and α is the scaling exponent for chain-length dependence. Note that primary radical termination is still neglected.

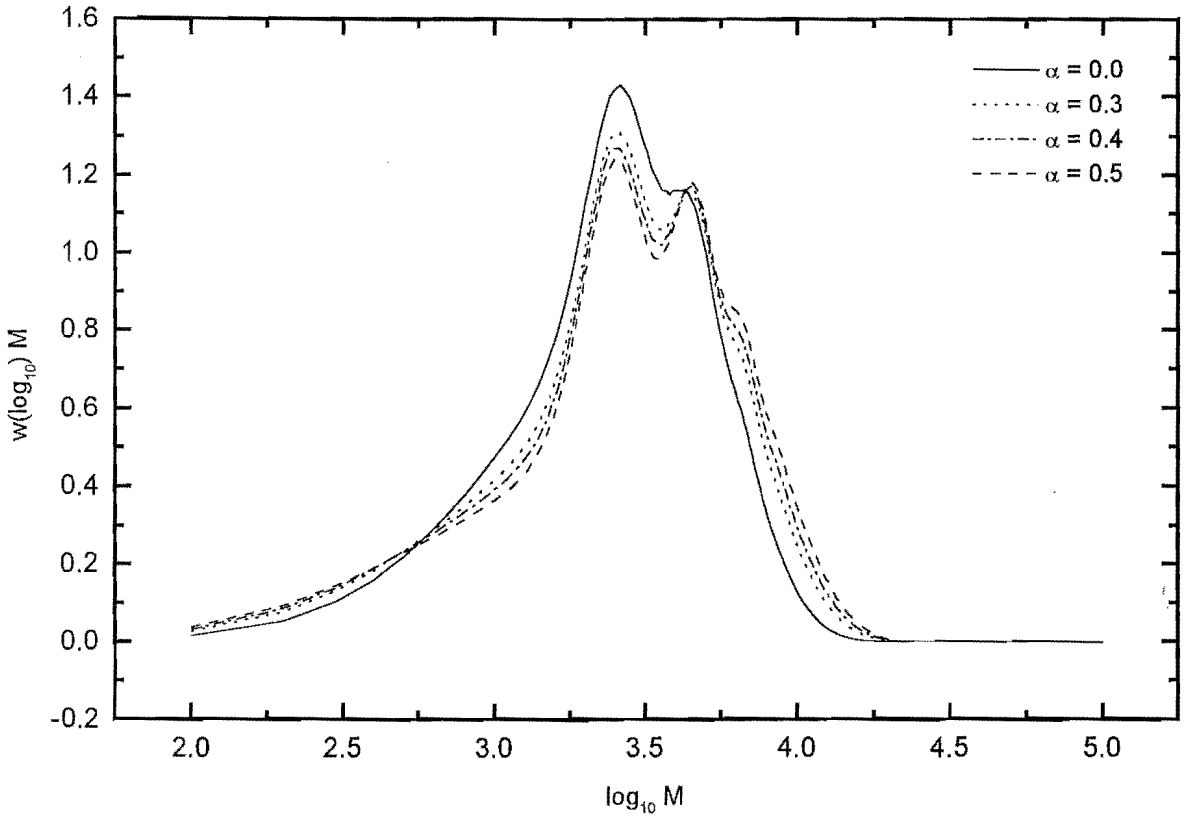

Figure 6-10: The effect of chain-length dependent termination.

A series of simulated MWDs where k_t is chain-length dependent are shown in figure 6-10. In these simulations, the value of $k_t^{1,1}$ has been adjusted to ensure that the average value of k_t across a period of ten laser pulses was always equal to $1 \times 10^7 \text{L.mol}^{-1}.\text{s}^{-1}$. Note the method of averaging k_t used in these simulations is that recommended by Olaj et. al.[38] This meant that as the value of α was increased, so did the value of $k_t^{1,1}$ used in these calculations. From these plots it is clear that chain-length dependent termination has several effects on the MWD. Firstly, as the magnitude of the chain-length dependence (α) is increased, the height of the higher order overtones increases relative to the height of the primary peak. This is due to a decrease of the rate coefficient for termination as the chain length of the terminating radical

increases, i.e., a 'long' radical terminates slower than a 'short' radical. Thus radicals survive to longer chain lengths, which ultimately leads to the formation of more long chains. In the present case this is evident not just as a secondary peak of enhance intensity, but also a high MWT tail of enhanced intensity (see figure 6-10). Interestingly, the same trends are also evident in figure 6-9 as k_t is lowered, With chain-length dependent termination one effectively has a lower k_t for long chains than for short chains - hence the results of figure 6-10. As expected, this effect is accentuated if the value of α is increased.

A chain-length dependent model for k_t also caused the dead chain MWD to give a larger proportion of very low MWT polymer. This can be understood as a consequence of the elevated termination rates for very small radicals.

Referring to figure 6-8, it is evident that experiment produced more high MWT material than could be predicted by simulation. So one result of allowing k_t to depend on chain length is that it causes the simulated MWD to be a slightly better fit to the experimental MWD. However the improvement was not substantial enough to be significant; the effect is merely noted because it is qualitatively as expected. As chain-length dependent termination has such a small effect, it will not be included in further modelling.

As an aside, it is interesting to note that although including a chain-length dependence in the termination rate coefficient only has a small effect, this effect is greater than in other PLP systems. The reason for this is clear: the characteristic chain length of dead polymer and therefore living radicals in this study is low: $L_0 = 20$ monomer units. Hence, as the rate of change in the microscopic termination rate constant in a chain-length dependent model (see equation 6.28) is greatest at low chain length, e.g., the difference between $k_t^{10,10}$ and $k_t^{11,11}$ is greater than the difference between $k_t^{100,100}$ and $k_t^{101,101}$, chain-length dependent termination should have a more noticeable effect in the present simulations than in ones with high values of L_0.

$$\frac{dk_t^{i,i}}{di} = -\alpha k_t^{1,1} i^{-(1+\alpha)} \tag{6.28}$$

Therefore, all the effects of chain-length dependent termination are expected to be enhanced the present system. However this remains to be thoroughly investigated.

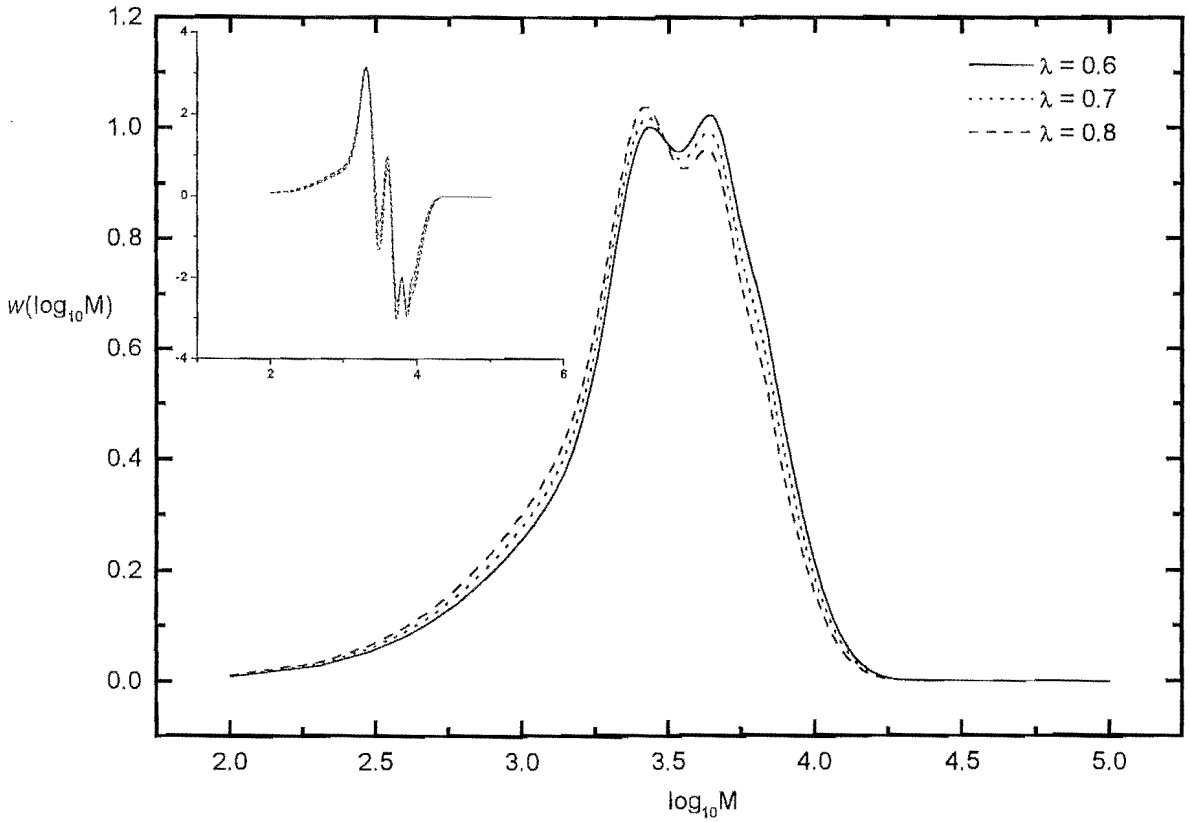

Figure 6-11: The effect of the proportion of termination by disproportionation on the GPC MWD distribution.

GPC Modeling: The Effect of λ on the GPC MWD

In this section I explore the effects of λ upon the dead chain MWD. This is an important investigation, for the fit between the simulated and experimental MWD has been used as the basis for extracting rate parameters assuming a value of λ. Thus if λ has a strong effect on the dead chain MWD, the rate parameters extracted could be incorrect.

Figure 6-11 contains a series of MWDs where only the ratio λ has been varied. From these MWDs it is clear that the ratio of λ does alter the shape of the MWD. In order to analyze how this impacts on the extraction of k_p, the derivatives of these distribution were taken (see

inlay, figure 6-11). The plots of these derivatives indicate that the position of the inflection point, and therefore the extracted value of k_p, is not affected by the ratio λ. The same is not true for the product $k_t\rho t_0$. The value of this product was obtained by fitting a simulation to the experimental MWD, where special care was taken to reproduce the relative peak heights of the primary peak and the first overtone. Figure 6-11 shows that the ratio λ affects the relative heights of these two peaks; therefore the ratio λ will to some extent affect the value acquired for the product $k_t\rho t_0$. To obtain the correct estimates of these two values, $k_t\rho t_0$ and λ, an iterative procedure is used. This involves fitting the GPC MWD to estimate $k_t\rho t_0$, then using this value to fit the ratio N_1/N_2 for λ (see below). The GPC MWD is then fitted again to obtain a value for $k_t\rho t_0$, this time using the new value for λ. This process was repeated until the values of $k_t\rho t_0$ and λ do not change significantly with successive iterations. The value $k_t\rho t_0$ given above is the best fit value as has been obtained by this procedure; similarly the value of λ below. In this way all the available MWD data has been used to obtain unique values of λ and $k_t\rho t_0$.

The above notwithstanding, it is noted that the GPC MWD could not be fitted with arbitrary variation of λ. For example, using $\lambda = 0$ did not enable the GPC MWD to be nearly as well fitted as achieved in figure 6-5. Thus modelling the GPC MWD in entirety does give some idea of the value of λ, and it was evident that the optimum fit of the GPC MWD was consistent with termination being predominately by disproportionation.

GPC Modeling: The Effect of Chromatographic Broadening on the GPC MWD

GPC is a size exclusion technique that suffers from chromatographic broadening. A GPC separates dead polymer chains on the basis of how long they take to elute through a chromatographic column. The large dead polymer molecules of a sample emerge from this column first, followed by the smaller dead polymer species. However, dead polymer chains of the same chain length do not all emerge at the same time. There are a large number of paths that a polymer molecule can take through a column, and each path takes a slightly different amount of time. The majority of paths that polymer molecules of the same chain length take through a GPC column require approximately the same elution time, with a few taking longer and a few taking a shorter time. The range of elution times for dead polymer of chain length i is well modeled by a Gaussian distribution. Importantly, there is overlap between the slowest times taken by

a polymer of one chain length and the fastest times taken by polymer chains of lower chain length. This means that GPC is unable to resolve the signals of individual chain lengths and a GPC MWD is said to contain chromatographic broadening.

Here a theoretical MWD (without chromatographic broadening) is broadened by transforming the concentration of dead polymer for one chain length into a Gaussian distribution. The contribution of the 'Gaussian tails' from other polymer chain lengths is then added in, i.e., the broadened signal at particular log i is equal to the sum of all the Gaussian portions that make a contribution to that log i. This procedure thus mimics what actually happens in a GPC. This procedure for modeling chromatographic broadening has been described in detail by Lammel et. al.[12] Figure 6-12 shows how chromatographic broadening changes the shape of the dead polymer MWD. The notation used to define the amount of chromatographic broadening is the same as that used by Lammel et. al.[12] They define $\sigma_v b$ as the degree of broadening, or equivalently, the width of the Gaussian that describes the GPC signal for a single polymer chain length. The two components of this variable, σ_v and b, are obtained experimentally: σ_v is a function of the GPC setup, and b is calculated from the slope of the log-linear molecular weight calibration, i.e., it is defined via equation 6.29. In this expression y is the elution time (or equivalently, the elution volume).

$$log_{10}M = a - by \tag{6.29}$$

It is important to stress that it is the individual $w(\log_{10} M)$ values that are transformed into Gaussians.

Chromatographic broadening reduces the definition of the dead chain MWD. It is clear from 6-12 that increasing the amount of broadening ($\sigma_v b$) causes features such as the primary peak and overtones to become less well defined. In general, chromatographic broadening also causes the overall width of the distribution to increase slightly. Although this brings simulated and experimental MWDs into closer agreement, the change is very small. Note that typical experimental values of the broadening parameter have been used: $\sigma_v b = 0.05$ corresponds to a set-up with very little broadening, while $\sigma_v b = 0.1$ is about as high as one would expect.[12]

In their study, Lammel et. al.[12] noted that chromatographic broadening alters the posi-

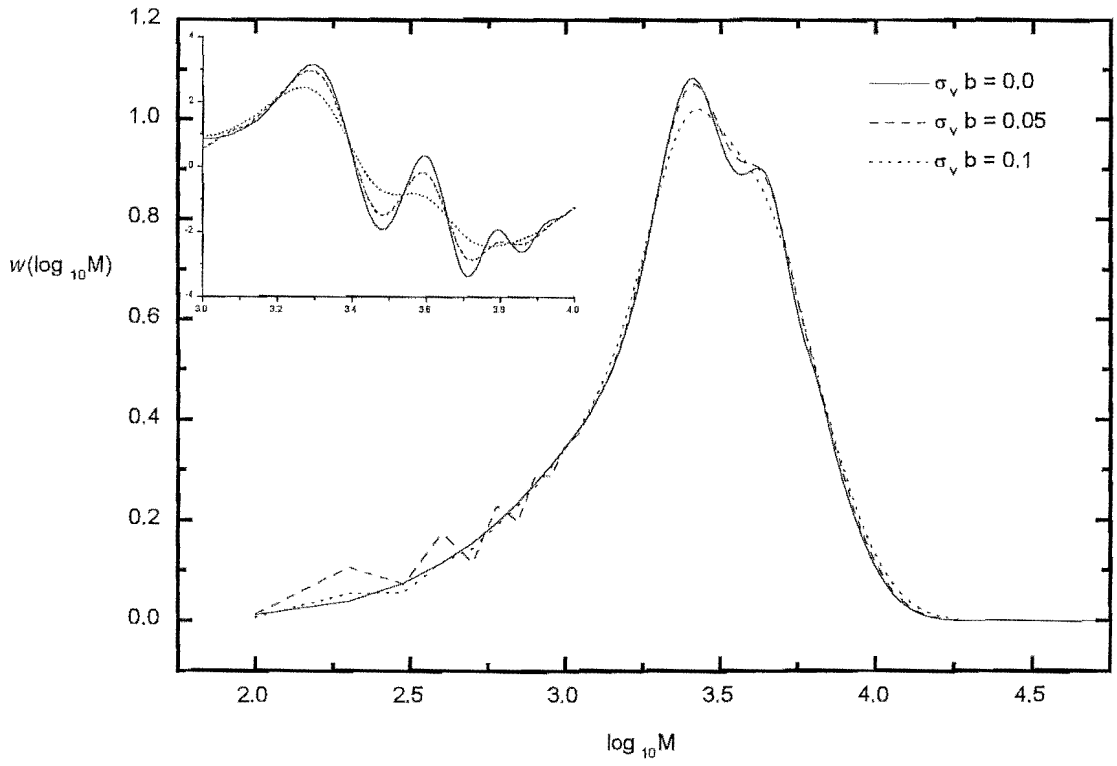

Figure 6-12: Chromatographic Broadening: Three MWDs are given where various amounts of broadening have been applied. Rate parameters are the best fit values of figure 6.5. The inlay gives the MWD derivative.

tions of all low molecular weight inflection points. The derivative inlay included in figure 6-12 confirms that chromatographic broadening moves the position of the low molecular weight side inflection points to lower MWT. Thus chromatographic broadening causes the value of k_p calculated from the inflection point to underestimate the actual value of k_p. Again the magnitude of this effect is small; here it causes approximately 5% error.

GPC Modeling: Comparison of Theory and Experiment

It is clear from figure 6-5 that the agreement between theory and experiment is excellent everywhere except in the high MWT region. In fact this agreement between simulation and exper-

iment is as good as has ever been obtained for PLP. In particular, the simulated MWD fits the experimental MWD very well in the region that contains the primary peak and the first overtone. This is important as these are features that are used to extract rate parameters, for example k_p.

The failure of this kinetic model to fit the entire MWD suggests that another effect, be it another polymerization process or an artifact of the measurement of the MWD is important to this system. An obvious candidate is spontaneous thermal initiation before or after the PLP. Spontaneous thermal initiation involves the thermal decay of initiator or the thermal activation of monomer to produce species that can initiate free-radical polymerization. Because the rate of initiation is low, high MWT is produced, in accord with experimental results here. An obvious difficulty with this suggestion is that the rate of thermal initiation in methyl methacrylate is very low and thus it will lead to the production of only a very small amount of polymer. However, less polymer is produced in the present PLP than in most other PIPs. This is because of the low temperature (0.2°C) and thus low k_p.

The anomalous high MWT polymer could also be an artifact of sample treatment before and after the PLP. Radical activity was quenched following the polymerization by the precipitation of polymer in hexane and polymerization was prevented before PLP by inhibitor. Neither of these methods are 100 % effective, and each could conceivably lead to artifacts. Finally, it is worthwhile noting that this problem of anomalous high MWT material is common to all PLPs, as a perusal of all modelling studies to date revealed.

6.2.4 Theoretical Foundations for N_1 / $(2N_2)$ Plots

The idea at the heart of this study is that information about the termination mechanism can be extracted from the MALDI-MS MWDs. The kinetics of this system demand that termination by the combination mechanism will produce chains with two initiator-derived endgroups, while the disproportionation mechanism will produce chains with only one of these endgroups. Therefore, it seems that if the ratio of polymer chains with one endgroup to those with two endgroups was evaluated, that information about the termination mechanism could be obtained. A problem remains though: how does the termination mechanism affect the ratio of chains with one endgroup to those with two endgroups? And what other factors influence this ratio?

To investigate this, an expression is derived for the ratio N_1 / $(2N_2)$ in a steady-state polymerization. I then move on to consider pseudo-steady state conditions. Note that we take the ratio of N_1 / $(2N_2)$ rather than N_1/N_2 to account for the fact that the disproportionation mechanism produces two dead polymer chains, while combination produces only one. The idea is that N_1 / $(2N_2)$ might of itself give some sort of idea of the value of $\frac{k_{td}}{k_{tc}}$.

The Ratio N_1 / $(2N_2)$ in a Steady-State Polymerization

By definition a steady-state polymerization has a constant rate of initiation, R_{init}, and a constant total concentration of all radical species that is equal to $\sqrt{R_{init}/2k_t}$. The steady-state dead polymer chain-length number distribution for chains with one initiator derived group of chain length i , i.e., chains formed by disproportionation, is

$$N_1(i) = F_n(1-s)s^{i-1} \tag{6.30}$$

It is assumed here that there is no dead chain formation by transfer. The number distribution of dead polymer species of chain length i with two initiator-derived endgroups, i.e., chains formed by combination, is

$$N_2(i) = (1-F_n)(1-s)^2(i-1)s^{i-2} \tag{6.31}$$

F_n is the number fraction of dead chains formed by disproportionation (see equation 6.34), i.e., it ensures that equations 6.30 and 6.31 are weighted correctly relative to each other. These two expression can be used to derive an expression for the ratio N_1 / $(2N_2)$ for chain length i:

$$\frac{N_1}{2N_2}(i) = \frac{F_n s}{2(1-F_n)(1-s)(i-1)} \tag{6.32}$$

Here

$$s = \frac{k_p \mathrm{M}}{k_p \mathrm{M} + 2k_t \mathrm{R}} \qquad \text{where } \mathrm{R} = \sum_{i=0}^{\infty} \mathrm{R}_i^1 \tag{6.33}$$

and,

$$F_n = \frac{k_{td}}{k_{td} + \frac{1}{2}k_{tc}} \tag{6.34}$$

The parameter s is recognizable as the probability of propagation. Therefore, if equations 6.33 and 6.34 are substituted into equation 6.32, and R is replaced by $\sqrt{R_{init} \ / \ 2k_t}$

$$\frac{N_1(i)}{2N_2(i)} = \frac{k_{td}k_pM}{k_{tc}(i-1)\sqrt{R_{init}\ 2k_t}} \tag{6.35}$$

While it is clear from equation 6.35 that $N_1 \ / \ (2N_2)$ is indeed related to $\frac{k_{td}}{k_{tc}}$ as anticipated, it is also clear that $N_1 \ / \ (2N_2)$ depends upon several additional rate parameters. Moreover, equation 6.35 also depends on the chain length of the dead polymer chain. i.e.,

$$\frac{N_1(i)}{2N_2(i)} \propto \frac{1}{i-1} \tag{6.36}$$

This expression says that the proportion of dead chains with two initiator endgroups increases with chain length. This means that the proportion of chains formed by combination is greater at high MWT than it is at low MWT. To understand this, consider the ways that a dead chain of a particular chain length can be formed via the combination termination mechanism. There are far more ways that a chain containing 100 monomer units can be formed than there are ways that a chain containing 10 monomer units can be made by the same mechanism. However, the number of ways that a chain can be formed by the disproportionation termination mechanism is independent of the polymer chain length. This is a statistical effect that is a result of the kinetics of the two termination mechanisms.

In short, combination favors formation of long chains, hence the dependence of equation 6.36. Note that equations for the case of chain transfer occurring have also been derived (then one additionally has $N_0(i)$), but they are not presented here because of their added complexity and because they are not relevant to the present experimental results (see earlier discussion).

The Ratio $N_1 \ / \ (2N_2)$ in an Intermittently-Initiated Polymerization

The radical and dead polymer chain distributions for an intermittently-initiated polymerization are significantly more complicated than those for a continuously-initiated polymerization. To avoid introducing the complicated mathematics that are required to describe these distributions, we take a qualitative approach to exploring the way that the $N_1 \ / \ (2N_2)$ plots depend on various rate parameters.

Given this, it is reasonable to expect N_1 / $(2N_2)$ for an intermittently-initiated system should show the same dependencies as a continuously-initiated polymerization. Figure 6-13 contains three plots of the simulated ratio N_1 / $(2N_2)$ against chain length for a PLP. Each line shown in this plot is calculated from a system with a different rate of initiation. It is clear that as the rate of initiation increases, N_1 / $(2N_2)$ decreases. This is trend is predicted by equation 6.35. Calculations have also been performed where each of the rate parameters contained in equation 6.35 was varied. These calculations confirm that the ratio N_1 / $(2N_2)$ has the same dependencies in a PLP as it does it a continuously-initiated polymerization.

Nonetheless, there are significant differences between the two plots. Whereas the N_1 / $(2N_2)$ against chain length plot for a steady-state polymerization decays with increasing chain length, each line in figure 6-13 is punctuated by periodic increases. At certain chain lengths (typically multiples of L_0) the value N_1 / $(2N_2)$ increases before continuing to decay. In summary, the PLP results show the same overall trends as for steady-state, but there are periodic perturbations in the PLP results.

To understand the reason for these increases in N_1 / $(2N_2)$, the position of these changes were analyzed. It was clear from this that termination by disproportionation becomes more important at chain lengths that are multiples of the characteristic chain length, i.e., jL_0; where j is a counting number. The reason for this is clear: when a laser pulse arrives the sharp increase in the number of small radicals means that termination is dominated by termination involving short radicals, whether it be termination between small radicals or between a small radical and an existing longer radical chain. As most existing longer radicals have chain lengths of $j\mathrm{L}_0$, a lot of dead polymer of chain length jL_0 is added to the dead polymer chain-length distribution. Thus there is a surge in production of species of chain length jL_0, due to disproportionation. However the same surge in the combination rate gives longer species, and so N_1 / $(2N_2)$ is boosted around jL_0. In some ways this is as if radicals of chain length jL_0 are created by steady-state initiation, and N_1 / $(2N_2)$ decays for i beyond this lengths, much as given by equation 6.36.

An interesting (and understandable) result of this is that the inflection points of the low molecular weight sides of the peaks in the N_1 / $(2N_2)$ can be used to extract k_p in the standard way, according to $L_i = (i-1)k_\mathrm{p}\mathrm{M}t_0$. This is evident from figure 6-13.

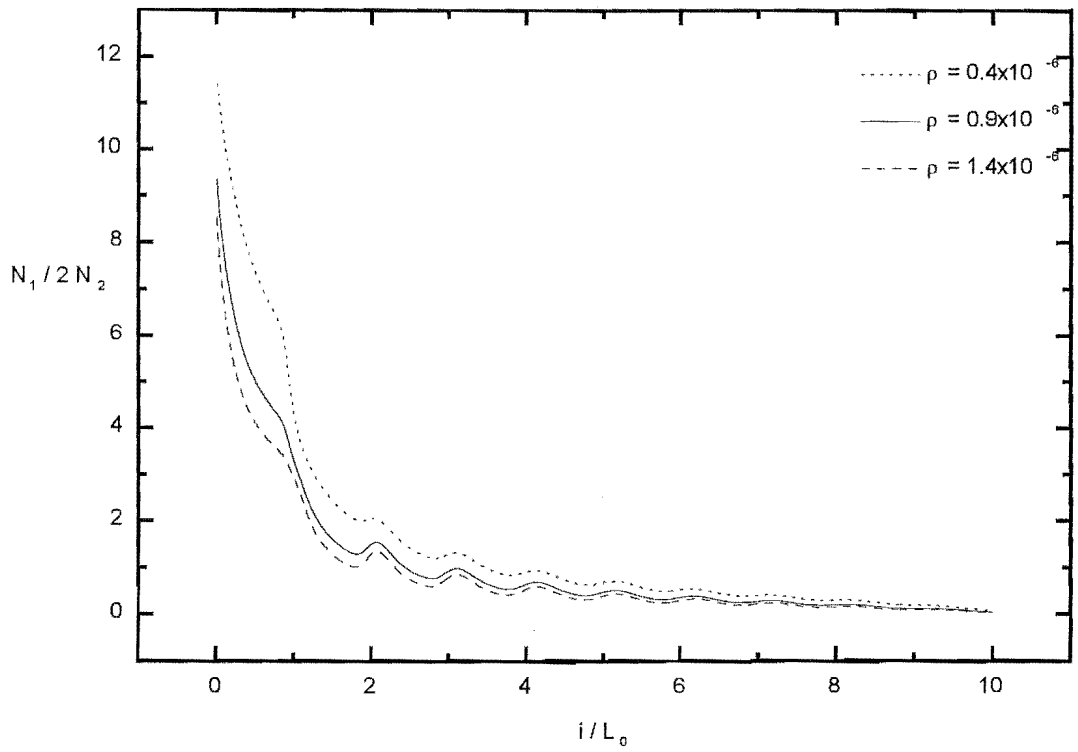

Figure 6-13: PLP simulation results for $N_1/(2N_2)$ versus i/L_0. Rate Parameters: M = 10.0 mol.L^{-1} otherwise as per figure 6.5.

Two points must be stressed about the relationship between N_1 / $(2N_2)$ and λ. Firstly, the relationship between these two ratios in a PLP system is complex. It is not possible to calculate the ratio of N_1 / $(2N_2)$ for any particular chain length and use this as λ. To gain an accurate value λ a numerical simulation must be performed and the value of λ extracted by fitting simulation to experimental data.

Secondly, N_1 / $(2N_2)$ depends on several rate coefficients in addition to λ. Thus the values of these rate coefficients have to be known before λ can be extracted. Fortunately, the comparison of simulation with the GPC (and potentially the MALDI-MS) MWD allows all of the rate parameters involved in this relationship (see equation 6.35) to be calculated. The extraction of these parameters was described above.

6.2.5 MALDI-MS Modeling

Having established the qualitative relationship between N_1 / $(2N_2)$ and λ, and having extracted the values of all of the necessary rate parameters, λ can be determined.

MALDI-MS Modeling: The Value of λ

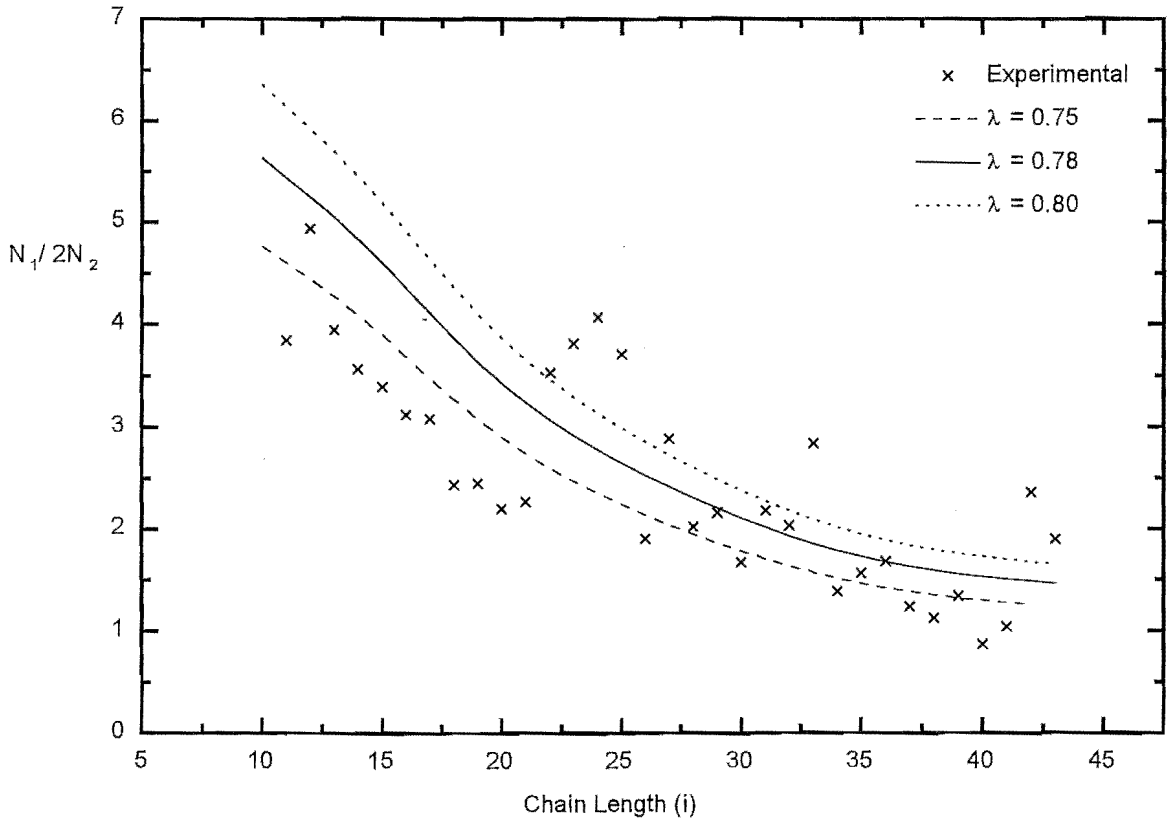

Figure 6-14: Best fit of simulated $N_1/(2N_2)$ curves to experimental data. Rate Parameters: as per figure 6.5.

Figure 6-14 contains the experimental ratio, N_1 / $(2N_2)$ and three simulated curves. The three curves given in this plot are the best fit to experiment (solid line) and the upper and lower limits for values of λ respectively (dotted and dashed lines). From figure 6-14 it is clear that

the best fit value for λ is 0.78 ± 0.03. This means that k_{td} / $k_{tc} = 3.5 \pm 0.1$, i.e. the termination mechanism of MMA at 0.2°C is dominated 3.5 to 1 by the disproportionation mechanism. This value for the ratio of the rate constant for termination by disproportionation to that for combination is higher than other values for this ratio in the literature.[34][51] Although there are few studies for temperatures as low as in this experiment, the Arrenhius plot of these high temperature values predicts a value of k_{td} / k_{tc} equal to at most 1.5 for MMA at 0.2°C. Thus the value I have calculated suggests that termination by disproportionation is a lot more prevalent than has been previously thought. As already discussed, it is believed that the present study overcomes limitations of previous studies, and the presently obtained value of λ is the best yet available.

Several intrinsic properties of the radical, as well as a number of physical properties of the polymerizing system, are known to affect the value of λ. The mechanism of termination by disproportionation most likely involves the abstraction of a β-hydrogen. Hence the availability of these atoms influences the value of λ. Although MMA has three such hydrogens, there is no evidence to suggest the propensity for two radicals to terminate by disproportionation is related to the number of β-hydrogens, i.e., that anything other than statistical factors are involved.[34] For some radicals the value λ can be rationalized in terms of the greater influence of steric factors on the combination mechanism. This has been shown by a good correlation between $\log(k_{td}/k_{tc})$ and the Taft steric factors (an empirical measurement of substituent 'bulkiness').[34] The MMA radical is a tertiary radical that has two reasonably sized groups adjacent to the radical center (see figure 6-15). However, modelling studies performed by Fischer et. al.[48] suggest that steric factors do not significantly affect the value of λ: some tertiary radicals undergo combination in preference to disproportionation, e.g., cyanisopropyl radicals.

A possible explanation for the prevalence of disproportionation in MMA is based on the nature of the radical-radical encounter complexes that lead to each type of termination reaction. There are many more ways that two radicals can encounter that will lead to the abstraction of a $\beta-$ hydrogen than to them combining. Thus it may be that for MMA the reaction barrier for disproportionation is so small that radicals will always disproportionate if they encounter in such a way that disproportionation is possible, i.e., the half-life of the encounter complex with a geometry that can lead to disproportionation is less than the time taken for reorientation. For

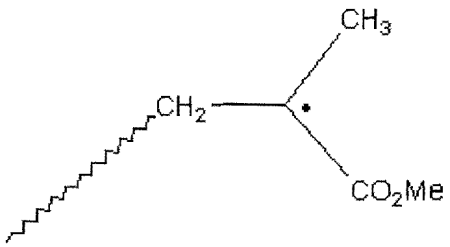

Figure 6-15: The radical center of a poly-methyl methacrylate chain.

this argument to hold there can not be a significant barrier to disproportionation. However, there can be a barrier and that barrier can be greater than that for termination by combination, and yet disproportionation still be the dominant termination mechanism.

There is some experimental evidence to support this proposition. Fischer et. al.[19] have shown that λ is strongly dependent on viscosity, where the proportion of termination that occurs by the disproportionation mechanism increases with viscosity for some monomers. They go on to rationalize this using a similar argument to that used above. They show using space filling models that the shape of the monomer influences how easy it is for the encounter complex to rotate. For example, they show that the shape of the tert-butyl radical is such that for the majority of encounter complex geometries it is more difficult for radicals to rotate into the geometry that allows combination than into that for disproportionation. This effect is accentuated by an increase in viscosity: at higher viscosity it becomes more difficult for the encounter complex to rotate. Thus the reorientation to a geometry where combination can occur becomes increasingly more difficult (than that required for disproportionation). Hence the proportion of termination by disproportionation increases.

This supports the argument given to explain a value of $\lambda = 0.78 \pm 0.03$ above as it shows that the value of λ can be successfully rationalized in terms of the possible encounter complexes that lead to each termination reaction. Interestingly, Fischer also found $k_{td}/k_{tc} \approx 4$ for t-butyl radicals at the viscosity of the present MMA experiments.[19] This affords confidence in the values of λ found here.

Note that this argument is not damaged by experimental studies that show that λ is not correlated to the number of β-hydrogens[34], for it is not necessarily the case that the presence

of more β-hydrogens means that there are more encounter complexes that lead to disproportionation.

6.2.6 Discussion of Possible Problems with Interpretation of Data

As the methodology used here is novel we will offer several criticisms of this method. These fall into two categories: misleading experimental results and flawed mechanistic assumptions.

Misleading Experimental Results

There are several ways that systematic errors in the MALDI-MS experimental data could affect the conclusions drawn in this study. Although the comparison of the MWDs measured by GPC and MALDI-MS has shown that these distributions agree well, it is possible that this comparison missed significant but subtle differences that could bias these results.

Chain-length Dependence in the Ionization and/or Desorption Process. The ionization and subsequent desorption of polymer from the matrix are processes fundamental to MALDI-MS.[14] If these processes depended on the chain length of the dead polymer chain involved, they could lead to a MALDI-MS MWD that was biased in favor of high or low MWT polymer. Fortunately, this type of bias would not affect the mechanistic conclusions drawn in this study. The conclusions drawn here are based on the ratio of N_1 to N_2. The value of this ratio would not be affected by chain length effects that influence N_1 and N_2 to the same extent, because the ratio N_1 to N_2 would still be accurate.

Endgroup Dependence in the Ionization and/or Desorption Process. The possibility exists that the desorption and/or ionization of polymer species that occurs during the measurement of a MALDI-MS MWD could depend upon the number of initiator-derived endgroups in a polymer chain. If these initiator-derived endgroups retarded the rate of ionization and/or desorption, then the MALDI-MS would contain less polymer chains with two cyanoisopropyl residues than it 'should'. This could mean that the value of λ extracted from a MALDI-MS MWD would be biased in favor of the disproportionation mechanism. However, this effect would almost certainly be more important for short, than long dead polymer chains, i.e., an

endgroup has less influence on a large molecule than a small molecule. Fortunately this means that the method used here is not sensitive to bias of this type. In this study we have used only the central region of the MWD. It is reasonable to assume the dead polymer chains in this region are large enough to be unaffected by error of this type.

Note that if the presence of these initiator-derived endgroups enhanced the rate of desorption and/or ionization, then the amount of termination by the disproportionation mechanism would be underestimated. In fact it is thought more likely that if anything the endgroups will enhance the ionization/desorption.

Flawed Mechanistic Assumptions

The methodology used to extract the ratio λ is model dependent. There are a number of assumptions that have been made in the process of extracting λ, that if shown to be false, could affect the value of the ratio λ. In this section we will discuss the appropriateness of several of these assumptions and explore what effect if any they would have on λ, if shown to be false.

Chain Transfer to Monomer It has been assumed throughout this study that chain transfer does not significantly affect the kinetics or MWDs. This assumption is based on two pieces of information: the rate constant for transfer to monomer measured for this system in separate studies, and the absence of dead polymer chains with no initiator-derived endgroups in the MALDI-MS MWD. If this assumption was shown to be invalid, i.e. it was shown that chain transfer processes were important, then the information extracted about the termination mechanism would also be invalid. Chain transfer alters the relationship between λ and the ratio of N_1 to N_2. This is clear from the population-balance differential equations for both systems, equations 6.6 - 6.16 as compared to equations 6.17 - 6.22. Whereas a model that excludes chain transfer is described by a set of population-balance differential equations where only termination by combination produces chains with two initiator-derived endgroups and disproportionation dead polymer chains with one endgroup, the same is not true if chain transfer processes are included. In this case, the combination termination mechanism can produce dead polymer chain with either one or two initiator-derived endgroups. However, the presence of

chain transfer does not make the methodology used here invalid, i.e., fitting a simulated curve to the ratio of N_1 to N_2 will still give information about the termination mechanism.

It does mean, though, that the rate constant for transfer must be known. Therefore, although the magnitude of chain transfer to monomer processes does affect the ratio λ extracted by the method used in this study, the evidence that the contribution of chain transfer to monomer process is very small justifies its exclusion.

Primary Radical Termination There is a fear that if the termination in this system was dominated by the termination of a macroradical and an initiator fragment, i.e., primary radical termination, that the value of λ extracted in this study would not be valid for 'normal' radical-radical termination. This concern is based upon the idea that the mechanism of termination for a primary radical and a macroradical could be different from that of two macroradicals. To investigate this, simulations were performed to measure the proportion of termination that involved a primary radical. These simulations counted all of the dead polymer formed by termination between a primary radical and some other species. These calculations were run with and without the chain-length dependent model for termination ($k_t^{1,1} = 1 \times 10^9$; $\alpha = 0.5$). In both cases the proportion of termination that involved primary radicals was small (7% in the strong chain-length dependent case and 1% in the chain-length independent case). Therefore, I conclude that it is unlikely that primary radical termination biases my results.

In conclusion then, the mechanistic information extracted by the method used in this work is insensitive to the major experimental errors or dependencies of MALDI-MS. In addition to this, the processes used to extract the value λ avoids common mechanistic flaws by fitting the ratio of N_1 to N_2 with a kinetic model where the rate parameters have been extracted from a series of modeling studies of the GPC MWD. I assert that this study has unambiguously obtained the value of the ratio λ, arguably the most accurate study to date.

6.2.7 MALDI-MS: Further Possibilities

This work has illustrated the power of MALDI-MS in concert with careful modeling studies as a method for elucidating detailed kinetic information. I believe that power of MALDI-MS, primarily in its ability to resolve polymer species that differ by very small masses, is yet to be

fully utilized.

Many criticisms have been leveled at MALDI-MS, of which the majority are concerned with the dependence of the ionization and desorption processes on the chain length and number of endgroups of the polymer samples. While these concerns are legitimate, this study has shown that careful modeling studies and comparisons with more firmly established techniques, such as GPC, mean that MALDI-MS can be used with some confidence. There are several examples of types information that could be obtained from MALDI-MS MWD; I now wish to explore a few.

The Mechanism of Disproportionation The power of MALDI-MS apparatus has increased since the experimental work modelled in this study was undertaken. Currently, many MALDI-MS apparatus are able to separate dead polymer chains that differ in mass by as little as 1 Dalton. This resolution will allow MALDI-MS to resolve out the two products of disproportionation (see figure 6-1): the saturated and the unsaturated dead chains. A study could be performed to investigate the mechanism of disproportionation, to confirm that these two products are present in equal numbers, as is predicted by the mechanism shown in figure 6-1.

The Mechanism of Chain Transfer MALDI-MS could be used to study the mechanism and the rate coefficient for chain transfer to monomer. It is clear from differential equations 6.6 – 6.16 that dead polymer chains with no initiator-derived endgroups can only be present in a MWD if chain transfer is occurring. Thus simulation studies that model the ratio of dead chains with no initiator-derived endgroups (N_0) to those with one initiator derived group (N_1) would produce values of the rate coefficient for transfer. Moreover, the transfer mechanism is believed to involve the transfer of a hydrogen from the α-methyl group of a macroradical to MMA monomer (see figure 6-16 for one of the two possible mechanisms). This pathway is believed to be favored because it produces an allylic radical. Thus the transfer reaction produces a dead polymer chain with an initiator endgroup and a unsaturated endgroup. The ability of MALDI-MS to resolve dead chains that are very similar in mass could possibly be used to study this mechanism.

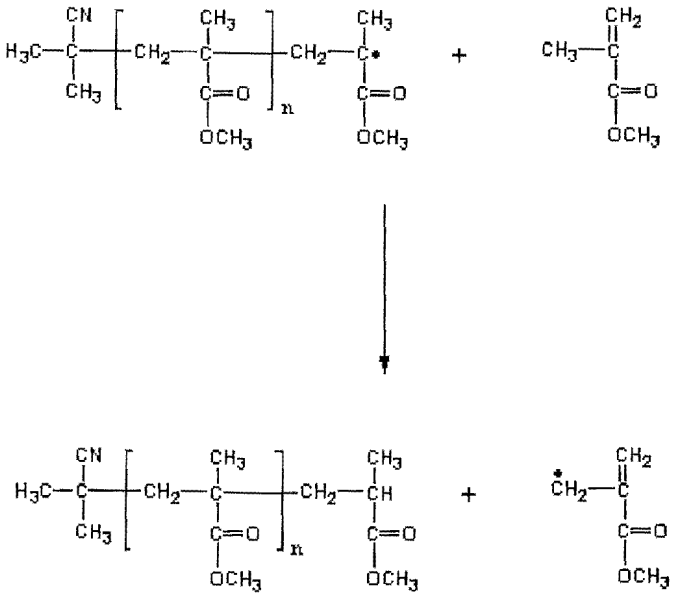

Figure 6-16: One of the two possible mechanism for chain transfer to monomer by a poly-methyl methacrylate radical.

6.2.8 New Theory

In this section ideas are developed to explain the lack of definition of the high order overtones in the simulated MWDs. An explanation is given for the difference in the appearance of the simulated MWDs shown in figure 6-17. It is important to note that both of these MWDs are simulated, not experimental. In both cases effects such as chromatographic broadening have not been added. In one case essentially the best fit parameters from figure 6-5 have been used, except $k_p M t_0 = 17$ is a bit lower than the best fit value of about 20. In the second simulation only $k_p M t_0$ has been changed, being increased by a factor of 10. It is evident that this results in much better resolution of the peaks.

In order to understand the source of this effect, it is necessary to look at the radical chain-length distribution. It is well known, and already mentioned previously, that the radical chain-length distribution for an intermittently-initiated polymerization consists of a number of equally spaced Poisson distributions; a typical example is given in figure 6-18 (solid line). The first radical 'wave' is a Poisson distribution consisting of radicals that were initiated by the last burst of initiation, while subsequent 'waves' correspond to radicals that have survived for successive

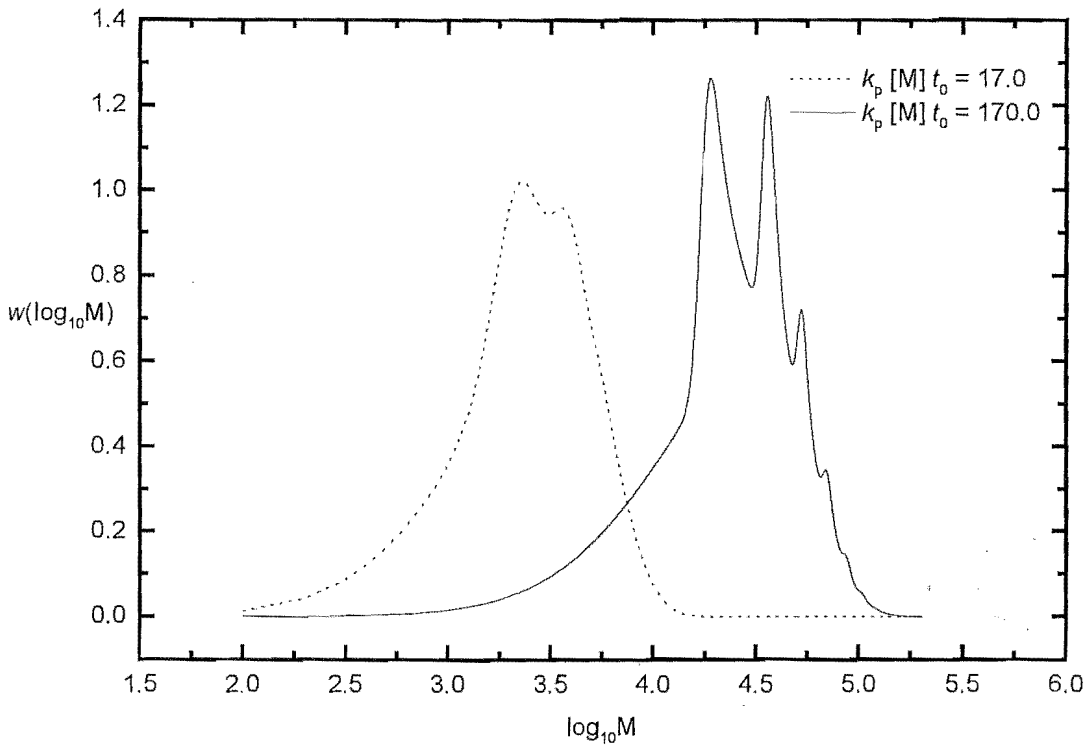

Figure 6-17: Two simulated MWDs based upon the default rate parameter set. The only difference between these two distributions is that indicated.

numbers of laser pulse periods. For example, the second Poisson distribution, counting from the low MWT, has survived one complete laser pulse period, the third Poisson distribution two pulse periods, and so on. Naturally, the heights of these Poisson distributions decrease as the length of time these radicals have lived increases as a result of radical annihilation processes, i.e., bimolecular termination (and chain transfer if it occurs). It is evident that quite a large fraction of radicals terminate between pulses in figure 6-17. In addition to this effect of termination, the absolute width of the distribution increases with time which also results in a decreasing height. This broadening is a result of the stochastic nature of the propagation process. The chain length to which radicals have grown after a certain period of time is a random variable with a Poisson distribution about the most probable chain length. The most probable chain

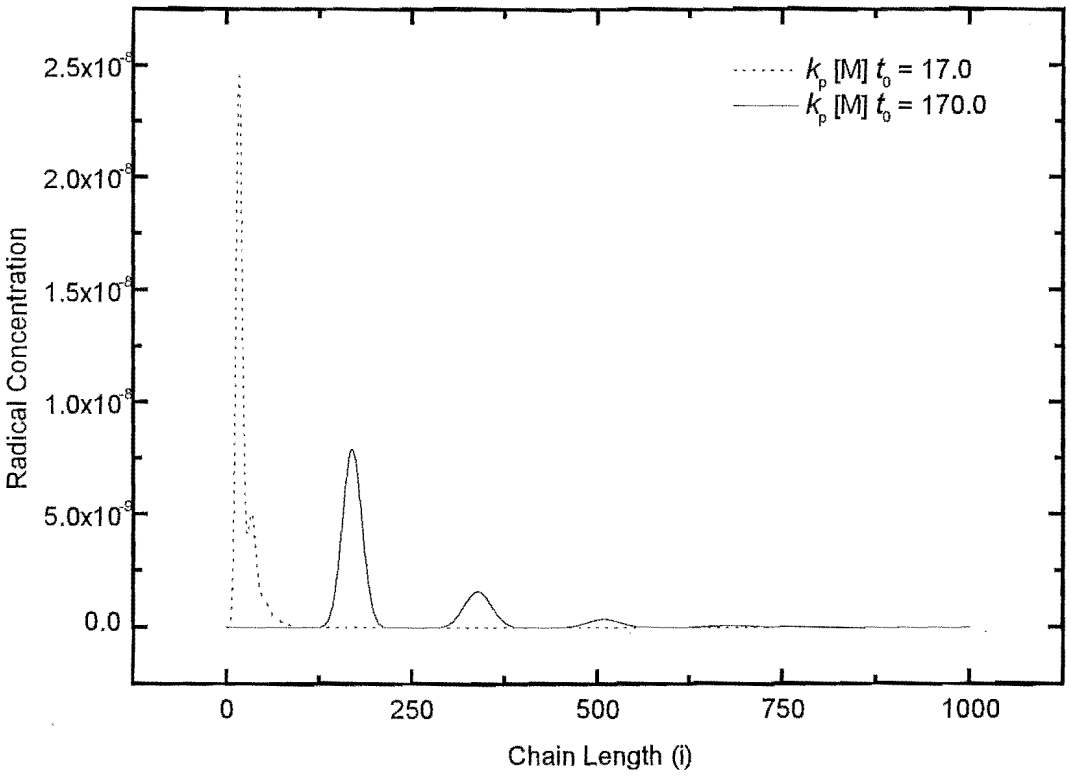

Figure 6-18: Radical chain-length distributions from simulations of figure 6-17, at times just prior to the arrival of a pulse.

length that a radical will grow to in j initiation periods is equal to $L_j = jk_pMt_0$. Moreover, the width at half height of this Poisson distribution is equal to $\sqrt{k_pMt}$. This means that at any given time most radicals are approximately the same chain length, while the probability of a radical being of any other chain length decreases the difference between that chain length and the most probable chain length increases.

It is clear from figure 6-18 that the key difference between these two radical chain-length distributions is the separation of the radical waves. In one case the difference in chain lengths between successive radical waves is less than the width of those waves, while in the other case the separation (in chain length) between successive Poisson distributions is much greater than

their width. This means that in one case all of the radical waves are resolved, while in the other case they are overlapping.

The resolution of the living radical chain-length distribution is directly correlated to the resolution of the dead polymer chain MWD. If the living radical chain-length distribution consists of a single peak then the dead polymer molecular weight distribution will only consist of a single peak. If on the other hand, the living radical chain-length distribution consists of several well resolved peaks then the dead polymer MWD is likely to also contain corresponding peaks. Note the dead chain MWD will always be broader than the living radical distribution, as it is a cumulative distribution and also because of the nature of the combination termination mechanism. Hence, the reason why the features of the 'unresolved' dead chain MWD in figure 6-17 (dotted line) are not like those of the 'resolved' MWD in figure 6-17 (solid line) is because the radical 'waves' in the living radical chain-length distribution are poorly separated in the former case.

This means that if one wants well-defined overtones in the dead polymer chain MWD, then the living radical chain-length distribution must contain a series of well separated radical waves.

Here I will develop a criterion that can be used to assess whether the radical waves in a PLP living radical chain-length distribution will be well separated or not. This criterion is based upon the empirically based assertion that if two radical waves are separated by a chain length greater than the sum of the respective widths at half height, then the resulting peak will be well-resolved. Moreover, as the absolute breadth of a radical wave increases as time passes, I use the time right before the arrival of the next pulse as the point where this criteria is applied, i.e., the time when these waves are broadened by the greatest amount. This leads to expression 6.37. This expression says that radical wave j is well resolved if the sum of the width at half height of wave j and $j+1$ is less than the separation of radical waves.

$$\sqrt{jk_{\mathrm{p}}\mathrm{M}t_0} + \sqrt{(j+1)k_{\mathrm{p}}\mathrm{M}t_0} < k_{\mathrm{p}}\mathrm{M}t_0 \tag{6.37}$$

Hence,

$$k_{\mathrm{p}}\mathrm{M}t_0 > 2j + 1 + 2\sqrt{j(j+1)} \tag{6.38}$$

Table 6.1 contains the minimum values of $k_{\mathrm{p}}\mathrm{M}t_0$ that must be used to ensure the resolution

Resolved Pulse	Min. k_pMt_0
1	5.8
2	9.9
3	13.9
4	17.9
5	22.0
6	26.0

Table 6.1: Table of minimum values for mean number of monomer units that a chain must grow in a dark time to ensure resolution of a particular pulse.

of a particular peak. It is clear from this table and equation 6.38 that the value of k_pMt_0 that is required increases as the number of peaks to be resolved increases. Moreover, it is also clear that the limiting values of k_pMt_0 are far less than those typically used in PLP experiments. Nonetheless, this does impose a limitation on the values of M and t_0 that can be used with a particular monomer. Note that this limitation can become important with slowly propagating monomers such as $\alpha-$methyl styrene. In the present experiments $k_pMt_0 \approx 20$, and indeed, only the first two peaks in the GPC distribution are resolved. Table 6.1 predicts that the first four peaks should be resolved. However, not only is criterion 6.37 overly charitable, but also ignores SEC broadening. So in fact the theory developed here is quite a good guideline.

6.3 Visible Light Pulsed-OPO-Laser Polymerization at 450 nm Employing a Bisacylphosphine Oxide Photoinitiator

The second section of this chapter concerns the modeling of a PLP system where a novel initiator was used. The population-balance differential equations that characterize this kinetic system are more complex than those for the standard kinetic model. These simulations were performed using the simulation strategy developed in this thesis. This strategy allowed accurate modelling to be performed in a minimal period of time.

6.3.1 Introduction

The use of PLP along with a method of obtaining the MWD of dead polymer chains (described in chapter one) is simple and well tested. However, this does not mean that this method is not without difficulties.[8] A major difficultly is that standard size exclusion (SEC), for example

GPC, analysis relies on calibration with polymer standards. Another limitation of the PLP-SEC technique is imposed by the use of a fixed UV wavelength generated by a pulsed laser. The wavelengths most commonly used are 355 nm as the third harmonic from a Nd:YAG laser, 351 nm from an excimer laser, or 308 nm, also from an excimer laser. These wavelengths preclude a number of important monomers (e.g. N-vinyl carbazole and many substituted styrenes) from analysis as the monomers themselves absorb strongly at these UV wavelengths, and thus the generation of primary radicals from photoinitiators is undermined. It is therefore of interest to overcome this limitation. Two options can be taken: (1) The use of a photoinitiation system which operates at the second harmonic of the Nd:YAG laser, 532 nm; or (2) The use of a tunable pumped laser operating at longer wavelengths, e.g. 450 nm, together with an appropriate photoinitiator system.

The work detailed represents an attempt to overcome the problem caused by the absorption of laser light by monomer using the second of the two approaches mentioned above. A previously untried photoiniator is used with a tunable pumped laser to generated primary radicals in a PLP experiment.

The most logical choice of photoinitiator for PLP is one that undergoes an α-cleavage (type 1) mechanism, as there is no requirement for electron transfer or abstraction reactions in the PLP initiation process (in fact such processes may disturb a PLP by not giving fast initiation). So in this work a phosphine oxide photoinitiator was chosen for study as such an initiator can be expected to deliver polymerizing radicals both rapidly and simply at 450 nm. A Nd:YAG laser pumped oscillator/power oscillator (OPO) system was selected for generating the pulsed light. This contrasts with cheaper alternatives such as a Raman shifter or dye lasers, these being unable to deliver sufficiently high laser powers for optimal PLP experiments (a low radical flux is usually undesirable[8][5]).

6.3.2 Results

Here a brief discussion will be given of the MWD obtained from this polymerization. For a detailed description of the experimental setup refer to Rees et. al.[44]

Homopolymerization of Methyl Methacrylate and Styrene

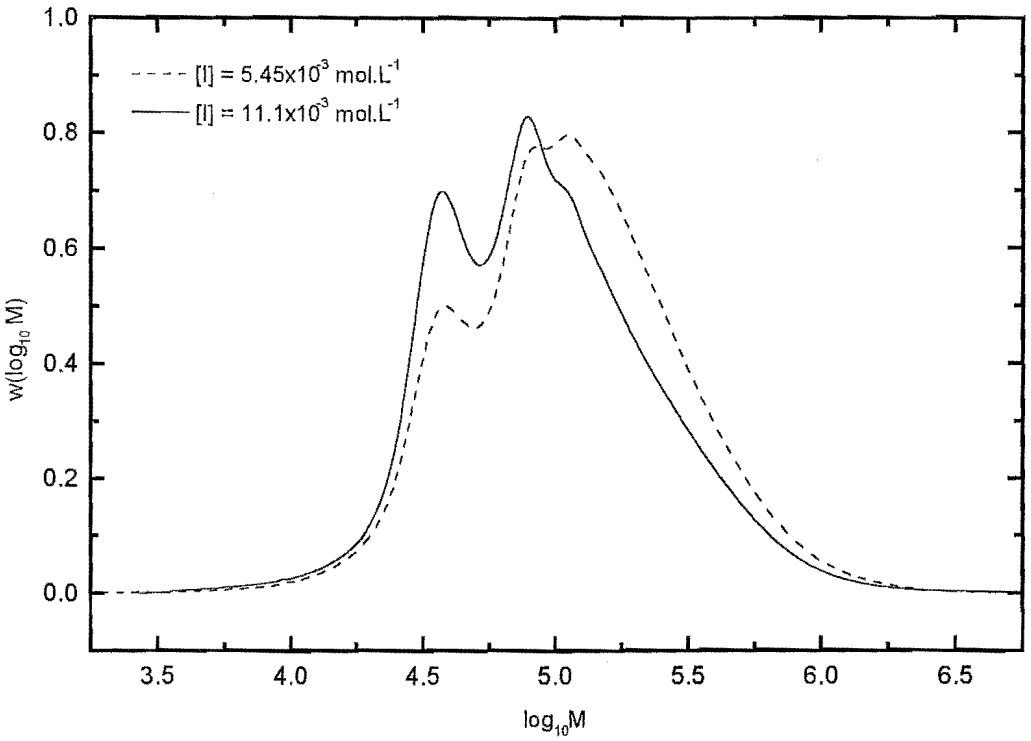

Figure 6-19: The MWD for the PLP of MMA for a range of BAPO concentrations.

The monomers methyl methacrylate (MMA) and styrene (STY) were polymerized with the photoiniator initiator bis(2, 6−dimethoxybenzoyl)−2, 4, 4− trimethylpentylphosphine oxide (BAPO) at 450 nm, 10 Hz and 20°C. A variety of photoinitiator concentrations were employed. The resulting MWDs are presented in figures 6-19 (MMA polymerizations) and 6-20 (STY polymerizations) as $w(log_{10}M)$, where w denotes weight fraction and M molecular weight. This is essentially the form in which standard SEC analysis (differential refractive index detection) yields MWDs. The structure of this MWDs suggests that reliable values of k_p may be obtained from these results. The values of k_p which are listed in table 6.2 were determined using equation 6.25, with L_0 set equal to the chain length of the inflection point on the low molecular weight side of the lowest molecular weight peak of SEC results in the form of number MWD. Such an inflection point is clearly evident as the first maximum of a plot of the derivative of the MWD;

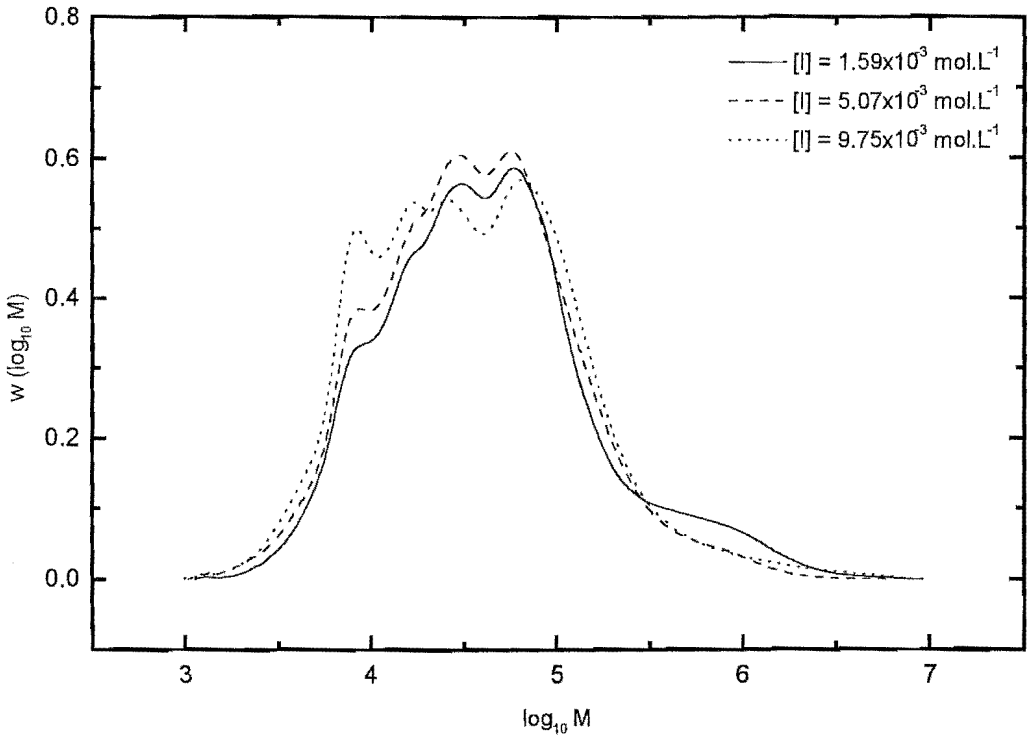

Figure 6-20: The MWD for the PLP of STY for a range of BAPO concentrations.

a typical derivative plot is shown in figure 6-21.

PLP Consistency Checks

A number of consistency checks have been recommended by an IUPAC working party to verify the accuracy of data generated from PLP experiments.[8] As this work deals with a modification to the conventional PLP experiment, it is appropriate to ensure that the novel photoinitiation conditions do not interfere with the k_p measurement. The most essential consistency check is considered to be that so-called 'overtone' inflection points be evident in a MWD at chain lengths $2L_0, 3L_0$, etc...[8] These features correspond to chains surviving for two, three, etc. pulse periods before undergoing termination. Such overtones are clearly evident in all the MWDs of

Experiment	Monomer	[BAPO] (mol.L^{-1})	L_0	k_p
1	MMA	5.45×10^{-3}	263	281
2	MMA	11.1×10^{-3}	267	285
3	STY	1.59×10^{-3}	54.6	63
4	STY	5.07×10^{-3}	58.9	68
5	STY	9.75×10^{-3}	58.3	67

Table 6.2: Propagation rate coefficient evaluation for the monomers MMA and STY from visible light PLP experiments.

figures 6-19 and 6-20, and one may formally see this in the typical derivative plot of figure 6-21, in which a number of maxima corresponding to the primary inflection point (used to determine k_p) and subsequent overtones are evident.

The IUPAC working party also recommends[8] the carrying out of additional consistency checks, most notably that k_p be shown to be invariant to changes in photoinitiator concentration, incident pulse energy or dark time t_0 between laser pules. Unfortunately it is impossible to conduct studies by varying t_0 as the OPO can only be operated at 10 Hz (so as to prevent damaging the optics). Varying the incident pulse energy was also not easy, so it was decided to vary the BAPO concentration as a consistency check. The results of table 6.2 show that the obtained k_p are indeed independent of [BAPO], giving further confidence that these k_p values are indeed reliable.

Finally, the k_p values of table 6.2 may be compared with the benchmark values recommended by the IUPAC working party, viz. $k_p = 277$ L.mol^{-1}.s^{-1} for MMA[5] at 20°C and $k_p = 69$ L.mol^{-1}.s^{-1} for STY[8] at 20°C. These values agree excellently with those of the present study, which in a sense is definitive proof of the 'consistency' of these k_p values. The relevance of this in the context of the present work is that we have shown that this novel photoinitiation system performs as desired, and could therefore be used for reliable k_p determination in systems for which k_p is not already known.

Peculiarities due to BAPO photoinitiation.

While the MWDs of figures 6-19 and 6-20 have the overall form one expects from PLP, they do however have one unusual aspect: there is a far greater contribution to the MWD from high molecular weight species than one usually observes. Usually the 'primary' peak containing the

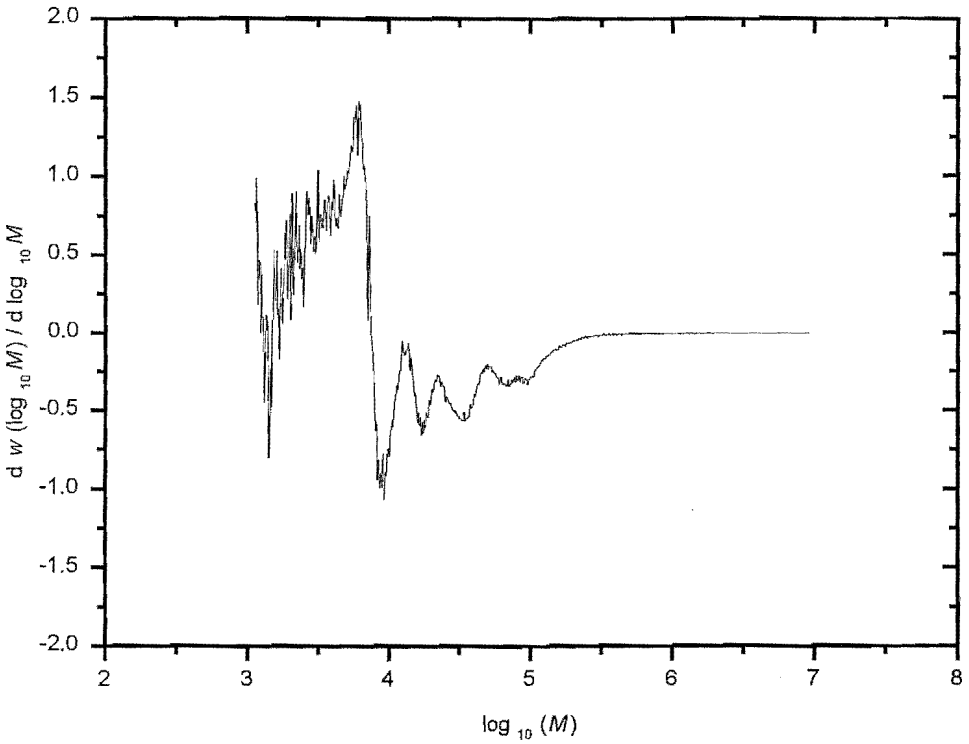

Figure 6-21: The deriative of the MWD for the PLP of STY with a BAPO concentration of 1.59×10^{-3}mol.L^{-1}.

chain length L_0 dominates the MWD, with the overtone features - corresponding to multiples of L_0 - being less prominent. However these results show the opposite behavior. This is especially the case for the STY results (Figure 6-20). Since it has been established that our PLP results are not artifactual (see above), it is against this background that the enhanced contribution to the MWD of polymer corresponding to multiples of L_0 must be explained. I suggest that the unique photoinitiation process contributes to this behavior, as now explained.

Several publications[46][27][15] have dealt with the photoinitiation chemistry of phosphine oxides. Monoacyl phosphine oxides (MAPO) undergo facile solvolytic cleavage of the carbon-phosphorus bond with high efficiency ($\phi = 0.6$) to yield an aroyl-phosphinoyl radical pair. Bisacyl phosphine oxides (BAPO) are particularly useful for initiating at higher wavelengths

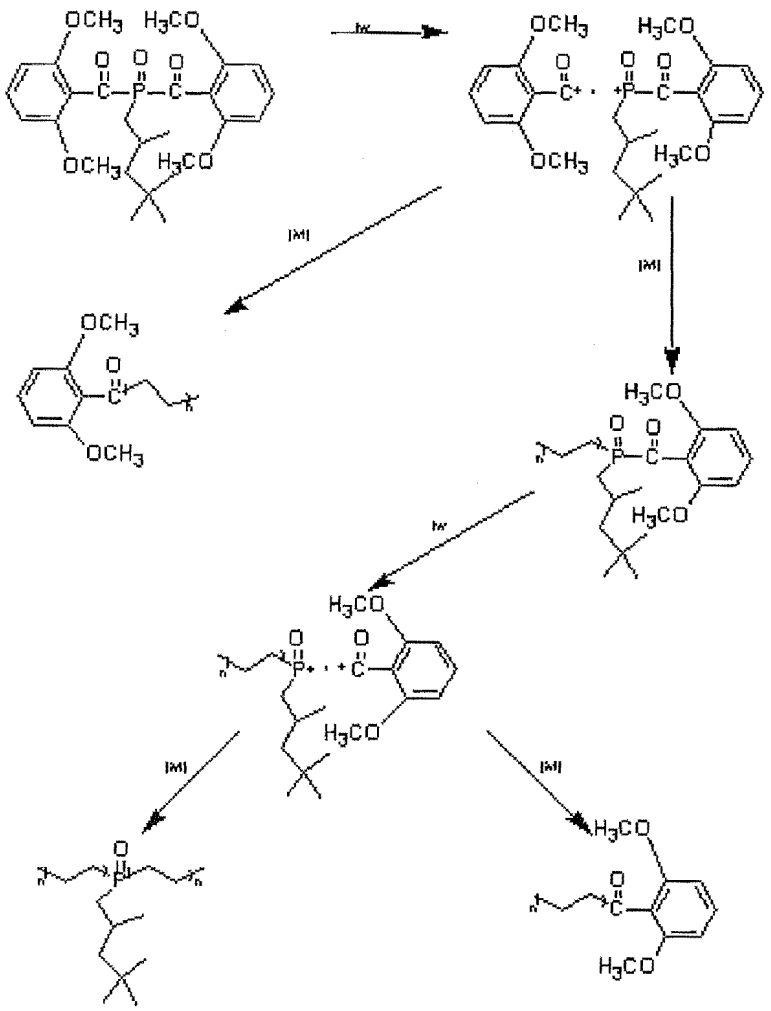

Figure 6-22: Reaction Scheme for the intiation of polymerization by BAPO (see text for further explanation)

as the $\pi \rightarrow \pi^*$ transition exhibits a significant extinction coefficient at 400 nm, which has been interpreted in terms of a specific interaction between the carbonyl and the phosphonyl groups. In the particular case of BAPO it has been established that the molecule undergoes a two-step cleavage reaction generating four radical sites, as indicated in figure 6-22. In a PLP experiment it seems most reasonable that the initial cleavage step is followed by propagation (as opposed to the second cleavage step), thus leading to the production of polymer with an 'active' chain end, which can then undergo reactivation at a subsequent laser pulse, and further propagation will follow. This is all illustrated in figure 6-22.

This initiation mechanism has implications for PLP. It may be anticipated that half (or approximately half, if the two types of primary radicals from the first cleavage step have different efficiencies) of the polymerizing radicals generated from the BAPO photoinitiator will contain a $2,4,4-$ trimethylpentylphosphine oxide unit (i.e. a MAPO unit) as endgroup. It may be further anticipated that almost all of these polymerizing radicals undergo a termination reaction of some sort before the 'active' endgroup undergoes reinitiation. This is so because in PLP the greater fraction of radicals usually experiences termination before the next pulse arrives, and even if a radical survives longer than one pulse period, it is unlikely that reinitiation will be immediate (with each pulse only a small fraction of photoinitiator groups undergo absorption). This means that almost all reinitiation must involve nominally dead chains. Thus a MAPO-ended chain which ordinarily would have remained a dead chain of chain length, say, n can undergo reinitiation and end up growing to chain length, say, $2L_0$, at which point it might for example undergo termination with a primary radical (giving a species of chain length $2L_0$) or combination with another species of length $2L_0$ (giving a chain of length $4L_0$). It is thus clear that the incorporation of 'reinitiatable' endgroups into half the polymer chains will lead to a reduction in the number of polymer molecules of relatively small chain lengths and an enhancement of the MWD at higher chain lengths. This is as observed. I now detail simulations which have been carried out to investigate these ideas further.

6.3.3 Simulation Studies

Right from the beginning[5], kinetic simulations have been indispensable in seeking to understand PLPs. It is therefore appropriate to attempt to investigate the ideas arising from the

above experiments by performing kinetic simulations. I begin with a standard kinetic scheme. In this way I develop a foundation on which to build a description of PLP with reinitiatable endgroups.

Standard Kinetic Model.

A standard kinetic model for free-radical polymerization includes the reactions of chain initiation, chain propagation, chain termination by disproportionation and chain termination by combination. Such a set of reactions may be represented schematically as follows, with the reactions in the order just given:

$$A - X - B \longrightarrow 2\mathrm{R}_0 \tag{6.39}$$

$$\mathrm{R}_i + \mathrm{M} \xrightarrow{k_\mathrm{p}} \mathrm{R}_{i+1} \tag{6.40}$$

$$\mathrm{R}_i + \mathrm{R}_j \xrightarrow{k_\mathrm{td}} \mathrm{D}_i + \mathrm{D}_j \tag{6.41}$$

$$\mathrm{R}_i + \mathrm{R}_j \xrightarrow{k_\mathrm{to}} \mathrm{D}_{i+j} \tag{6.42}$$

Here R_i denotes a living radical of chain length i, D_i dead polymer chain of length i, $A-X-B$ molecular initiator, and R_0 the so-called primary radicals from initiator decomposition (in other words, a radical of chain length 0, although obviously it is recognized that the two moieties from initiator decomposition may be different, as indeed they are in the case of BAPO). The rate coefficients k are subscripted to indicate to which of the above reactions they correspond. Clearly our model assumes that all rate coefficients are chain-length independent and that the contribution of chain transfer is insignificant. The latter is reasonable on account of the low temperature of the experiments we seek to model (MMA and STY undergo negligible chain transfer to monomer at 20°C). This was confirmed in additional simulations in which chain transfer to monomer was included and sensible estimates were used for rate coefficients for chain transfer to monomer.

Population Balance Equations for Standard Kinetic Model.

From the above scheme one may write down population balance differential equations which describe how the concentrations of all species change with time t. These are as follows.

Living Radicals:

$$\frac{d\mathrm{R}_0}{dt} = R_{init} - k_\mathrm{p}\mathrm{M}\mathrm{R}_0 \tag{6.43}$$

$$\frac{d\mathrm{R}_1}{dt} = k_\mathrm{p}\mathrm{M}\mathrm{R}_0 - k_\mathrm{p}\mathrm{M}\mathrm{R}_1 - 2k_\mathrm{t}\mathrm{R}_1\sum_{j=1}^{\infty}\mathrm{R}_j \tag{6.44}$$

$$\frac{d\mathrm{R}_i}{dt} = k_\mathrm{p}\mathrm{M}\mathrm{R}_{i-1} - k_\mathrm{p}\mathrm{M}\mathrm{R}_i - 2k_\mathrm{t}\mathrm{R}_i\sum_{j=1}^{\infty}\mathrm{R}_j \qquad i \geq 2 \tag{6.45}$$

Dead Polymer Chains:

$$\frac{d\mathrm{D}_1}{dt} = 2k_\mathrm{td}\mathrm{R}_1\sum_{j=1}^{\infty}\mathrm{R}_j \tag{6.46}$$

$$\frac{d\mathrm{D}_i}{dt} = 2k_\mathrm{td}\mathrm{R}_i\sum_{j=1}^{\infty}\mathrm{R}_j + k_\mathrm{tc}\sum_{j=1}^{i-1}\mathrm{R}_j\mathrm{R}_{i-j} \qquad i \geq 2 \tag{6.47}$$

In these expressions all symbols stand for the same species as they did above, e.g. R_0 represents the concentration of primary radicals, however these symbols now denote the concentration, whereas previously the stood for an individual species. The total rate coefficient for termination is given by $k_\mathrm{t} = k_\mathrm{td} + k_\mathrm{tc}$. Note that the 'American' convention for termination rates has been employed, i.e., the overall termination rate is given by $-2k_\mathrm{t}\mathrm{R}^2$, where R is the total radical concentration. For these PLP simulations it is assumed that there is no background initiation, so that the rate of initiation R_{init} is zero except at the arrival of a pulse. I define ρ as the total concentration of primary radicals produced by a pulse, assumed to be constant throughout a PLP (i.e., negligible initiator consumption is assumed).

As is clear from equation 6.43, I also assume that there is negligible termination involving primary radicals; this was verified in simulations in which primary radical termination was included (by not allowing R_0 species to terminate one gains the convenience of not having to define dead chains of length zero).

Simulations Results

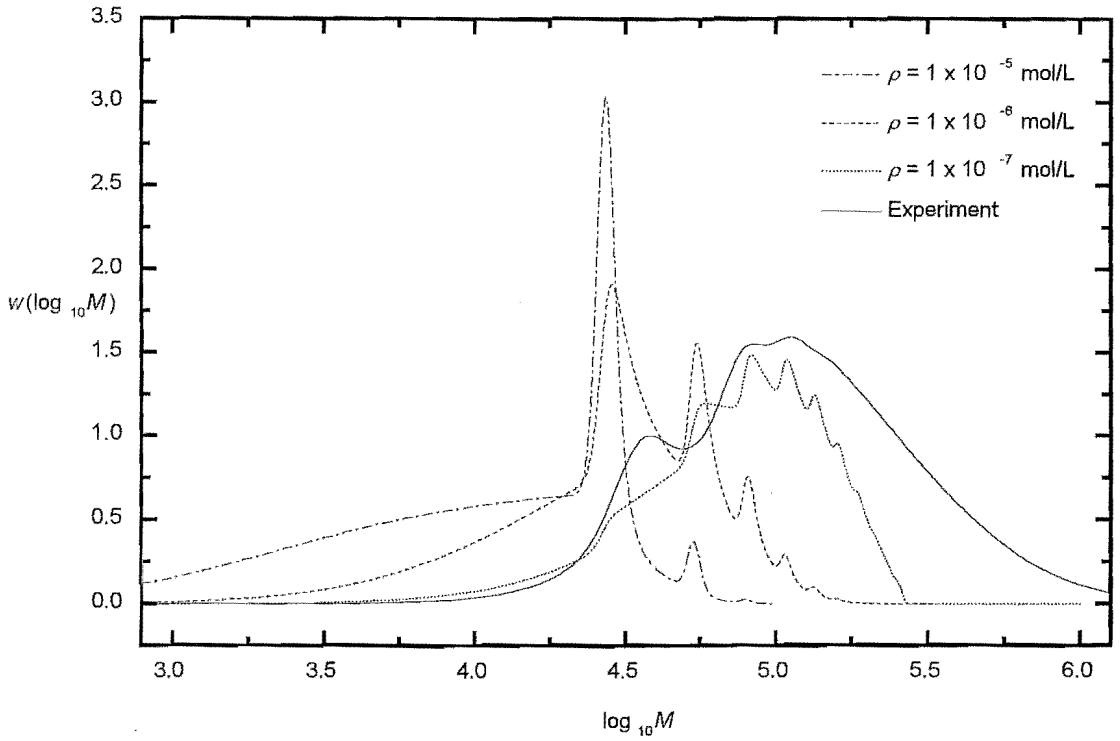

Figure 6-23: Molecular weight distributions for polymerization 1 of table 6.2: MMA with [BAPO] $= 5.45 \times 10^{-3}$mol.L^{-1}. The full line is the experimentally obtained MWD, the broken lines are MWDs from simulations with the standard kinetic model

A number of simulations were carried out with the above standard kinetic model, where the Modified Euler method was used for numerical solution of equations 6.43 - 6.47 above. Differential equations for individual chain lengths up to and including $i = 10,000$ were solved, with a single differential equation for all species of greater chain length being used (a truncation chain length of $10,000$ was found to cover the entire MWD in all cases). All R_i were initially set equal to zero and allowed to build up to their pseudo-steady state profile. Simulations were carried out for 10 pulses of polymerization, this being long enough for a pseudo-steady state to be well and truly obtained. Thus the cumulative MWD at the end of a simulation is effectively equivalent to the MWD one would obtain from a PLP. I therefore present the simulation results as normalized cumulative MWDs. Through careful monitoring it is ensured

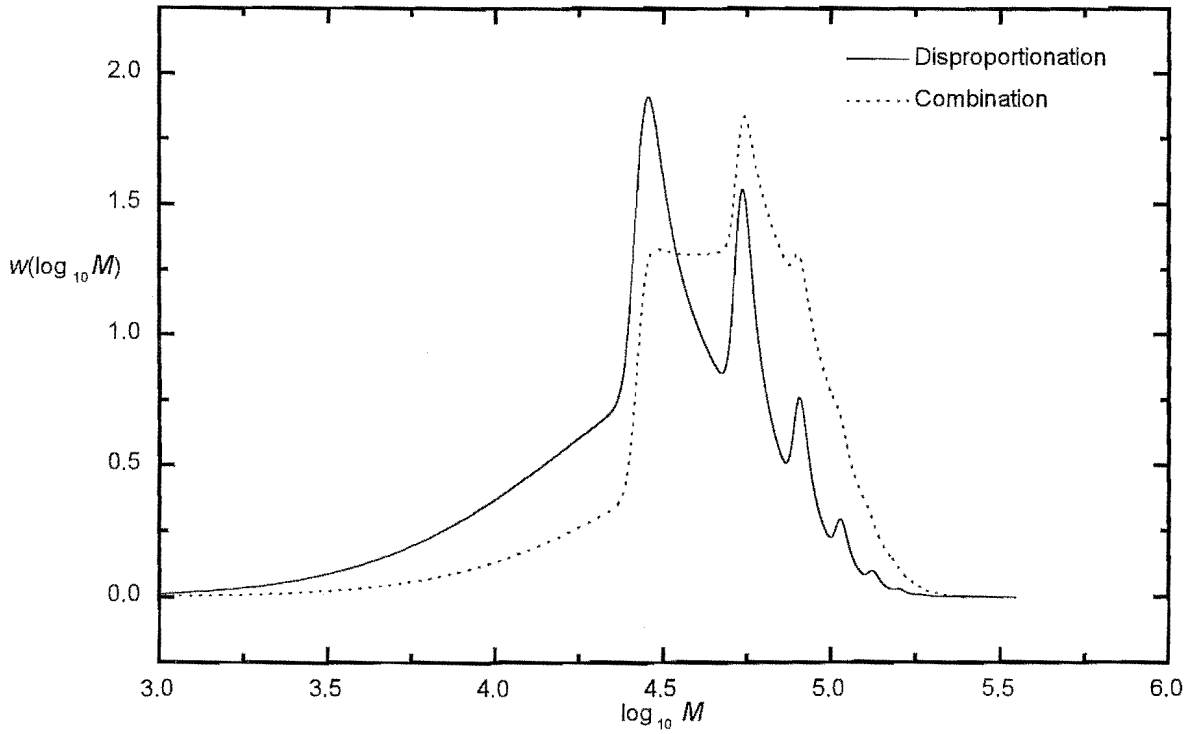

Figure 6-24: Simulated molecular weight distributions for cases of termination by disproportionation only (full line; $\rho = 1.0 \times 10^{-6}$ mol.L^{-1} results of previous figure) and termination by combination only (dotted line; same parameter values except termination ocurrs exclusively by the combination termination mechanism).

that error from numerical solution of this system of differential equations remained negligible at all times (see chapter five).

Results of simulations using the standard kinetic model are presented in figures 6-23 and 6-24 (rate parameters: $k_p = 280$ L.mol^{-1}s^{-1}, $k_{td} = 1.0 \times 10^7$L.mol^{-1}s^{-1}, $k_{tc} = 0$, M= 9.321 mol.L^{-1}, $t_0 = 0.1$s, $\rho = 1.0 \times 10^{-5}, 1.0 \times 10^{-6}$ and 1.0×10^{-7}mol.L^{-1} as indicated). First of all I discuss figure 6-23, which compares simulation results with the experimental MWD from the MMA PLP with the lowest BAPO concentration. Appropriate parameter values were used in simulations, as indicated. In particular we mention that $k_{td}/k_t = 1$ was used. This ratio has recently been

measured [56] as being 0.8 for MMA at 0°C, thus confirming the generally accepted view[34] that MMA termination is predominantly by disproportionation. I have here taken the simple option of using $k_{td}/k_t = 1$ because simulations without combination are considerably quicker, and the character of results is not changed by the occurrence of a little combination only. With t_0 fixed and k_{td}/k_t and k_p known for the system of interest, the only adjustable parameter value was $k_t\rho$, results not depending on the individual values of k_t and ρ.[37] The value of $k_t\rho$ was varied by setting k_t equal to the reasonable value of 1.0×10^7 L.mol^{-1}.s^{-1} and varying ρ. Unfortunately I have no idea of the concentration of radicals created per pulse in these PLPs, so simulations spanning $\rho = 1.0 \times 10^{-5}$mol.L^{-1} (a high value) and $\rho = 1.0 \times 10^{-7}$mol.L^{-1} (at the low end of the range of usual values) were carried out. Figure 6-23 confirms the well known result (e.g. reference [12]) that MWDs are crucially dependent on the value of ρ, decreasing ρ giving decreasing rates of termination, and therefore longer chains. In figure 6-23 it is evident that $\rho = 1.0 \times 10^{-7}$mol.L^{-1} gives the best agreement between simulation and experiment. Given that pulse energies and photoinitiator concentrations in these experiments were normal in value, the results of figure 6-23 thus suggest that BAPO might give rise to low primary radical fluxes (which could be due either to a low extinction coefficient or low photoinitiator efficiency). This is an obvious area for further investigation before these PLP results can be completely understood.

Whereas termination in MMA systems is predominantly by disproportionation, in STY systems it is almost exclusively by combination.[34] This major difference between the polymerizations of these monomers was investigated by carrying out simulations in which all termination was by combination, i.e., $k_{td} = 0$ and $k_{tc} = k_t$. The results of one such simulation are shown in figure 6-24, in which are also presented the analogous results (from figure 6-23) for the case of disproportionation only. As expected, longer chains are produced by combination, with the result that the intensities of PLP overtones are enhanced while the intensity of the PLP fundamental peak is diminished. The different termination mechanisms operative are thus surely a major factor in explaining the differences between our MMA and STY results (compare figures 6-19 and 6-20). It is unclear if there are other MMA-STY differences contributing toward the differences between the results of figures 6-19 and 6-20. It is possible, for example, that identical conditions might give rise to different ρ in STY and MMA systems (e.g. photoinitiator

efficiencies might be significantly dependent on environment).

Referring back to figure 6-23, it is evident that although reasonable agreement between experiment and simulation can be obtained with $\rho = 1.0 \times 10^{-7}$mol.L^{-1}, the agreement cannot be called close. Of particular note is that what is clearly evident as a fundamental peak (admittedly of reduced intensity) in the experimental results is only a shoulder in the simulation results. It should also be borne in mind that these experimental SEC results have been broadened by axial dispersion, an effect not accounted for in these simulations. If it were, then for usual extents of SEC broadening the $\rho = 1.0 \times 10^{-7}$mol.L^{-1} simulation results of figure 6-23 would become almost structureless.[12] This contrasts with our experimental results, which retain PLP features, even though many chains much longer in length than $k_p M t_0$ are produced. This suggests that it is justified to carry out further simulations in order to see if these experimental results can be better explained by the phenomenon of endgroup reinitiation, which I postulate is occurring in our PLPs with BAPO.

Modified Kinetic Model

There are many ways in which the standard kinetic scheme may be refined. For example, chain-length-dependent rate coefficients - and in particular chain-length-dependent termination rate coefficients - may be introduced. In the present work our interest obviously lies in extending the standard kinetic scheme to incorporate reinitiation of terminated polymer molecules: recall from figure 6-22 that it is anticipated that the use of BAPO as photoinitiator will lead to many polymer chains having a monoacyl phosphine oxide (MAPO) endgroup, and it is believed that these can undergo further photoinitiation. In particular I am interested in how significantly such reinitiation will affect PLP results, and to what extent it gives closer agreement between the results of simulations and experiments.

Reaction Scheme for Modified Kinetic Model

In order to develop a kinetic scheme that allows the reinitiation of initiator-derived endgroups, polymer chains and living radicals must be resolved on the basis of the number of MAPO endgroups they contain. In the scheme outlined below and in all subsequent expressions, R_i^k denotes a living radical of chain length i containing k MAPO endgroups ($k = 0$ or 1) and D_i^k

analogous for non-living chains ($k = 0, 1$ or 2). We thus have a modified reaction scheme as follows.

Initiation:

$$A - X - B \longrightarrow \mathrm{R}_0^0 + \mathrm{R}_0^1 \tag{6.48}$$

Reinitiation:

$$\mathrm{D}_i^1 \longrightarrow \mathrm{R}_0^0 + \mathrm{R}_i^0 \tag{6.49}$$

$$\mathrm{D}_i^2 \longrightarrow \mathrm{R}_0^0 + \mathrm{R}_i^1 \tag{6.50}$$

Propagation:

$$\mathrm{R}_0^0 + \mathrm{M} \xrightarrow{k_\mathrm{I}} \mathrm{R}_1^0 \tag{6.51}$$

$$\mathrm{R}_0^1 + \mathrm{M} \xrightarrow{k_\mathrm{I}} \mathrm{R}_1^1 \tag{6.52}$$

$$\mathrm{R}_i^k + \mathrm{M} \xrightarrow{k_\mathrm{p}} \mathrm{R}_{i+1}^k \qquad i \geq 1 \tag{6.53}$$

Termination (combination and disproportionation):

$$\mathrm{R}_i^0 + \mathrm{R}_j^0 \xrightarrow{k_\mathrm{td}} \mathrm{D}_i^0 + \mathrm{D}_j^0 \tag{6.54}$$

$$\mathrm{R}_i^0 + \mathrm{R}_j^0 \xrightarrow{k_\mathrm{tc}} \mathrm{D}_{i+j}^0 \tag{6.55}$$

$$\mathrm{R}_i^0 + \mathrm{R}_j^1 \xrightarrow{k_\mathrm{td}} \mathrm{D}_i^0 + \mathrm{D}_j^1 \tag{6.56}$$

$$\mathrm{R}_i^0 + \mathrm{R}_j^1 \xrightarrow{k_\mathrm{tc}} \mathrm{D}_{i+j}^1 \tag{6.57}$$

$$\mathrm{R}_i^1 + \mathrm{R}_j^1 \xrightarrow{k_\mathrm{td}} \mathrm{D}_i^1 + \mathrm{D}_j^1 \tag{6.58}$$

$$\mathrm{R}_i^1 + \mathrm{R}_j^1 \xrightarrow{k_\mathrm{tc}} \mathrm{D}_{i+j}^2 \tag{6.59}$$

Here $A - X - B$ symbolizes the molecular initiator (BAPO), R_0^1 denotes $A - X\bullet$, a MAPO primary radical, and R_0^0 denotes $A\bullet$ and $B\bullet$, the primary radicals with no labile bonds, i.e., the primary radicals which become standard endgroups (see figure 6-22). In the experiments of this work $A\bullet$and $B\bullet$ are identical, but in general they need not be. Also not that here k_I is the rate coefficient for the propagation for primary radicals.

Population Balance Equations for Modified Kinetic Model.

From the above reaction scheme the following population balance differential equations can be written down.

Living Radicals ($k = 0, 1$):

$$\frac{d\mathrm{R}_0^k}{dt} = R_{init} - k_\mathrm{I}\mathrm{M}\mathrm{R}_0^k \tag{6.60}$$

$$\frac{d\mathrm{R}_1^k}{dt} = k_\mathrm{I}\mathrm{M}\mathrm{R}_0^k - k_\mathrm{p}\mathrm{M}\mathrm{R}_1^k - 2k_\mathrm{t}\mathrm{R}_1^k \sum_{j=1}^{\infty}(\mathrm{R}_j^0 + \mathrm{R}_j^1) \tag{6.61}$$

$$\frac{d\mathrm{R}_i^k}{dt} = k_\mathrm{p}\mathrm{M}\mathrm{R}_{i-1}^k - k_\mathrm{p}\mathrm{M}\mathrm{R}_i^k - 2k_\mathrm{t}\mathrm{R}_i^k \sum_{j=1}^{\infty}(\mathrm{R}_j^0 + \mathrm{R}_j^1) \qquad i \geq 2 \tag{6.62}$$

Dead Polymer Chains:

$$\frac{d\mathrm{D}_1^0}{dt} = 2k_\mathrm{td}\mathrm{R}_1^0 \sum_{j=1}^{\infty}(\mathrm{R}_j^0 + \mathrm{R}_j^1) \tag{6.63}$$

$$\frac{d\mathrm{D}_1^1}{dt} = 2k_\mathrm{td}\mathrm{R}_1^1 \sum_{j=1}^{\infty}(\mathrm{R}_j^0 + \mathrm{R}_j^1) \tag{6.64}$$

$$\frac{d\mathrm{D}_1^2}{dt} = 0 \tag{6.65}$$

$$\frac{d\mathrm{D}_i^0}{dt} = 2k_\mathrm{td}\mathrm{R}_i^0 \sum_{j=1}^{\infty}(\mathrm{R}_j^0 + \mathrm{R}_j^1) + k_\mathrm{tc}\sum_{j=1}^{i-1}\mathrm{R}_j^0\mathrm{R}_{i-j}^0 \qquad i \geq 2 \tag{6.66}$$

$$\frac{d\mathrm{D}_i^1}{dt} = 2k_\mathrm{td}\mathrm{R}_i^1 \sum_{j=1}^{\infty}(\mathrm{R}_j^0 + \mathrm{R}_j^1) + 2k_\mathrm{tc}\sum_{j=1}^{i-1}\mathrm{R}_j^0\mathrm{R}_{i-j}^1 \qquad i \geq 2 \tag{6.67}$$

$$\frac{d\mathrm{D}_i^2}{dt} = k_\mathrm{tc}\sum_{j=1}^{i-1}\mathrm{R}_j^1\mathrm{R}_{i-j}^1 \qquad i \geq 2 \tag{6.68}$$

Once again for convenience it has been assumed that primary radical termination is a negligible fraction of the overall termination rate.

In these simulations the rate of initiation R_{init} is set equal to zero for the time between pulses. As before, photoinitiation due to molecular initiator is accounted for by increasing the primary radical concentration by a concentration ρ, this being apportioned equally between R_0^1 and R_0^0 species (see figure 6-22), i.e., each of these populations is increased by $\rho/2$ to simulate the effect of pulsing. As well as photoinitiation due to BAPO, we must also now allow for the

reinitiation of species with MAPO endgroups which occurs upon pulsing. This is quantified by defining a physically plausible parameter REI which I call the reinitiation factor. This is the fraction of MAPO endgroups which undergo reinitiation upon pulsing. For example, if REI = 0.1 then there is a one in ten chance of a MAPO endgroup being reinitiated, i.e., if at the instant of pulse arrival there were one thousand polymer chains containing one MAPO endgroup, then after the pulse there would be 900 chains of this type. Hence one has the following general equations which were used to describe the population changes due to reinitiation which occur upon the arrival of a pulse:

$$D_i^1 = (1 - \mathrm{REI}) \times D_i^1 \tag{6.69}$$

$$D_i^2 = (1 - 2 \times \mathrm{REI}) \times D_i^2 \tag{6.70}$$

$$R_i^0 = R_i^0 + \mathrm{REI} \times D_i^1 \qquad i \geq 1 \tag{6.71}$$

$$R_i^1 = R_i^1 + 2 \times \mathrm{REI} \times D_i^2 \qquad i \geq 2 \tag{6.72}$$

$$R_0^0 = \mathrm{REI} \sum_{i=1}^{\infty} (D_i^1 + 2D_i^1) \tag{6.73}$$

The factors of 2 in the above equations are due to D_i^2 species having two reinitiatable endgroups. Note that equation 6.73 represents the updating of R_0^0 due to reinitiation only (this population is also incremented to account for initiation, as already explained).

It is evident from above that negligible biradical formation has been assumed. Such species may be formed either by the simultaneous reinitiation of both MAPO endgroups of a D_i^2 species (as formed by combination, see equation 6.59) or by the reinitiation of the MAPO endgroup of a R_i^1 living radical. However the probability of simultaneous reinitiation of both ends of a D_i^2 species will be extremely small. As for reinitiation of living chains, the number of MAPO endgroups attached to living chains will be negligibly small relative to the number attached to non-living chains (except of course at the very beginning of a PLP when there has been little time for dead chain accumulation). For these reasons it is justified to neglect biradical formation. To make absolutely sure of this, a kinetic model that allowed formation of biradicals by both the above mechanisms was postulated. Kinetic equations based on this model were

derived and then solved numerically. I do not include explicit details because of the complexity of the equations. However I can report from this examination that the contribution of biradicals was found to be unimportant at all but the very early stages of simulated PLPs, exactly as expected.

Simulation Results

Simulation studies of PLP usually make allowance for the fact that it takes several pulses to reach a pseudo-steady state. This can be done easily and in either of two ways: (1) The time-scale of a simulation is increased until the contribution of the polymer formed prior to a pseudo-steady state has become insignificant (this is the approach we used in our simulations with the standard kinetic model); or (2) Once a pseudo-steady state is reached, the simulation is carried out for one more pulse period and only the polymer formed during this period is registered. With this modified kinetic model, however, the treatment of the period prior to the establishment of a pseudo-steady state was found to be more difficult. This is because the populations of D_i^1 and D_i^2 species do not endlessly increase (as opposed to the concentrations D_i^0 of truly dead chains); rather, these species with reinitiatable endgroups are both formed and consumed by initiation and reinitiation processes. A pseudo-steady state is reached when the rate of creation of MAPO endgroups is equal to their rate of loss by reinitiation, i.e., when

$$\rho/2 = \mathrm{REI}\sum_{i=1}^{\infty}(D_i^1 + 2D_i^1) \tag{6.74}$$

This relation reveals a number of things: (1) The concentrations D_i^1 and D_i^2 must buildup before a pseudo-steady state can be reached. Because the reinitiation probability REI is expected to be well less than 1 (having REI close to 1 in value is inconsistent with the fact that the probability of absorption by photoinitiator is low), it follows from equation 6.74 that the total concentration of reinitiatable endgroups (the sum in equation 6.74) must buildup to much greater than $\rho/2$ for a pseudo-steady state to be attained. This obviously takes a large number of pulses, because each pulse gives a net change of at most $\rho/2$ in the MAPO concentration. Hence the number of pulses required to attain pseudo-steady state will be greater than 1/REI, (2) The lower the value of REI, the higher the values of D_i^1 and D_i^2 which are necessary for equation 6.74 to

be satisfied, and so the longer it takes for a system to buildup to a pseudo-steady state. (3) Equation 6.74 also reveals that endgroup reinitiation leads to higher radical concentrations. In fact it is evident from equation 6.74 that a pseudo-steady state will be characterized by each pulse generating a concentration 2ρ of new radicals (ρ from BAPO, ρ from reinitiation). This situation will not be reached until the D_i^1 and D_i^2 have reached a pseudo-steady state, i.e., the radical population now takes an equally long time to attain a pseudo-steady state (as opposed to the situation without endgroup reinitiation).

It was found that of order 100 pulses were typically necessary to reach a pseudo-steady state in these simulations with endgroup reinitiation. I was therefore faced with the need to carry out simulations for a far larger number of pulses than one needs to with a standard kinetic model. The approach taken with the modified kinetic model was to simulate exactly 100 pulses of polymerization. In some cases (REI = 0.1) this was sufficient for a pseudo-state to be reached, while in others (REI = 0.01 or less) a pseudo-steady state was only approached (see points (1) and (2) above). Even in the latter cases, however, the simulations were still long enough to evaluate the effect of reinitiatable endgroups on PLP results, which is the aim of these simulations. In all cases more complete results would have been obtained by carrying on the simulations for a larger number of pulses. However each of these simulations with the modified kinetic scheme took almost one day of dedicated CPU time of a large VAX computer (not surprisingly, simulation times per pulse are considerably lengthened by adopting the modified kinetic model). It was therefore not considered feasible to carry out longer simulations.

Otherwise simulation details are the same as before, except that the chosen parameter values were such that a truncation chain length of 2000 was found to be adequate. It should also be affirmed that simulation results are once again presented as cumulative MWDs, i.e., they include the chains generated in the buildup to pseudo-steady state. I take this approach because the experimental MWDs will also include such chains, and if the buildup to pseudo-steady state really is a significant portion of a PLP with BAPO (as our simulations suggest), then it is appropriate to compare experimental results with cumulative MWDs from simulations. The sum $D_i^0 + D_i^1 + D_i^2$ is taken as being the number MWD that would be measured experimentally; results are presented as this number MWD appropriately transformed.

Figure 6-25 (rate parameters: $k_p = k_I = 100$ L.mol^{-1}.s^{-1}, $k_{td} = 1.0 \times 10^6$L.mol^{-1}.s^{-1},

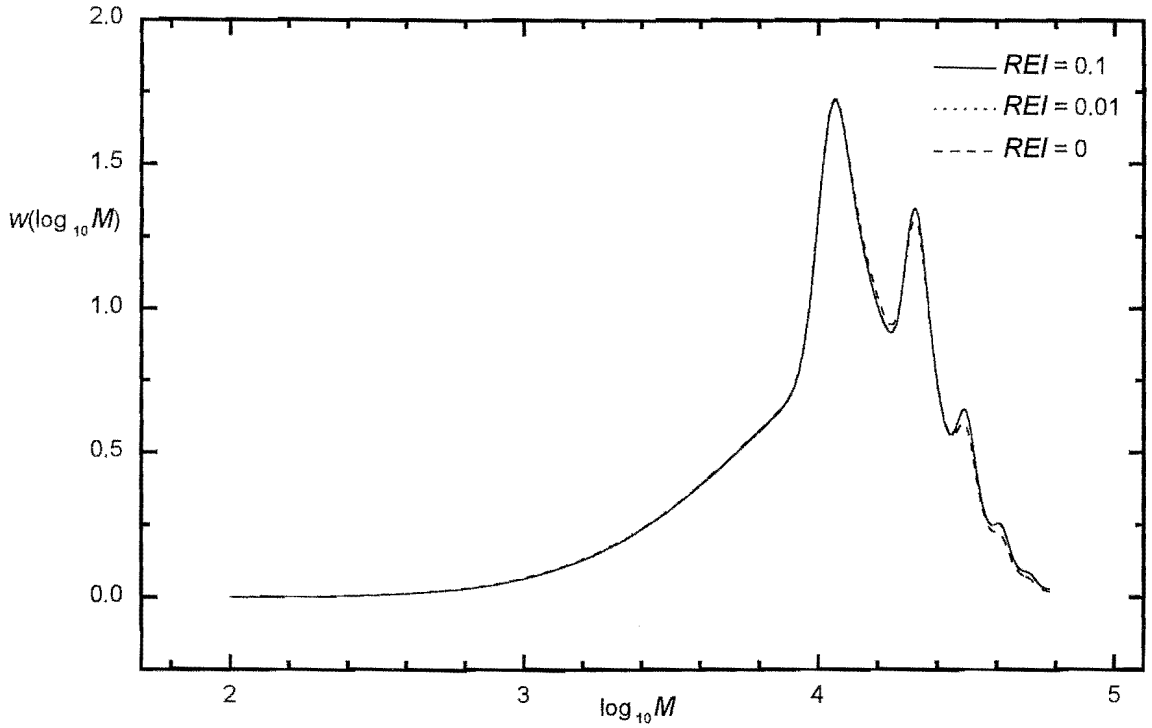

Figure 6-25: Simulated molecular weight distributions illustrating the effect of endgroup reinitiation

$k_{tc} = 0$, M = 10.0 mol.L^{-1}, $t_0 = 0.1$ s, $\rho = 1.0 \times 10^{-5}$mol.L^{-1}, REI= 0.1, 0.01 and 0 as indicated; note that REI = 0.1 and REI = 0.01 results are barely distinguishable), illustrates the effect of varying the rate of reinitiation of reinitiatable endgroups. Model parameter values have been used. In particular note the use of a relatively low k_p (100 L.mol^{-1}.s^{-1}) and $k_{tc} = 0$: both these choices speed up simulations considerably (a small truncation chain length can be used, and the combination sums in equations 6.66 - 6.68 do not need to be evaluated). The value of $k_t = 1 \times 10^6$L mol^{-1} s^{-1} may look low, but it is compensated for by the high value of $\rho = 1 \times 10^{-5}$mol.L^{-1} (it is only the value of the product of $k_t\rho$ which is important). The use of these model parameter values (as opposed to values corresponding as closely as possible to the experimental conditions) in no way precludes commenting on these experimental results on

the basis of what these simulations show.

The first result which is evident from figure 6-25 is that reinitiation has the expected effect on MWDs: there is an enhancement in the intensity of the overtone PLP peaks (compare the simulation without reinitiation with those with non-zero REI). This of course does not definitively prove that endgroup reinitiation occurred in these experiments with BAPO, however it does confirm that the process of reinitiation will give rise to overtone PLP peaks of greater intensity, the phenomenon observed experimentally. This said, it is clear from the simulation results of figure 6-25 that the extent to which overtone intensities were increased in our experiments cannot be explained by the mechanism of reinitiation alone. Indeed, it is perhaps surprising how little this process seems to affect MWDs. One reason for this is that only 50 % of all chains may undergo reinitiation in the first place, i.e., half of the primary radicals from BAPO decomposition go on to form truly dead chains (i.e., D_i^1 species). Another reason is that as discussed, the phenomenon of reinitiation results in higher radical concentrations, an effect which acts to suppress overtone features (see figure 6-23). A further reason is that simulations were stopped (due to time constraints, see above) after simulation of only 100 pulses worth of polymerization, i.e., after at most a relatively short period of pseudo-steady state polymerization (as already discussed). Thus at the end of these simulations a relatively large number of chains exist as D_i^1 species as compared to the number of D_i^1 species which have been reinitiated, i.e., the reported MWDs overemphasize the contribution of D_i^1 species (these being exactly as from a conventional PLP). Close inspection of these simulations indeed confirmed that the high molecular weight portions of these MWDs do get more pronounced as the number of pulses mounts and more D_i^1 species have had time to undergo reinitiation. However there is no evidence to suggest that if it were feasible to carry out simulations for thousands of pulses, then a significantly larger enhancement of overtone features would be found. What is perhaps more likely is that chain-length-dependent termination is operative, and that this leads to reinitiated chains, already relatively long, being exposed to reduced rates of termination and therefore polymerizing for much longer than they do in these simulations (in which the one k_t is used for all chain lengths). Most likely, however, is that low values of ρ are the main factor responsible for the unusual shape of the MWDs: the trends of figure 6-23 apply equally with the modified kinetic model. If this is the case, then the sharpness of PLP features in these experimental

MWDs must be owed to very low extents of SEC broadening.[12]

One extra possible effect that we have investigated here is that of initiator consumption (this has been neglected in all simulations to date). This was done as follows. Since REI is defined as the probability of a MAPO endgroup undergoing reinitiation, it seems logical to expect that 2× REI is close to the probability of a BAPO molecule undergoing photoinitiation (either of 2 identical bonds may be photolytically cleaved in the symmetric BAPO molecule). Hence one expects

$$\frac{\rho}{2} = 2 \times \text{REI}\,[A-X-B] \tag{6.75}$$

Here $[A-X-B]$ denotes the initial BAPO concentration. The use of $\rho/2$ in equation 6.75 reflects that each decomposition event produces two radicals. Simulations were carried out in which $[A-X-B]$ was used as a variable instead of ρ. Consistent with equation 6.75 is that the initiator concentration be adjusted as follows with each simulated pulse:

$$[A-X-B] = [A-X-B](1-2\times\text{REI}) \tag{6.76}$$

Equation 6.76 thus mimics the effect of initiator consumption, which will clearly be faster as REI is increased. However equation 6.75 makes clear that a larger REI gives a larger ρ, an effect which of itself influences PLP results (see figure 6-23). In order not to mix together different effects, simulations were carried out with the identical starting value of $\rho = 1 \times 10^{-5}\text{mol.L}^{-1}$. This was achieved by decreasing the starting $[A-X-B]$ as REI was increased. It should be noted that the inclusion of initiator consumption in the kinetic model precludes the establishment of a truly pseudo-steady state (because ρ is always decreasing).

The results of simulations are shown in figure 6-25. Although ρ is the same at the start of each simulation, it decreases more quickly as REI is increased, because of faster initiator consumption (see equation 6.76). Thus one gets lower rates of termination, and hence the obtained MWD is more pronounced at higher molecular weights. Of course reinitiation - also operative in these simulations - additionally gives this effect, however we have already seen in figure 6-24 that its contribution is quantitatively small, regardless of the value of REI. So the considerable enhancement of overtone features in the REI = 0.1 results of figure 6-25 must primarily be an effect of initiator consumption. This raises the possibility that high initiator

consumption could have been a major factor contributing to the unexpected shape of our MWDs. This said, it is thought to be unlikely that there was significant initiator consumption in these experiments. Further, a value as high as REI = 0.1 - the value found to be necessary to give a significant initiator consumption effect in these simulations - is also thought to be unlikely. However it must be remembered that these simulations were only of 100 pulses of polymerization, whereas in reality experiments will usually be carried out for of order a thousand pulses, and this may be long enough to give significant initiator consumption even for lower REI. The true value of REI is of course genuinely unknown. In these simulations I have used a wide variety of REI values. A value of order 0.001 or lower is perhaps what one might expect in reality for REI; these simulations suggest that such a value produces very weak reinitiation effects. As noted, however, it may be that reinitiation effects only emerge slowly over a very large number of pulses, and hence were not fully seen in these simulations. Interestingly, if REI is of order 0.001 in reality, then experimental systems would take thousands of pulses to reach a pseudo-steady state, i.e., experiments would either entirely or mostly be conducted in a state of approach to pseudo-steady state. On the other hand, if REI is high (say, 0.1), then the discussion above makes clear that high initiator consumption must be expected.

In summing up these simulations with the modified kinetic model, it must said that as many questions have been raised as answered. While it is clear that endgroup reinitiation does indeed give the anticipated effect of higher proportions of long chains, these simulations suggest that this might only be a minor effect in explaining the experimental MWDs. It is clear that a better understanding of these MWDs will only be possible once more is known about photoinitiation with BAPO, for these simulations have suggested that either a low value of ρ or a large extent of initiator consumption could be more important factors than endgroup reinitiation as such in explaining the experimental MWDs. Further, it would clearly be useful to have some idea of the real reinitiation probability (REI). Since these simulations indicate that these BAPO systems approach pseudo-steady state relatively slowly, it would be of interest to determine how MWDs evolve as pulses are applied; MALDI-mass spectroscopy, which can identify endgroups, would be especially useful in this respect. Equally, it is also clear that being able to carry out longer simulations would be useful in seeking to understand experimental results. Not only could greater numbers of pulses be simulated, but it would also be desirable to carry out simulations

with combination. The results of figure 6-23 still indicate the effect of combination on MWDs, but it would be preferable to be able to model our styrene results directly.

Conclusion

Through the study of MMA and STY, I have confirmed that the use of a visible light photoinitiator such as BAPO should offer the opportunity of determining accurate values of k_p for monomers which absorb strongly at UV wavelengths. We have also seen here that the use of BAPO as a PLP photoinitiator leads to MWDs in which overtone peaks are more pronounced and the fundamental peak less evident than is usual. This is qualitatively consistent with the phenomenon of endgroup reinitiation, which one expects to occur when BAPO is used as a photoinitiator. This may be a process which occurs, at least to some small degree, in all free-radical polymerizations. Simulations were therefore carried out to investigate to what extent endgroup reinitiation alters MWDs. Although these simulations indicate that endgroup reinitiation probably has only a small quantitative effect on MWDs, this is nevertheless a significant result because of it being unexpected. Indeed, endgroup reinitiation would seem to have a number of subtle, unexpected effects, most notably long approaches to pseudo-steady state. Other simulations suggest that the high numbers of high molecular weight species produced in these experiments are more likely to be due to either low primary radical fluxes or high initiator consumption. This emphasizes the need for further quantitative information about the photoinitiation properties of the novel PLP photoinitiator BAPO before BAPO PLP results can be completely understood.

6.4 Concluding Remarks

The simulations performed in this chapter showcase the methods developed in chapters three to five. The developed numerical simulation techniques have allowed these complex kinetic systems to be simulated in a manageable length of computing time with assured accuracy.

The work presented in this chapter is a selection of the kinetic simulation studies that have been preformed in this thesis. A number of other investigations have been completed that have not been documented here. These include a simulation study of the mechanism of

Atom Transfer Radical polymerization and simulations of PLP MWDs where long dark times have been used, i.e., long times between bursts of initiation. The latter study involved the use of simulations to ensure that transfer-dominated conditions where obtained during these experiments. Moreover, computer-based simulations were used to check the accuracy of the value of the rate coefficient for transfer extracted from these experimental MWDs.

Chapter 7

Conclusion

Although this thesis has dealt with many facets of pulse initiated polymerization (PIP), the main aim of this work was to develop and assess strategies for the simulation of PIP. To do this, this study has focussed on methods - analytical and numerical - for solving the population-balance differential equations (DEs) that characterize PIP. By investigating these DEs, I have hoped to develop an efficient method for solving these equations, a method suited to modelling PIP. In this chapter the work performed in this thesis will be brought together and used to answer the question: what is the best strategy for simulating PIP?

It should be mentioned at the outset that this study has elucidated a lot of information in addition to the answer to this question. In particular, the form and the numerical solution of the DEs that characterize PIP are now well understood. Here a summary of the information gained about the structure of these DEs and the form of their solution will be given. This information not only informs us about PIP, but also about the modeling of free-radical polymerization in general. Although the solution of the DEs for continuously-initiated polymerization differs in some ways to those for intermittently-initiated polymerization, there are many similarities.

Finally, the results obtained from the two modelling studies of PIP experimental data presented in this thesis will be summarized. These studies have showcased the solution methods developed in this thesis, as well as facilitating the development of a better understanding of free-radical polymerization.

7.1 The Structure and the Solution of the Differential Equations that Characterize Pulse Initiated Polymerization

Right at the beginning of this study it was realized that a detailed understanding of the mathematical structure of the population-balance DEs for PIP was imperative, because unless these DEs were fully understood, it would be difficult to solve them well. Although the main aim of examining these DEs was to allow them to solved well, the information gained is useful in its own right. For these reasons, a brief summary will now be given of the insights gained into the structure of these DEs and their solution.

The DEs that model the concentrations of living radical species in a free-radical polymerization are numerous, stiff, coupled, and non-linear. Collectively these properties mean that they are not easy to solve. Moreover, if a periodic initiation profile is used then these difficulties are amplified. Both the solution to these DEs and the methods that must be used to solve them become more complicated. In particular, an intermittent rather than continuous initiation profile exacerbates the problem of stiffness. The solution to the DEs for PIP contain more transients that those for normal continuously initiated polymerization, i.e., the DEs are stiffer. This means that there are more regions in time and chain-length where extra care must be taken in obtaining a solution. This became clear when the Euler method was applied in chapter three. The appearance of transients (radical 'waves') meant that more error was incurred when a radical species had the most probable chain-length. Moreover, it meant the maximum integration step-size was limited to a value less than $\frac{1}{k_p M}$, i.e., 10^{-3}s for the default parameters of this thesis. This proved to be a limitation that was universal for explicit finite-difference based solution methods.

The error in the total radical concentration was smaller in magnitude and also less prone to divergence than had been expected. An analysis of the time dependence of the error incurred by the Euler method revealed that the error in the total radical concentration is self-correcting. This self-correction is caused by the balance between two types of error. The first type of error, truncation error, is fundamental to the way that finite-difference based solution methods work. They approximate the value of DEs during a small time interval by a simple function, the approximation function, and in doing so introduce error. This truncation error was shown to

be closely related to the rate of change in the DEs. Moreover, as the total radical concentration decreases for almost all of an initiation period, this error is negative; it means that the radical concentration is underestimated. The second type of error is initial-condition error. Initial-condition error originates from the fact the initial conditions for the next integration step are equal to the final conditions of the last step. Hence, if error was introduced in the last integration step, the initial conditions for the next step contain error. Thus, as the rate of termination during a step is proportional to square of the radical concentration at the start of a step, the underestimation of the initial radical concentration leads to an underestimation of the rate of termination during that step. Therefore the total radical concentration decreases less than is expected during that time step, i.e. initial-condition error compensates for the truncation error already present in the total radical concentration. The balance between the truncation error added and the initial-condition error removed, means that the error in these DEs does accumulated unabated, rather a situation is reached where the truncation error added during an initiation period is equal to the initial-condition error removed. The balance between these two types of error causes the odd situation of a pseudo-steady-state error to be established.

The error incurred in the solution of the DEs for dead polymer species has also been investigated. The DEs that model the rate of change in the concentrations of dead chains are significantly less complicated than those for growing radicals. This because they only contain simple gain terms that are not coupled to one other, i.e., the dead chain DEs are only coupled to the DEs for the living radicals not for other dead chains. For these reasons it was hypothesized that these DEs would be less difficult to solve; this was in fact the case. The analysis performed in chapter five demonstrated that the numerical solution of the dead chain DEs incurs little error.

This lead to the suggestion that a different numerical solution method should be used to solve these DEs for dead chains than that which is used to solve the DEs for living radicals. It was argued that this will normally involve using a slow yet accurate method for the living radical DEs and a faster but less accurate method for the dead polymer chain DEs, i.e., lower-level approximation function and/or longer time-step. Trial calculations indicated that this significantly decreases the time taken to simulated PIP. Moreover, these calculations showed that the reduction in computer time was greater when the termination can occur via the combination

mechanism.

Another analysis was performed upon the dead chain DEs. This explored the effects of error in the living radical distribution upon dead chain molecular weight distribution (MWD). By adding error to the analytically obtained (and therefore error-free) radical chain-length distribution, I was able to investigate the effect of various types of error on the final product of a simulation, the dead chain MWD. In this study it was clearly shown that it is error in the total radical concentration that has the greatest effect on the dead chain MWD.

7.2 The Optimal Solution Strategy

In this study both analytic and numerical solution strategies have been employed. In chapter two, three analytic solutions were tested. These methods proved to have little value as practical solution strategies. The major problem faced when using any of these expressions was generating the dead polymer chain-length distribution from the concentrations of growing radicals. It was not possible to obtain an analytic expression for the dead polymer MWD. In each case the only way that such a distribution could be obtained was by numerically integrating an expression for some facet of the living radical distribution (which is equivalent in may ways to numerical solution of the dead chain DEs). This appears to be a general feature of analytic solutions for this type of polymerization: although some feature of the living radical chain-length distribution can be predicted analytically, for example the dependence of the rate of termination on chain-length, the dead polymer MWD can only be evaluated numerically. However, this alone does not preclude the use of these solutions to model PIP. It is the fact that these expressions are computationally expensive to evaluate that causes the real problem. The numerical integration of any function means that it must be evaluated many times. Thus if that function takes a long time to evaluate, the numerical integration will take a much longer time. Performing a typical simulation with one of these analytic expressions took many minutes of computer time (typically two hours).

These analytic solutions have an additional disadvantage that is more typical of analytic solutions: any change in the reaction scheme means that they must be re-derived. Thus the modelling of PIP MWDs with an analytic solution is not recommended unless a solution can

be found that overcomes the problems noted above.

Numerical solution strategies met with more success. The Taylor series and Runge-Kutta methods used in this thesis can be used to solve this system of DEs accurately in a short period of time. These methods are recommended as the solution algorithms that should be used to model PIP. To decide which of the three tested methods that proved successful – the Euler, Modified Euler and fourth-order Runge-Kutta method – should be used, the following strategy is recommended. A trial calculation should be performed with the Euler method. If this calculation is completed quickly, i.e., within a matter of minutes, then the fourth-order Runge-Kutta should be used, because it too is likely to run quickly and its accuracy is best. If this calculation takes a moderate amount of time, then the Modified Euler method should be used. Otherwise the Euler method should be used as it runs the fastest. Also the error in the total radical concentration should be monitored if possible, for example using the analytic expression for the total radical concentration (see chapter one). It should be ensured that this error is always below 1%. If it is not then the step-size should be decreased or a more accurate method used.

It is also recommended that the step-size profile based upon the rate of change in the differential equations that was developed in chapter three should be used. Calculations performed in chapters three and four established that using this step-size profile increases the efficiency of all of these methods. This step-size profile provides the simulation strategy with information about the error in these differential equations, informing it when to be careful and when to be bold.

Although the strategy outlined above is suited to a wide range of conditions, there are some situations when another strategy will give much faster simulation times. Firstly, in some cases an implicit, rather than an explicit, method could be used. It is recommended that if the ratio $\frac{k_p[M]t_0}{2}$ is greater than 100, then an implicit method could be used to some advantage. This being said, it is advisable to initially use both an implicit and explicit method and to compare these methods before deciding on a strategy. Implicit methods may be faster, but this will be at the expense of accuracy. In general an explicit method with a time-step less than $(k_pM)^{-1}$is a fail-safe option. It may take longer that an implicit method with a much longer time-step, but accuracy is assured. This in fact is an important finding of this thesis: despite the stiff nature of

the differential equations describing free-radical polymerization, explicit methods with a small enough time-step (less than $(k_p M)^{-1}$) always solve these differential equations accurately.

Finally, if the number of types of chemical species in a polymerization is extraordinary high, then the modified Monte Carlo algorithm is recommended. For most polymerization systems the Monte Carlo algorithm is a lot less efficient than any of the finite-difference based methods. However, if a lot of chemical species have to be resolved, then the Monte Carlo method can be the optimal strategy. Probably this is only the case when one wishes to include processes such as chain transfer to polymer in modelling.

It is believed that the judicous use of the strategy outlined above is the optimal solution strategy for the simulation of PIP. Not all workers will be in a position to carry out this strategy to the letter, and for such workers the fourth-order Runga-Kutta method is recommended as being fail-safe.

7.3 Information Gained from Modeling Studies

Two case studies have been performed where the methods developed in this thesis have been used to model PIP. In the first study MWD data obtained by MALDI-MS has been simulated to extract information about the mechanism of termination for methyl methacrylate. This study extracted a value of λ $(k_{td}/(k_{td} + k_{tc}))$ equal to 0.78 at 0°C.

The second case study was an investigation of a novel visible light initiator that can be used to initiate PIP. The MWDs obtained when this initiator was used were different in several ways from typical PIP MWDs (the first overtone was greater than the primary peak). This analysis attempted to explain causes of this abnormality. To do this the effects that the reinitiation of initiator-derived endgroups contained in dead polymer had on these MWDs were studied. It became clear that this reinitation had only a small effect on these MWDs. It was concluded that the atypical MWDs obtained from these experiments could be explained by initiator consumption and effects of the termination mechanism.

Very importantly, these two case studies illustrate how flexibility is invariably needed in modelling of free-radical polymerization data. In neither case could the analytic solutions of chapter two be used to model the data, because either more information was needed or

additional processes have to be added to the reaction scheme. For this reason it is simplest to stick to the numerical solution of DEs rather than attempt to develop one-off analytic solutions. Hence the importance of chapters three to five of this thesis.

7.4 Future Work

There are number of areas where the work of this thesis has raised questions that could be tackled in further investigations. A selection of these includes:

- **Continuously-Initiated Polymerization** It could be necessary to perform modelling studies of continuously-initiated polymerizations where the DEs have to be solved numerically, i.e., systems where one can not generate an analytic solution by making the steady-state assumption. For example, one may wish to model a continuously-initiated polymerization over a range of conversion conditions. To develop methods suitable for modelling of this type of polymerization, a study similar to that outlined in this thesis should be performed. In particular, attention should be payed to the solution of the DEs when they are far from the steady-state, e.g., in the initial stages of the polymerization, as well as when they are close to a steady-state, e.g., when the only changes occurring are due to, for example, changes in conversion.

- **Chain Transfer to Polymer** It was mentioned several times in this thesis that the best method for modelling chain transfer to polymer is likely to be the Monte Carlo method. I suggest that methods could be developed to allow this modelling to take place efficiently. For example, we saw it chapter three that the efficiency of the MC method was drastically increased when the propagation reaction was treated as a Normal distribution. The potential exists for a similar treatment to be used for chain transfer to polymer, for example, a distribution based treatment could be used for the position of branch points.

- **Living Radical Polymerization** Living radical polymerization is an important industrial processes. An investigation similar to that of this thesis could be conducted into the solution of the DEs for the living radical and dead polymer chain-length distributions in these systems. The work of this thesis should be a excellent staging point for an inves-

tigation of these systems because of the many similarities between living and standard free-radical polymerization systems.

- **MALDI-MS Modelling** MALDI-MS MWDs contain a wealth of, as yet, untapped information. Experimental and modelling studies should be performed of these MWDs to extract information about, for example the mechanism of the termination by disproportionation and the mechanism and rate of chain transfer.

Bibliography

[1] A.P. Alexsandrov, V.N. Genkin, M.S. Kitai, I.M. Smirnova, and V.V. Solokov. *Sov. J. Quantum Electron. (Engl. Transl.)*, 7:547, 1977.

[2] P.W. Atkins. *Physical Chemistry.* Oxford Uni. Press, 4th edition, 1990.

[3] S.W. Benson and A.M. North. *J. Am. Chem. Soc.*, 84:935, 1962.

[4] K.C. Berger and G. Meyerhoff. *Polymer Handbook.* J. Wiley and Sons, New York, 3rd edition, 1989.

[5] S. Beuermann, M. Buback, T.P. Davis, R.G. Gilbert, R.A. Hutchinson, O.F. Olaj, G.T. Russell, J. Schweer, and A.M. van Herk. *Macromol Chem. Phys.*, 198:1545, 1997.

[6] W.E. Boyce and R.C. DiPrima. *Elementary differential equations and boundary value problems.* John Wiley and Sons, Inc., 1992.

[7] M. Buback, M. Busch, and R. Lammel. *DECHEMA Monographs*, 131:569, 1995.

[8] M. Buback, R.G. Gilbert, R.A. Hutchinson, B. Klumperman, F-D. Kutcha, B.G. Manders, K.F. O'Driscoll, G.T. Russell, and J. Schweer. *Macromol. Chem. Phys.*, 196:3267, 1995.

[9] M. Buback and F-D. Kuchta. *Macromol. Chem. Phys.*, 198:1455, 1997.

[10] M. Buback and R. Lammel. *Macromol. Theory and Simul.*, 6:145–150, 1997.

[11] M. Buback and R. Lammel. *Macromol. Theory and Simul.*, 7:197, 1998.

[12] M. Buback, R. Lammel, and M. Busch. *Macromolecular Theory and Simulations*, 5:845–861, 1991.

[13] R.L. Burden and J.D. Faires. *Numerical Analysis.* PWS Publishing Company, 1993.

[14] H.S. Creel. *Trends in Polymer Science*, 1:335–342, 1993.

[15] A.F. Cunningham, V. Desobry, K. Dietliker, R. Husler, and D.G. Leppard. *Chimia*, 48:223, 1994.

[16] M. Deady, A.W.H. Mau, G. Moad, and T.S. Spurling. *Makromol. Chem*, 194:1691–1705, 1993.

[17] A.V. Evseev and A.N. Nikitin. *Laser Chem.*, 16:83, 1995.

[18] A.V. Evseev and A.N. Nikitin. *Macromolecular Reports*, A33:187, 1996.

[19] H. Fischer and H. Paul. *Acc. Chem. Res.*, 20:200–206, 1987.

[20] C. W. Gear. *Numerical initial value problems in ordinary differential equations.* Prentice-Hall, 1971.

[21] D.T. Gillespie. *J. Phys. Chem.*, 81:2340, 1977.

[22] J. He, H. Zhang, and Y. Yang. *Macromol. Theory and Simul.*, 4:811, 1995.

[23] J.P.A. Heuts. *Dynamics of Propagation and Transfer Reactions in Free-Radical Polymerization.* PhD thesis, University of Sydney, 1996.

[24] J.P.A. Heuts, R.G. Gilbert, and L. Radom. *Macromolecules*, 28:8771, 1995.

[25] J.P.A. Heuts, A. Pross, and L. Radom. *J. Phys. Chem.*, 100:17087–17089, 1996.

[26] R.A. Hutchinson, D.A. Paquet Jr, and J.H. McMinn. *Macromolecules*, 28:5663, 1995.

[27] U. Kolczak, G. Rist, K. Dietliker, and J. Wirz. *J. Am. Chem. Soc.*, 118:6477, 1996.

[28] D. Kukulji, T.P. Davis, and R.G. Gilbert. *Macromolecules*, 29:994–999, 1998.

[29] J. Lu, H. Zhang, and Y. Yang. *Makromol. Chem. Theory and Simu.*, 2:747, 1993.

[30] B. Manders. *Pulsed Initiation Polymerization.* PhD thesis, Technical University of Eindhoven, 1997.

[31] K.W. Mclaughlin, D.D. Latham, C.E. Hoyle, and M.A. Tripp. *J. Phys. Chem*, 93:3643–3647, 1989.

[32] G. Moad, D.A. Shipp, T.A. Smith, and D.H. Solomon. *Macromolecules*, 30:7627, 1997.

[33] G. Moad and D.H. Solomon. *Comprehensive Polymer Science: The Synthesis, Characterization, Reactions and Applications of Polymers*, volume 3, page 147. Pergamon: Oxford, 1989.

[34] G. Moad and D.H. Solomon. *The Chemistry of Free Radical Polymerization*. Peragamon: Oxford, 1st edition, 1995.

[35] M. Monterio, K.F. O'Driscoll, and B. Klumperman. *J. Polym. Sci., Part A: Polym. Chem.*, 35:515, 1997.

[36] K.F. O'Driscoll and M.E. Kunidersma. *Macromol. Theory Simul.*, 3:469, 1994.

[37] O.F. Olaj, I. Bitai, and F. Hinkelmann. *Macromol. Chem.*, 188:1689, 1987.

[38] O.F. Olaj, A. Kornherr, and G. Zifferer. *Macromol. Rapid Comm.*, 18:997, 1997.

[39] O.F. Olaj, A. Kornherr, and G. Zifferer. *Macromol. Rapid Commun.*, 19:89, 1998.

[40] O.F. Olaj and G. Zifferer. *Makromol. Chem. Theory and Simul.*, 1:71, 1992.

[41] O.F. Olaj and G. Zifferer. *DECHEMA Monographs*, 131:579, 1995.

[42] O.F. Olaj and G. Zifferer. *Macromolecular Theory and Simulations*, 7:157–169, 1998.

[43] W.H. Press, B.P. Flannery, S.A. Teuloksy, and W.T. Vetterling. *Numerical Recipes*. Cambridge University Press, 1987.

[44] M.T.L. Rees, G.T. Russell, M.D. Zammit, and T.P. Davis. *Macromolecules*, 31:1763–1772, 1998.

[45] G.T. Russell. *Macromol. Theory Simul.*, 4:497, 1995.

[46] W. Rutsch, K. Dietliker, D. Leppard, M. Kohler, L. Misev, U. Kolczak, and G. Rist. *Prog. Org. Coat.*, 27:227, 1996.

[47] J. Sarnecki and J. Schweer. *Macromolecules*, 28:4080–4088, 1995.

[48] H.F. Schuh and H. Fischer. *Helv. Chim. Acta.*, 61:2463–2478, 1978.

[49] J. Schweer, J. Sarnecki, F. Mayer-Posner, K. Mullen, H.J. Rader, and J. Spickermann. *Macromolecules*, 29:4536–4543, 1996.

[50] M. Seebelberg and M. Thorn. *Macromol. Theory Simul*, 3:825–843, 1994.

[51] M. Stickler. Private Communication.

[52] M. Stickler and G. Meyerhoff. *Makromol. Chem.*, 179:2729, 1978.

[53] J. Stoer and R. Bulirsch. *Introduction to numerical analysis.* Springer-Verlag, 1980.

[54] A.M. van Herk, H. De Brouwer, B.G. Manders, L.H. Luthjens, M.L. Hom, and A. Hummel. *Macromolecules*, 29:1027–1030, 1996.

[55] M. Wulkow. *Macomol. Theory and Simul.*, 5:393, 1996.

[56] M.D. Zammit, T.P. Davis, and D.M. Haddleton. *Macromolecules*, 29:492–494, 1996.

[57] G. Zifferer and O.F. Olaj. *Macromol. Theory and Simul.*, 5:901, 1996.

[58] G. Zifferer and O.F. Olaj. *Macromol. Theory and Simul.*, 5:923, 1996.